Universitat Autònoma de Barcelona

Complex Neuroimaging Changes in Metabolite, Cortical Structures and Regional Vulnerabilities in the Alzheimer Disease Continuum

Victor Montal Blancafort

Doctoral Thesis

Complex Neuroimaging Changes in Metabolite, Cortical Structures and Regional Vulnerabilities in the Alzheimer Disease Continuum

Victor Montal Blancafort
victor.montal [at] protonmail [dot] com

Thesis director:
Dr. Juan Fortea

Thesis tutor:
Dr. Alberto Lleo

Neurobiology of dementia Unit – Memory Unit
Institut d'Investigació Biomèdica Sant Pau
Hospital de la Santa Creu i Sant Pau

Programa de Doctorat en Neurociències
Institut de Neurociències
Universitat Autònoma de Barcelona

Barcelona. October 2021

Certificate of direction

Dr. Juan Fortea Ormaechea, who obtained his PhD in Medicine in the Universitat de Barcelona, specialist in Neurology at Hospital de Sant Pau and medical director of the Alzheimer – Down Syndrome Unit and Dr. Alberto Lleó Bisa, who obtained his PhD in Medicine in the Universitat de Barcelona, Head of the Memory Unit in the Neurology Department in Hospital de la Santa Creu i Sant Pau and aggregate professor in the Universitat Autònoma de Barcelona Certify:

That the work “Complex neuroimaging changes in metabolite, cortical structures and regional vulnerabilities in the Alzheimer disease continuum”, presented by Victor Montal Blancafort to qualify for Doctor in Neurosciences for the Universitat Autònoma de Barcelona has been done under our direction and meets all the requirements to be presented and defended in the presence of the corresponding Thesis Committee.

Dr Juan Fortea, Director
Director of the Alzheimer – Down Syndrome Unit
Hospital de la Santa Creu i Sant Pau

Dr Alberto Lleo, Tutor
Head of the Memory Unit
Hospital de la Santa Creu i Sant Pau

“*Thoroughly conscious ignorance*
is the prelude to every real advance in science”

James Clerk Maxwell

Table of Contents

Abstract

Alzheimer disease (AD) is the most important cause of dementia. Its histopathological hallmarks are intracellular hyperphosphorylated tau and extracellular amyloid plaques, which start to accumulate decades before the onset of clinical symptoms and eventually lead to neurodegeneration and brain atrophy. Magnetic resonance imaging (MRI) provides a window to characterize in vivo the cortical changes in the preclinical and clinical phases of the disease. This thesis studied the cortical macrostructural, microstructural and metabolite changes along the AD continuum. It highlights the complex and non-linear alterations in the preclinical phase and analyzes the characteristic regional vulnerability underlying the spread of tau in early stages of the disease. Specifically, the first work of the thesis mathematically modeled the trajectory of cortical thickness and cortical mean diffusivity in autosomal dominant Alzheimer disease. This work demonstrated a biphasic trajectory of cortical alterations, in which the initial increases of amyloid were associated with increased cortical thickness and decreased cortical diffusivity, but were followed by cortical thinning and increased cortical diffusivity once tau becomes abnormal (15 years prior to symptom onset). The second work of this thesis characterized the alterations of metabolites along the AD continuum in a cohort of Down Syndrome using magnetic resonance spectroscopy (MRS). This work showed the potential of MRS to detect AD-related inflammation and neurodegeneration. The third work of this thesis investigated the potential of cortical diffusivity as a marker of neurodegeneration and its relationship with the accumulation of tau in preclinical AD. This work showed cortical diffusivity decreases were associated with the accumulation of tau in inferior temporal regions and predicted clinical deterioration. The fourth work of this thesis studied the genetic regional vulnerability associated to the stereotypical pattern of tau accumulation. This work developed a novel graph-theory-based framework to characterize the spread of tau integrating a high-resolution data of gene expression. This thesis has several important potential implications. First, it consolidates the biphasic trajectory of cortical alterations that reconciles previous conflicting results in the literature, greatly expand the potential of MRI to track changes in preclinical AD and provides a rationale to understand the (otherwise) paradoxical findings of increased atrophy in the active

arm of anti-amyloid trials. Second, this thesis showed MRS could be a good noninvasive disease-stage biomarker in Down syndrome to track neurodegeneration and neuroinflammation. Third, it shows cortical mean diffusivity could be a more sensitive marker of neurodegeneration than cortical thickness that could be implemented in clinical trials. Finally, it provides a new framework to analyze the regional vulnerability underlying the spread of tau which could lead to the identification of new drug targets. In conclusion, this thesis highlights the complexity of the cortical changes preclinical AD and their regional vulnerability, but also demonstrates the potential of MRI to track these changes when using a multimodal approach, non-linear models and new analytical frameworks.

Resumen

La enfermedad de Alzheimer es la principal causa de demencia. Patológicamente, está caracterizada por tau hiperfosforilada intracelular y el depósito de placas de amiloide extracelular. Estos procesos fisiopatológicos empiezan décadas antes de que aparezca el deterioro cognitivo, y conllevan atrofia cerebral y neurodegeneracion. La imagen por resonancia magnética (RM) nos permite caracterizar “in-vivo” los cambios corticales en las fases preclínicas de la enfermedad. Esta tesis incluye trabajos donde se estudian los cambios macroestructurales, microestrucutrales y de metabolitos corticales a lo largo del continuo de la EA. Este trabajo destaca la complejidad de estos cambios y su trayectoria no lineal, y analiza la vulnerabilidad regional que subyace a la propagación de tau en las fases tempranas de la enfermedad. En concreto, en el primer trabajo de esta tesis, se modeló matemáticamente la trayectoria de cambios de grosor cortical y difusividad cortical en la EA autosómica dominante. Demostramos que existe los cambios corticales siguen una trayectoria bifásica, donde en el inicio y relacionado con el acúmulo de amiloide, aparece un incremento del grosor cortical y un descenso de la difusividad cortical, que siguen a cambios hacia atrofia e incrementos de difusividad una vez tau adquiere valores patológicos (15 años antes de que empiecen los síntomas clínicos). En el segundo trabajo de esta tesis se caracterizó las alteraciones de metabolitos en el continuo de la EA en una muestra de adultos con Síndrome de Down usando resonancia magnética por espectroscopia (RMS). Este estudio demuestra el potencial de la RMS para detectar alteraciones relacionadas con la neurodegeneracion en la EA. En el tercer trabajo de esta tesis se investigó el potencial de la difusividad cortical como marcador de neurodegeneracion, y su relación con el acúmulo patológico de tau en las fases preclínicas de la EA. En el cuarto trabajo de esta tesis se estudió el perfil genético de la vulnerabilidad regional asociada al patrón de propagación de tau. Para este trabajo se desarrollaron herramientas basadas en teoría de grafos para caracterizar la propagación de tau, integrando información de alta resolución sobre expresión génica. Esta tesis supone potenciales implicaciones. En primer lugar, consolida la presencia de un modelo bifasico de cambios corticales que proporciona una explicacion a resultados aparentemente adversos en la literatura, y propone el potencial de la RM para capturar alteraciones estructurales en las etapas tempranas de la enfermedad. En

segundo lugar, demuestra el potencial de la RMS como marcador no invasico para medir la neurodegeneracion e inflamacion en la poblacion con Sindrome de Down. En tercer lugar, propone que la difusividad cortical es un potencial marcador de neurodegeneracion mas sensible que el grosor cortical, con potencial para ser usado en ensayos clinicos. En ultimo lugar, propone un marco analitico para estudiar las vulnerabilidades regionales asociadas a la propagacion de tau, cuyos resultados pueden suponer una guia de investigacion a nuevas dianas farmacologicas. En conclusion, esta tesis destaca la complejidad de los cambios corticales en etapas preclinicas de la EA y su vulnerabilidad regional.

List of Abbreviations

Aβ	Amyloid β
ABA	Allan Brain Atlas
AD	Alzheimer Disease
ADAD	Autosomal dominant Alzheimer disease
AIBL	Australian Imaging, Biomarker & Lifestyle Flagship Study of Ageing
ALS	Amyotrophic lateral sclerosis
APOE	Apolipoprotein E
APP	Amyloid precursor protein
bvFTD	Behavioural variant of frontotemporal dementia
CERAD	Consortium to Establish a Registry for Alzheimer's Disease
cMD	Cortical mean diffusivity
CSF	Cerebrospinal fluid
CSK3β	Glycogen synthase kinase 3
DIAN	Dominantly Inherited Alzheimer Network
DKI	Diffusion kurtosis imaging
DONSURF	Diffusion on surface
DS	Down Syndrome
DW-MRS	Diffusion-weighted magnetic resonance spectroscopy
DWI	Diffusion weighted imaging
FDA	Food and Drug Agency
FDG	Fluorodeoxyglucose
GWAS	Genome-wide association study
HABS	Harvard Aging Brain Study
HARDI	High angular resolution diffusion imaging
LOESS	Locally estimated scatterplot smoothing
MAO-B	Monoamine oxidase B
MAPT	Microtubule associated protein tau
mI	Myo-inositol
MRI	Magnetic resonance imagine
MRS	Magnetic resonance spectroscopy
NAA	N-acetyl-aspartate
NFL	Neurofilament light chain

NFT	Neurofibrillary tangles
NIA-AA	National Institute on Aging and Alzheimer's Association
DTI	Diffusion tensor imaging
NODDI	Neurite orientation dispersion and density imaging
PET	Positron emission tomography
PSEN1	Presenlilin 1
PSEN2	Presenlilin-2
pTau	Hyperphosphorilated tau
RNA	Ribonucleic acid
sTREM2	Soluble triggering receptor expressed on myeloid cells 2
YKL-40	Chitinase 3-like I

List of publications

1) **Montal V,** Vilaplana E, Pegueroles J, Bejanin A, Alcolea D, Carmona-Iragui M, Clarimón J, Levin J, Cruchaga C, Graff-Radford NR, Noble JM, Lee JH, Allegri R, Karch CM, Laske C, Schofield PR, Salloway S, Ances B, Benzinger T, McDale E, Bateman R, Blesa R, Sánchez-Valle R, Lleó A, Fortea J; Dominantly Inherited Alzheimer Network (DIAN). ***Biphasic cortical macro- and microstructural changes in autosomal dominant Alzheimer's disease***. Alzheimers Dement. 2021 Apr;17(4):618-628. doi: 10.1002/alz.12224. Epub 2020 Nov 16. PMID: 33196147; PMCID: PMC8043974.

2) **Montal V**, Barroeta I, Bejanin A, Pegueroles J, Carmona-Iragui M, Altuna M, Benejam B, Videla L, Fernández S, Padilla C, Aranha MR, Iulita MF, Vidal-Piñeiro D, Alcolea D, Blesa R, Lleó A, Fortea J; Down Alzheimer Barcelona Neuroimaging Initiative. ***Metabolite Signature of Alzheimer's Disease in Adults with Down Syndrome.*** Ann Neurol. 2021 Jul 26. doi: 10.1002/ana.26178. Epub ahead of print. PMID: 34309066.

3) Rodriguez-Vieitez E*, **Montal V***, Sepulcre J, Lois C, Hanseeuw B, Vilaplana E, Schultz AP, Properzi MJ, Scott MR, Amariglio R, Papp KV, Marshall GA, Fortea J, Johnson KA, Sperling RA, Vannini P. ***Association of cortical microstructure with amyloid-β and tau: impact on cognitive decline, neurodegeneration and clinical progression in older adults.*** Mol Psychiatry. In press

4) **Montal V**, Diez I, Chanmie K, Orwig W, Bueichekú E, Bejanin A, Pegueroles J, Dols-Icardo O, Vannini P, El-Fakhri G, Johnson KA, Sperling RA, Fortea J, Sepulcre J. ***Neurogenetic Vulnerability of Tau Spreading in the Aging Brain***. In preparation

1. Introduction

1.1 Alzheimer Disease

1.1.1 A Global Health Problem

Dementia, a term used to describe the affectation of memory, thinking, behaviour and emotion in several brain disorders, is estimated to be affecting over 55 million people in 2021. Alzheimer disease (AD) is the most important cause of dementia, accounting for 50-60% of people with cases. Alzheimer's disease is the most common cause of dementia in the world, with more than 6.8 million people aged 65 or older suffering of AD dementia only in the United States[1]. Unfortunately, there is no cure, despite the recent FDA approval of Aduhelm[2]. Thus, the global burden of AD, and the tremendous impact on both patients and caregivers makes research in AD a priority of the utmost importance.

1.1.2 Pathological hallmarks of the disease

Part of the complexity to understand and characterize AD might stem from the fact that it is the only neurodegenerative disease associated with two proteinopathies[3]. AD has two core pathological hallmarks: the presence of extracellular amyloid plaques (composed mainly by amyloid 1-42) and the accumulation of intracellular hyperphosphorylated species of the microtubule-associated tau protein in neurofibrillary tangles.

Amyloid plaques are formed through the accumulation of extracellular soluble fragments of amyloid-β (Aβ). Aβ is the result of the sequential cleavage of the Amyloid Precursor protein (APP)[4], which is mainly found in neurons, by three protease activities. The cleavage of APP by the beta- and gamma-secretase, generates Aβ peptides between 40 and 43 amino acids in length that are prone to aggregation. The most frequent species in amyloid plaques is the Aβ1-42 peptide[5]. Amyloid plaques can be found in several conformations, the two most frequent being diffuse and dense-core plaques. Topographically, amyloid deposition starts in the isocortex, and later spreads to subcortical areas[3].

Neurofibrillary tangles (NFT) result from the pathological accumulation of intraneuronal paired helical filaments of hyperphosphorilated tau (pTau)[3]. Tau is expressed by the microtubule associated protein tau (MAPT). Tau can be phosphorilated by several kinases, the most important of which is the glycogen synthase kinase 3 (CSK3β)[6]. Hyperphosophorilated tau dissociates from the microtubules and accumulates in tangles[3]. The topography of the pathological accumulation of tau in AD follows a stereotypical pattern, which starts at the locus coeruleus, expands to medial temporal cortex, to subsequently accumulate in the neocortex[7].

Even though amyloid plaques and NFT are the most prominent hallmarks, AD also presents several other pathological findings that are important in the progression of the disease[8]. In this sense, the role of glia cells in the progression of AD has recently received enormous atztention due to the consistent findings in GWAS studies implicating innate immunity[9]. The complex changes of astrocytes and microglia from their homeostatic state to its reactivity is only beginning to be understood, but clearly modulate the accumulation and spread of both amyloid and tau[10]. In addition, recent findings also point to the direct toxic effect of reactive glia to cause neuronal death[11].

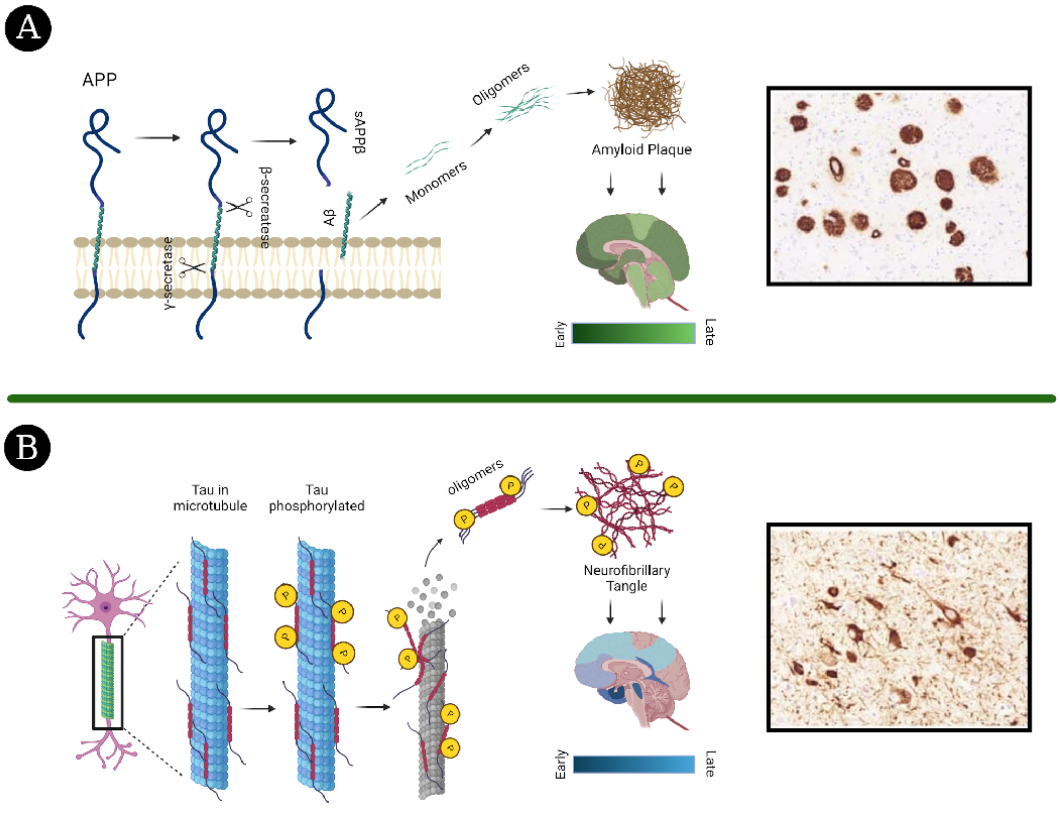

Figure 1. Pathological hallmarks of AD. (A) Amyloid plaques formation and (B) NFT formation

Amyloid plaques and tau tangles have been described pathologically for more than a century with silver staining methods among others. The biochemical composition, however, was not described until the 1980s, and together with the development of immunohistochemistry, eventually led in the 2000s to the development of several protocols and scales to measure the burden of each proteinopath[7,12]. For amyloid

deposition, the two most widely used scales are the CERAD[12] (for neuritic plaques) and the Thal scales (for Aβ deposition)[13]. For tau, the Braak staging criteria is the most widely used. It proposes a sequential propagation of tau in the brain and describes six stages[7]. Microglia was first described by Pío del Río Hortega, who beautifully described its different morphological states[14]. However, there are not standardized scales to quantify the amount of pathological glia, probably because its importance has been neglected until very recently. This will probably change as there is very active research in this topic.

1.1.3 Sporadic and familial Alzheimer Disease

AD dementia is clinically characterized by a progressive loss of memory and executive functions. Its more common presentation is initially characterized by a gradual deterioration of episodic memory that disturbs the ability to acquire and recall recently learnt information[15]. AD is a complex multifactorial disease, in which the combination of genetic vulnerability, risk factors and epigenomic changes lead to the development of the disease. Nevertheless, recent genetic studies with thousands of participants identified 38 loci that increase the risk of developing AD, being APOE the most important one[9]. Among the risk factors for sporadic AD the most important is age[16]. In most individuals, the disease occurs between 70 and 90 years of age.

Currently, there are two frameworks to diagnose the disease. On the one hand, the NIA-AA framework proposes a biological definition of the disease based solely on biomarkers (i.e amyloid and tau)[17]. The clinical symptoms or syndromes stage the disease (e.g. AD dementia in those individuals with pathological amyloid and pathological tau and a dementia syndrome). On the other hand, the International Working Group, in addition to the considering the presentation of pathological changes, requires the presence of a clinical syndrome to diagnose an individual with AD[18].

Despite the high heritability (estimated in about 70%[19], Figure 2-A), less than 1% of AD dementia presentations arise from autosomal dominant mutations. Concretely, autosomal dominant Alzheimer Disease (ADAD) is caused by mutations in the APP, presenlilin-1 (PSEN1) and presenilin-2 (PSEN2) genes[20]. The clinical symptomatology in ADAD resembles that of sporadic AD, even though it appears more than 20 or 30 years before late onset AD. Importantly, the topography and laminar distribution of amyloid and tau accumulations are very similar between the two forms.

Another population recently categorized as genetic form of dementia is Down Syndrome(DS)[21]. Recent epidemiologic studies have shown that the lifetime risk of Alzheimer’s disease in people with DS is more than 95%[22]. This ultra-high risk stems from the trisomy of chromosome 21 itself, where the APP gene its coded, resulting into an over-production of amyloid since birth. Importantly, the trajectory of

biomarkers and clinical changes of AD in the DS population (DSAD) is identical to that of ADAD[21] (Figure 2-B). ADAD and DSAD are both thus genetically determined forms of AD.

Genetically determined forms of AD present a unique opportunity to study AD pathophysiology over sporadic AD. Most importantly, the age of presentation of clinical symptoms in these two forms of familial AD is highly predictable[21,23], which allow to estimate the years to symptom onset and thus study the chrono-pathophysiology of the disease even in cross-sectional studies (often referred to, in this context, as pseudo-longitudinal studies). This predictability (and unavoidability) of the disease even in asymptomatic individuals makes these populations ideal for both primary and secondary preventive trials.

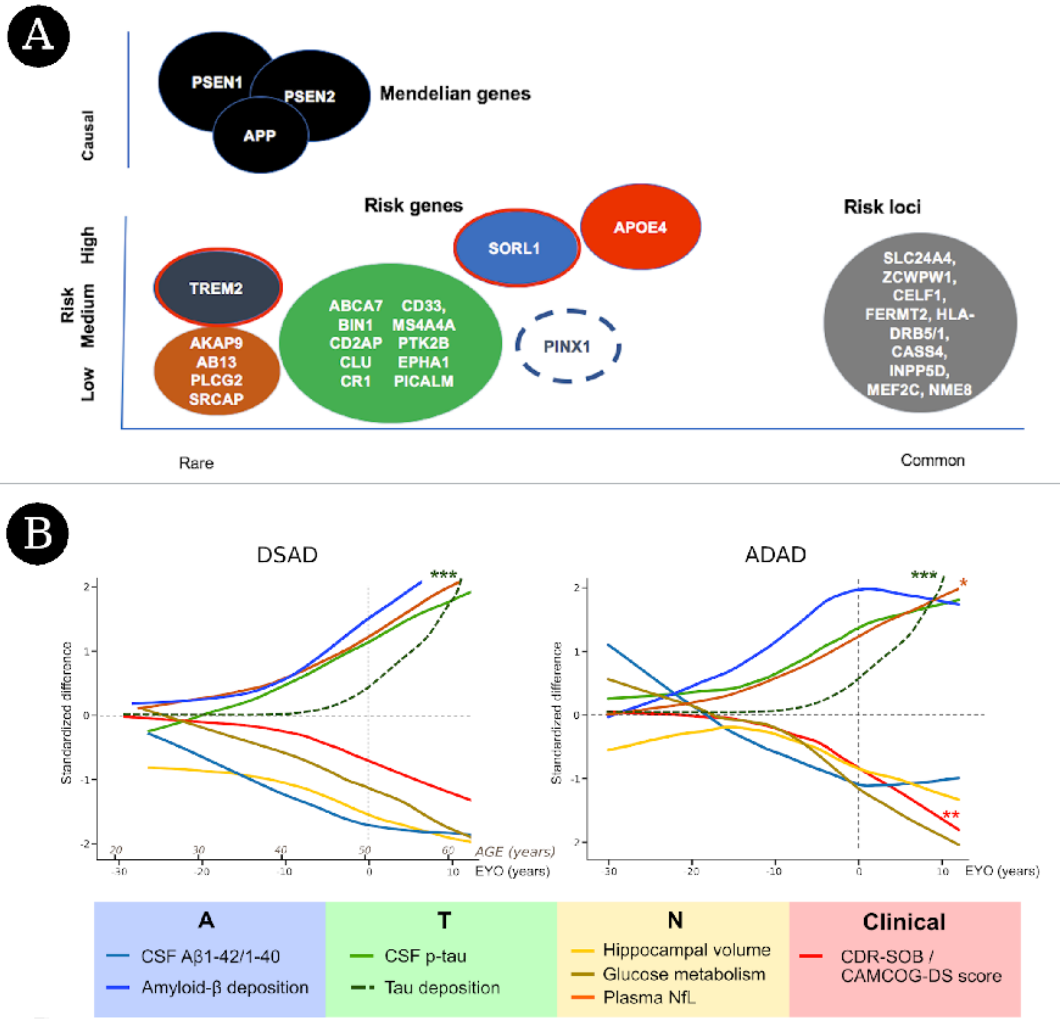

Figure 2. Genetic landscape in Alzheimer Disease. (A) Genetic risk genes and their prevalence in the genera population (adapted from Alzforum) and (B) Biomarker trajectories in ADAD and DS.

1.2 Biomarker for Alzheimer Disease

A biomarker is a measurable indicator of some biological state or condition, that can be objectively and reliably quantified. Many biomarkers have been discovered and validated to diagnose and study the AD pathophysiology[24]. Due to the diverse properties of those biomarkers, it is possible to group them in diverse ways, for example by the nature of the biomarkers, such as differentiating between biochemical and imaging biomarkers. The biomarkers of particular interest in this PhD are cerebrospinal fluid (CSF) and plasma biomarkers in the biochemical subgroup, and the positron emission tomography (PET), structural and diffusion magnetic resonance and magnetic resonance spectroscopy biomarkers, for the imaging biomarkers.

1.2.1 Biochemical Biomarkers

i) Cerebrospinal Fluid Biomarkers

Cerebrospinal fluid (CSF), which can be obtained through a lumbar puncture[25], is in direct contact with the extracellular space of the brain. Thus, CSF biomarkers are ideally poised to measure the AD pathological changes. CSF has been used for more than two decades in AD and other neurodegenerative diseases. There are three main proteins that have been studied in CSF: 1) Aβ1-42 (decrease in AD), 2) pTau (increased in AD) and 3) total Tau (increased in AD)[24]. These core AD biomarkers have repeatedly been shown to correlate with brain pathology, both in postmortem pathological studies[26] or when using amyloid or tau PET data as a proxy of brain pathology[27,28]. Researchers have also used CSF data to measure and study other pathophysiological alterations such as neuroinflammation, neurodegeneration (through neurofilament-light chain -NfL) or synaptic loss[29].

ii) Plasma Biomarkers

Plasma is a very accessible biofluid that might provide important information both for research and clinical practice because of its low-cost and availability. In the last 3 years, in parallel with major technical advancements, several plasma biomarkers have been developed in the AD field[24]. One of the earliest and most successful is plasma NfL, which reliable measure neurodegeneration, although it is not specific for AD as it is increased in all other neurodegenerative conditions. Other recent advancements have also allowed to measure different tau isoforms (pTau181 and pTau217 and pTau231)[24,30,31], which showed potential to track pathological alterations in early stages of the disease. Importantly, plasma pTau biomarkers showed high correlation with tau (and amyloid) PET and CSF measurements[30,32], reinforcing its potential to be used in clinical practice.

1.2.2 Imaging Biomarkers

i) Positron emission tomography biomarkers

Positron emission tomography (PET) is a nuclear medicine technique that enables the measurement and spatially location of specific protein aggregates or receptors in-vivo through the use of radiotracers. It is grounded on several radioisotopes based on fluoride, carbon or oxygen that emit positrons and that can be incorporated in different molecules (named radiotracer or ligands)[33]. These radiotracers are injected into the bloodstream, cross the brain blood barrier and reach their target. The collision of the emitted positrons with electrons generate gamma rays that can be measured in the PET. Fluorinated tracers have a much longer halve life than those based on carbon and are thus much better suited to be used in clinical practice. The ligands more widely used in the AD field are fluorodeoxyglucose (FDG), amyloid tracers and, more recently tau tracers. FDG has been used to measure brain metabolism for more than 30 years. AD dementia patients typically show hypometabolism in temporoparietal regions. Amyloid tracers (such as Florbetapir, florbetaben or flutemetamol) measure the deposition of amyloid, whereas tau tracers (such as FTP, RO948, PI2620 or MK6240) measure tau pathology[34]. PET can also be used to measure other pathological processes such as reactive astrocytosis[35] (e.g using Deprenyl-PET) or microglia activation[36] (using TSPO-PET). Compared to other biomarkers that provide only a scalar measure of brain pathology, PET provides topographical information. However, it does have some technical caveats such as low spatial-resolution (compared to other imaging techniques), non-specific tissue binding and/or partial volume contamination[37].

ii) Strucutral MRI

Magnetic resonance imaging (MRI) is a radiological technique that enables the visualization and study of the biophysical properties of the brain in-vivo. MRI is based on the use of strong magnetic fields, magnetic field gradients, and radio waves that can be measured via antennas, to generate images of the brain[38]. In dementia clinical practice, MRI is used to rule out the presence of morphological alterations that might justify or contribute to the symptomatology, such as vascular lesions or brain tumours. However, with advanced settings of the acquisition parameters, is it also viable to study more concrete biophysical properties. One of the most widely used is the T1-weighted MRI which has a high signal-to-noise ratio and maximizes tissue-class differentiation (gray matter vs white matter and vs CSF). It results into a spatial high-resolution snapshot of the brain, that helps to study its morphology (shape, size, and integrity). It is based on short echo time (interval between the magnetic pulse and acquisition of the radio-frequency signal) and short repetition time (interval between the different magnetic pulses). In research, T1w-MRI are processed using various software to obtain measurements that can eventually be used as biomarkers[39]. One of the most used software is Freesurfer, which

return a map of cortical thickness (i.e the normal distance between the white matter surface and the pial surface –the cortex height)[40]. Using cortical thickness, researchers have widely characterized the cortical thinning pattern commonly found in AD, that mainly affects the temporal and parieto-occipital regions[41]. These measurements have been validated against time-consuming postmortem neuropathological studies[42]. The use of MRI with other biomarkers enable multimodal studies that have identified associations such as that of cortical thinning and tau deposition as measured by PET[43]. Overall, these findings suggest that cortical thickness, obtained from T1w-MRI, might be a potential non-invasive biomarker of neurodegeneration associated with tau accumulation.

iii) Diffusion-Weighted Imaging MRI

Diffusion-weighted imaging (DWI) is another type of MRI sequence, developed to study the movement of water molecules in the brain. It is mainly used to infer the microstructural alterations of the tissue[44]. In 1905, Albert Einstein described that water molecules, in free-space, follow a random distribution of movement named Brownian movement[45]. However, water molecules in the brain are strongly constrained by the local cellular architecture, namely cell membranes, fibres and other macromolecules/proteins[44,46]. The cumulative effect of such constrains limits the displacement of the water molecules. Thus, properly modelled, DWI can inform about the microstructural changes of the different tissues in AD. The raw DWI data in research settings obtained with over 30 gradient directions is not directly interpretable: it provides high-dimensional information and is hard to inspect visually. Thus, there have been efforts to develop models over DWI data to interpret it more easily[47]. The most widely used, diffusion tensor imaging (DTI), is grounded in the idea of computing a tensor representation (i.e 3 directions) summarizing the information of all the gradients[46,48]. After the decomposition of the high-dimensional signal to the tensor, it is possible to compute several metrics that might help to study and interpret the displacement of water molecules. One of the most widely used metric driven from DTI is mean diffusivity[49], which average the magnitude of diffusion over the 3 tensor decompositions. Mean diffusivity can be interpreted as: how isotropic/spheric is the displacement of water? If we are assessing the microstrucure of the cerebrospinal fluid surrendering the cortex, we will observe high mean diffusivity due to the lack of physical barriers. Nevertheless, if we study the microstuructural architecture of brain tissue, such as the cortex, mean diffusivity will be reduced due to the presence of more physical barriers that constrains water displacement. This decrease is more prominent in the white matter, where the inherent directionality of the axons limit the water displacement. Importantly, in the presence of neurodegeneration where there is cell death and breakdown of biological barriers, water can move more freely which result into higher mean diffusivity compared to a healthy state[50].

Most literature in the AD field has focused on the study of white matter microstructure. Nevertheless, DWI can also be used to measure microstructural changes in the grey matter[51,52]. The cortex diffusivity is isotropic as there is not such a well-defined directionality of the intracortical bundles compared to the white matter. Thus, an isotropic metric derived from DTI such as mean diffusivity, is very well poised to evaluate microstructural alterations. Neurodegeneration will be reflected as increases in mean diffusivity due to the breakdown of biological physical barriers that restricts the movement of water molecules[50]. However, cortical diffusivity is only rarely studied in detail due to some methodological caveats, being the partial volume contamination from the CSF the most important one[53]. In this sense, our group recently developed a surface-based approach (DONSURF), combining several neuroimaging toolbox, to create a robust pipeline to compute cortical mean diffusivity (cMD) overcoming several major preprocessing caveats[54]. In previous work by our group, we demonstrated that cMD was robust against CSF partial volume contamination, and that it was able to track neurodegenerative-related changes in AD patients compared to healthy controls[54]. These results have been recently replicated by others[55,56]. We have also shown that cMD is a sensitive and robust biomarker of neurodegeneration in other diseases such as the behavioural variant of frontotemporal dementia (bvFTD)[57], multiple sclerosis[58], primary progressive aphasia (under review) or in amyotrophic lateral sclerosis (ALS)[59] patients. Importantly, in previous works, we showed that cMD was able to detect subtle microstructural alterations even in the absence of atrophy[57], suggesting it could be a more sensitive marker of neurodegeneration than atrophy.

iv) Magnetic ressonance spectroscopy

Magnetic resonance spectroscopy (MRS) is a nuclear magnetic technique designed to measure metabolites (or the neurochemical state) of the brain. MRS is based on the physical properties of the chemicals, which have different magnetic resonance frequencies. Thus, with a MRS acquisition, we can quantify several metabolites in the brain[60]. These metabolites have shown to change along the AD continuum and to inform of the pathophysiological process[61,62]. Even though several metabolites (including lipids) can be measured with MRS, two of the most studied metabolites in the AD field are N-Acetyl-aspartate (NAA)[61] and myo-inositol (mI)[62]. NAA is a general marker of neuron integrity and it has been shown to be reduced in AD participants compared to healthy controls[63]. mI is a sugar, synthesized mainly in astrocytes. It is considered to be a marker of neuroinflammation[64], and contrary to NAA, mI is increased in AD participants compared to healthy controls[63]. These metabolite alterations are region-specific and might differ depending on which region is assessed[63]. Nevertheless, despite its potential as a biomarker in AD, MRS is not routinely used due to its lower spatial resolution (it is usually acquired in a specific region of 8mm^3) and to the more complicated processing it requires compared to more conventional MRI techniques.

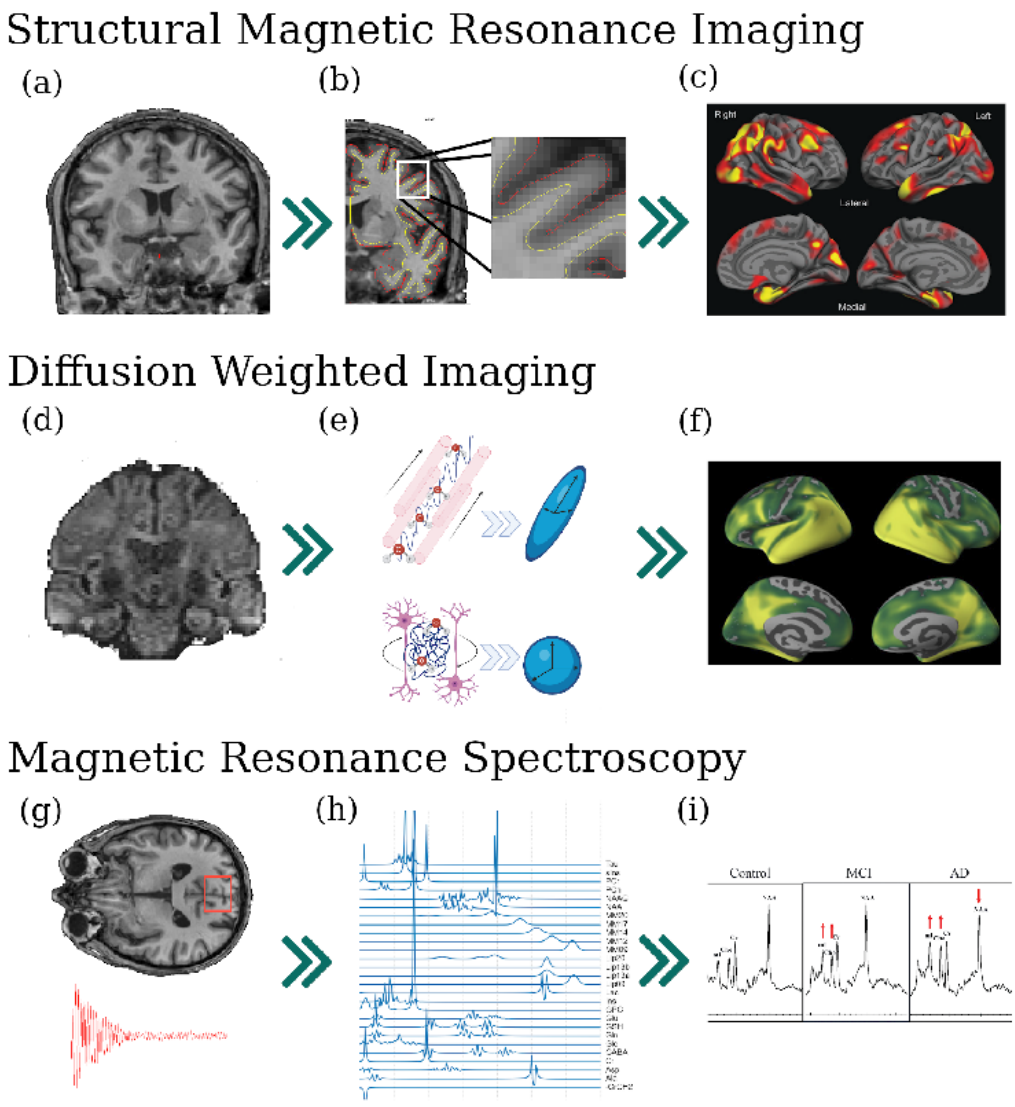

Figure 3. MRI-based imaging markers. a) raw T1w MRI; b) Cortical thickness segmentation; c) AD atrophy pattern; d) raw DWI; e) tensor decomposition (DTI); f) AD increased diffusivity pattern; g) MRS voxel localization and raw signal; h) metabolite fitting; i) AD pattern of metabolite changes.

1.3 Preclinical Alzheimer Disease

AD is characterized by a long preclinical phase of more than 20 years[65], in which pathological alterations occur in the absence of clinical symptoms. This preclinical phase was first identified in large post-mortem pathological studies[66]. With the development of in-vivo biomarkers, it has been consistently demonstrated in many observational studies, both in the general population[67] and in

autosomal dominant AD[68]. The NIA-AA criteria framework[17] classifies cognitively unimpaired participants into different groups based on their biomarker profile: participants with normal levels of amyloid and tau (A-T-), those with abnormal levels of amyloid but normal levels of tau (A+T-), and finally those with abnormal levels of both amyloid and tau (A+T+).

Our group has been particularly interested in the study of the changes in cortical thickness in preclinical AD. We have proposed a biphasic model of cortical structural alterations to reconcile apparently contradictory changes in this long phase of the disease. In early stages of this preclinical phase, in the presence of pathological amyloid levels, but normal tau (A+T-), we found increased cortical thickness[51,54,69], and a positive relationship between more amyloid pathology and thicker cortex[70]. However, those participants with pathological levels of amyloid and tau (A+T+) had more atrophy compared to age-matched participants with normal biomarkers. Our biphasic model is also congruent with longitudinal findings, where we reported that A+T- participants have lower rates of atrophy when compared to A-T-, whereas A+T+ have higher atrophy rates[71]. Importantly, we also found the aforementioned biphasic model when analysing cortical microstrutural alterations using cortical diffusivity: A+T- participants revealed a pattern of decreased diffusivity that evolved into significant increases of water diffusion in A+T+[51,54]. We hypothesized that these early alterations in A+T- are caused by an amyloid-related inflammation that causes neuronal hypertrophy and/or glia reactivity and recruitment, leading to the increase in cortical thickness and the decrease in cortical diffusivity. In our model, we posit that once tau also becomes abnormal, the synergistic toxic effect of amyloid and tau leads to neurodegeneration, as reflected in cortical atrophy and increased water diffusivity. Our group has extensively studied this relationship between inflammation and cortical alterations in the early stages of the disease. One example is a proof-of-concept study that targeted the amyloid-related neuroinflammation[72]. In this study we found that increased astrocyte reactivity (as measured by deprenyl PET) was directly associated to increased cortical thickness and decreased cortical diffusivity in a small sample of ADAD participants. However, there are several other biomarkers of inflammation that could be used to study the interplay between neuroinflammation and cortical alterations. A potential candidate that has not being explored before, is the quantification of metabolites related to neuroinflammation is myo-inositol (as measured by MRS).

1.4 Regional Vulnerability in Early Stages of the Disease

The pathological accumulation of amyloid and tau are not randomly distributed in the brain but rather follow a stereotypical spatial pattern that recapitulates the large-scale networks described in functional MRI. Consequently, it has been suggested that AD (and the rest of the neurodegenerative diseases) are network-afflicting diseases[73–78], in which the different neurodegenerative diseases target specific and

distinct brain networks. Similarly, neurodegeneration and atrophy have also shown to be localized in specific brain areas[41,77,79]. In this sense, in our neuroimaging studies in preclinical AD, we also identified that the regions showing increased cortical thickness and decreased cortical diffusivity overlap[54]. The study of the specific vulnerability of the different neurodegenerative diseases and AD in particular, is increasingly recognized as one of the major topics of research[80,81]. Investigating the factors that make these vulnerable brain regions unique is essential. The study of regional vulnerability might best be studied from different angles: from exploring the morphology of the most vulnerable cell types using in-vitro studies[82], to investigating the genetic fingerprint that might contribute to such vulnerabilities[83].

The study of cortical transcriptomic data has led to the discovery of novel pathways that might be affected (or more prone to be affected) in AD[83,84]. Nevertheless, the use of bulk RNA or single-nuclei RNA transcriptomic analyses have been focused on specific brain regions, thus neglecting the extent of the entire cortex, mainly due to its expensive cost. To overcome some of these limitations, in 2012, researchers from the Allen Institute made publicly-available the Allan Brain Atlas (ABA) dataset[85]. This dataset contains the expression of 10027 genes from 3,702 postmortem slices from 6 healthy volunteers across the cortex. This database has enabled the analysis of regional vulnerability in multiple cognitive disorders[86–88], and the study of the relationship between the expression of APP and MAPT and amyloid accumulation and neurodegeneration[89]. Unfortunately, most of the analyses using the ABA have neglected the large-scale and network nature of the stereotypical pattern of amyloid and tau accumulation, having focused only on local measurements of such proteins.

1.5 The complexity of the cortical alterations in the continuum of AD

During the last decade, the study of macrostructural and microstructural alterations in preclinical AD have witnessed an important increase in publications (from 22 studies in 2010 to 84 in 2020; Pubmed). Nevertheless, there are still some challenges that need to be addressed to better comprehend and characterize the cortical structural alterations in this early phase of the disease.

A major challenge preclinical AD research is the assessment of the trajectory of changes of biomarkers along the AD continuum. For decades, researchers have compared biomarkers between the different groups of the AD continuum (e.g participants with AD dementia compared to cognitively unimpaired or patients with mild cognitive impairment), and/or how the biomarkers (linearly) change with age or the (linear again) relationship between biomarkers (e.g assess the association between tau CSF values and cognitive performance). Nevertheless, recent studies increasingly highlight the limitations of these (simplistic) approaches or models, which in addition require strong a priori assumptions (i.e changes are linear)[54,90]. In this sense, a large and rapidly growing body of research is trying to overcome these limitations using new analytic models, such as non-linear models[90], LOESS or linear mixed effects

models[91]. In addition to these statistical approaches, researchers have also developed and applied novel (and more abstract) methods such as graph theory, to investigate non-trivial relationships. Graph theory is a field in mathematics that allows the abstraction of complex systems, and provides analytical tools to study such systems[92,93]. In short, graph theory is based in the study of graphs or networks, which are mathematical structures used to model pairwise relations between objects. A graph/network is composed of abstract entities (e.g biomarkers, participants, brain regions) named nodes, and the pairwise relationship between them (correlation, co-occurrence, etc) represented by links[93–95]. Graph theory in AD has been mainly used to study the relationship between the functional and/or structural connectome alterations AD-core biomarkers, or to study difference between diagnostic groups[96].

Our group have intensely work to overcome such modeling limitations. Although we have been able to show using diverse statistical approaches a biphasic model of cortical alterations, we were not able to determine the exact temporal moment in the disease continuum in which those alterations take place. A continuous approach, as opposed to stratifying subjects into diagnostic categories, using genetically determined AD, allows to temporarily position subjects along the disease continuum and the determination of the temporal points in which the dynamics of cortical structural alterations occur. The first study of this thesis aimed to tackle these issues using an international multicentre cohort of autosomal dominant AD.

Another challenge when evaluating our biphasic model is the measurement of neuroinflammation. Neuroinflammation is certainly complex, but different studies have used different approaches such as the measurement of different cytoquines or proteins in biofluids or through PET ligands, such as the aforementioned deprenyl[72]. However, no study has assessed the metabolites obtained from MRS data in relation with cortical thickness, which would have obvious advantages as its acquisition could easily be included in MRIs protocols. The second study of this thesis assessed these relationships in a cohort of adults with DS, another model of genetically determined AD.

Another hurdle in AD research is the validation of novel biomarkers. In this sense, our group have previously demonstrated that cortical diffusivity is a novel and promising biomarker that has been successful to track the biphasic model. Nevertheless, little is known about its relationship to pathological markers (i.e tau or amyloid PET) and its potential to serve as a prognostic marker of cognitive decline. The third study of this thesis assessed the relationship between cortical diffusivity and in-vivo measurements of tau-PET and evaluate its prognostic value.

Finally, the study of local vulnerability to accumulate amyloid and tau dates from several decades ago. Nevertheless, two questions remain unstudied. First, the study of this vulnerability across the whole cortical mantel (as opposed of a focus only in the entorhinal or hippocampus). There is a need to

develop an analytical framework that enables capturing a gradient of characteristics (e.g gene expression) that accompany the stereotypical pattern of protein accumulation and thus explain the temporality of the spread of the pathology. Second, the use of novel methodological frameworks (such as graph theory) to merge multi-domain and multiscale information in order to characterize the AD-related regional vulnerabilities. These questions were addressed in the fourth work of this PhD.

2. Hypothesis and Objectives

This thesis is based on the following hypothesis:

1. Cortical macrostructure and microstructure alterations start more than two decades before symptom onset in AD and follow a biphasic trajectory in parallel to the development of amyloid first and then tau biomarker alterations.

2. Early-disease neuroinflammation measured as measured by MRS is related to increased cortical thickness and core AD biomarkers in preclinical AD.

3. Cortical diffusivity is able to capture the microstructural alterations in preclinical AD related to the accumulation of tau in early Braak stages, and can be used as a prognostic marker of cognitive decline.

4. The stereotypical temporal and regional pattern of tau spreading is related to regional vulnerability as reflected in gradual gene expression alterations along the spreading topographical pattern.

The specific objectives of this thesis are:

1. To mathematically model the non-linear trajectory of cortical thickness and cortical diffusivity in autosomal dominant Alzheimer disease in relation to age and CSF AD biomarkers.

2. To measure the alterations of metabolite levels measured using MRS in the Alzheimer Disease continuum in adults with Down Syndrome, and its correlation to core AD biomarkers and brain structure.

3. To study the association between cortical diffusivity and medial temporal lobe tau-PET accumulation in preclinical Alzheimer disease, and how cortical diffusivity predicts future cognitive decline.

4. To determine the gradient of gene expression that fingerprints tau spreading, measured via tau-PET, using graph theory tools and high-spatial-resolution gene expression data.

3. Publications

Biphasic cortical macro- and microstructural changes in autosomal dominant Alzheimer's disease

Victor Montal[1,2;] Eduard Vilaplana[1,2;] Jordi Pegueroles[1,2]; Alex Bejanin[1,2]; Daniel Alcolea[1,2]; María Carmona-Iragui[1,2,3]; Jordi Clarimón[1,2]; Johannes Levin[4,5]; Carlos Cruchaga[7,8,9]; Neill R Graff-Radford[10]; James M Noble[11]; Jae-Hong Lee[12]; Ricardo Allegri[13]; Celeste M. Karch,[14]; Christoph Laske[15,16]; Peter Schofield[17,18]; Stephen Salloway[19]; Beau Ances[6,7,9,20]; Tammie Benzinger[9,20]; Eric McDale[6,9]; Randall Bateman[6,7,9]; Rafael Blesa[1,2]; Raquel Sánchez-Valle[21] ; Alberto Lleó[1,2], Juan Fortea[1,2,3] for the Dominantly Inherited Alzheimer Network (DIAN)

(1) Sant Pau Memory Unit, Department of Neurology, Hospital de la Santa Creu i Sant Pau, Biomedical Research Institute Sant Pau, Universitat Autònoma de Barcelona, Barcelona, Spain. (2) Center of Biomedical Investigation Network for Neurodegenerative Diseases (CIBERNED), Madrid, Spain (3) Barcelona Down Medical Center. Fundació Catalana de Síndrome de Down. Barcelona, Spain. (4) Department of Neurology, Ludwig-Maximilians-Universität München, Munich, Germany; (5) German Center for Neurodegenerative Diseases; Munich Cluster for Systems Neurology (SyNergy), Munich, Germany (6) Department of Neurology, Washington University School of Medicine, St Louis, MO, USA (7) The Hope Center for Neurological Disorders, St Louis, MO, USA (8) NeuroGenomics and Informatics, Washington University School of Medicine, St. Louis, MO, USA
(9) Knight Alzheimer's Disease Research Center, Washington University School of Medicine, St Louis, MO, USA
(10) Department of Neurology, Mayo Clinic, Jacksonville, FL, USA (11) Department of Neurology, Taub Institute for Research on Alzheimer's Disease and the Aging Brain, Columbia University Irving Medical Center, New York, NY, USA (12) Department of Neurology, University of Ulsan College of Medicine, Asan Medical Center, Seoul, Korea (13) Department of Cognitive Neurology, Institute for Neurological Research Fleni, BuenosAires, Argentina (14) Department of Psychiatry, Washington University School of Medicine, Saint Lous, MO, USA (15) German Center for Neurodegenerative Diseases (DZNE) Tübingen, Germany (16) Section for Dementia Research, Hertie Institute for Clinical Brain Research and Department of Psychiatry and Psychotherapy, University of Tübingen, Germany (17) Neuroscience Research Australia, Sydney, Australia. (18) School of Medical Sciences, University of New South Wales, Sydney, Australia. (19) Neurology and the Memory and AgingProgram, Butler Hospital, Providence, RI, USA_(20) Department of Radiology, Washington University in St. Louis, St. Louis, MO, Missouri, USA (21) Alzheimer's Disease and Other Cognitive Disorders Unit, Hospital Clínic, Fundació Clínic per a la Recerca Biomèdica, Institut d'Investigacions Biomèdiques August Pi i Sunyer (IDIBAPS), Universitat de Barcelona, Barcelona, Spain

Alzheimers Dement (2021) (4):618-628 doi: 10.1002/alz.12224

ABSTRACT

A biphasic model for brain structural changes in preclinical Alzheimer Disease could reconcile some conflicting and paradoxical findings in observational studies and anti-amyloid clinical trials. In this study we tested this model fitting linear vs quadratic trajectories and computed the timing of the inflection points vertexwise of cortical thickness and cortical diffusivity–a novel marker of cortical microstructure–changes in 389 participants from the Dominantly Inherited Alzheimer's Network. In early preclinical AD, between 20 to 15 years before estimated symptom onset, we found increases in cortical thickness and decreases in cortical diffusivity followed by, cortical thinning and cortical diffusivity increases in later preclinical and symptomatic stages. The inflection points 16 to 19 years before estimated symptom onset are in agreement with the start of tau biomarker alterations. These findings confirm a biphasic trajectory for brain structural changes and have direct implications when interpreting MRI measures in preventive AD clinical trials.

BACKGROUND

Alzheimer disease has a long preclinical phase in which multiple pathophysiological alterations coexist. Individuals who carry mutations in the Presenilin-1, Presenilin-2 or amyloid precursor protein genes are destined to develop symptomatic Alzheimer´s disease. Although autosomal dominant Alzheimer disease (ADAD) is an etiologically distinct form of Alzheimer disease (AD), it shares pathological features, and a similar clinical presentation, to sporadic Alzheimer´s disease.[1,2] The Dominantly Inherited Alzheimer Network (DIAN) Observational Study evaluates mutation carriers with standardized clinical and cognitive testing, brain imaging, and biochemical biomarkers with the goal of determining the sequence of changes in pre-symptomatic carriers. It is thus a unique population in which to study the timing of events in Alzheimer´s disease pathophysiology.[3–5]

We have recently proposed a biphasic model of cortical changes in the preclinical stage of sporadic AD based on cross-sectional[6-8] and longitudinal data.[9] In this model, early pathological cortical thickening in Alzheimer´s disease vulnerable regions is found in subjects with pathological CSF amyloid levels and normal CSF tau levels. This phase, which might be due to early neuroinflammatory changes,[10] is followed by atrophy once CSF tau also becomes abnormal.[7–9,11,12] Several cross-sectional studies have analyzed the brain structural changes in ADAD showing different cortical changes at different preclinical stages. Cortical thinning occurs in the precuneus, and temporal lateral regions seven to three years prior to symptom onset.[3] However, in young presymptomatic mutation carriers increased cortical thickness[10,13–16] and increased volumes in subcortical regions[13,17,18] have been described in small cohorts of ADAD.

Diffusion tensor imaging enables the study of the brain microstructure. Most diffusion weighted imaging studies in AD have focused on the white matter. However, it can also be used to study the cortical microstructure.[13,19] Cortical mean diffusivity has been proposed as a new biomarker in neurodegenerative diseases that could be more sensitive than cortical thickness to detect cortical changes, especially on symptomatic phases of the disease.[8,13,19–21] Importantly, cortical mean diffusivity also follows a biphasic trajectory in sporadic AD, with early decreases associated with cortical thickening and increases in later preclinical phases.[8] Interestingly, previous small cohort studies of ADAD reported cortical mean diffusivity

decreases in early presymptomatic ADAD[10,13,17] and later increases in symptomatic mutation carriers.[13,17]

Therefore, a biphasic trajectory of cortical changes might reconcile the aforementioned changes in ADAD (and sporadic Alzheimer´s disease). However, this biphasic model is based on the comparison between the different stages of preclinical Alzheimer´s disease,[8,9] or on observations in small ADAD studies.[10,13,17] It has not been mathematically tested. ADAD offers the opportunity to compare different mathematical models (ie. linear vs quadratic) to detect the inflection points at which these changes occur.

Using the largest sample of ADAD, the multicenter DIAN cohort, we aimed to confirm and test this biphasic model of cortical changes in preclinical AD. Specifically, (i) we explored the trajectories of cortical thickness and cortical mean diffusivity comparing mutation carriers and non-carriers in relation to estimated years to symptoms onset, (ii) compared the fit of a biphasic (or quadratic) model as opposed to the linear one and computed the inflection point for cortical changes, and (iii) assess the influence of CSF pTau in the relationship between cortical alterations and estimated years to symptoms onset. A better characterization of the trajectory of MRI structural changes in ADAD and the confirmation and characterization of this biphasic model in ADAD would inform the use of MRI outcome in current anti-amyloid preventive trials and future anti-inflammatory trials.

METHODS

Participants

Individuals from families with mutations in the presenilin-1, presenilin-2 and amyloid precursor protein genes were recruited from 14 sites participating in the DIAN observational study. We included all participants who had genetic, clinical data and an available quality checked MRI from the 12th data-freeze. The period of recruitment was January 2009 to December 2017. Estimated years to expected symptoms onset was computed as the difference between the participant's current age and the mutation-specific expected age of clinical symptoms onset.[3,22]. All participants provided written informed consent. Local ethical approval was obtained at each participating DIAN site.

Structural and diffusion MRI

MRI acquisition parameters were based on the ADNI protocol. Briefly, all subjects underwent a 3 Tesla T1-weighted scan at resolution of 1.1 x 1.1 x 1.2 mm voxels. Scans with artifacts were excluded. Images were processed with Freesurfer 5.3 and normalized to a standard space and smoothed using a Gaussian kernel of 15mm for statistical analysis as commonly done in cortical thickness analyses. A final number of 389 subjects with correctly preprocessed T1w images were included. Diffusion weighted images were available for a subset of the participants (N=300) with one b=0 and 64 directions at b=1000 with an isotropic voxel size of 2.5mm. We excluded 11 subjects due to image artifacts. We computed cortical mean diffusivity using a surface-based in-house pipeline as previously reported.[8] Briefly, we computed a rigid-body registration between the b=0 and the 64 b=1000 volumes to correct for motion effects. After removing non-brain tissue, a tensor model was fitted using FSL's dtifit command, and we computed the mean diffusivity metric. We then coregistered the b=0 scan to the segmented T1w image. Eight additional subjects were excluded due to incorrect registration. We then sampled the mean diffusivity volume for each participant at the midpoint cortical ribbon and projected it to each individual surface, previously

constructed by Freesurfer, in order to generate individual cortical mean diffusivity maps. Finally, cortical diffusivity maps were normalized a standard surface template (fsaverage) and smoothed using a 15mm kernel. A total number of 281 participants were finally included in the cortical mean diffusivity analyses.

Biochemical quantifications of pTau

A subset of 327 individuals also underwent a lumbar puncture. CSF sample collection and measurement in the DIAN cohort has been previously described[23]. Briefly, CSF pTau181 (further referred as pTau) was measured by immunoassay using Luminex bead-based multi-plexed xMAP technology (INNO-BIA AlzBio3, Innogenetics).

Statistical analysis

Demographics were compared using the non-parametric test Man-Whitney U test and the Fisher´s exact test as implemented in the R statistical software.

We designed three independent, but interrelated analyses to specifically assess the biphasic model in ADAD, using EYO as a proxy of disease staging. We first performed an exploratory analysis to compare cortical thickness and cortical mean diffusivity between mutation carriers and non-carriers in 5-year intervals with respect estimated symptom onset (ranges from -25 to +5) computing the vertex-wise Cohen's d effect size maps in order to explore group differences. We then used a 2-class general linear model to identify regions with statistically significant differences, including sex and education as nuisance factors. To avoid false positives, we corrected the results with a cluster-sized based MonteCarlo simulation with 10,000 repeats as implemented in Freesurfer (familywise error [FWE], $p < 0.05$).

Second, we compared different mathematical models (ie. linear vs quadratic). We initially assessed the linear relationship between both neuroimaging metrics and age in non-carriers, finding a significant association in non-carriers (Suppl Fig 1). Therefore, in order to mitigate this age-related effect and model the changes in mutation carriers, we first normalized each mutation carrier individual map using a W-score approach.[24,25] We finally compared the linear model and, the linear model with the addition of a quadratic term of estimated years to symptoms' onset to the model at each surface vertex:

$$\text{Wscore-NI} \sim \text{EYO}^2 + \text{EYO}$$

We applied the Akaike information criterion (AIC) to assess the improvement in the model with the inclusion of the quadratic term. Importantly, the AIC penalizes model complexity to avoid the risk of overfitting the data. Afterwards, we assessed the statistical significance of the quadratic model in those regions were the addition of the quadratic term improved the fitting. In addition, we computed interaction analyses to assess if the quadratic relationship of the imaging biomarkers with EYO were significantly stronger in the mutation carriers compared to the non carriers, using the following model at each vertex:

$$\text{NI} \sim \text{EYO}^2 * \text{MutationStatus} + \text{EYO} + \text{Sex}$$

Only those regions that survived multiple comparisons based on cluster-extension Monte Carlo simulations are shown (FWE, $p < 0.05$). Then, to assess the inflection point for the cortical changes we fitted a second-order polynomial equation (i.e a parabola) and computed the first derivative of the polynomial in a vertex-wise basis. Of note, we only report the inflection points in those regions

where the addition of the quadratic term improved the fitting of our data. The second-order polynomial fitting and the AIC metric were computed using the python packages numpy[26] and statsmodels[27], respectively.

Finally, we compared if the relationship between both imaging markers and EYO differed depending on the CSF pTau positivity status in asymptomatic mutation carriers. We computed a threshold of pTau positivity based on a ROC analyses comparing asymptomatic vs symptomatic mutation carriers, using the Youden's algorithm. This threshold was used to categorize mutation carrier individuals into positive or negative pTau individuals. Then, we used a vertex-wise interaction model defined as:

$$\text{Wscore-NI} \sim \text{EYO}*\text{pTauStatus}$$

Only regions that survived multiple comparisons based on cluster-extension Monte Carlo simulations are shown (FWE, $p < 0.05$).

RESULTS

Participants

Table 1 summarizes the demographics and clinical data of all participants. There were no statistical differences in age, sex distribution, estimated years to symptoms onset or mutation type frequency between the mutation carriers and the non-carriers. As expected, we found significant differences in global CDR scores and CSF pTau measurements ($p < 0.001$).

Cortical macro and microstructural changes with respect estimated years to symptom onset

We first compared the cortical thickness and cortical mean diffusivity between carriers and non-carriers in 5-year age intervals (Figure 1 and Suppl Fig 2). The youngest mutation carriers (25 to 20 years before symptom onset) showed significant cortical thinning in middle temporal regions and increased diffusivity on the insula, with non-significant middle-to-high effect size differences in the precuneus and in the anterior cingulate and medial prefrontal cortex. Between 20 to 15 years before estimated symptom onset there was a shift, and mutation carriers showed significant increased cortical thickness in the occipital fusiform and insula and non-significant middle-to-high effect size in the precuneus, lateral temporal cortex, whereas mutation carriers showed significant reduced diffusivity on the left insula and frontal-parietal cortices and non-significant middle-to-high effect size differences posterior cingulate and lateral temporal regions. In the decade before symptom onset, mutation carriers showed significant cortical thinning in temporoparietal and occipital areas and increased cortical mean diffusivity in the precuneus and lateral and medial occipitotemporoparietal regions that further extended after the onset of clinical symptoms.

Cortical thickness and cortical diffusivity change following a quadratic model in preclinical AD

We then compared a quadratic vs a linear modeling for the normalized cortical changes (W-scores) in the mutation carriers individuals. Specifically, we first calculated if the addition of a quadratic term of EYO to the linear model at each surface vertex W-scores improved data fitting (Suppl Fig 3). Fig 2 (left panels) show the regions where the quadratic term of estimated years to onset for both neuroimaging metrics were significant after correcting for overfitting using the AIC criteria and correcting for multiple comparisons. The normalized cortical thickness

(Fig 2 top row) showed a significant quadratic relationship in regions of the temporal cortex, temporoparietal junction, and parts of the precuneus and parieto-occipital regions. The normalized cortical mean diffusivity revealed a more widespread pattern of regions with significant quadratic relationships, especially in the lateral and medial temporal cortex, the precuneus, and temporoparietal regions. Of note, the results are qualitatively the same when restricting the analyzing the PSEN1 carriers alone and when analyzing the PSEN2 and APP mutation carriers combined (results not shown).

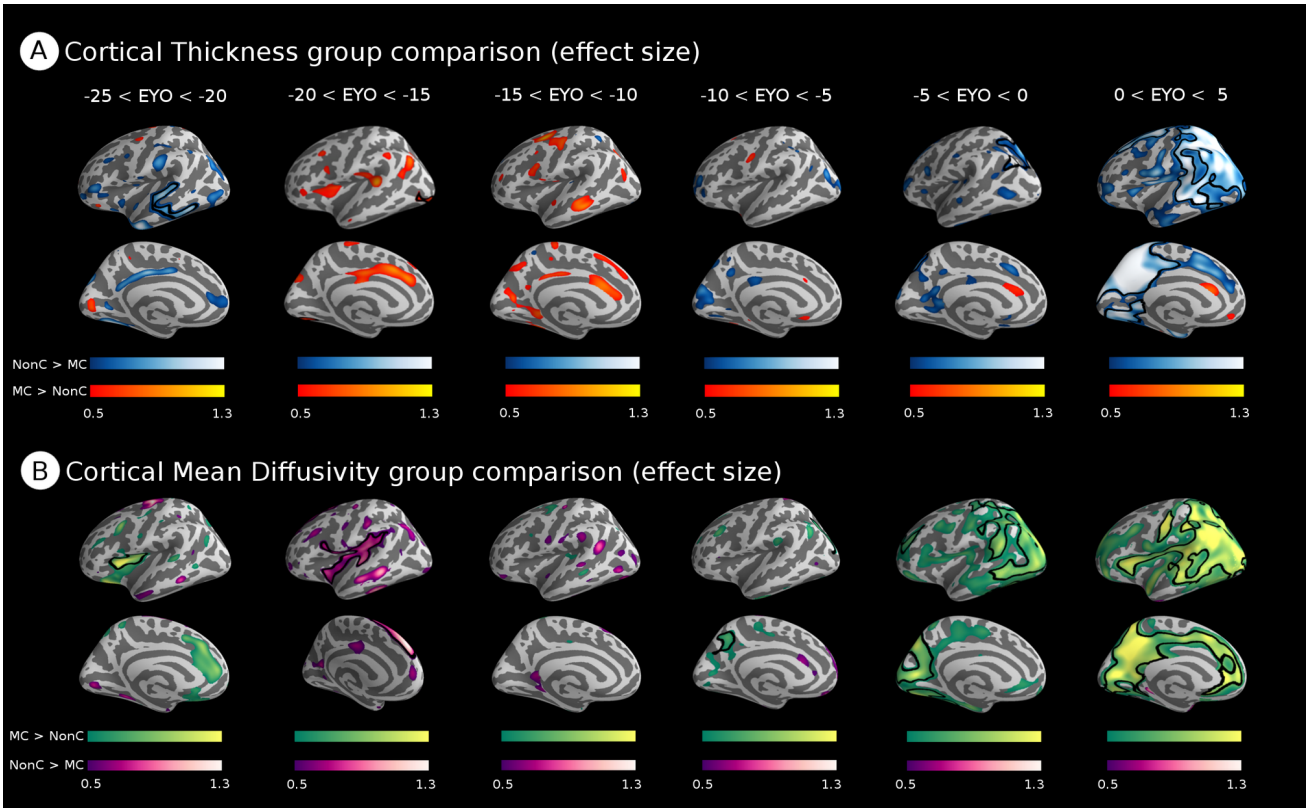

Figure 1. Group comparisons in cortical thickness and cortical mean diffusivity between carriers and non-carriers in 5-year age intervals. We show the Cohen's d effect sizes to show trajectory of changes. Of note, only mid to high effect sizes are shown. Furthermore, statistically significant group differences clusters are outlined in black. For display purpose, only results in the left hemisphere are shown but the right hemisphere revealed similar changes. A) Cortical thickness effect size differences between the mutation carriers (MC) and the non-carriers (NonC) for different subsets of estimated years to onset. Blue is associated to less cortical thickness in the mutation carriers, whereas orange-yellow reflects higher cortical thickness in comparison to the non-carriers. B) Cortical mean diffusivity differences between mutation carriers and non-carriers for different subsets of estimated years to onset. Green is associated with increases of cortical mean diffusivity in the mutation carrier group, whereas purple reflects decreases in cortical mean diffusivity in comparison to the non-carriers. EYO = estimated years to onset; NonC = Non-carriers; MC = Mutation Carriers.

Structural MRI markers inflection points are coincident with biochemical neurodegenerative biomarkers

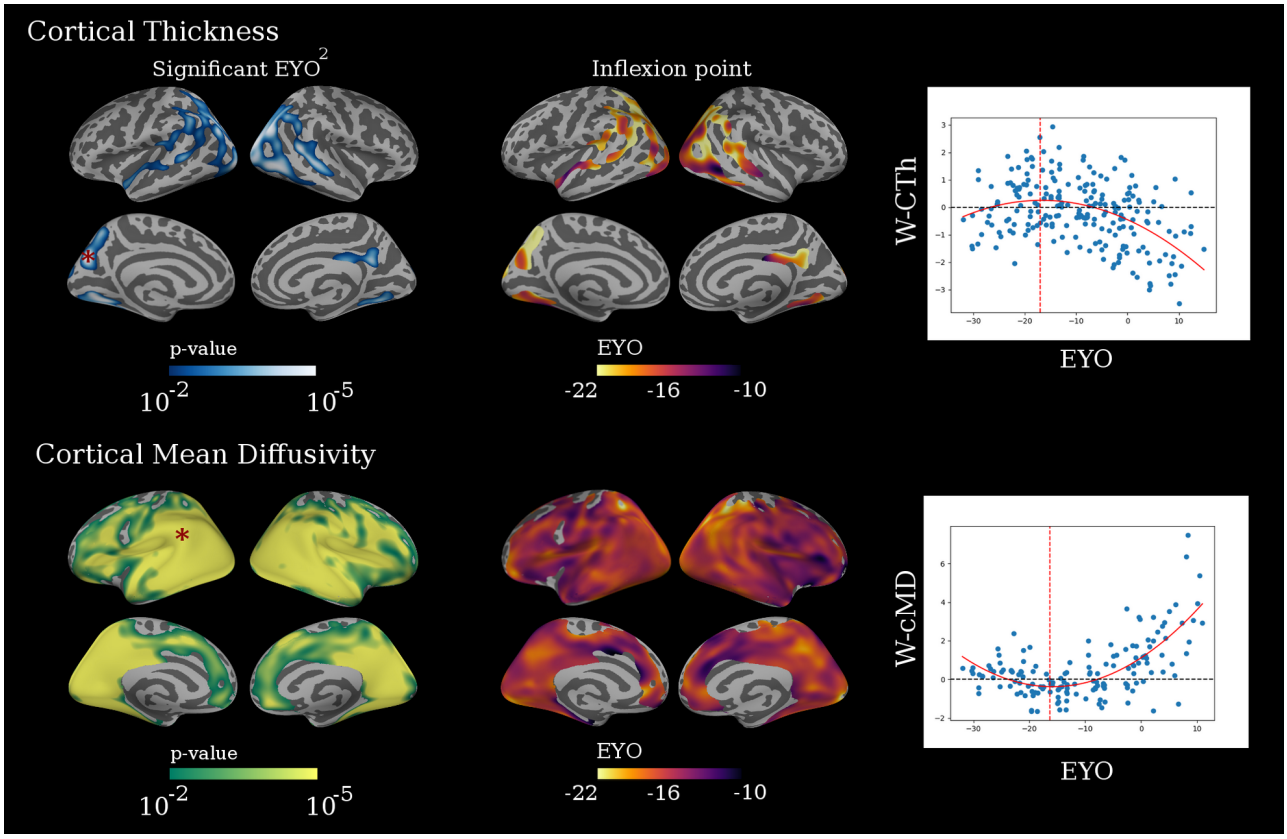

Figure 2. Brain regions showing a significant quadratic association with estimated years to symptom onset in mutation carriers. Left panel shows the significant clusters for the association between the normalized cortical thickness (W-CTh; top row) and the normalized cortical mean diffusivity (W-MD; lower row) and the squared of estimated years of onset in mutation carriers participants. The middle panels show the inflection points for the W-CTh and W-MD (ie. the EYO at which W-CTh change from increasing to decreasing (top row) and where the W-MD change from decreasing to increasing (lower row). The right panels show the scatter plots for the fitting of the second order polynomial in the most significant vertex of the cortical mantle (marked as *) for both W-CTh (top row) and W-cMD (lower row).

We then calculated the inflection points for both the normalized cortical thickness and the normalized cortical mean diffusivity after fitting a second-order polynomial in the regions where the quadratic term was significant. To this aim, we computed the first derivative of the polynomial in a vertex-wise basis. Our data show that for cortical thickness, the trajectory changed around -18.8 years of onset and for cortical mean diffusivity around -16.25 years of onset. Of note, similar results were found when excluding the individuals with EYO>0 (Suppl. Fig 5).

The association between both cortical thickness and cortical mean diffusivity and estimated years to symptom onset depends on CSF pTau status

We dichotomized mutation carriers into pTau positive (pTau+) or negative (pTau-) using a threshold of 52.8

pg/ml, in order to run interaction analyses of the relationship between imaging markers and EYO by pTau status. Figure 3 shows the brain areas where/in which these interactions were significant. Specifically, we found a cluster of significant interaction for cortical thickness in parieto-occipital regions of the left hemisphere (Figure 3 top-row left panel) that was driven by increases of cortical thickness related to EYO in the pTau- and atrophy in the pTau+ (Figure 3 top-row right panel).

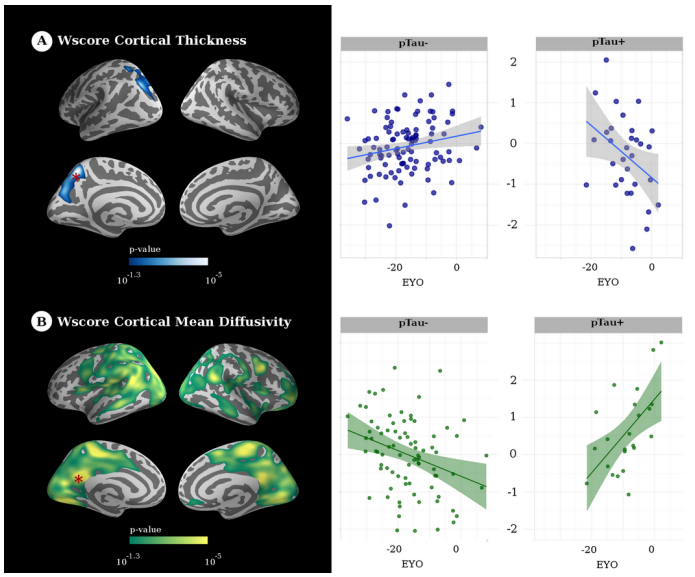

Figure 3. Interaction analyses between estimated years to symptom onset and CSF pTau positivity status on cortical thickness and cortical mean diffusivity. Left panel: Brain regions with a significant interaction for both cortical thickness (top row) and cortical mean diffusivity (bottom row). Right panel: scatter plots for the interaction analyses in cortical thickness (upper right panel) and cortical mean diffusivity (lower right panel) in the most significant vertex for each interaction analysis (marked as red *)

For cortical mean diffusivity, we found a more widespread pattern of significant interactions, encompassing parieto-occipito-temporal areas bilaterally, and frontal regions for the right hemisphere (Figure 3 lower-row left panel). These interactions were driven by decreases of cortical diffusivity in relationship to EYO in the pTau- subgroup and diffusion increases in the pTau+ subgroup (Figure 3 top-row right panel).

A biphasic model of structural changes along the Alzheimer's Disease continuum

We finally integrate the proposed biphasic model for cortical macro and microstructural changes in relation with the reported pathophysiological biomarker changes in ADAD using the AT(N) framework[28] (Figure 4). Importantly, we did not categorize our individuals based on their biomarkers profiles, but contextualized the hypothetical biphasic model of alterations with previous findings in ADAD. Mutation carriers with EYO at the A-T- range present cortical thinning and increased cortical mean diffusivity. The onset of amyloid biomarker changes varies across ADAD studies, but between 25 to 20 years before estimated symptom onset, the rates of change in CSF Aβ42 values and amyloid uptake values start to occur.[29,30] This is 10 to 5 years before the earliest increases in CSF pTau levels have been reported.[31] Mutation carriers with EYO in the A+T- phase showed the first signs of increased cortical thickness and decreased cortical mean diffusivity changes in mutation carriers. The reported onset for CSF pTau increases is close to our calculated inflection points for the trajectory of changes in both neuroimaging metrics. Thereafter, when comparing mutation carriers and non–carriers with EYO in the A+T_{CSF}+ phase, we did not see differences until the earliest reported alterations in tau PET, which occur 6 years before the symptoms onset[32]. When comparing individuals with EYO in this A+TPET+ phase we found a widespread pattern of cortical thinning and increased cortical mean diffusivity. It is important to note that this biphasic trajectory does not occur in all the

regions of the brain, but in specific regions. Furthermore, the temporality might vary in different areas of the cortex.

Table 1. Demographics from DIAN sample

	Non-Carriers	Mutation Carriers
N (% DTI)	166 (74.7)	223 (70.4)
Asymptomatic (%)	N/A	68.1
Age (median, IQR)	36.74 [30.15 – 46.46]	36.48 [30.31 – 46.52]
Female (%)	57.2	54.7
Family Mutation *PSEN1/PSEN2/APP* (%)	65 / 12 / 23	72 / 9 / 17
EYO (median, IQR)	-10.41 [-19.1 - -2.5]	-9.13 [-18.56 - -1.31]
CDR (median, IQR)	0·0 [0 - 0]	0 [0 – 0.5]
CSF pTau pg/ml (median, IQR)	26.76 [21.9 – 34.22]	44.48 [31.1 – 83.5]

DISCUSSION

This study confirms that cortical thickness and cortical mean diffusivity follow a biphasic trajectory in ADAD. This model reconciles the apparently conflicting initial observations in small cohort studies. This biphasic trajectory should be considered when analyzing the MRI endpoints in preventive Alzheimer´s disease clinical trials.

This study confirms initial observations from small ADAD cohorts, which had already reported cortical thickening and decreased cortical mean diffusivity in early preclinical AD in a small independent samples of presenilin-1 mutation carriers in Spain,[13–15] Colombia,[16] and Sweden.[10] Similarly, we and others have also reported increases of volume in subcortical structures.[13,17,18] Cortical mean diffusivity has also been assessed in a subset of the aforementioned studies. In agreement with our results, early decreases in cortical mean diffusivity were found in association with increased cortical thickness.[13] The present study not only confirms this early phase of cortical thickening, but importantly, it also shows, for the first time, that these changes are not neurodevelopmental, but pathological. Indeed, the youngest mutation carriers in the present study showed cortical thinning and increased cortical mean diffusivity. Cortical thickening and decreased mean diffusivity only emerged 20 to 15 years before estimated symptom onset. Atrophy, on the other hand, has been consistently reported in later preclinical (and symptomatic) ADAD. In this sense previous cross-sectional studies in DIAN and in other independent cohorts demonstrated cortical thinning in the precuneus ~7 to 4 years before symptom onset, a timing which is in agreement with our results.[3,33–36] Of note, although the main analyses show an overlapping pattern of changes for MD and CTh and between regions with the early increased cortical thickness and decreased cortical mean diffusivity and the later decreased cortical thickness and increased cortical mean diffusivity, some differences between modalities and regions should be further explored. We have previously shown that MD might have superior sensitivity than CTh[20], especially in frontal and insular regions. Furthermore, not all regions follow or are at the same pathophysiological stage in a given time-point[9], and some of the changes at early stages of the disease (co-occuring with presumably amyloid related inflammation as shown in a proof-of-concept deprenyl study in ADAD[10]) might not overlap completely with the later tau-related atrophy.

This paper provides the first mathematical modeling for a biphasic trajectory of changes in ADAD. The addition of a quadratic term significantly improved the linear model in several Alzheimer´s disease vulnerable regions.[8,37] This analysis enabled us to calculate the inflection points for both the normalized cortical thickness and normalized

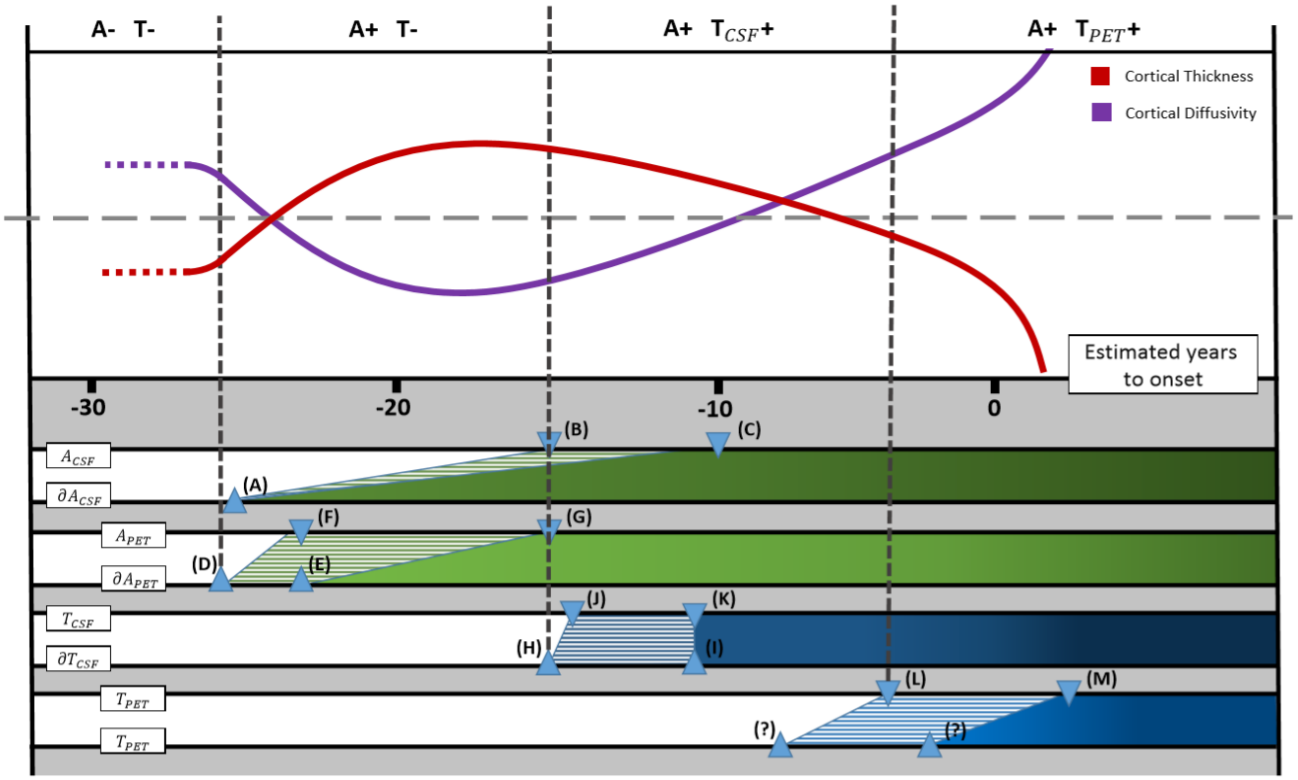

Figure 4. Hypothetical model of cortical thickness and cortical diffusivity changes in the presymptomatic phase of autosomal dominant Alzheimer´s disease. Top: Summary of MRI findings reported in the present study for cortical thickness (red) and cortical diffusivity (purple) Bottom: Previously reported time-points of pathophysiological biomarker changes. The ordering of the biomarkers correspond to: CSF amyloid levels, cross-sectional and rate of change (ACSF and δACSF, respectively); amyloid PET, cross-sectional and rate of change (APET and δAPET, respectively); CSF pTau levels, crossectional and rate of change (TCSF and δTCSF, respectively); and Tau PET, crossectional and rate of change (TPET and δTPET, respectively; the later hypothetical*). The letters refer to the different studies which report the estimated years to symptom onset at which these changes occur: (A) McDade et al 2018, (B) Bateman et al 2012, (C) McDade et al 2018, (D) McDade et al 2018, (E) Gordon et al 2018, (F) McDade et al 2018, (G) Bateman et al 2012, (H) Llibre-Guerra et al 2019, (I) Llibre-Guerra et al 2019, (J) Bateman et al 2012, (K) McDade et al 2018, (L) Quiroz et al 2018 and (M) Gordon et al 2019. *As there are no published longitudinal studies using Tau PET in autosomal dominant Alzheimer´s disease, (?) refers to unknown event time-point of Tau PET longitudinal changes. Shaded color-lines reflect uncertainty of biomarker positivity due to discrepancies in the literature.

cortical mean diffusivity, which occurred 16 to 19 years before the expected symptom onset. This type of analyses can only be performed in ADAD, in which years to symptom onset can be reliably estimated. However, these analyses also require a large cohort of mutation carriers, which were not available in the aforementioned studies in the small independent ADAD cohorts. This biphasic trajectory of changes substantially expands the possibilities of MRI to detect the changes in preclinical Alzheimer´s disease, if properly modeled. Indeed, it shows dynamic changes in the two

decades prior to symptom onset as opposed to the aforementioned capability to detect atrophy in the last decade before symptom onset.

The interaction analyses showed clear differences when comparing the trajectories between CSF pTau+ and pTau- subgroups. In early preclinical Alzheimer´s disease, in individuals with low CSF pTau values, cortical thickness increased and mean diffusivity decreased in mutation carriers, whereas in later stages, in those individuals with high CSF pTau values, there was cortical thinning and increases in cortical mean diffusivity. Interestingly, a previous longitudinal study in the DIAN cohort showed accelerated rates of atrophy up to 13 years before symptom onset in the precuneus,[30] earlier than the aforementioned cross-sectional studies. We speculate that longitudinal atrophy begins after CSF pTau levels start to increase, theoretically around 15 years before symptom onset (or earlier) in the DIAN cohort.[1,31] In this sense, we had previously shown that increased longitudinal atrophy rates can co-occur with increased cross-sectional cortical thickness.[14]

We finally integrate the cortical macro and microstructural changes in relation to the reported pathophysiological biomarker changes in ADAD. The timing of the cortical changes is strikingly congruent with those of amyloid and tau. The increase in cortical thickness and the decrease in cortical diffusivity coincided with the start of fibrillar amyloid accumulation,[15,30] around 20 years before symptom onset. However, 16 years before symptom onset, most regions had reached an inflection point, in agreement with the aforementioned reported increases in atrophy rates,[14,30] and the beginning of the increases in CSF pTau levels.[1,29,31] These results support the hypothesis previously reported by our group and others[8,9,38] that amyloid and tau have a toxic synergistic effect that might drive the inflexion point in cortical changes, leading to cortical atrophy and increases in cortical mean diffusivity. Finally, we found widespread cortical thinning and increased cortical mean diffusivity in subjects close to symptoms onset (EYO -5). Interestingly, this is the age-range at which the earliest increases in the uptake of tau PET have been reported.[32,39] Further work is needed in order to test the A/T/N framework in ADAD. This biphasic trajectory of changes is not unique to ADAD; our group and others have already shown early pathological cortical thickening and decreased cortical mean diffusivity in Alzheimer´s disease vulnerable regions in cognitively unpaired subjects from the general population with pathological CSF Aβ42 levels and normal CSF tau levels.[8,40,41] Cortical thinning, and increases in mean diffusivity, only occurred in the presence of both abnormal amyloid and tau biomarkers.[6–9] The atrophy and increased mean diffusivity found in the youngest mutation carriers might reflect neurodevelopmental abnormalities. In this sense, in animal models using Tg2576 mice, decreased spine density and reduced levels of synaptophysin, in addition to behavioral changes have been described months prior to amyloid plaque deposition[42]. Similarly, in humans, Quiroz et al[43] reported cognitive vulnerabilities in verbal comprehension, processing speed and interpersonal relations tests, decades before the symptom onset. However, further studies with larger sample sizes in this age-range and earlier time-points are needed to confirm this neurodebelopmental hypothesis. The rationale for cortical diffusivity decreases and cortical thickness increases early in AD has been previously reviewed.10 In short, these changes could be related to amyloid-related inflammatory processes. Several studies have shown early astrocytic activation prior to neurodegeneration in animal models (see[44] for a review) and even prior to amyloid plaque accumulation in humans.[45] A local relationship has been demonstrated

between astrocytosis measured using deprenyl PET and increases of cortical thickness and decreases of diffusivity in a Swedish ADAD cohort.[10]

Our results have important implications for the design of clinical trials with anti-amyloid therapies such as the Colombian (NCT01998841) and DIAN-TU (NCT01760005) cohorts. MRI measures are commonly used as endpoints, but under the assumption of a linear trajectory of changes. A biphasic trajectory in the design and interpretation of such trials outcomes should be considered. Our model might help understand the paradoxical findings in anti-amyloid trials (e.g. AN1792, solanezumab or bapineuzumab) where the active arm showed increased atrophy rates with respect to placebo (i.e a drug that effectively decreased amyloid related inflammation could lead to the counterintuitive effect of increasing atrophy, as it has been repeatedly shown in anti-amyloid trials). Our model also has immediate implications for secondary prevention trials in sporadic AD such as the A3 study (1R01AG054029-01), the A4 study (NCT02008357), ADAPT (NCT00007189) or TOMORROW (NCT01931566) trials as well as in future trials with anti-inflammatory drugs. Finally, this study confirms the sensitivity of cortical mean diffusivity to track the cortical microstructural changes in Alzheimer´s disease.

The main strength of this study are the inclusion of the largest cohort of ADAD and the mathematical modeling of the biphasic trajectory using two complementary imaging measures. Our methodology to measure cortical mean diffusivity is another strength as it overcomes limitations previously reported when using voxel-based approaches, such as partial volume contamination and kernel-sensitive CSF inclusion during data smoothing.[46] Interestingly, cortical mean diffusivity captured the biphasic trajectory of changes in more widespread regions than cortical thickness. However, future studies should compare the sensitivity of cortical thickness and cortical mean diffusivity in the continuum of AD (both sporadic and ADAD), as it has been demonstrated in bvFTD[20]. This study also has several limitations. First, this study relies on the concept of estimated years to onset; however, several external factors might affect clinical presentation. Second, despite the use of a previously validated surface-based in-house pipeline developed to minimize CSF contamination, the cortical diffusivity might still be contaminated by partial volume effect related to the DWI low resolution. Finally, only a longitudinal study with long follow-ups periods with individual amyloid, tau, metabolic (PET-FDG) and inflammatory biomarkers will determine with accuracy the trajectory of changes at the individual level and the interplay between them. These analyses might become soon possible with the advent of plasma amyloid, tau and neurodegenerative biomarkers.

In summary, we showed that cortical changes in the preclinical ADAD follow a biphasic trajectory with early cortical thickening and decreases in cortical mean diffusivity followed by atrophy and increases cortical mean diffusivity around 16 years before symptom onset, an age when CSF Tau levels start to increase. This biphasic trajectory might be crucial when interpreting MRI measures in current and future preventive trials in Alzheimer´s disease.

ACKNOWLEDGMENTS

We acknowledge the altruism of the participants and their families and contributions of the DIAN research and support staff at each of the participating sites for their contributions to this study. Data collection and sharing for this project was supported by The Dominantly Inherited Alzheimer’s Network (DIAN, UF1AG032438) funded by

the National Institute on Aging (NIA), the German Center for Neurodegenerative Diseases (DZNE), Raul Carrea Institute for Neurological Research (FLENI), Partial support by the Research and Development Grants for Dementia from Japan Agency for Medical Research and Development, AMED, and the Korea Health Technology R&D Project through the Korea Health Industry Development Institute (KHIDI).This manuscript has been reviewed by DIAN Study investigators for scientific content and consistency of data interpretation with previous DIAN Study publications. In addition, this project was founded by the Fondo de Investigaciones Sanitario (FIS), Instituto de Salud Carlos III (PI14/01126 and PI17/01019 to JF, PI13/01532 and PI16/01825 to RB, PI18/00335 to MCI, PI18/00435 to DA, PI14/1561 and PI17/01896 to A.L) and the CIBERNED program (Program 1, Alzheimer Disease to Alberto Lleó and SIGNAL study, www.signalstudy.es), partly jointly funded by Fondo Europeo de Desarrollo Regional, Unión Europea, Una manera de hacer Europa. This work was also supported by the National Institutes of Health (NIA grants 1R01AG056850 - 01A1; R21AG056974 and R01AG061566 to JF), Departament de Salut de la Generalitat de Catalunya, Pla Estratègic de Recerca i Innovació en Salut (SLT002/16/00408 to A.L), Fundació La Marató de TV3 (20141210 to JF, 044412 to RB); V. Montal is supported by Fondo de Investigaciones Sanitario (FI18/00275). This work was also supported by Generalitat de Catalunya (SLT006/17/00119 to JF, SLT006/17/95 to EV and SLT006/17/00125 to DA) and a grant from the Fundació Bancaria La Caixa to RB.

REFERENCES

1. Bateman RJ, Xiong C, Benzinger TLS, et al. Clinical and Biomarker Changes in Dominantly Inherited Alzheimer's Disease. N Engl J Med. 2012;367(9):795-804. doi:10.1056/NEJMoa1202753

2. Tang M, Ryman DC, McDade E, et al. Neurological manifestations of autosomal dominant familial Alzheimer's disease: a comparison of the published literature with the Dominantly Inherited Alzheimer Network observational study (DIAN-OBS). Lancet Neurol. 2016;15(13):1317-1325. doi:10.1016/S1474-4422(16)30229-0

3. Benzinger TLS, Blazey T, Jack CR, et al. Regional variability of imaging biomarkers in autosomal dominant Alzheimer's disease. Proc Natl Acad Sci U S A. 2013;110(47):E4502-9. doi:10.1073/pnas.1317918110

4. Reiman EM, Quiroz YT, Fleisher AS, et al. Brain abnormalities in young adults at genetic risk for autosomal dominant AD. Lancet Neurol. 2012;11(12):1048-1056. doi:10.1016/S1474-4422(12)70228-4.BRAIN

5. Ridha BH, Barnes J, Bartlett JW, et al. Tracking atrophy progression in familial Alzheimer's disease: a serial MRI study. Lancet Neurol. 2006;5(10):828-834. doi:10.1016/S1474-4422(06)70550-6

6. Fortea J, Sala-Llonch R, Bartrés-Faz D, et al. Cognitively Preserved Subjects with Transitional Cerebrospinal Fluid ß-Amyloid 1-42 Values Have Thicker Cortex in Alzheimer Disease Vulnerable Areas. Biol Psychiatry. 2011;70(2):183-190.

7. Fortea J, Vilaplana E, Alcolea D, et al. Cerebrospinal Fluid ß-Amyloid and Phospho-Tau Biomarker Interactions Affecting Brain Structure in Preclinical Alzheimer Disease. Ann Neurol. 2014;76(2):223-230. doi:10.1002/ana.24186

8. Montal V, Vilaplana E, Alcolea D, et al. Cortical microstructural changes along the Alzheimer's disease continuum. Alzheimer's Dement. 2017;(October):1-12. doi:10.1016/j.jalz.2017.09.013

9. Pegueroles J, Vilaplana E, Montal V, et al. Longitudinal brain structural changes in preclinical Alzheimer disease. Alzheimer's Dement. 2016;9(September):1-11. doi:10.1016/j.jalz.2016.08.010

10. Vilaplana E, Rodriguez-vieitez E, Ferreira D, et al. Cortical microstructural correlates of astrocytosis in autosomal- dominant Alzheimer ' s disease. Neurology. 2020;94:1:11.

11. Desikan RS, McEvoy LK, Thompson WK, et al. Amyloid-β associated volume loss occurs only in the presence of phospho-tau. Ann Neurol. 2011;70(4):657-661. doi:10.1002/ana.22509

12. Pascoal TA, Mathotaarachchi S, Mohades S, et al. Amyloid-β and hyperphosphorylated tau synergy drives metabolic decline in preclinical Alzheimer's disease. Mol Psychiatry. 2016;(October 2015):1-6. doi:10.1038/mp.2016.37

13. Fortea J, Sala-Llonch R, Bartrés-Faz D, et al. Increased cortical thickness and caudate volume precede atrophy in psen1 mutation carriers. J Alzheimer's Dis. 2010;22(3):909-922. doi:10.3233/JAD-2010-100678

14. Sala-Llonch R, Lladó A, Fortea J, et al. Evolving brain structural changes in PSEN1 mutation carriers. Neurobiol Aging. 2015;36(3):1261-1270. doi:10.1016/j.neurobiolaging.2014.12.022

15. Sala-Llonch R, Falgàs N, Bosch B, et al. Regional patterns of 18F-florbetaben uptake in presenilin 1 mutation carriers. Neurobiol Aging. 2019;81:1-8. doi:10.1016/j.neurobiolaging.2019.04.010

16. Quiroz YT, Schultz AP, Chen K, et al. Brain Imaging and Blood Biomarker Abnormalities in Children With Autosomal Dominant Alzheimer Disease. JAMA Neurol. 2015;02114:1-8. doi:10.1001/jamaneurol.2015.1099

17. Ryan NS, Keihaninejad S, Shakespeare TJ, et al. Magnetic resonance imaging evidence for presymptomatic change in thalamus and caudate in familial Alzheimer's disease. Brain. 2013;136(Pt 5):1399-1414. doi:10.1093/brain/awt065

18. Quan M, Zhao T, Tang Y, et al. Effects of gene mutation and disease progression on representative neural circuits in familial Alzheimer's disease. Alzheimers Res Ther. 2020;12(1):14. doi:10.1186/s13195-019-0572-2

19. Weston PSJ, Simpson IJA, Ryan NS, Ourselin S, Fox NC. Diffusion imaging changes in grey matter in Alzheimer ' s disease : a potential marker of early neurodegeneration. Alzheimers Res Ther. 2015;7(47):1-8. doi:10.1186/s13195-015-0132-3

20. Illán-Gala I, Montal V, Borrego-Écija S, et al. Cortical microstructure in the behavioural variant of frontotemporal dementia: looking beyond atrophy. Brain. 2019;142(4):1121-1133. doi:10.1093/brain/awz031

21. Vogt NM, Hunt JF, Adluru N, et al. Cortical Microstructural Alterations in Mild Cognitive Impairment and Alzheimer's Disease Dementia. Cereb Cortex. December 2019:bhz286. doi:10.1093/cercor/bhz286

22. Ryman DC, Acosta-Baena N, Aisen PS, et al. Symptom onset in autosomal dominant Alzheimer disease: A systematic review and meta-analysis. Neurology. 2014;83(3):253-260. doi:10.1212/WNL.0000000000000596

23. Fagan AM, Xiong C, Jasielec MS, et al. Longitudinal Change in CSF Biomarkers in Autosomal-Dominant Alzheimer ' s Disease. 2014;6(226). doi:10.1126/scitranslmed.3007901

24. La Joie R, Perrotin A, Barre L, et al. Region-Specific Hierarchy between Atrophy, Hypometabolism, and -Amyloid (A) Load in Alzheimer's Disease Dementia. J Neurosci. 2012;32(46):16265-16273. doi:10.1523/JNEUROSCI.2170-12.2012

25. Bejanin A, La Joie R, Landeau B, et al. Distinct Interplay Between Atrophy and Hypometabolism in Alzheimer's Versus Semantic Dementia. Cereb Cortex. 2018;(May):1-11. doi:10.1093/cercor/bhy069

26. van der Walt S, Colbert SC, Varoquaux G. The NumPy Array: A Structure for Efficient Numerical Computation. Comput Sci Eng. 2011;13(2):22-30. doi:10.1109/MCSE.2011.37

27. Seabold S, Perktold J. statsmodels: Econometric and statistical modeling with python. In: 9th Python in Science Conference. ; 2010.

28. Jack CR, Bennett DA, Blennow K, et al. NIA-AA Research Framework: Toward a biological definition of Alzheimer's disease. Alzheimer's Dement. 2018;14(4):535-562. doi:10.1016/j.jalz.2018.02.018

29. McDade E, Wang G, Gordon BA, et al. Longitudinal cognitive and biomarker changes in dominantly inherited Alzheimer disease. Neurology. 2018:10.1212/WNL.0000000000006277. doi:10.1212/WNL.0000000000006277

30. Gordon BA, Blazey TM, Su Y, et al. Spatial patterns of neuroimaging biomarker change in individuals from families with autosomal dominant Alzheimer's disease: a longitudinal study. Lancet Neurol. 2018;17(3):211-212. doi:10.1016/S1474-4422(18)30028-0

31. Llibre-Guerra JJ, Li Y, Schindler SE, et al. Association of Longitudinal Changes in Cerebrospinal Fluid Total Tau and Phosphorylated Tau 181 and Brain Atrophy With Disease Progression in Patients With Alzheimer Disease. JAMA Netw open. 2019;2(12):e1917126. doi:10.1001/jamanetworkopen.2019.17126

32. Quiroz YT, Sperling RA, Norton DJ, et al. Association between amyloid and tau accumulation in young adults with autosomal dominant Alzheimer disease. JAMA Neurol. 2018;75(5):548-556. doi:10.1001/jamaneurol.2017.4907

33. Weston PSJ, Nicholas JM, Lehmann M, et al. Presymptomatic cortical thinning in familial Alzheimer disease: A longitudinal MRI study. Neurology. 2016;87(19):2050-2057. doi:10.1212/WNL.0000000000003322

34. Wang G, Coble D, McDade EM, et al. Staging biomarkers in preclinical autosomal dominant Alzheimer's disease by estimated years to symptom onset. Alzheimer's Dement. 2019;1:1-9. doi:10.1016/j.jalz.2018.12.008

35. Kinnunen KM, Cash DM, Poole T, et al. Presymptomatic atrophy in autosomal dominant Alzheimer's disease: A serial magnetic resonance imaging study. Alzheimer's Dement. 2018;14(1):43-53. doi:10.1016/j.jalz.2017.06.2268

36. Knight WD, Kim LG, Douiri A, Frost C, Rossor MN, Fox NC. Acceleration of cortical thinning in familial Alzheimer's disease. Neurobiol Aging. 2011;32(10):1765-1773. doi:10.1016/j.neurobiolaging.2009.11.013

37. Dickerson BC, Bakkour A, Salat DH, et al. The cortical signature of Alzheimer's disease: regionally specific cortical thinning relates to symptom severity in very mild to mild AD dementia and is detectable in asymptomatic amyloid-positive individuals. Cereb Cortex. 2009;19(3):497-510. doi:10.1093/cercor/bhn113

38. Pascoal TA, Mathotaarachchi S, Shin M, et al. Amyloid and tau signatures of brain metabolic decline in preclinical Alzheimer's disease. Eur J Nucl Med Mol Imaging. 2018:259-18. doi:10.1007/s00259-018-3933-3

39. Gordon BA, Blazey TM, Christensen J, et al. Tau PET in autosomal dominant Alzheimer's disease: relationship with cognition, dementia and other biomarkers. Brain. 2019. doi:10.1093/brain/awz019

40. Johnson SC, Christian BT, Okonkwo OC, et al. Amyloid burden and neural function in people at risk for Alzheimer's Disease. Neurobiol Aging. 2014;35(3):576-584. doi:10.1016/j.neurobiolaging.2013.09.028

41. Chételat G, Villemagne VL, Pike KE, et al. Larger temporal volume in elderly with high versus low beta-amyloid deposition. Brain. 2010;133(11):3349-3358. doi:10.1093/brain/awq187

42. Jacobsen SJ, Redwine JM, Morrison JH, et al. Early-onset behavioral and synaptic deficits in a mouse model of Alzheimer's disease. Proc Natl Acad Sci. 2006;103(13):5161-5166. doi:10.1073/pnas.0600948103

43. Quiroz YT, Pulsifer M, Chen K, et al. Cognitive Vulnerabilities in Presenilin-1 E280a Mutation-Carrying Children From the World'S Largest Autosomal-Dominant Alzheimer'S Disease Kindred. Alzheimer's Dement. 2017;13(7):P225-P226. doi:10.1016/j.jalz.2017.07.108

44. Drummond E, Wisniewski T. Alzheimer's disease: experimental models and reality. Acta Neuropathol. 2017;133(2):155-175. doi:10.1007/s00401-016-1662-x

45. Rodriguez-Vieitez E, Saint-Aubert L, Carter SF, et al. Diverging longitudinal changes in astrocytosis and amyloid PET in autosomal dominant Alzheimer's disease. Brain. 2016:awv404. doi:10.1093/brain/awv404

46. Coalson TS, Van Essen DC, Glasser MF. The impact of traditional neuroimaging methods on the spatial localization of cortical areas. Proc Natl Acad Sci. 2018;115(27):E6356-E6365. doi:10.1073/pnas.1801582115

SUPPLEMENTARY MATERIAL

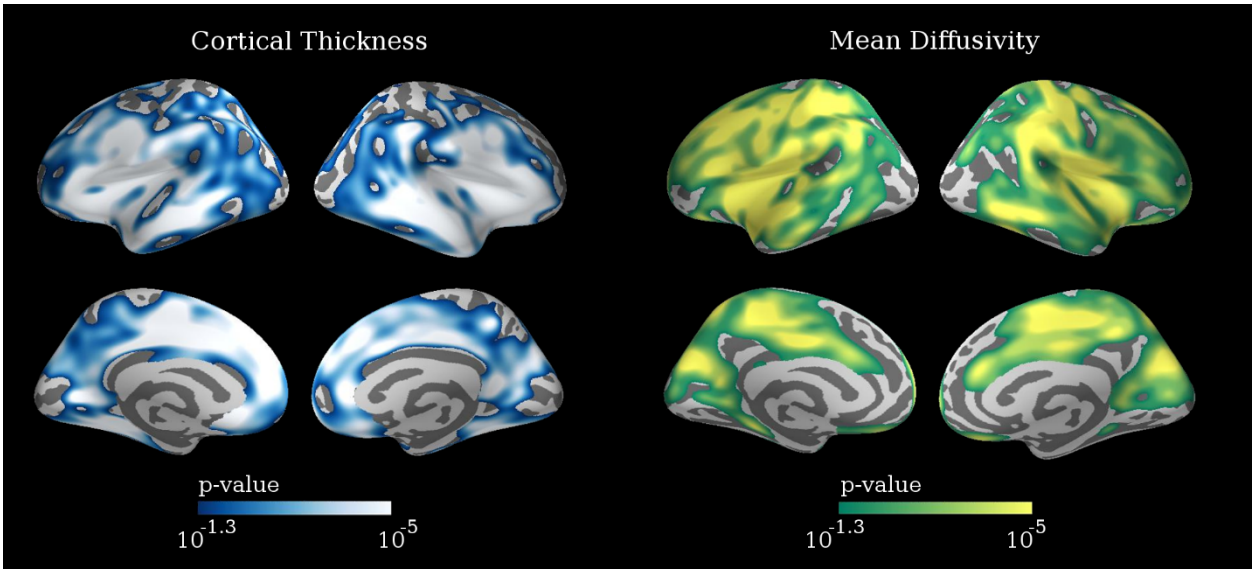

Supplementary Figure 1. Correlation between age and cortical thickness and cortical mean diffusivity in non-carriers. Both cortical thickness (left) and cortical mean diffusivity (right) showed a widespread pattern of significant correlation with age. Blue-white colors reflect negative association of age with cortical thickness, whereas green-yellow colors reflect increases of cortical mean diffusivity related to age.

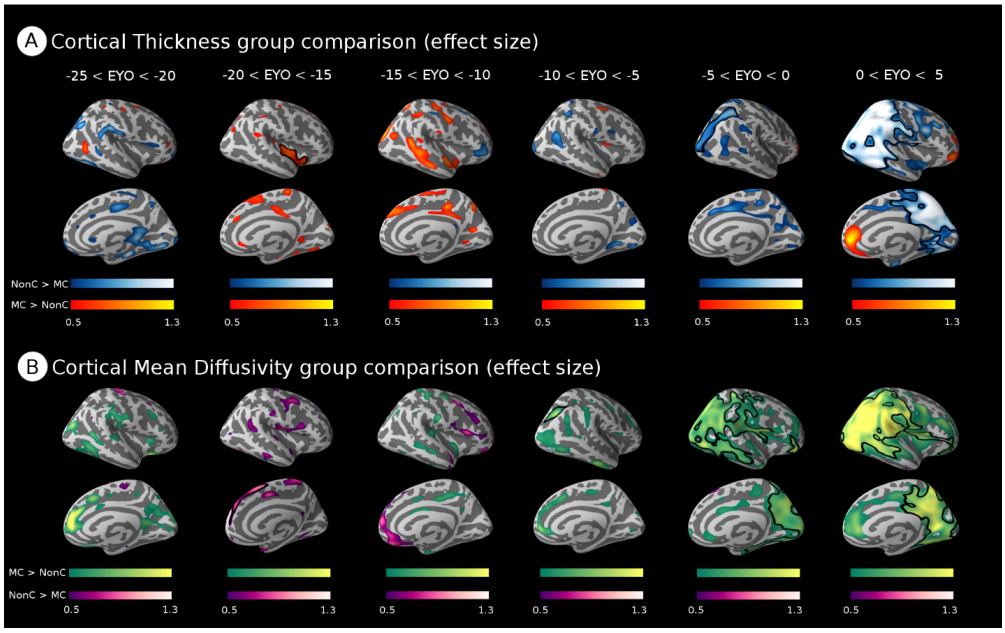

Supplementary Figure 2. Right hemisphere group comparisons in cortical thickness and cortical mean diffusivity between carriers and non-carriers in 5-year age intervals.

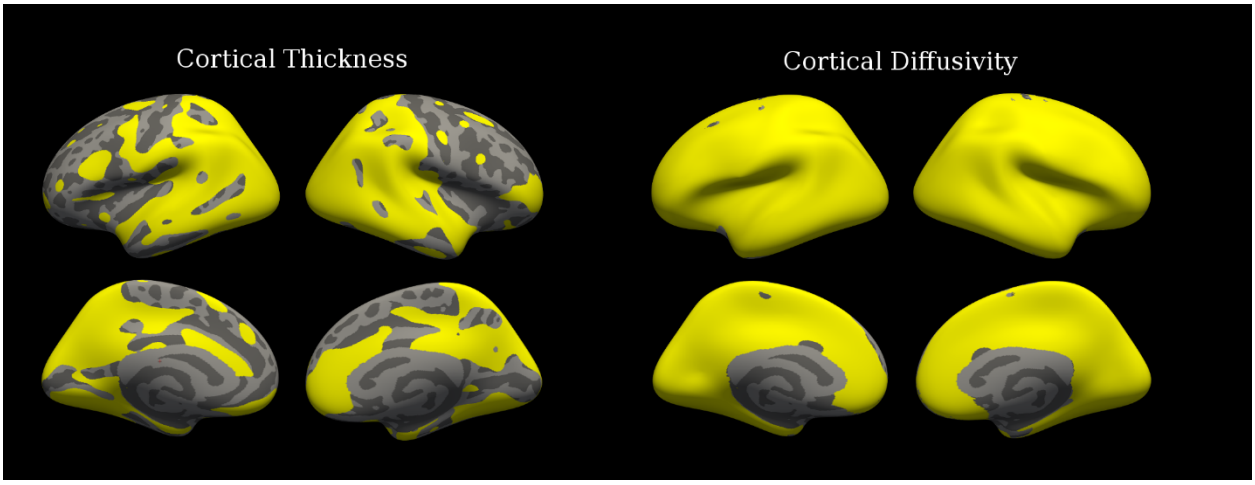

Supplementary Figure 3. Regions where the inclusion of the quadratic term improved the fitting of our data. Regions (in yellow) where the inclusion of the quadratic term of estimated years to symptoms onset improved the modeling of the cortical thickness (left) and cortical diffusivity (right) data in relation to EYO using the AIC criterion. Figure shows a binarized map of the regions were AIC was lower for the model including the quadratic model. No quantitative measure of the AIC difference is shown, since it is not interpretable.

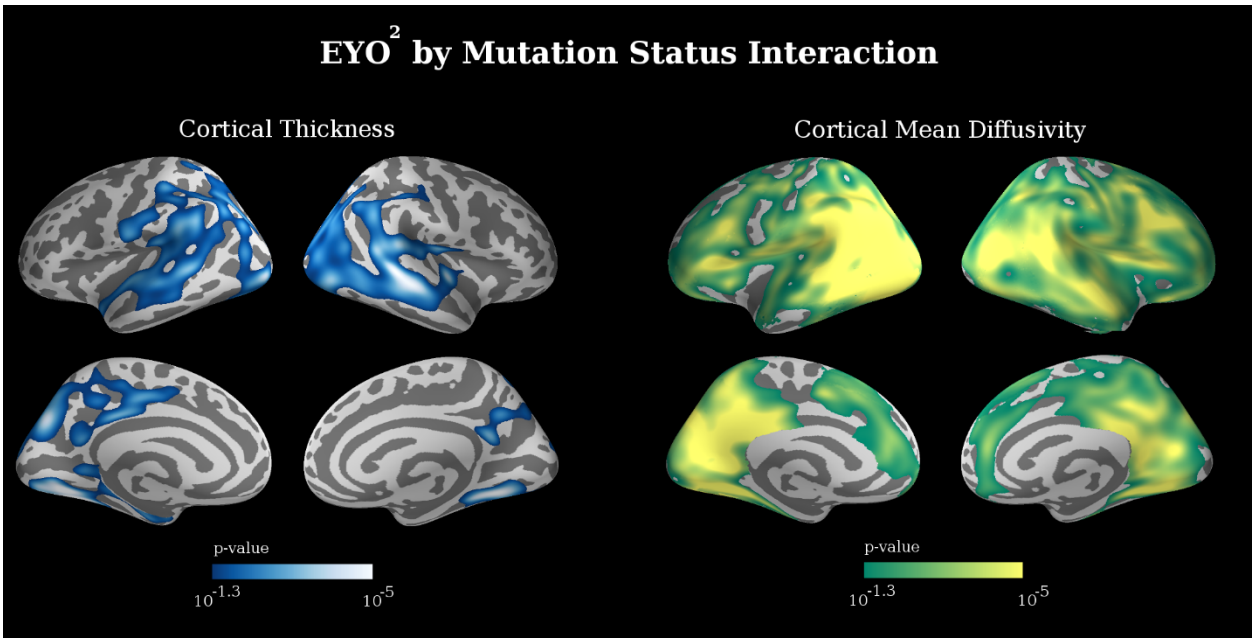

Supplementary Figure 4. Interaction analyses of the relationship between cortical thickness (left) and cortical mean diffusivity (right) with EYO², depending on mutation status. Colored vertex represents those brain regions were data in mutation carriers follow a statistically significant stronger quadratic relationship compared to non carriers

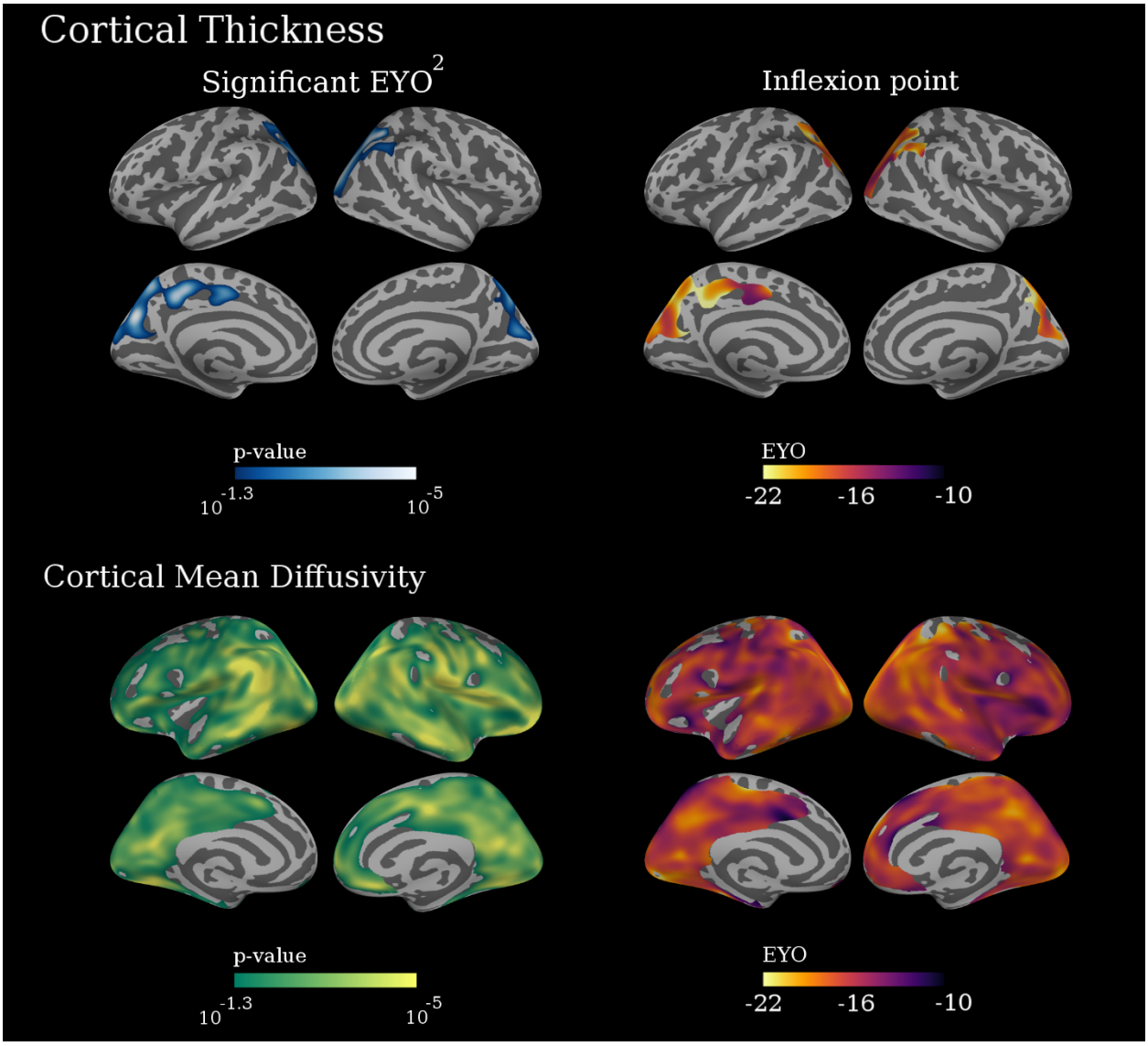

Supplementary Figure 5. Biphasic model of neuroimaging markers in preclinical ADAD mutation carriers alone. The left panels show the clusters where the association between W-CTh (top row) and W-cMD (lower row) and EYO^2 were significant and survived multiple comparisons. The right panels show the EYO for the inflection points vertexwise for W-CTh (upper right panel) and W-cMD (lower right panel).

Metabolite Signature of Alzheimer's Disease in Adults with Down Syndrome

Victor Montal[1,2]; Isabel Barroeta[1,2]; Alexandre Bejanin[1,2]; Jordi Pegueroles[1,2]; María Carmona-Iragui[1,2,3]; Miren Altuna[1,3]; Bessy Benejam[3]; Laura Videla[1,3]; Susana Fernández[3]; Concepcion Padilla[1]; Mateus Aranha[1]; Florencia Iulita[1,2]; Didac Vidal-Piñeiro[4]; Daniel Alcolea[1,2]; Rafael Blesa[1,2]; Alberto Lleó[1,2]; Juan Fortea[1,2,3]; Down Alzheimer Barcelona Neuroimaging Initiative

(1) Sant Pau Memory Unit, Department of Neurology, Hospital de la Santa Creu i Sant Pau, Biomedical Research Institute Sant Pau, Universitat Autònoma de Barcelona, Barcelona, Spain. (2) Center of Biomedical Investigation Network for Neurodegenerative Diseases (CIBERNED), Madrid, Spain. (3) Barcelona Down Medical Center. Fundació Catalana Síndrome de Down, Barcelona, Spain. (4) Centre for Lifespan Changes in Brain and Cognition, Department of Psychology, University of Oslo, Oslo 0317,Norway

Annals of Neurology (2021) (3):407-416. doi: 10.1002/ana.26178

ABSTRACT

To examine the Alzheimer's Disease metabolite signature through magnetic resonance spectroscopy in adults with Down syndrome and its relation with Alzheimer's Disease biomarkers and cortical thickness.

We included 118 adults with Down syndrome from the Down Alzheimer Barcelona Imaging Initiative and 71 euploid healthy controls from the Sant Pau Initiative on Neurodegeneration cohort. We measured the levels of myo-inositol (a marker of neuroinflammation) and N-acetyl-aspartate (a marker of neuronal integrity) in the precuneus using magnetic resonance spectroscopy. We investigated the changes with age and along the disease continuum (asymptomatic, prodromal Alzheimer's Disease, and Alzheimer's Disease dementia stages). We assessed the relationship between these metabolites and Aβ42/Aβ40 ratio, phosphorylated tau-181, NfL, and YKL-40 Cerebrospinal fluid levels as well as amyloid positron emission tomography uptake using Spearman correlations controlling for multiple comparisons. Finally, we computed the relationship between cortical thickness and metabolite levels using Freesurfer.

Asymptomatic adults with Down syndrome had a 27.5% increase in the levels of myo-inositol, but equal levels of N-acetyl-aspartate compared to euploid healthy controls. With disease progression, myo-inositol levels increased while N-acetyl-aspartate levels decreased in symptomatic stages of the disease. Myo-inositol was associated with amyloid, tau, and neurodegeneration markers, mainly at symptomatic stages of the disease, whereas N-acetyl-aspartate was related to neurodegeneration biomarkers in symptomatic stages. Both metabolites were significantly associated with cortical thinning, mainly in symptomatic participants.

Magnetic resonance spectroscopy detects Alzheimer's disease related inflammation and neurodegeneration, and could be a good noninvasive disease-stage biomarker in Down syndrome.

INTRODUCTION

The lifetime risk of symptomatic Alzheimer´s disease (AD) in adults with Down syndrome (DS) is over 90%.[1] This ultra-high risk is mainly caused by the extra copy of the amyloid precursor protein gene, coded on chromosome 21. DS is consequently conceptualized as a genetically determined form of AD.[2] The clinical and biomarker changes of AD in adults with DS are strikingly similar to those described in autosomal dominant AD (ADAD).[3] DS thus offers, likewise ADAD, a unique opportunity to determine the sequence of changes from preclinical AD to symptomatic stages.[3]

The study of regional metabolite levels using proton magnetic resonance spectroscopy (MRS) has shown potential to track brain alterations in vivo along the AD continuum in sporadic AD.[4,5] There is a strong convergence of findings reporting increases in myo-inositol (mI), a marker of astrocytosis neuroinflammation, and decreases in N-acetylaspartate (tNAA), a neuronal marker, with disease progression in various brain areas.[4–8] This metabolic signature correlates to both in vivo imaging measures of amyloid[5,6,9] and to postmortem AD pathology.[10]

The few MRS studies in people with DS, have identified a similar pattern of changes in MRS metabolites, with increases of mI and decreases of tNAA. These changes might arise from AD-related pathological alterations, but in the case of mI, could also result from the presence of the mI transporter gene in the chromosome 21.[11,12] However, the temporality of MRS changes with age and their relationship with core-AD biomarkers and brain atrophy is still unknown. Taking advantage of the Down Alzheimer Neuroimaging Initiative (DABNI), a large cohort of adults with DS with

available MRI, MRS, PET and cerebrospinal fluid (CSF) biomarkers, we aimed to determine the metabolite levels changes i) with age and ii) along the diagnostic groups of the AD continuum, and assess the relationship between metabolite alterations and iii) core-AD CSF biomarkers and iv) cortical thickness.

METHODS

Participants

This is a single-center cross-sectional study. We recruited 118 adults with DS aged 18 or older from the population-based Down Alzheimer Barcelona Neuroimaging Initiative (DABNI) cohort.[3] We also included a convenience sample of 71 cognitively normal euploid subjects (controls) from the Sant Pau Initiative of Neurodegeneration SPIN cohort.[13] The study was approved by the Sant Pau Research Ethics Committee, following the standards for medical research in humans recommended by the Declaration of Helsinki. All participants or their legally authorized representatives gave written informed consent.

Adults with DS were clinically evaluated to assess their clinical and cognitive status, including the administration of a semi-structured health questionnaire (Cambridge Examination for Mental Disorders of Older People with Down Syndrome, CAMDEX-DS)[14] and a neuropsychological battery including the Cambridge Cognitive Examination for Older Adults with Down's syndrome (CAMCOG-DS) Spanish version.[14] As in previous studies,[15,16] participants were classified during a consensus meeting between the neurologist and neuropsychologist into the following clinical groups: asymptomatic (aDS), when there was no clinical suspicion of AD-related cognitive decline, prodromal AD (pDS), when there was evidence of cognitive decline due to AD, but no significant impact on baseline activities of daily living (ADL), and AD dementia (dDS) when the cognitive decline impacted ADL. This classification was blinded to biomarker data. Eleven individuals were excluded for having medical or psychiatric conditions.

1H-MRS acquisition and analysis

MRS was performed on a 3T Philips Achieva magnet scanner, using the point-resolved spectroscopy single-voxel (PRESS) sequence, with an echo time of 2000 ms and repetition time of 35 ms, flip angle of 90º, and 1024 points. The metabolite data profile was acquired in a 2x2x1.1 mm voxel placed in a region of interest (ROI) located in the posterior cingulate cortex (PCC) and the precuneus. This region was selected due to its reported sensitivity to detect metabolite differences in sporadic AD.[17] We processed MRS data using Spectroscopy Analysis Tools (SPANT) v1.4.0 (https://martin3141.github.io/spant/index.html), an open-source R toolbox which relies on iteratively adapted baseline fitting of MRS signal based on multiple penalized splines.[18] We preprocessed the raw MRS data removing the residual water signal using an HSVD filter, and realigning the data to 2.01 reference point (tNAA peak). We then run the SPANT::fit_mrs() with the ABFIT method to quantify different metabolites, providing measures for mI, tNAA, and total Cr (TCr). We used the ratio by TCr (phosphocreatine + creatine) for the two metabolites (i.e., ml and tNAA) in all statistical analyses given the stability of its resonance peak.[8] Moreover, TCr did not change along the age-span in our sample (both DS and controls with Spearman rho < 0.15, data not shown), as previously shown in the literature.[8] Moreover, by normalizing with TCr, we control inter-individual differences that might arise from different amount of water due to atrophy and/or voxel location.

Quality control criteria included a signal-to-noise ratio higher than 5, a FWHM lower than 0.15ppm, and a Q value

(a measure of quality fitting)[19] lower than 2. In addition, SPANT provides estimated SDs (based on Cramér-Rao lower bounds), which reflect the quality of the expected fitting. Due to the disease-associated changes, the SDs in a cohort along the whole AD continuum are increased with respect to those in homogeneous samples. Thus, we imposed a liberal threshold of less than 50% of SDs as a quality criterion. Four participants did not fulfill the aforementioned quality control criteria.

CSF acquisition and analysis

A subset of 73 adults with DS underwent a lumbar puncture to obtain CSF sampling, following international recommendations.[20] We measured core AD biomarkers (Aβ42, Aβ40, phosphorylated tau 181 -pTau) using the Lumipulse G assays on LUMIPULSE G600II automated platform (Fujirebio). In addition, we quantified CSF levels of YKL-40 (chitinase-3-like protein 1), a marker of reactive astroglia in AD,[21] and neurofilament light (NfL), a marker of neurodegeneration,[22,23] using ELISA Kit MicroVue (Quidel, San Diego, CA) and NF-light (UmanDiagnostics, Umeå, Sweden), respectively. All euploid controls had normal core AD biomarkers levels, assessed in the same conditions and with the same technique.[13]

Amyloid PET acquisition and processing

A subset of 38 participants with DS also underwent an amyloid PET scan using the tracer 18F-florbetapir. We initially only offered amyloid PET to those subjects that also consented to CSF analyses due to grant protocol restraints. We had to stop the florbetapir PET recruitment due to restricted access in Spain for research. Florbetapir PET was acquired using a Philips Gemini TF scan 50 min after injection of 370mBq of 18F-florbetapir, with 2 mm slice thickness and 128x128 image size. The images were processed to obtain a unique value that represents the global amyloid load in the brain.[24] Briefly, florbetapir PET images were normalized to a standard space using a two-step registration approach: native florbetapir image to structural T1-weighted MRI, and T1-weighted MRI to standard MNI152 template. We computed a global amyloid PET measure, averaging the signal across the cingulate, parietal, frontal and temporal cortical areas, previously normalized using the whole cerebellum as the reference regions. Such global amyloid scalar value, referenced as Landau's florbetapir signature along the manuscript, has been shown to accurately differentiate amyloid positive patients in sporadic AD.

Structural T1-MRI acquisition and processing

Structural T1-weighted images were acquired with a 3 Tesla Philips Achieva scanner, using an MPRAGE protocol with 0.94x0.94x1 mm voxel resolution, 8.1 ms and 3.7 ms of repetition time and echo time, respectively, and 160 slices. We computed cortical thickness using Freesurfer package v6.0 (https://surfer.nmr.mgh.harvard.edu/) following a procedure previously described.[25,26] Briefly, Freesurfer automatically delineates the white matter and pial surfaces in order to compute a cortical thickness value for each vertex in the brain. Each individual cortical thickness map is then normalized to the standard space (fsaverage) and smoothed using a gaussian kernel of 15mm. From the initial set of 108 adults with DS with good quality MRS data, 26 subjects were excluded due to erroneous segmentation.

Table 1. Participants demographics

	Controls (N= 71)	All Down syndrome (N= 103)	Asymptomatic Down syndrome (N= 62)	Prodromal Down syndrome (N= 21)	Demented Down syndrome (N= 20)	Statistical Differences (p-value)
Age	54.3 (49.4-57.1)	44.8 (36.9-53.2)	40.2 (31-46.3)	49.8 (44.8-53.6)	54.1 (49.9-56.2)	<0.001
Sex (N Female)	45	39	25	7	7	0.118
Total-CAMCOG	NA	74 (58-83)	78 (65-85)	73 (58-78)	52 (39-63)	<0.001
CSF $A\beta_{42}/A\beta_{40}$ ratio	NA	0.061 (0.042-0.084)	0.08 (0.062-0.094) (N=35)	0.041 (0.030-0.051) (N=31)		<0.001
Florbetapir Landau Signature (SUVr)	NA	1.16 (1.02-1.3)	1.04 (1-1.19) (N=24)	1.27 (1.21-1.37) (N=14)		0.002
CSF pTau 181 (pg/mL)	NA	58.7 (27.9-122.7)	29.6 (17.1-56.7) (N=40)	146.4 (96.3-209.6) (N=33)		<0.001
CSF NfL (pg/mL)	NA	475.5 (305.4-764.5)	353.2 (201-450.1) (N=36)	766.3 (684.5-1618.5) (N=28)		<0.001
CSF YKL-40 (ng/mL)	NA	107.3 (90.4-214.2)	134 (70-178) (N=34)	206.3 (204.6-323) (N=18)		<0.001

To assess differences in baseline demographic characteristics and metabolites levels between the diagnostic groups, we used a Kruskal-Wallis rank sum test, with pairwise comparisons using the Dwass-Steel-Critchlow-Fligner test. In addition, for the metabolite analyses, we controlled for multiple comparisons using the Benjamin & Hochberg false discovery rate (FDR) method. All these analyses were performed using the R package StatsExpressions.[27]

To test the diagnostic performance of each metabolite, we used receiver operating characteristic (ROC) curves and assessed the area under the curve (AUC) for each metabolite. We used the Youden's index to compute the optimal threshold that differentiates between the clinical groups.

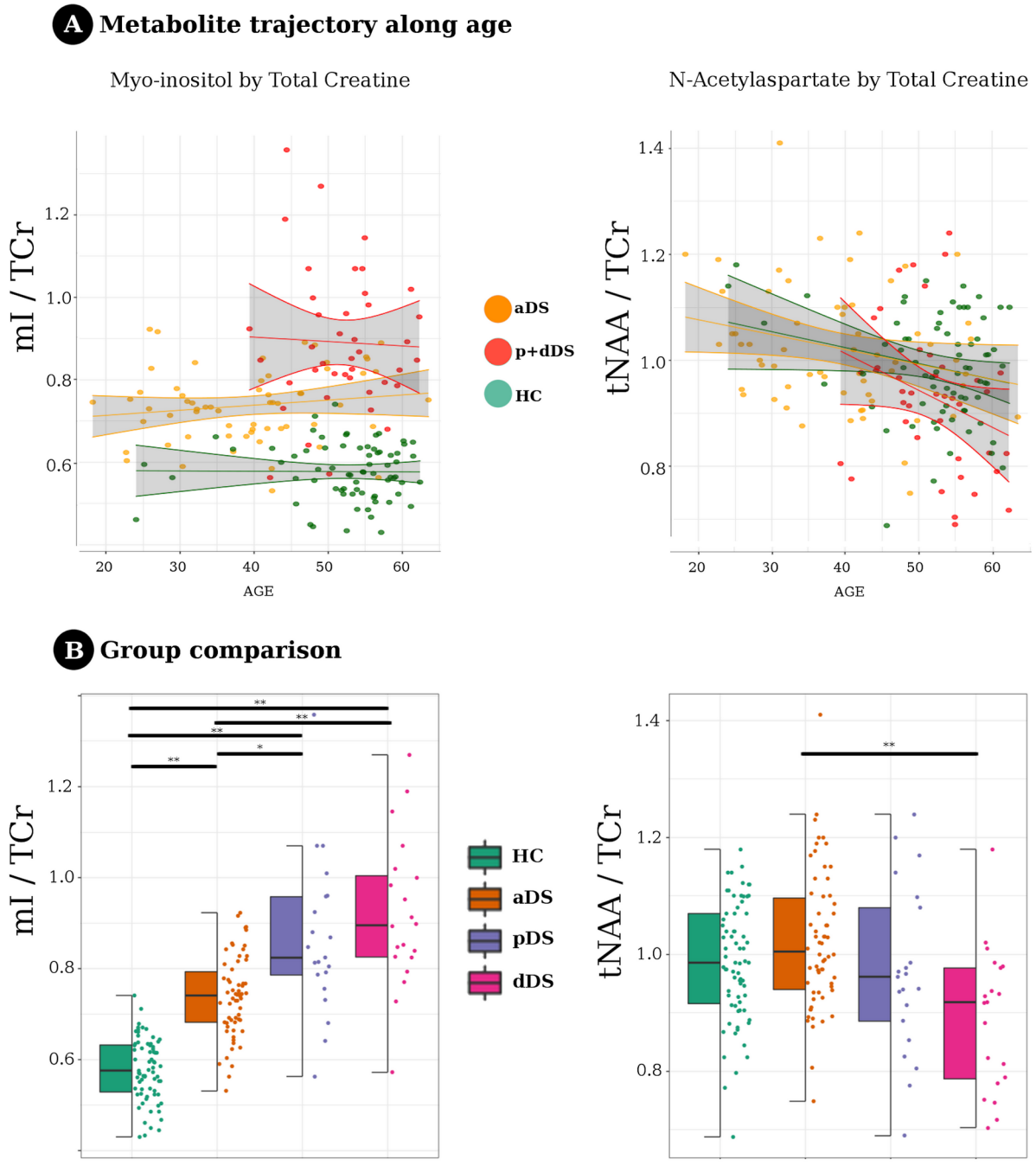

Fig 1. mI and tNAA changes with age and along the AD continuum in Down syndrome. Panel A) The association for mI/TCr (left) and tNAA/TCr (right) with age. Lines were obtained fitting a linear model for each subgroup. Panel B) Boxplot (median and inter-quartile ranges) and data-point distribution for mI/TCr (left) and tNAA/TCr (right) for each subgroup. HC = euploid healthy controls; aDS = asymptomatic Down Syndrome; pDS = prodomal Down Syndrome; dDS = Down Syndrome with dementia; ** = $p < 0.01$ FDR corrected; * = $p < 0.05$ FDR corrected

To investigate the relationship between the metabolite's ratio levels and AD biomarkers (i.e ratio Aβ42/Aβ40, pTau, YKL-40, NfL, and Landau's florbetapir signature), we performed Spearman correlation tests both in all adults with DS and separately in aDS and symptomatic DS (i.e., pooling pDS and dDS together due to the relatively small sample size). We considered significant those correlations with a p-value < 0.05 after controlling for multiple comparisons using the Benjamin & Hochberg FDR test. To further visualize the stability of our associations, we ran bootstrap analyses, subsetting and shuffling our DS sample 1000 times using the R package boot and recomputing the Spearman Rho estimate using the package ppcor. We plotted the original estimate and the interquartile range of these 1000 permutations.

Finally, to study the association between metabolite ratios and cortical thickness, we used a general linear model with sex as a nuisance factor, for each vertex of the surface, as implemented in Freesurfer. We performed this analysis for the whole DS sample, and aDS and symptomatic patients separately.

We controlled for false positives using a cluster-extent MonteCarlo approach also implemented in Freesurfer.[28] Only results that survived multiple comparisons (FWE $p<0.05$) are shown. Adjusting by age in autosomal dominant AD and Down syndrome studies is a topic of debate, addressed with different approaches in the literature. In Down syndrome, AD pathology is universal by age 40, and the cumulative incidence is over 90% in the seventh decade. Therefore, the concept of healthy aging in this population is very problematic and very difficult to dissect from preclinical AD (i.e. we cannot remove the effect of normal aging from that of the disease process). However, on the other hand, the shared association with age of several variables makes the epiphenomenological association between such variables problematic. Hence, in the present study, we decided to perform both adjusted and unadjusted (by age) statistical analyses. For the group comparisons, in addition to the non-parametric approach we repeated the analyses using a ANCOVA. We also performed the ROC analyses adjusting by age. For the association between AD-core biomarkers, we corrected age-related effect using a partial Spearman correlation. For cortical thickness analyses, we re-run the analyses using a GLM with age as nuisance factor, as implemented in Freesurfer.

RESULTS

Sample

The final sample included 71 controls and 103 adults with DS, of whom 62 were asymptomatic, 21 pAD and 20 dAD. Table 1 shows the demographics and biomarker data of the participants. As expected, there were significant statistical differences in age and all biomarker levels between the different clinical groups.

Changes in MRS metabolites profiles along the AD continuum in DS

Fig 1A shows the relationship between age and both mI/TCr and tNAA/TCr in adults with DS and controls. mI/TCr was increased in all DS compared to controls, and further increased in the early 40s. tNAA/TCr decreased with age in both adults with DS and controls. Asymptomatic adults with DS showed comparable tNAA levels as controls, although tNAA levels started to decrease in their mid-40s.

Fig 1B shows the mI/TCr and tNAA/TCr ratios along the AD continuum. There were significant group differences for both mI/TCr ($p < 0.001$) and tNAA/TCr ($p = 0.002$). All the DS subgroups had a higher mI/TC ratio than controls ($p < 0.001$ FDR corrected). pDS and dDS groups had increased levels compared to aDS (both with $p < 0.01$ after FDR corrected), but there were no significant differences between

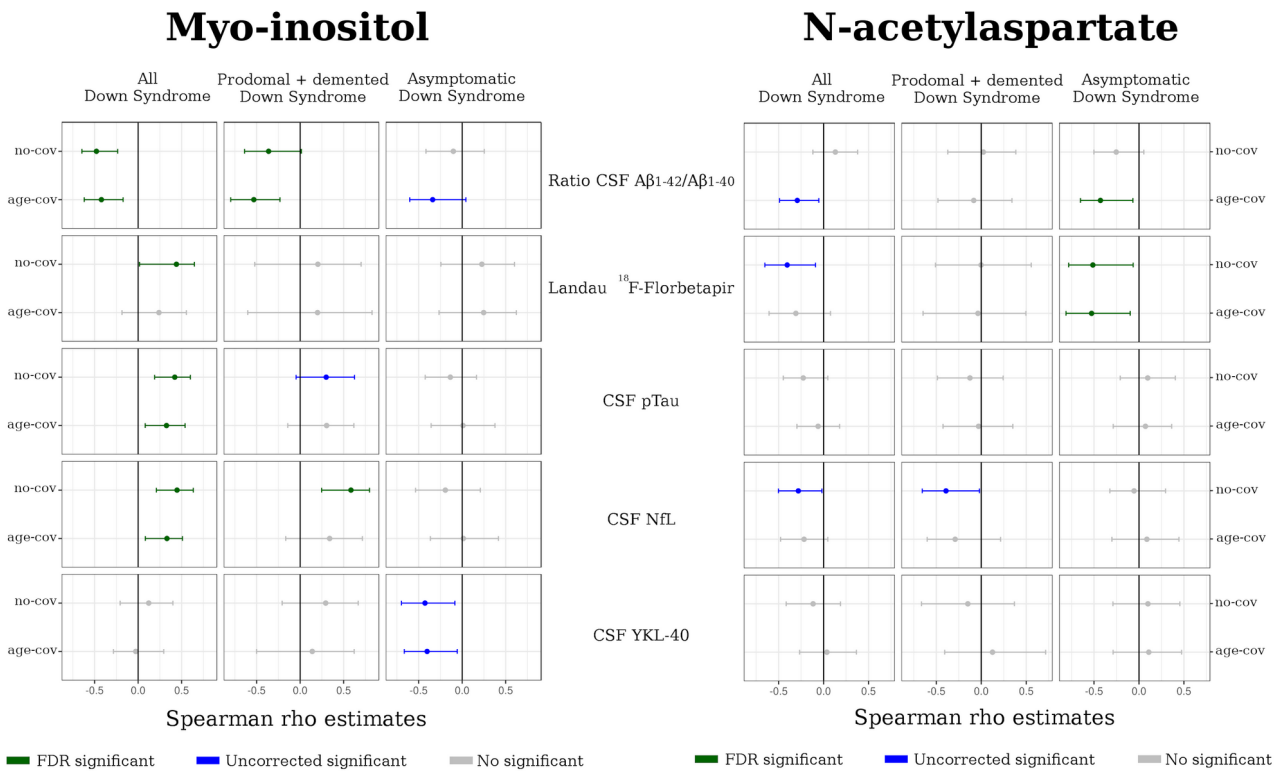

Fig 2. mI and tNAA correlate with AD-core biomarkers. Association between AD biomarkers and mI/TCr and tNAA/TCr for the whole sample (left column), prodromal and Down Syndrome with dementia (central column) and asymptomatic Down Syndrome (right column). Midpoint shows the (partial) Spearman Rho value for the included sample, whereas the line represents the CI for bootstrap with 1000 permutations. For each biomarker, we compute both the adjusted (age-cov) and no-adjusted (no-cov) Spearman Rho value.

pDS and dDS. We identified the same pattern of significant results when adjusting the comparisons by age. The ROC analyses showed an AUC of 0.74 (cut-point=0.786; CI=0.76-0.87) and 0.85 (cut-point=0.824; CI=0.77-0.89), when comparing aDS vs pDS and aDS vs dDS, respectively. For the tNAA/TCr ratio, the pairwise comparisons only revealed statistical differences between aDS and dDS (p = 0.001 FDR corrected). In the ROC analyses, the AUC analyses showed an AUC of 0.62 (cut-point=0.98; CI=0.88-1.00) and 0.78 (cut-point=0.938; CI=0.89-1.03), when comparing aDS vs pDS and aDS vs dDS, respectively. We found similar results when adjusting by age. Concretely, for mI, we obtained an AUC of 0.75 and 0.88 when comparing aDS against pDS and dDS, respectively, and an AUC of 0.65 and 0.82 when comparing tNAA levels of aDS against pDS and dDS, respectively.

Metabolite associations with core AD and inflammatory biomarkers

We next studied the relationship between both the mI/TC and tNAA/TC ratios and AD biomarkers (Fig 2). The mI/TC ratio was significantly associated with amyloid biomarkers, both with the CSF Aβ42/Aβ40 ratio and with the Landau's florbetapir signature in the whole sample of DS ($p < 0.05$

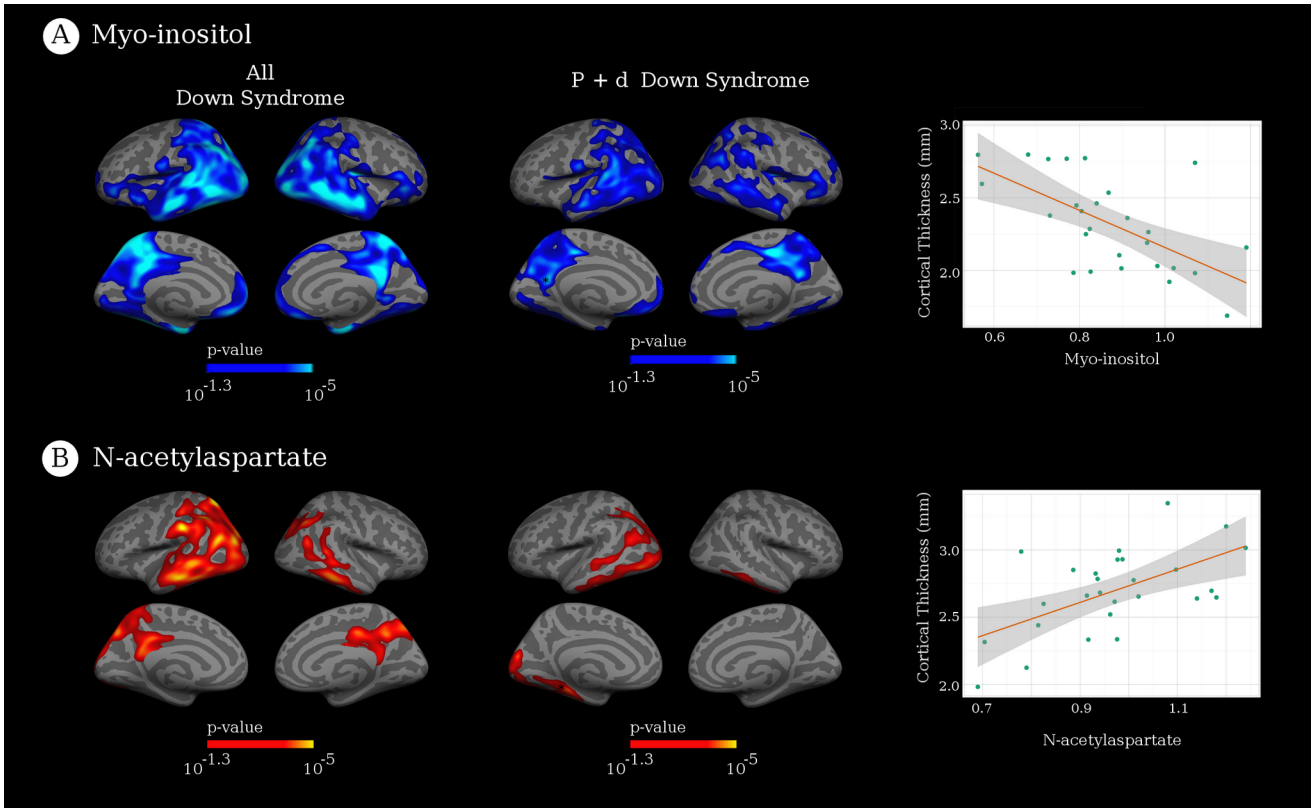

Fig 3. mI and tNAA are related to cortical atrophy in the AD continuum in Down syndrome. Cortical surface representation of significant negative (blue) association between mI/TCr and cortical thickness and positive (red) association between tNAA/TCr. Scatterplots show the associations for the most significant vertex (marked with black *).

FDR corrected for both biomarker). However, when splitting our sample into subgroups, only those with symptomatic AD showed a significant association with CSF Aβ42/Aβ40 ratio. The mI/TC ratio was also significantly associated with CSF pTau levels in the whole sample ($p < 0.05$ FDR corrected). When splitting the sample, no association survived multiple comparisons. We also found a significant positive association between the mI/TCr ratio and CSF NfL both in the whole sample and in the symptomatic AD subgroup ($p < 0.05$ FDR corrected). We did not find any correlation that survived multiple comparisons between mI/Tcr and CSF YKL-40. The tNAA/TCr ratio was associated with Laundau's florbetapir signature in both the whole sample and in aDS (both $p < 0.05$, uncorrected), but these associations did not survive multiple comparisons. The tNAA/TCr ratio was also associated with CSF NfL in the whole sample and in the symptomatic AD subgroup (both $p < 0.05$, uncorrected). When adjusting correlations by age using partial Spearman correlation, we found similar results.

Cortical thickness is associated with MRS metabolite alterations

Fig 3 shows the association between the mI/TCr and tNAA/TCr ratios and cortical thickness in the whole sample and in symptomatic patients. We found a widespread pattern of cortical thinning with increasing mI/TC ratios in AD

vulnerable regions, encompassing the precuneus, temporo-parietal and lateral temporal areas bilaterally, the medial temporal in the right hemisphere, and part of the medial inferior frontal cortex in the left hemisphere. This association was mainly driven by symptomatic patients. Similarly, the tNAA/TCr ratio was associated with cortical thickness in an overlapping (but less extended) pattern, both in the whole sample and in symptomatic patients. We found no significant association between the mI/TC ratio and cortical thickness in the aDS subgroup, and only a small cluster in the left superior frontal gyrus for the tNAA/TCr analysis (results not shown). When adjusting by age, we found a similar pattern of results, even though no cluster-extend multiple comparisons clusters survived for the tNAA analyses.

DISCUSSION

This study investigated for the first time the MRS changes with age and along the AD continuum, as well as their diagnostic performance and association with core AD, inflammatory biomarkers and cortical thickness. Metabolite levels are altered in symptomatic AD and are associated with core AD biomarkers changes in adults with Down syndrome. Despite the lower diagnostic performance with respect core AD biromarkers, MRS is able to track AD-related neuroinflammatory and neurodegenerative changes, and has the advantage with respect CSF or PET biomarkers, that it could be easily included in the MRI acquisition in longitudinal studies. MRS could thus be used as a disease-staging biomarker in DS, with potential of demonstrating target engagement in disease-modifying therapies.

This study showed MRS metabolic alterations associated with DS and with AD pathophysiology. The mI/TCr had clear differences even in the youngest asymptomatic individuals (and throughout all ages) with respect to controls, while the tNAA/TCr was unchanged in asymptomatic individuals. These results underscore the importance of considering the neurodevelopmental or constitutive differences in individuals with DS when interpreting biomarker results.[3] The increases of mI in asymptomatic DS individuals are not only a result of aging, as previously reported for the general population,[29–31] but probably also due to the presence of the inositol transporter gene on chromosome 21[12] and/or a consequence of neuroinflammation[32–34] resulting from an increase in inflammatory cytokine expression.[35] A prior study with a smaller sample size11 (17 aDS and 5 dDS) also found increases in mI in aDS compared to controls, but was not able to detect differences between the DS subgroups. We did find changes both in the mI/TC and tNAA/TC ratios along the AD continuum. The larger sample size in our study enabled us the identification of a gradient of increases along the AD continuum in the mI/TC ratio. These results are congruent with previous reports in sporadic AD, in which participants with mild cognitive impairment and AD dementia showed increases in the mI/TC ratio compared to controls.[4,5,7,8,36,37] The tNAA/TC ratio was less sensitive to detect changes with disease progression. We only found differences in the aDS vs dDS comparison, in agreement with previous reports.[11] Further research positioning the MRS voxel in a more prominent and early-stage neurodegenetion region, such as the temporal cortex, might enhance the sensitivity of tNAA/TCr. Despite the differences between clinical groups, the ROC analyses for MRS showed lower diagnostic performance than plasma or CSF biomarkers.[3]

This study also assessed the relationship between MRS metabolite alterations and AD biomarkers. The mI/TC ratio was more strongly associated with AD biomarkers than tNAA, and was the only metabolite to survive multiple

comparisons correction. The mI/TC ratio was associated with amyloid biomarkers (both the CSF Aβ42/Aβ40 ratio and amyloid PET uptake), CSF pTau, and CSF NfL levels in the whole sample, and with the CSF Aβ42/Aβ40 ratio and CSF NfL (and a trend for CSF pTau levels) in the symptomatic patients. Previous studies had also found a positive association between mI and amyloid PET uptake[5,6,9] or amyloid neuropathology[10] in sporadic AD. In our study, mI was also correlated with tau and neurodegeneration markers. While previous studies in sporadic AD did not find an association between neurofibrillary tangles and mI10, others have shown a co-localization of neurofibrillary tangles and reactive astrocytes (see Laurent et al[38] for a review), suggesting a possible association between both markers. Alternatively, the positive correlation between mI and CSF pTau might be driven by the group differences along the AD continuum as the association within each subgroup did not survive the multiple comparison correction in the stratified analyses. Further studies using in-vivo local measures of tau pathological changes (such as tau PET) might resolve these discrepancies between CSF biomarkers and postmortem quantifications.

Contrary to our expectations, there were no associations between mI and CSF YKL-40 levels (only a counterintuitive negative association in asymptomatic subjects). This is surprising given that both mI and YKL-40 have been proposed as markers of astrocytosis,[21] and both are increased with disease progression.[4,39] It is possible that both biomarkers reflect different astrocytic and neuroinflammatory responses in AD, or that they track changes in different astrocyte subtypes.[40,41] This suggests to us that the inflammatory processes measured by both biomarkers are different. The inflammatory response in AD is complex and probably evolves in different phases along the disease course. Further research using in-vivo markers of inflammation (such as deprenyl or SMBT-1 PET tracer) or animal studies will help further understand these associations. Although no correlation survived multiple comparisons correction for tNAA, we found significant (uncorrected) correlations between tNAA and both CSF NFL levels and florbetapir PET uptake. As expected the correlation with amyloid biomarkers were found in asymptomatic subjects, and the correlation with neurodegeneration in symptomatic subjects.

Metabolite levels are also associated with neurodegeneration. We found an association between both the mI/TC and tNAA/TC ratios in the precuneus and the cortical thinning in widespread regions typically affected in AD. Of note, the AD-vulnerable regions are similar in sporadic amnesic AD[26,42] and DS.[16,43,44] These associations were more prominent in symptomatic stages of the disease. To our knowledge, it is the first study reporting these relationships in DS. In sporadic AD, there are some previous reports assessing the association between MRS metabolites and local neuroimaging changes in AD. For instance, a recent work by Sheikh-Bahaei and colleagues[9] investigated the local relationship between metabolite levels and amyloid and FDG PET uptake. Others have focused on the local relationship between structural imaging alterations and metabolites levels in subcortical regions and the white matter, using both whole-brain MRS,[45,46] or investigating specific structures, such as the hippocampus.[47] However, no previous study had assessed the impact of the metabolite signature on the whole cortical mantle.

The main strength of this study is the inclusion of a large population-based cohort of adults with DS with available multimodal biomarker data, including MRS, MRI, florbetapir PET and CSF biochemical biomarkers. The population-based cohort of adults with DS with subjects in

all the clinical stages of the AD continuum and the control group helped to disentangle the neurodevelopmental and AD-associated changes. Furthermore, the multimodal assessments helped us to investigate the relationship with the AD pathophysiology. Despite the lower diagnostic performance of MRS with respect to plasma or CSF biomarkers, our results suggest that MRS can detect neuroinflammatory and neurodegenerative changes associated with AD in adults with DS. MRS is more accessible (and far cheaper) than PET studies and easier to implement in longitudinal designs than CSF studies. Therefore, MRS could be used to assess target engagement or as surrogate markers of efficacy in disease modifying therapies.

This study also has limitations. Metabolite levels were assessed in only one specific location using single-voxel MRS. The acquisition of multi-voxel MRS could provide further insights into the pattern of metabolite alterations beyond the precuneus. Moreover, our MRS acquisition protocol is not suitable to use state-of-the-art models, such as the MRS-diffusion model, that would allow the measurement not only of metabolite levels, but also the measurement of the within-cellular displacement of metabolites that might change due to glia morphological alterations in early stages of the disease.48 In addition, the discrepancies between mI and CSF YKL-40 suggest that further work, with more specific cytokine-expression should be done to understand the origin of the mI alterations. Finally, longitudinal studies are required to better characterize the longitudinal alterations of these metabolites in a single-subject basis.

In summary, this study supports the use of MRS to characterize pathophysiological alterations in DS and its potential to track AD pathophysiology in AD clinical trials in DS.

ACKNOWLEDGEMENTS

This study was supported by the Fondo de Investigaciones Sanitario, Instituto de Salud Carlos III, and the CIBERNED programme, partly jointly funded by the EU European Regional Development Fund. This work was also supported by the National Institutes of Health, Departament de Salut de la Generalitat de Catalunya, Pla Estratègic de Recerca i Innovacio en Salut, and Fundació La Marató de TV3. VM is supported by the Fondo de Investigaciones Sanitario, Instituto de Salud Carlos III. MFI is supported by the Jérôme Lejeune and Sisley D'Ornano Foundations. AB is supported from a Juan de la Cierva-Incorporacion grant from the Spanish Ministery of Economy (IJCI-2017-32609) and a Miguel Servet I grant (2020, CP20/00038) from the Carlos III Health Institute. Fundació Catalana Síndrome de Down, Fundació Víctor Grífols i Lucas, and the Jérôme Lejeune Foundation also partly supported this work. Finally, this work was supported by Generalitat de Catalunya and a grant from the Fundació Bancaria La Caixa to RB. We thank all the participants with Down's syndrome, their families, and their carers for their support of, and dedication to, this research. We also acknowledge the Fundació Catalana Síndrome de Down for global support; Laia Muñoz, Soraya Torres and Shaimaa El Bounasri for laboratory and sample handling; Reyes Alcoverro, Marta Salinas, and Tania Martínez for administrative support; and Concepción Escola and Diana Garzón for nursing handling.

REFERENCES

1. Rubenstein E, Hartley SL, Bishop L. Epidemiology of Dementia and Alzheimer Disease in IndividualsWith DownSyndrome. JAMA Neurol. 2019;77(2):262–264.

2. Dubois B, Feldman HH, Jacova C, et al. Advancing research diagnostic criteria for Alzheimer ' s disease : the IWG-2 criteria. Lancet Neurol 2014;13(June)

3. Fortea J, Vilaplana E, Carmona-Iragui M, et al. Clinical and biomarker changes of Alzheimer's disease in adults with Down

syndrome: a cross-sectional study. Lancet 2020;395(10242):1988–1997.

4. Kantarci K, Jack CR, Xu YC, et al. Regional metabolic patterns in mild cognitive impairment and Alzheimer's disease: A 1H MRS study [Internet]. Neurology 2000;55(2):210–217.[cited 2014 Oct 14] Available from: http://www.neurology.org/cgi/doi/10.1212/WNL.55.2.210

5. Voevodskaya O, Sundgren PC. Myo-inositol changes precede amyloid pathology and relate to APOE genotype in Alzheimer disease. 2016;0

6. Kantarci K, Lowe V, Przybelski SA, et al. Magnetic resonance spectroscopy, beta-amyloid load, and cognition in a population-based sample of cognitively normal older adults. [Internet]. Neurology 2011;77(10):951–958.Available from: http://www.ncbi.nlm.nih.gov/pubmed/21865577

7. Voevodskaya O, Poulakis K, Sundgren P, et al. Brain myoinositol as a potential marker of amyloid-related pathology. 2019;0:395–406.

8. Valenzuela MJ, Sachdev PS. Magnetic resonance spectroscopy in AD. Neurology 2011;10(MAY)

9. Sheikh-bahaei N, Manavaki R, Sheikh-bahaei N. PET-guided MR Spectroscopy in Alzheimer's disease. Ann. Neurol. [date unknown];1–21.

10. Murray ME, Przybelski SA, Lesnick TG, et al. Early Alzheimer's disease neuropathology detected by proton MR spectroscopy. [Internet]. J. Neurosci. 2014;34(49):16247–55.Available from: http://www.pubmedcentral.nih.gov/articlerender.fcgi?artid=4252542&tool=pmcentrez&rendertype=abstract

11. Lin A-L, Powell D, Caban-Holt A, et al. 1H-MRS metabolites in adults with Down syndrome: Effects of dementia [Internet]. NeuroImage Clin. 2016;Available from: http://linkinghub.elsevier.com/retrieve/pii/S2213158216300997

12. Berry GT, Mallee JJ, Kwon HM, et al. The human osmoregulatory Na+/myo-inositol cotransporter gene (SLC5A3): Molecular cloning and localization to chromosome 21. Genomics 1995;25(2):507–513.

13. Alcolea D, Clarimón J, Carmona-Iragui M, et al. The Sant Pau Initiative on Neurodegeneration (SPIN) cohort: a dataset for biomarker discovery and validation in neurodegenerative disorders. Alzheimer's Dement. Transl. Res. Clin. Interv. 2019;5:597–609.

14. Esteba-Castillo S, Dalmau-Bueno A, Vidal N, et al. Adaptación y validación del Cambridge Examination for Mental Disorders of Older People with Down's Syndrome and Others with Intellectual Disabilities (CAMDEX-DS) en población española con discapacidad intelectual. Rev. Neurol. 2013;57:337.

15. Fortea J, Carmona-Iragui M, Benejam B, et al. Plasma and CSF biomarkers for the diagnosis of Alzheimer's disease in adults with Down syndrome: a cross-sectional study. Lancet Neurol. 2018;17(10):860–869.

16. Fortea J, Vilaplana E, Carmona-iragui M, et al. Clinical and biomarker changes of Alzheimer ' s disease in adults with Down syndrome : a cross-sectional study. Lancet 2020;395

17. Öz G. MR spectroscopy of the brain for radiologists [Internet]. Radiology 2007;270(3):3:e12.Available from: http://pubs.rsna.org/doi/10.1148/radiol.13130531

18. Wilson M. Adaptive baseline fitting for 1 H MR spectroscopy analysis. Magn Reson Med 2021;(February 2020):13–29.

19. Wilson M, Reynolds G, Kauppinen R a, et al. A constrained least-squares approach to the automated quantitation of in vivo 1H magnetic resonance spectroscopy data. [Internet]. Magn. Reson. Med. 2011;65(1):1–12.[cited 2014 Aug 29] Available from: http://www.ncbi.nlm.nih.gov/pubmed/20878762

20. Vanderstichele HMJ, Janelidze S, Demeyer L, et al. Optimized Standard Operating Procedures for the Analysis of Cerebrospinal Fluid Aβ42 and the Ratios of Aβ Isoforms Using Low Protein Binding Tubes. J. Alzheimer's Dis. 2016;53(3):1121–1132.

21. Querol-Vilaseca M, Colom-Cadena M, Pegueroles J, et al. YKL-40 (Chitinase 3-like I) is expressed in a subset of astrocytes in Alzheimer's disease and other tauopathies. J. Neuroinflammation 2017;14(1):1–10.

22. Gaetani L, Blennow K, Calabresi P, et al. Neurofilament light chain as a biomarker in neurological disorders. J. Neurol. Neurosurg. Psychiatry 2019;1–12.

23. Delaby C, Alcolea D, Carmona-Iragui M, et al. Differential levels of Neurofilament Light protein in cerebrospinal fluid in patients with a wide range of neurodegenerative disorders. Sci. Rep. 2020;10(1):1–8.

24. Landau SM, Breault C, Joshi AD, et al. Amyloid-β imaging with Pittsburgh compound B and florbetapir: comparing radiotracers and quantification methods. [Internet]. J. Nucl. Med. 2013;54(1):70–7.[cited 2014 Jan 28] Available from: http://www.pubmedcentral.nih.gov/articlerender.fcgi?artid=3747730&tool=pmcentrez&rendertype=abstract

25. Fischl B, Dale AM. Measuring the thickness of the human cerebral cortex from magnetic resonance images. [Internet]. Proc. Natl. Acad. Sci. U. S. A. 2000;97(20):11050–5.Available from: http://www.pubmedcentral.nih.gov/articlerender.fcgi?artid=27146&tool=pmcentrez&rendertype=abstract

26. Montal V, Vilaplana E, Alcolea D, et al. Cortical microstructural changes along the Alzheimer's disease continuum [Internet]. Alzheimer's Dement. 2017;(October):1–12.Available from: http://linkinghub.elsevier.com/retrieve/pii/S1552526017337676

27. Patil I. statsExpressions: “ggplot2” Expressions with Statistical Details. 2019;

28. Hagler DJ, Saygin AP, Sereno MI. Smoothing and cluster thresholding for cortical surface-based group analysis of fMRI data. Neuroimage 2006;33(4):1093–1103.

29. Reyngoudt H, Claeys T, Vlerick L, et al. Age-related differences in metabolites in the posterior cingulate cortex and hippocampus of normal ageing brain: A 1H-MRS study [Internet]. Eur. J. Radiol. 2012;81(3):e223–e231.Available from: http://dx.doi.org/10.1016/j.ejrad.2011.01.106

30. Suri S, Emir U, Stagg CJ, et al. Effect of age and the APOE gene on metabolite concentrations in the posterior cingulate cortex. Neuroimage 2017;152(March):509–516.

31. Marjańska M, McCarten JR, Hodges J, et al. Region-specific aging of the human brain as evidenced by neurochemical profiles measured noninvasively in the posterior cingulate cortex and the occipital lobe using 1H magnetic resonance spectroscopy at 7 T. Neuroscience 2017;354(May):168–177.

32. Huggard D, Kelly L, Ryan E, et al. Increased systemic inflammation in children with Down syndrome [Internet]. Cytokine 2020;127(July 2019):154938.Available from: https://doi.org/10.1016/j.cyto.2019.154938

33. Wilcock DM, Griffin WST. Down’s syndrome, neuroinflammation, and Alzheimer neuropathogenesis. J. Neuroinflammation 2013;10:1–10.

34. Patkee PA, Baburamani AA, Long KR, Dimitrova R. Neurometabolite Mapping Highlights Elevated Myo-inositol Profiles within the Developing Brain in Down Syndrome. 2020;1–26.

35. Flores-Aguilar L, Iulita MF, Kovecses O, et al. Evolution of neuroinflammation across the lifespan of individuals with Down syndrome. Brain 2020;

36. Kantarci K, Xu YC, Shiung MM, et al. Comparative diagnostic utility of different MR modalities in mild cognitive impairment and Alzheimer’s disease. Dement. Geriatr. Cogn. Disord. 2002;14(3–4):198–207.

37. Kantarci K. Proton MRS in mild cognitive impairment. [Internet]. J. Magn. Reson. Imaging 2013;37(4):770–7.Available from: http://www.pubmedcentral.nih.gov/articlerender.fcgi?artid=3609038&tool=pmcentrez&rendertype=abstract

38. Laurent C, Buée L, Blum D. Tau and neuroinflammation: What impact for Alzheimer’s Disease and Tauopathies? Biomed. J. 2018;41(1):21–33.

39. Alcolea D, Martínez-Lage P, Sánchez-Juan P, et al. Amyloid precursor protein metabolism and inflammation markers in preclinical Alzheimer disease. [Internet]. Neurology 2015;85(7):626–33.Available from: http://www.ncbi.nlm.nih.gov/pubmed/26180139

40. Liddelow SA, Guttenplan KA, Clarke LE, et al. Neurotoxic reactive astrocytes are induced by activated microglia [Internet]. Nature 2017;541(7638):481–487.Available from: http://dx.doi.org/10.1038/nature21029

41. Habib N, McCabe C, Medina S, et al. Disease-associated astrocytes in Alzheimer’s disease and aging [Internet]. Nat. Neurosci. 2020;1–6.Available from: http://www.nature.com/articles/s41593-020-0624-8

42. Dickerson BC, Bakkour A, Salat DH, et al. The cortical signature of Alzheimer’s disease: regionally specific cortical thinning relates to symptom severity in very mild to mild AD dementia and is detectable in asymptomatic amyloid-positive individuals. [Internet]. Cereb. Cortex 2009;19(3):497–510.[cited 2014 Jan 22] Available from: http://www.pubmedcentral.nih.gov/articlerender.fcgi?artid=2638813&tool=pmcentrez&rendertype=abstract

43. Matthews DC, Lukic AS, Andrews RD, et al. Dissociation of Down syndrome and Alzheimer’s disease effects with imaging [Internet]. Alzheimer’s Dement. Transl. Res. Clin. Interv. 2016;2(2):69–81.Available from: http://dx.doi.org/10.1016/j.trci.2016.02.004

44. Rafii MS, Lukic AS, Andrews RD, et al. PET Imaging of Tau Pathology and Relationship to Amyloid, Longitudinal MRI, and Cognitive Change in Down Syndrome: Results from the Down Syndrome Biomarker Initiative (DSBI). J. Alzheimer’s Dis. 2017;60(2):439–450.

45. Su L, Blamire AM, Watson R, et al. Whole-brain patterns of 1H-magnetic resonance spectroscopy imaging in Alzheimer’s disease and dementia with Lewy bodies. Transl. Psychiatry 2016;6(8):1–8.

46. Constans JM, Meyerhoff DJ, Gerson J, et al. H-1 MR spectroscopic imaging of white matter signal hyperintensities: Alzheimer disease and ischemic vascular dementia. Radiology 1995;197(2):517–523.

47. Kantarci K, Petersen RC, Przybelski SA, et al. Hippocampal volumes, proton magnetic resonance spectroscopy metabolites, and cerebrovascular disease in mild cognitive impairment subtypes. Arch. Neurol. 2008;65(12):1621–1628.

48. Ligneul C, Palombo M, Hernández-Garzón E, et al. Diffusion-weighted magnetic resonance spectroscopy enables cell-specific monitoring of astrocyte reactivity in vivo. Neuroimage 2019;191(December 2018):457–469.

Association of cortical microstructure with amyloid-β and tau: impact on cognitive decline, neurodegeneration, and clinical progression in older adults

Elena Rodriguez-Vieitez[1,2,3,†], **Victor Montal**[4,5,†], Jorge Sepulcre[1,6], Cristina Lois[1,6], Bernard Hanseeuw[1,6,7], Eduard Vilaplana[4,5], Aaron P. Schultz[1,2], Michael J. Properzi[1,2] Matthew R. Scott[1,2] Rebecca Amariglio[1,2,8], Kathryn V. Papp[1,2,8], Gad A. Marshall[1,2,8], Juan Fortea[4,5], Keith A. Johnson[1,6], Reisa A. Sperling[1,2,8], Patrizia Vannini[1,2,8]

†These authors contributed equally to this work.

(1) Massachusetts General Hospital, Harvard Medical School, Boston, MA 02114, USA (2) Athinoula A. Martinos Center for Biomedical Imaging, Charlestown, MA 02129, USA (3) Karolinska Institutet, Department of Neurobiology, Care Sciences and Society, Stockholm 14152, Sweden (4) Hospital de la Santa Creu i Sant Pau, Barcelona 08041, Spain (5) Centre of Biomedical Investigation Network for Neurodegenerative Diseases (CIBERNED), Madrid 28031, Spain (6) Gordon Center for Medical Imaging, Boston, MA 02114, USA (7) Saint Luc University Hospital, Université Catholique de Louvain, Brussels 1200, Belgium (8) Brigham and Women's Hospital, Harvard Medical School, Boston, MA 02115, USA

Molecular Psychiatry (2021) doi: 10.1038/s41380-021-01290-z.

ABSTRACT

Non-invasive biomarkers of early neuronal injury may help identify cognitively-normal individuals at risk of developing Alzheimer's disease (AD). A recent diffusion-weighted imaging (DWI) method allows assessing cortical microstructure via cortical mean diffusivity (cMD), suggested to be more sensitive than macrostructural neurodegeneration. Here, we aimed to investigate the association of cMD with amyloid-β and tau pathology in older adults, and whether cMD predicts longitudinal cognitive decline, neurodegeneration and clinical progression. The study sample comprised n=196 cognitively-normal older adults (mean[SD] 72.5[9.4] years; 144 women[58.3%]) from the Harvard Aging Brain Study. At baseline, all participants underwent structural MRI, DWI, 11C-Pittsburgh compound-B-PET, 18F-flortaucipir-PET imaging and cognitive assessments. Longitudinal measures of Preclinical Alzheimer Cognitive Composite-5 were available for n=186 individuals over 3.72 (1.96)-year follow-up. Prospective clinical follow-up was available for n=163 individuals over 3.2 (1.7)-years. Surface-based image analysis assessed vertex-wise relationships between cMD, global amyloid-β, and entorhinal and inferior-temporal tau. Multivariable regression, mixed-effects models and Cox proportional-hazards regression assessed longitudinal cognition, brain structural changes and clinical progression. Tau, but not amyloid-β, was positively associated with cMD in AD-vulnerable regions. Correcting for baseline demographics and cognition, increased cMD predicted steeper cognitive decline, which remained significant after correcting for amyloid-β, thickness and entorhinal tau; there was a synergistic interaction between cMD and both amyloid-β and tau on cognitive slope. Regional cMD predicted hippocampal atrophy rate, independently from amyloid-β, tau and thickness. Elevated cMD predicted progression to MCI. Cortical microstructure is a non-invasive biomarker that independently predicts subsequent cognitive decline, neurodegeneration and clinical progression, suggesting utility in clinical trials.

INTRODUCTION

Alzheimer's disease (AD) is characterized by the misfolding and deposition of amyloid-β (Aβ) and hyperphosphorylated tau in the brain[1, 2], a process that begins years before clinical onset[3]. Accumulating evidence from preclinical and clinical studies supports the notion that Aβ and tau pathologies interact synergistically in the preclinical stages of AD, contributing to faster neurodegeneration and cognitive decline[4–7]. Therefore, in-vivo imaging biomarkers of AD proteinopathy, neuronal injury and neurodegeneration are of interest to elucidate the dynamic interplay among biological mechanisms underlying disease progression.

Although Aβ positivity and even sub-threshold Aβ load have been shown to predict cognitive decline happening over longer time periods[8–10], Aβ alone is not accurate enough to predict short-term cognitive decline or clinical progression[11, 12]. Therefore, complementary non-invasive imaging biomarkers of subtle neuronal injury whether alone or in combination with Aβ may help select participants at the earliest stages with an enhanced risk of impending cognitive decline or clinical progression. Biomarkers for identification of at-risk individuals prior to widespread neurodegeneration are of great interest for optimization of secondary prevention trials[13–15], and as outcome measures of therapeutic efficacy.

While neurodegeneration is typically reflected in macrostructural changes including atrophy and cortical thinning measured by structural MRI, a recent diffusion-weighted imaging (DWI) method has allowed to assess

microstructural properties of the grey matter (GM) [16, 17] by means of cortical mean diffusivity (cMD). Increased cMD is thought to reflect the early breakdown of microstructural integrity due to damage to cellular membranes and dendritic processes[18], and therefore cMD has been proposed as a sensitive biomarker of subtle microstructural injury, prior to overt neurodegeneration measured by atrophy or cortical thinning[19, 20]. Previous cross-sectional studies have reported increased cMD in prodromal and dementia stages of sporadic AD[16, 21], and a positive association between cMD values and years to symptom onset in autosomal-dominant AD[17, 22, 23]. In sporadic fronto-temporal degeneration and amyotrophic lateral sclerosis, increased cMD was more widespread, had a larger effect size and was more closely associated with disease severity compared with cortical thinning[24, 25]. Increased cMD has also been observed in AD-vulnerable regions in pre-dementia stages of AD at pathological levels of CSF Aβ and phospho-tau[16]. However, the relationship between cMD and the underlying in-vivo Aβ and tau burden in cognitively-normal adults is unknown. Moreover, the ability of cMD to predict subsequent cognitive decline, neurodegeneration and clinical progression in the AD-continuum remains unknown.

The specific aims of this study are to: (i) investigate the cross-sectional association of in-vivo Aβ and tau burden with cMD and in a cohort of cognitively-normal older adults, (ii) determine whether baseline cMD is associated with prospective longitudinal cognitive change and hippocampal atrophy rates, independently and/or interactively with Aβ and tau at baseline, (iii) determine whether baseline cMD predicts subsequent clinical progression.

METHODS

Participants

The study sample consisted of n=196 community-dwelling older adults from the Harvard Aging Brain Study (HABS) (Table 1), a longitudinal observational study of aging and preclinical AD conducted at Massachusetts General Hospital and Brigham and Women's Hospital in Boston, MA [26].

For the aims of this study, we selected participants with concurrent data on DWI, T1-weighted MRI, 11C-Pittsburgh Compound-B (PIB)-PET, 18F-flortaucipir (FTP)-PET and cognitive assessments summarized using the Preclinical Alzheimer Cognitive Composite-5 (PACC5)[27]. All assessments had been performed within one year of the T1-weighted MRI scan. Using these inclusion criteria, we got a group of n=196 participants (referred to as 'baseline'), all deemed cognitively-normal. Of note, the majority of participants had a Clinical Dementia Rating (CDR)=0, except for nine participants with CDR=0.5. Subsets of the cohort had longitudinal MRI, neuropsychological, CDR and clinical evaluations (Table 1). Ethical approvals, exclusion criteria and neuropsychological evaluations are detailed in Supplementary Methods.

MRI methods

All participants underwent a structural 3D T1-weighted magnetization-prepared rapid-acquisition gradient-echo (MPRAGE) sequence and a DWI sequence on a 3-Tesla TimTrio scanner (Siemens, Erlangen, Germany) with a 12-channel phased-array head coil (acquisition parameters in Supplementary Methods).

Structural MRI was processed for estimation of cortical thickness (CTh) and subcortical volumetric segmentation using FreeSurfer 6.0 (http://surfer.nmr.mgh.harvard.edu) [28]. Cortical segmentations were visually inspected to detect and correct processing errors and an automatic region-

Table 1. Sample composition

Characteristic	**All participants (*n* = 196)**	**Aβ- (*n* = 147)**	**Aβ+ (*n* = 49)**	***P* value**
No. (% of sample)				
Female, No. (%)	114 (58.2%)	86 (58.1%)	28 (57.1%)	0.87
White/non-hispanic, No. (%)	148 (75.5%)	105 (71.4%)	43 (87.8%)	0.02
APOE- 4+	53 (27.0%)	23 (15.6%)	30 (61.2%)	<0.001
CDR = 0.5	9 (4.6%)	8 (5.4%)	1 (2.0%)	0.32
Mean (SD)				
Age, years	72.5 (9.4)	70.9 (9.6)	77.3 (7.2)	<0.001
Years of education	16.2 (2.9)	16.2 (3.0)	16.0 (2.8)	0.63
MMSE	29.1 (1.12)	29.1 (1.13)	29.2 (1.11)	0.80
Logical memory, delayed recall	15.7 (3.86)	15.7 (3.86)	15.7 (3.89)	>0.99
PACC5	0.19 (0.75)	0.22 (0.75)	0.09 (0.74)	0.30
PIB-FLR DVR	1.17 (0.19)	1.08 (0.04)	1.45 (0.19)	<0.001
entFTP PVC SUVr	1.36 (0.29)	1.29 (0.23)	1.56 (0.34)	<0.001
i-tFTP PVC SUVr	1.44 (0.18)	1.40 (0.15)	1.56 (0.21)	<0.001
No. follow-up MRI scans	1.47 (0.52)	1.44 (0.50)	1.51 (0.56)	0.49
Prospective MRI follow-up, years	3.11 (1.52)	3.01 (1.50)	3.31 (1.55)	0.31
Subsample *n* / total *n* (%)	118/196 (60.2%)	79/147 (53.7%)	39/49 (79.6%)	
No. follow-up cognitive assessments	3.56 (1.80)	3.40 (1.81)	4.04 (1.71)	0.03
Prospective cognitive follow-up, years	3.72 (1.96)	3.50 (1.92)	4.34 (1.95)	0.01
Subsample *n* / total *n* (%)	186/196 (94.9%)	138/147 (93.9%)	48/49 (98.0%)	
Prospective clinical follow-up, years	3.2 (1.7)	3.1 (1.7)	3.4 (1.6)	0.30
Subsample *n* / total *n* (%)	163/196 (83.2%)	116/147 (78.9%)	47/49 (95.9%)	
Progressors to MCI, *n* /total (%)	11/163 (6.7%)	1/116 (0.86%)	10/47 (21.3%)	
Time to progression in those who progressed, years	3.3 (1.5)	4.5 (-)	3.2 (1.5)	
Prospective CDR follow-up, years	3.3 (1.7)	3.3 (1.6)	3.3 (1.8)	>0.99
Subsample *n* / total *n* (%)	165/187 (88.2%)	119/139 (85.6%)	46/48 (95.8%)	
Progressors to CDR=0.5, *n* /total (%)	15/165 (9.1%)	3/119 (2.5%)	12/46 (26.1%)	
Time to CDR=0.5 in those who progressed, years	2.7 (1.7)	3.4 (0.9)	2.5 (1.9)	

of-interest (ROI) parcellation was performed[29]. Hippocampal volume (HV), adjusted for intracranial volume, was assessed using Freesurfer.

DWI data were processed with an in-house surface-based diffusion tensor imaging (DTI) approach combining FSL (FMRIB Software Library) (http://fsl.fmrib.ox.ac.uk/fsl/fslwiki, v5.0.9) and FreeSurfer 6.0 tools [16]. This surface-based approach applies recently developed techniques [30–32] to overcome limitations of traditional voxel-based approaches. First, it reduces the contribution from CSF and white matter signal on GM voxels that can confound cMD measures. Second, it applies a surface-based smoothing procedure, less sensitive to smoothing kernel size compared with voxel-based analyses [33]. In the surface-based DTI approach, images were motion-corrected via rigid-body registration between the b=0 and the 30 b=700 volumes. After removing non-brain tissue, a tensor model was fitted using FSL's dtifit command, and we computed the cMD metric. The diffusion images were then coregistered to each subject's T1 using bbregister, a boundary-based registration algorithm in FreeSurfer [34]. The cMD maps resulting from DTI fitting were then sampled in the midpoint between white and pial surfaces, projected onto the subject's cortical surface space, and registered to FreeSurfer standard space. Finally, cMD maps were normalized to a standard surface template (fsaverage) and smoothed using a 15-mm 2D full-width half-maximum Gaussian kernel across the cortical mantle. cMD was extracted from eight AD-vulnerable ROIs: entorhinal, fusiform gyrus, inferior-temporal, middle-temporal, inferior-parietal, orbitofrontal, isthmus cingulate and parahippocampal gyrus. These eight ROIs are typically described as vulnerable to tau aggregation based on postmortem and in vivo staging (Braak and Braak, 1991; Jack et al. 2017; Schöll et al. 2016), and data-driven approaches (Sepulcre et al. 2017).

PET methods

All PIB and FTP-PET scans were acquired at the Massachusetts General Hospital PET facility (ECAT EXACT HR+ scanner; Siemens, Erlangen, Germany) [26, 35]; (acquisition parameters in Supplementary methods). Late-sum PIB and FTP-PET images were used to coregister the respective PET volumes to each subject's native T1 using mri_coreg in FreeSurfer, prior to quantification.

PIB-PET quantification: A Logan model was applied to dynamic PIB-PET images using cerebellar GM as reference to generate parametric non-partial volume corrected (non-PVC) Logan Distribution Volume Ratio (DVR) images, which were projected onto the cortical surface. Individual burden was extracted from a cortical composite including frontal, lateral-temporal, parietal and retrosplenial (PIB-FLR) regions [35, 36]. Participants were further stratified into Aβ+ and Aβ- sub-groups at baseline using non-PVC PIB-FLR Logan DVR=1.2 as cut-off, previously derived using Gaussian mixture modeling [12].

Tau PET quantification: FTP-PET images were projected onto the cortical surface space and partial volume corrected using the geometric transfer matrix method [37]. FTP-PET was then quantified using PVC standardized uptake value ratio (SUVr) using cerebellar GM as reference. Individual tau burden was extracted from the bilateral entorhinal and inferior-temporal cortices. Entorhinal FTP (entFTP) was used as a proxy for aging and early tau deposition in preclinical AD, while inferior-temporal FTP (i-tFTP) represents AD-related neocortical tau [5, 35, 38, 39].

Statistical analyses

Cross-sectional analyses

Surface-based analyses: To investigate the associations of A and tau with cortical microstructure, we applied a general linear model in FreeSurfer with vertex-wise cMD as dependent variable in three models. For each model, the independent predictor was global Aβ burden evaluated in the PIB-FLR cortical composite, entFTP or i-tFTP; age and sex were covariates. Vertex-wise analyses were corrected for multiple comparisons within FreeSurfer using a cluster extension criterion based on Monte Carlo simulation with 10,000 repeats, with family-wise error correction at P<0.05, two-sided test.

Regional-based analyses: Separate multivariable regression models were used to independently assess the ability of global Aβ burden (continuous or dichotomous PIB-FLR), entFTP and i-tFTP to predict regional cMD. Also, models were set-up to examine the interaction of global Aβ and either entFTP or i-tFTP in predicting regional cMD, and their respective independent contributions. All models included age and sex as covariates. Corrections for multiple regional comparisons were performed using a false discovery rate (q<0.05) approach, two-sided test.

Longitudinal analyses

Prediction of cognitive decline and neurodegeneration rates: To investigate whether regional cMD is associated with longitudinal cognitive and neurodegeneration rates, the longitudinal changes in PACC5 or HV were extracted from mixed-effects models with PACC5 or HV as outcome, using time (years from baseline) as fixed-effects predictor, and incorporating random intercepts and slopes at the subject level (Eq.1). From these models, we extracted an individual random slope of PACC5 and of HV for each participant, which represented the corresponding rates of change [40]:

$$Longitudinal\ PACC5\ or\ HV \sim time_{from\ baseline} + (time_{from\ baseline} | \text{subject } ID)$$

Multivariable regression models were then used to investigate whether regional cMD at baseline predicts slope of PACC5 or HV. All models included age and sex as covariates; in models predicting cognitive decline, baseline PACC5 and education were also added as covariates. Furthermore, we tested whether cMD interacted with dichotomous or continuous PIB-FLR, entFTP or i-tFTP on the slope of PACC5 or HV; models with interaction terms included all lower-order terms.

We further applied a hierarchical regression approach to test the ability of cMD to predict PACC5 or HV slopes when sequentially including PIB-FLR and CTh as independent predictors, and finally adding entFTP or i-tFTP as predictors. The statistical fit of different models was inter-compared using R2 and Akaike information criterion (AIC); lowest AIC indicates better fit. All statistical tests were two-sided.

Prediction of clinical outcomes: We used survival analysis to investigate whether cMD predicts subsequent clinical progression. Time-to-event was defined as years from baseline to the first follow-up visit when a participant was diagnosed as mild cognitive impairment (MCI). For comparison, separate survival models were set-up using progression from CDR=0 to 0.5 as a subtler definition of clinical progression [41]. We applied multivariable Cox proportional-hazards regression models to estimate hazard ratios (HRs) with 95% confidence intervals (CI) to investigate whether dichotomous regional cMD ("high cMD" defined as top-tertile cMD; "low cMD" otherwise) predicts subsequent diagnosis of MCI/AD, or progression to CDR=0.5. Cox regression analyses were controlled for baseline age, sex and education, to account for demographic differences across participants. Additional exploratory Cox

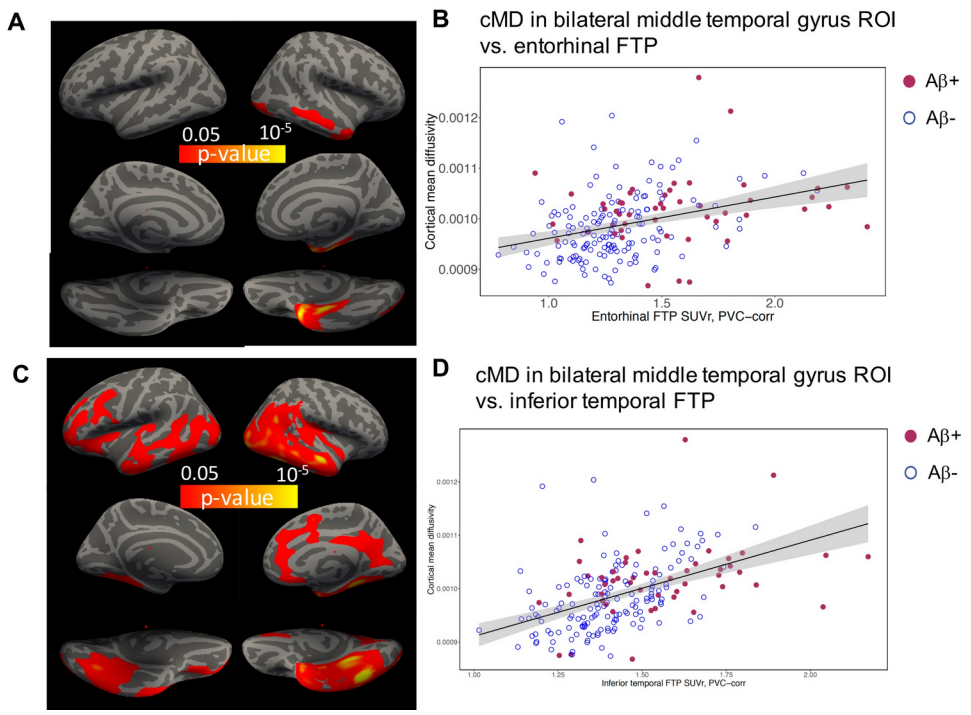

Figure 1. Cross-sectional associations of entorhinal and inferior-temporal tau with cMD. (A) Surface-based statistical map representing the clusters with significant association of vertex-wise cMD with entorhinal ^{18}F-flortaucipir (FTP) uptake; clusters survived correction for multiple comparisons implemented in FreeSurfer by using a cluster extension criterion in a Monte Carlo simulation with 10,000 repeats, with the family-wise error correction settled at $P < 0.05$. **(B)** Scatterplot illustrating the association of cMD in the middle-temporal gyrus region-of-interest (ROI) and entorhinal FTP uptake. **(C)** Surface-based statistical map representing the clusters with significant association of vertex-wise cMD with inferior-temporal FTP uptake; clusters survived correction for multiple comparisons implemented in FreeSurfer by using a cluster extension criterion in a Monte Carlo simulation with 10,000 repeats, with the family-wise error correction settled at $P < 0.05$. **(D)** Scatterplot illustrating the association of milddle-temporal cMD with inferior-temporal FTP uptake. cMD = cortical mean diffusivity; FTP = ^{18}F-flortaucipir; PVC = partial volume corrected; SUVr = standardized uptake value ratio.

regression analyses sequentially incorporated PIB status and CTh as predictors. Results were visualized using Kaplan-Meier curves. All statistical tests were two-sided. Further details about statistical tests and software are included in Supplementary methods.

RESULTS

Demographic and clinical data of the 196 participants with baseline data stratified into Aβ+ and Aβ- sub-groups are presented in Table 1. Aβ+ participants had greater prevalence of APOE-4 positivity, were older and had greater Aβ and tau pathology than the Aβ- sub-group; there were no significant differences in cognitive performance between Aβ+ and Aβ- sub-groups at baseline.

Cross-sectional associations of in-vivo Aβ and tau with cMD in older adults

No significant association was found between PIB-FLR and vertex-wise cMD after multiple-comparisons correction. In the ROI-based analysis, neither dichotomous nor continuous PIB-FLR were associated with regional cMD, corrected for multiple comparisons.

Entorhinal and inferior-temporal tau (entFTP, i-tFTP) showed a positive cross-sectional association with vertex-wise cMD across all n=196 participants (Fig. 1). The association of entFTP with vertex-wise cMD was localized to clusters in the entorhinal and inferior-middle temporal gyrus on the right hemisphere (Fig. 1A), while i-tFTP was associated to more widespread increases in cMD in bilateral clusters of entorhinal, isthmus cingulate, fusiform gyrus, inferior-middle temporal gyrus, and parts of lateral occipital, lateral orbitofrontal cortex and precuneus (Fig. 1C). These associations were confirmed when using ROI-based analyses for eight bilateral cMD ROIs (Supplementary Table 1). Both entFTP and i-tFTP had the strongest positive association with inferior-middle temporal gyrus cMD, where regression models explained up to 40-45% of the total variance in cMD (Supplementary Table 1). Scatterplots for the ROI-based analyses are illustrated for the middle-temporal gyrus (Figs. 1B, 1D). There was no significant interaction between entFTP or i-tFTP and either dichotomous or continuous PIB-FLR in predicting concurrent regional cMD (not shown). When either dichotomous or continuous PIB-FLR and entFTP or i-tFTP were entered as independent predictors, the PIB-FLR term was non-significant, while the predictive ability of entFTP or i-tFTP was not substantially altered (not shown).

Relationship between baseline cMD and subsequent rate of cognitive decline

Correcting for baseline demographics and cognitive status (PACC5), baseline cMD in all ROIs predicted steeper decline in PACC5 (Supplementary Table 2); illustrated in the lateral middle-temporal gyrus (Fig. 2A). In five ROIs (Table 2), cMD remained a significant predictor of PACC5 slope after correcting for PIB-FLR, and after simultaneously correcting for both PIB-FLR and regional CTh, indicating that baseline cMD is capturing variance in subsequent cognitive decline, independently from Aβ and CTh biomarkers. The observation that CTh was a non-significant predictor in four of the five ROIs (Table 2) supports the concept that cMD has higher sensitivity than CTh as a prognostic marker of cognitive decline. When entFTP was additionally included as predictor, cMD in the isthmus cingulate cortex remained a significant predictor of cognitive decline (Supplementary Table 3); when i-tFTP was used as predictor instead of entFTP, none of the regional cMD values remained predictive of cognitive decline, suggesting that the shared variance between cMD and subsequent cognitive decline is explained by increased neocortical tau pathology.

Cortical mean diffusivity is synergistic with amyloid-β and tau burden in predicting future cognitive decline

We observed a significant interaction between cMD and continuous or dichotomous PIB-FLR in predicting PACC5 slope; which was significant in all ROIs after multiple-comparisons correction (Supplementary Table 4). This interaction is illustrated in Fig. 2A where, as middle-temporal cMD increases, PACC5 declines with a steeper slope in the Aβ+ compared with the Aβ- sub-group. The interaction between cMD and continuous PIB-FLR is illustrated in Supplementary Fig. 1, which represents the association of baseline middle-temporal cMD with PACC5 slope for mean PIB-FLR ± 1 standard deviation (SD) range. In these interaction models, the individual terms PIB-FLR

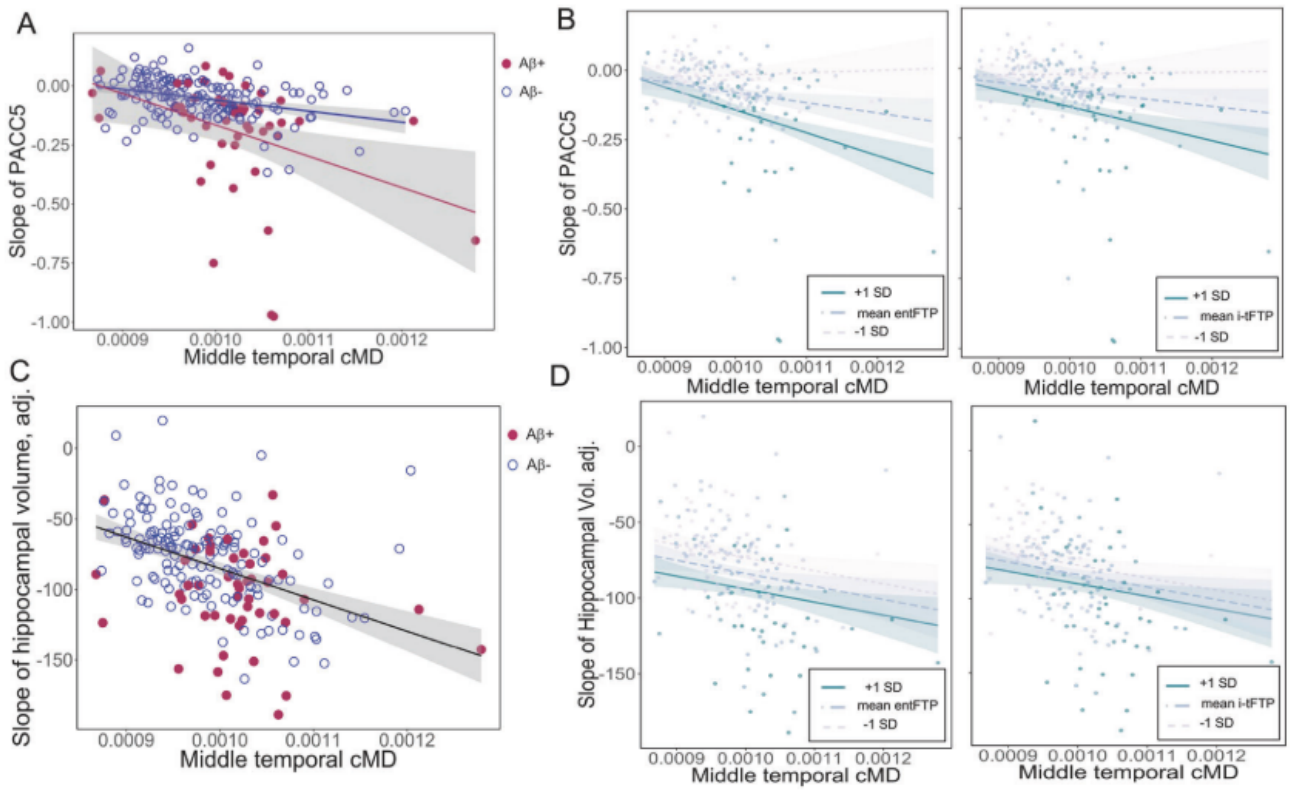

Figure 2. Associations of cMD with subsequent rates of cognitive decline and hippocampal volume loss. (A) Association of middle-temporal cMD at baseline with subsequent rate of cognitive decline as measured by the Preclinical Alzheimer Cognitive Composite-5 (PACC5), illustrating the significant interaction between cMD and dichotomized A burden. **(B)** Middle-temporal cMD interacts with tau burden (entFTP, i-tFTP) in predicting future rate of cognitive decline. **(C)** Association of middle-temporal cMD at baseline with subsequent rate of hippocampal volume loss. **(D)** Middle-temporal cMD does not significantly interact with tau burden (entFTP, i-tFTP) in predicting future rate of hippocampal volume loss. cMD = cortical mean diffusivity; entFTP = entorhinal ^{18}F-flortaucipir; i-tFTP = inferior-temporal ^{18}F-flortaucipir; PACC5 = Preclinical Alzheimer Cognitive Composite-5.

and regional cMD remained significant independent predictors.

There was also a significant interaction between regional cMD and tau burden as measured by either entFTP or i-tFTP (Supplementary Table 5) in predicting the rate of cognitive decline, as illustrated in Fig. 2B for cMD in the middle-temporal region. In these interaction models, the individual terms entFTP, itFTP and regional cMD remained significant independent predictors.

Relationship between baseline cMD and subsequent rate of HV loss

Regional cMD in all ROIs predicted rate of HV loss, after multiple-comparisons correction (Supplementary Table 6); illustrated in Fig. 2C for the middle-temporal gyrus cMD. The ability of regional cMD to predict rate of HV loss remained significant after correcting for PIB-FLR, regional

CTh and either entFTP (Supplementary Table 7) or i-tFTP (Supplementary Table 8).

Regional cMD did not interact with PIB-FLR (not shown). Also, the interaction of cMD with continuous measures of tau burden (entFTP or i-tFTP) was non-significant in predicting rate of HV loss (Fig. 2D).

Cortical mean diffusivity is predictive of subsequent clinical progression

Eleven participants (5.6% [11/196]) progressed to a clinical diagnosis of MCI within a mean (SD) progression time of 3.3 (1.5) years. Using CDR as outcome, we found that 15 participants (9.1% [15/187]) progressed to CDR=0.5 during 2.7 (1.7) years. Despite few participants progressed clinically during the study period, we observed that higher cMD predicted faster progression. In particular, entorhinal, middle-temporal and orbitofrontal cMD predicted shorter survival using MCI or CDR=0.5 as outcome, as illustrated in Fig. 3 for the orbitofrontal cMD. In all Cox proportional hazards models, which included age, sex and education as covariates, PIB status was the strongest predictor of clinical progression and showed an HR[95% CI]=25.98 [3.19 to 211.32], P=0.002 in predicting progression to MCI and HR[95% CI]=10.20 [2.82 to 36.93] in prediction progression to CDR=0.5. Orbitofrontal cMD remained significant after inclusion of PIB status and CTh as independent predictors (Fig. 3). Orbitofrontal cMD had an HR[95% CI]=11.06 [2.22 to 55.03], P=0.003 in predicting progression to MCI, and HR[95% CI]= 4.78 [1.57 to 14.59], P=0.006 in predicting progression to CDR=0.5. CTh did not significantly predict clinical progression in any of the clinical progression models (Fig. 3). Respective survival analyses in entorhinal and middle-temporal gyrus are illustrated in Supplementary Figs. 2 and 3.

DISCUSSION

In this study of 196 older adults, entorhinal and inferior-temporal tau, but not global Aβ, were positively associated with cMD in AD-vulnerable brain areas. Increased cMD at baseline predicted faster cognitive decline, which remained significant after correction for global Aβ, regional CTh and entorhinal tau. We also observed a synergistic interaction between cMD and global Aβ, and between cMD and tau burden, on subsequent rate of cognitive decline. Higher cMD at baseline predicted faster hippocampal atrophy and clinical progression to MCI. At baseline, entorhinal and inferior-temporal tau were positively associated with regional cMD, suggesting that elevated cMD is a marker of neuronal injury accompanying tau as it spreads into the neocortex. Our finding that increased cMD is associated to tau but not Aβ burden is consistent with the independent roles that these proteinopathies play in the brain [4, 42]. Recent studies[16, 17, 43] reported a non-linear effect of Aβ load on structural biomarkers in the brain in clinically-normal individuals prior to overt neuronal damage, which could explain the lack of a linear association between cMD and global Aβ in our cohort. We then assessed the relationship between baseline cMD and subsequent cognitive decline, neurodegeneration and clinical progression. We found that higher cMD values were strongly predictive of steeper cognitive decline and HV loss. The ability of regional cMD to predict subsequent cognitive decline remained significant after sequentially accounting for global Aβ burden, regional CTh and entorhinal tau, suggesting that cMD independently explains variance in cognitive decline, beyond those traditional imaging biomarkers. In contrast, regional cMD did not significantly

Table 2. Statistical regression analyses

Indep. pred.	**Std. (95% CI)**	***P* value**	***q* value**	**R^2 (AIC)**	**Indep. pred.**	**Std. (95% CI)**	***P* value**	***q* value**	**R^2 (AIC)**
	Slope PACC5 ~ fusiform cMD + PIB-FLR + PACC5 + (fusiform CTh)								
Fusiform cMD	-0.24 (-0.38 to -0.10)	$8x10^{-4}$	0.005	0.34 (489)	Fusiform cMD	-0.17 (-0.32 to -0.03)	0.022	0.043	0.37 (484)
PIB-FLR	-0.33 (-0.45 to -0.21)	$2x10^{-7}$	$3x10^{-7}$		PIB-FLR	-0.32 (-0.44 to -0.20)	$3x10^{-7}$	$4x10^{-7}$	
PACC5	0.27 (0.14 to 0.40)	$9x10^{-5}$	$1x10^{-4}$		PACC5	0.25 (0.12 to 0.38)	$2x10^{-4}$	$3x10^{-4}$	
					Fusiform CTh	0.17 (0.04 to 0.30)	0.012	0.046	
	Slope PACC5 ~ inferior temporal cMD + PIB-FLR + PACC5 + (inferior temporal CTh)								
Inf. temp. cMD	-0.23 (-0.39 to -0.08)	0.003	0.005	0.34 (491)	Inf. temp. cMD	-0.20 (-0.37 to -0.03)	0.020	0.043	0.34 (492)
PIB-FLR	-0.34 (-0.47 to -0.22)	$8x10^{-8}$	$2x10^{-7}$		PIB-FLR	-0.35 (-0.47 to -0.23)	$6x10^{-8}$	$2x10^{-7}$	
PACC5	0.27 (0.14 to 0.41)	$6x10^{-5}$	$1x10^{-4}$		PACC5	0.27 (0.14 to 0.40)	$8x10^{-5}$	$2x10^{-4}$	
					Inf. temp. CTh	0.06 (-0.08 to 0.19)	0.40	0.48	
	Slope PACC5 ~ isthmus cingulate cMD + PIB-FLR + PACC5 + (isthmus cingulate CTh)								
Isthmus cing. cMD	-0.21 (-0.34 to -0.08)	0.001	0.005	0.34 (490)	Isthmus cing. cMD	-0.21 (-0.34 to -0.08)	0.001	0.011	0.34 (491)
PIB-FLR	-0.34 (-0.46 to -0.22)	$1x10^{-7}$	$2x10^{-7}$		PIB-FLR	-0.34 (-0.46 to -0.21)	$2x10^{-7}$	$3x10^{-7}$	
PACC5	0.26 (0.13 to 0.39)	$1x10^{-4}$	$1x10^{-4}$		PACC5	0.26 (0.13 to 0.39)	$2x10^{-4}$	$2x10^{-4}$	
					Isthmus cing. CTh	0.04 (-0.09 to 0.16)	0.57	0.57	
	Slope PACC5 ~ lateral orbitofrontal cMD + PIB-FLR + PACC5 + (lateral orbitofrontal CTh)								
Lateral orbitofr.MD	-0.15 (-0.28 to -0.01)	0.034	0.039	0.32 (496)	Lateral orbitofr. MD	-0.16 (-0.29 to -0.02)	0.027	0.044	0.32 (497)
PIB-FLR	-0.35 (-0.47 to -0.23)	$6x10^{-8}$	$2x10^{-7}$		PIB-FLR	-0.35 (-0.48 to -0.23)	$6x10^{-8}$	$2x10^{-7}$	
PACC5	0.28 (0.14 to 0.41)	$6x10^{-5}$	$1x10^{-4}$		PACC5	0.28 (0.15 to 0.42)	$5x10^{-5}$	$2x10^{-4}$	
					Lateral orbitofr. CTh	-0.05 (-0.17 to 0.07)	0.42	0.48	
	Slope PACC5 ~ middle temporal cMD + PIB-FLR + PACC5 + (middle temporal CTh)								
Mid. temp. cMD	-0.24 (-0.39 to -0.09)	0.002	0.005	0.34 (490)	Mid. temp. cMD	-0.21 (-0.37 to -0.04)	0.016	0.043	0.34 (492)
PIB-FLR	-0.34 (-0.46 to -0.22)	$1x10^{-7}$	$2x10^{-7}$		PIB-FLR	-0.34 (-0.46 to -0.22)	$1x10^{-7}$	$2x10^{-7}$	
PACC5	0.26 (0.13 to 0.40)	$1x10^{-4}$	$1x10^{-4}$		PACC5	0.26 (0.13 to 0.39)	$1x10^{-4}$	$2x10^{-4}$	
					Mid. temp CTh	0.06 (-0.08 to 0.21)	0.37	0.48	

predict subsequent cognitive decline once inferior temporal tau was included as independent predictor. Our findings suggest that the shared variance between cMD and subsequent cognitive decline may be explained by increasing neocortical tau pathology, which is likely an underlying biological substrate driving the elevated cMD signal. Our results are in line with accumulating evidence that, while entorhinal tau can increase with aging without being an AD-specific process, inferior temporal tau is a stronger predictor of subsequent AD-specific cognitive decline (Cho et al 2019; Ossenkoppele et al 2021). In previous cross-sectional studies in patients with sporadic AD, fronto-temporal degeneration and amyotrophic lateral sclerosis[19, 20, 24, 25], cMD was associated with cognitive performance independently from CTh. Our study extends our knowledge about cMD to cognitively-unimpaired individuals, where we found that cMD has prognostic ability to predict short-term cognitive decline beyond that provided by Aβ structural biomarkers and entorhinal tau.

The regions where increased cMD was predictive of cognitive decline independently from CTh are consistent with regions undergoing hypometabolism in preclinical AD, in particular the isthmus cingulate located next to the posterior cingulate cortex[38], where a synergistic contribution of Aβ and tau leads to metabolic dysfunction in the absence of atrophy. Together with those previous reports, our findings support the notion that both cMD and 18F-fluorodeoxyglucose-PET are early biomarkers of tau-driven synaptic dysfunction preceding overt neuronal death and atrophy. Increased cMD in the absence of cortical thinning might also reflect early microstructural damage in response to tau oligomers that cause synaptic toxicity and dysfunction prior to neuronal death as demonstrated in preclinical studies[4], or to the accumulation of other protein oligomers or deposits of TDP-43 or -synuclein, for which no PET tracers are yet available.

Our study also showed that cMD and either Aβ or tau burden contribute independently and synergistically to subsequent cognitive decline over ~3.5 years. This finding suggests that in a clinical trial selecting Aβ participants[13, 15], the addition of the cMD biomarker would help to further select those participants most likely to decline over a relatively short term. Our finding adds to current efforts to compare the utility of different biomarkers of Aβ tau and neurodegeneration, whether used alone or in combination, to predict short-term cognitive decline and clinical progression[41, 44]. In line with previous observations (Farrell et al. 2020), we found that PIB status was the strongest predictor of clinical progression to MCI or CDR=0.5 during ~3.5 years follow-up. In addition, a novel finding of our stuy was that higher cMD independently predicted faster clinical progression to MCI or CDR=0.5, beyond that predicted by PIB status, while CTh did not provide any significant predictive value. These findings add support to the concept that cMD has higher sensitivity than CTh in the AD continuum and that it may be a useful biomarker for stratification of at-risk individuals for prevention trials that typically extend over three to five years.

Regional cMD showed prognostic ability for subsequently faster rate of hippocampal atrophy, demonstrating added value beyond imaging biomarkers of global Aβ, CTh and entorhinal or inferior-temporal tau; the absence of a synergistic effect between cMD and either Aβ or tau might be explained because longitudinal MRI data was available for only ~60% of baseline participants, having fewer longitudinal follow-ups compared to the more comprehensive longitudinal cognitive and clinical data available. Alternatively, the presence of co-pathologies

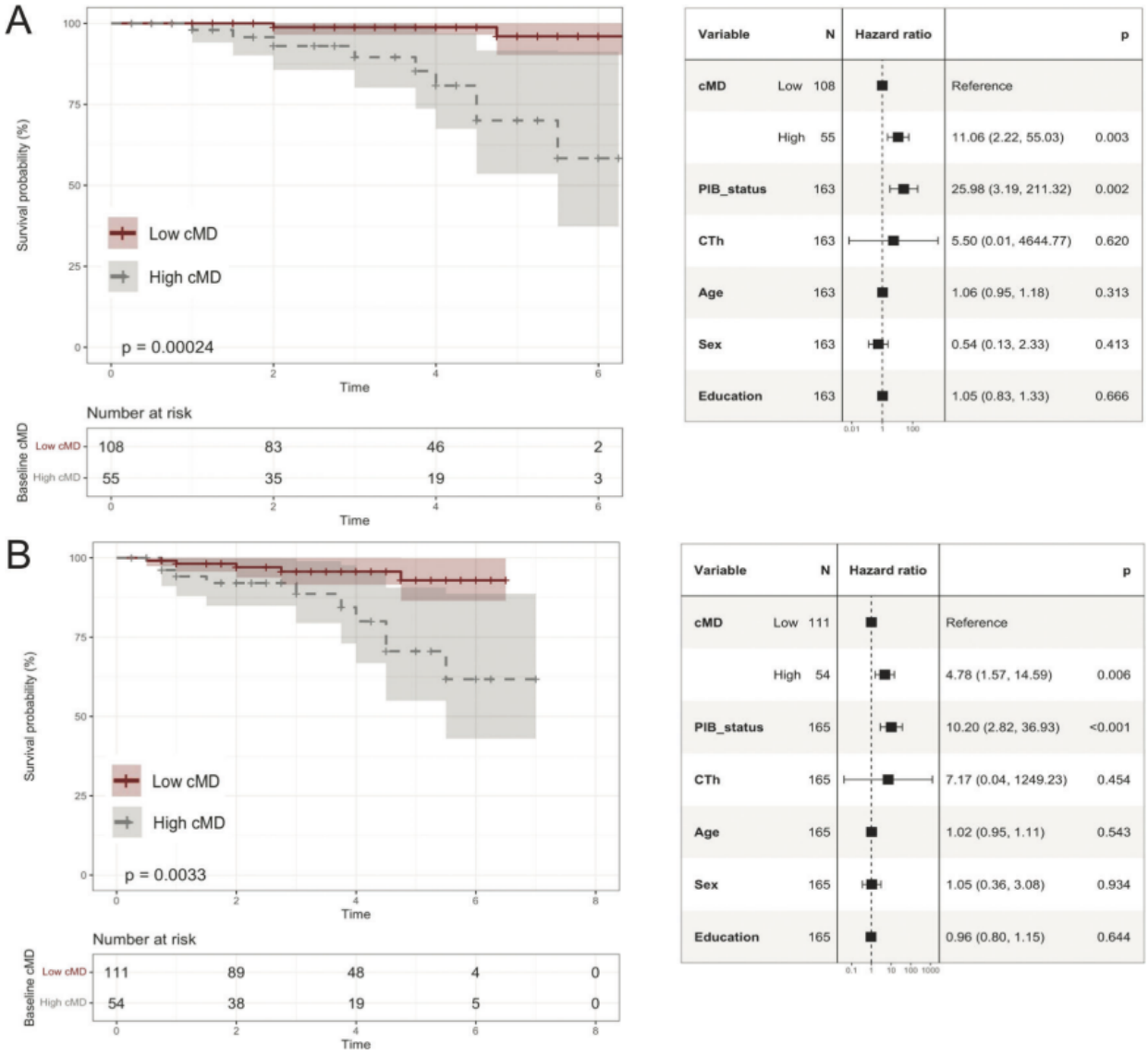

Figure 3. Survival analyses illustrating the ability of cMD to predict subsequent clinical progression. Kaplan-Meier curves and Cox proportional hazards regression results for lateral orbitofrontal cMD (high/low groups) predicting **(A)** progression to MCI**, (B)** progression to CDR = 0.5. cMD = cortical mean diffusivity; CTh = cortical thickness; PIB_status = A + vs A -; "High cMD" = top-tertile cMD values ("Low cMD", otherwise).

might in part explain the observed hippocampal atrophy. Previous reports have suggested that, while hippocampal atrophy is a rather specific feature of underlying AD pathology (Jack et al. 2002), neurodegeneration in this brain region may be due to a confluence of multiple underlying AD and non-AD co-pathologies including TDP-43 (Wilson et al. 2013). In particular, postmortem TDP-43 burden was found to be associated with antemortem hippocampal

atrophy as measured with MRI, independently from Aβ and tau pathology (Bejanin et al. 2019). Based on these previous reports, we speculate that the cMD signal in our study may be partly due to underlying TDP-43 pathology that contributes to HV loss independently from Aβ and tau pathology, and which may be associated with a slower rate of decline than AD pathology.

While our study focused on microstructural properties in the grey matter, three previous studies investigated white matter microstructural changes in the same cohort (Jacobs et al. 2018; Rabin et al. 2018, 2019). Increased mean diffusivity in the hippocampal cingulum white matter bundle was associated to greater downstream tau pathology in the posterior cingulate cortex, an effect that was enhanced at high levels of A burden, and suggesting that white matter tracts might serve as pathways for tau propagation. Our results are in line with Jacobs et al. with one key difference in that we studied microstructural properties in the grey matter. Our study found that AD pathology, in particular tau, is associated to microstructural injury in the grey matter. Further longitudinal studies are needed to investigate whether changes in cMD in the grey matter are locally and/or distally associated to longitudinal accumulation of tau, and whether they temporally precede or follow from degeneration of white matter tracts. A related study in older adults from HABS (Rabin et al 2018) found that global fractional anisotropy (FA) in nine WM tracts predicted longitudinal cognitive decline independently but not synergistically with A burden. A follow-up study (Rabin et al. 2019) reported that the synergistic interaction between FA in the fornix and A burden was associated to subsequently faster episodic memory decline. In common with these two reports (Rabin 2018 2019), we found that cMD is predictive of subsequent cognitive decline independently from Aβ status; in addition, we found that cMD is synergistic with A in predicting cognitive decline. From our results we conclude that in the continuum of AD, and especially in presymptomatic A -positive individuals, cMD could be a promising marker to identify individuals at enhanced risk of short-term cognitive decline and clinical progression, with utility for prevention trials.

HABS is a cohort study enrolling community-dwelling older adults that are followed over time. Our finding that cMD has prognostic value in a convenience sample such as HABS, not enriched for AD-risk factors, suggests that cMD is a sensitive marker of early and subtle neuronal injury, with promising potential as a prognostic biomarker with higher sensitivity compared with macrostructural biomarkers. Additional studies on the ability of cMD to predict cognitive decline and clinical progression in cohorts enriched for AD-risk factors such as APOE-4, autosomal-dominant mutations or other more stringent inclusion criteria, would be valuable to confirm our results.

A major strength of our study is its highly multimodal nature including concurrent T1-weighted MRI, DWI, Aβ and tau neuroimaging data. Also, the cohort was comprehensively characterized in terms of cognitive assessments and multiple longitudinal neuroimaging, neuropsychological and clinical data points. Since grey matter is considered mostly isotropic with respect to the motion of water molecules (Le Bihan et al. 2003; Weston et al. 2015), we selected cMD as an optimum metric to assess cortical microstructure in the grey matter. Although it could be technically possible to compute FA in the grey matter, its anisotropic-based computation would make it less informative and straightforward to interpret compared with cMD. Our study has some limitations. Only ~60% of the study participants had longitudinal MRI scans, which possibly limited the statistical power of the analyses involving HV loss. We only had longitudinal DWI in a small subset of participants so

DWI analyses were restricted to cross-sectional data; further longitudinal investigations would be valuable to explore relationships between changes in cMD, Aβ and tau to investigate the temporal dynamics of microstructural damage and proteinopathy accumulation.

Our study showed that cortical microstructure is a promising non-invasive technique, sensitive to early microstructural injury in older adults. Given that neuronal loss is irreversible, the ability of cMD to detect subtle microstructural damage prior to overt atrophy may have important clinical implications. We found that tau is an underlying pathological substrate associated with increases in cMD. As such, cMD might be a proxy for tau-induced neuronal injury, and cortical microstructure could serve as a lower-cost, non-invasive alternative to tau PET in clinical settings. The combination of multimodal baseline and longitudinal data allowed us to demonstrate the ability of cMD to predict cognitive and clinical progression using three different independent measures: slope of PACC5 and progression to MCI or to CDR=0.5; the confirmation of the prognostic ability of cMD using three different methods adds robustness to our findings. The ability of cMD to predict short-term cognitive decline and clinical progression suggests utility as outcome measure and to improve risk stratification of participants in clinical trials.

ACKNOWLEDGEMENTS

This project is supported by the US National Institute of Aging - NIH grants (1R21AG064348-01, R01AG061083 (PI: P. Vannini). The Harvard Aging Brain Study is funded by the National Institute on Aging (P01AG036694) (PI: R. A. Sperling) with additional support from several philanthropic organizations. E. R.-V. receives support from the Swedish Alzheimer Foundation (Alzheimerfonden) the Swedish Dementia Foundation (Demensfonden), and Erik and Edith Fernström and Karolinska Institutet Foundations, Sweden. We also thank the research staff and the very dedicated participants of the Harvard Aging Brain Study. The funders had no role in the design and conduct of the study; collection, management, analysis, and interpretation of the data; preparation, review, or approval of the manuscript; and decision to submit the manuscript for publication. Corresponding author Patrizia Vannini has full access to all the data in the study and takes responsibility for the integrity of the data and the accuracy of the data analysis.

REFERENCES

1. Arriagada PV, Growdon JH, Hedley-Whyte ET, Hyman BT. Neurofibrillary tangles but not senile plaques parallel duration and severity of Alzheimer's disease. Neurology. 1992;42:631–631.

2. Braak H, Braak E. Neuropathological stageing of Alzheimer-related changes. Acta Neuropathol. 1991;82:239–259.

3. Jack CR, Bennett DA, Blennow K, Carrillo MC, Dunn B, Haeberlein SB, et al. NIA-AA Research Framework: Toward a biological definition of Alzheimer's disease. Alzheimer's & Dementia. 2018;14:535–562.

4. Busche MA, Hyman BT. Synergy between amyloid-β and tau in Alzheimer's disease. Nat Neurosci. 2020;23:1183–1193.

5. Sperling RA, Mormino EC, Schultz AP, Betensky RA, Papp KV, Amariglio RE, et al. The impact of Aβ and tau on prospective cognitive decline in older individuals. Ann Neurol. 2018:ana.25395.

6. Ossenkoppele R, Smith R, Ohlsson T, Strandberg O, Mattsson N, Insel PS, et al. Associations between tau, Aβ, and cortical thickness with cognition in Alzheimer disease. Neurology. 2019;92:e601–e612.

7. La Joie R, Visani AV, Baker SL, Brown JA, Bourakova V, Cha J, et al. Prospective longitudinal atrophy in Alzheimer's disease correlates with the intensity and topography of baseline tau-PET. Sci Transl Med. 2020;12:eaau5732.

8. Farrell ME, Jiang S, Schultz AP, Properzi MJ, Price JC, Becker JA, et al. Defining the lowest threshold for amyloid-PET to predict future cognitive decline and amyloid accumulation. Neurology. 2020:10.1212/WNL.0000000000011214.

9. Donohue MC, Sperling RA, Petersen R, Sun C-K, Weiner MW, Aisen PS, et al. Association Between Elevated Brain Amyloid and Subsequent Cognitive Decline Among Cognitively Normal Persons. JAMA. 2017;317:2305–2316.

10. Bischof GN, Jacobs HIL. Subthreshold amyloid and its biological and clinical meaning: Long way ahead. Neurology. 2019;93:72–79.

11. Mormino EC, Betensky RA, Hedden T, Schultz AP, Ward A, Huijbers W, et al. Amyloid and APOE 4 interact to influence short-term decline in preclinical Alzheimer disease. Neurology. 2014;82:1760–1767.

12. Mormino EC, Betensky RA, Hedden T, Schultz AP, Amariglio RE, Rentz DM, et al. Synergistic Effect of β-Amyloid and Neurodegeneration on Cognitive Decline in Clinically Normal Individuals. JAMA Neurol. 2014;71:1379.

13. Sperling RA, Rentz DM, Johnson KA, Karlawish J, Donohue M, Salmon DP, et al. The A4 Study: Stopping AD Before Symptoms Begin? Science Translational Medicine. 2014;6:228fs13-228fs13.

14. Sperling RA, Aisen PS, Beckett LA, Bennett DA, Craft S, Fagan AM, et al. Toward defining the preclinical stages of Alzheimer's disease: Recommendations from the National Institute on Aging-Alzheimer's Association workgroups on diagnostic guidelines for Alzheimer's disease. Alzheimer's & Dementia. 2011;7:280–292.

15. Sperling R, Mormino E, Johnson K. The Evolution of Preclinical Alzheimer's Disease: Implications for Prevention Trials. Neuron. 2014;84:608–622.

16. Montal V, Vilaplana E, Alcolea D, Pegueroles J, Pasternak O, González-Ortiz S, et al. Cortical microstructural changes along the Alzheimer's disease continuum. Alzheimer's & Dementia. 2018;14:340–351.

17. Montal V, Vilaplana E, Pegueroles J, Bejanin A, Alcolea D, Carmona-Iragui M, et al. Biphasic cortical macro- and microstructural changes in autosomal dominant Alzheimer's disease. Alzheimers Dement. 2020. 16 November 2020. https://doi.org/10.1002/alz.12224.

18. Le Bihan D. Looking into the functional architecture of the brain with diffusion MRI. Nat Rev Neurosci. 2003;4:469–480.

19. Vogt NM, Hunt JF, Adluru N, Dean DC, Johnson SC, Asthana S, et al. Cortical Microstructural Alterations in Mild Cognitive Impairment and Alzheimer's Disease Dementia. Cerebral Cortex. 2020;30:2948–2960.

20. Weston PSJ, Simpson IJA, Ryan NS, Ourselin S, Fox NC. Diffusion imaging changes in grey matter in Alzheimer's disease: a potential marker of early neurodegeneration. Alz Res Therapy. 2015;7:47.

21. Torso M, Bozzali M, Zamboni G, Jenkinson M, Chance SA, for the Alzheimers Disease Neuroimage Initiative. Detection of Alzheimer's Disease using cortical diffusion tensor imaging. Hum Brain Mapp. 2020:hbm.25271.

22. Vilaplana E, Rodriguez-Vieitez E, Ferreira D, Montal V, Almkvist O, Wall A, et al. Cortical microstructural correlates of astrocytosis in autosomal-dominant Alzheimer disease. Neurology. 2020;94:e2026–e2036.

23. Weston PSJ, Poole T, Nicholas JM, Toussaint N, Simpson IJA, Modat M, et al. Measuring cortical mean diffusivity to assess early microstructural cortical change in presymptomatic familial Alzheimer's disease. Alz Res Therapy. 2020;12:112.

24. Illán-Gala I, Montal V, Borrego-Écija S, Vilaplana E, Pegueroles J, Alcolea D, et al. Cortical microstructure in the behavioural variant of frontotemporal dementia: looking beyond atrophy. Brain. 2019;142:1121–1133.

25. Illán-Gala I, Montal V, Pegueroles J, Vilaplana E, Alcolea D, Dols-Icardo O, et al. Cortical microstructure in the amyotrophic lateral sclerosis-frontotemporal dementia continuum. Neurology. 2020:10.1212/WNL.0000000000010727.

26. Dagley A, LaPoint M, Huijbers W, Hedden T, McLaren DG, Chatwal JP, et al. Harvard Aging Brain Study: Dataset and accessibility. NeuroImage. 2017;144:255–258.

27. Papp KV, Rentz DM, Orlovsky I, Sperling RA, Mormino EC. Optimizing the preclinical Alzheimer's cognitive composite with semantic processing: The PACC5. Alzheimer's & Dementia: Translational Research & Clinical Interventions. 2017;3:668–677.

28. Fischl B, Dale AM. Measuring the thickness of the human cerebral cortex from magnetic resonance images. Proceedings of the National Academy of Sciences. 2000;97:11050–11055.

29. Desikan RS, Ségonne F, Fischl B, Quinn BT, Dickerson BC, Blacker D, et al. An automated labeling system for subdividing the human cerebral cortex on MRI scans into gyral based regions of interest. NeuroImage. 2006;31:968–980.

30. Beer AL, Plank T, Meyer G, Greenlee MW. Combined diffusion-weighted and functional magnetic resonance imaging reveals a temporal-occipital network involved in auditory-visual object processing. Front Integr Neurosci. 2013;7.

31. Wu M, Lu LH, Lowes A, Yang S, Passarotti AM, Zhou XJ, et al. Development of superficial white matter and its structural interplay with cortical gray matter in children and adolescents: Development of SWM in Children and Adolescents. Hum Brain Mapp. 2014;35:2806–2816.

32. Coalson TS, Van Essen DC, Glasser MF. The impact of traditional neuroimaging methods on the spatial localization of cortical areas. Proc Natl Acad Sci USA. 2018;115:E6356–E6365.

33. Jones D, Symms M, Cercignani M, Howard R. The effect of filter size on VBM analyses of DT-MRI data. NeuroImage. 2005;26:546–554.

34. Greve DN, Fischl B. Accurate and robust brain image alignment using boundary-based registration. Neuroimage. 2009;48:63–72.

35. Johnson KA, Schultz A, Betensky RA, Becker JA, Sepulcre J, Rentz D, et al. Tau positron emission tomographic imaging in aging and early Alzheimer disease: Tau PET in Aging and Early AD. Ann Neurol. 2016;79:110–119.

36. Johnson KA, Gregas M, Becker JA, Kinnecom C, Salat DH, Moran EK, et al. Imaging of amyloid burden and distribution in cerebral amyloid angiopathy. Ann Neurol. 2007;62:229–234.

37. Rousset OG, Ma Y, Evans AC. Correction for partial volume effects in PET: principle and validation. J Nucl Med. 1998;39:904–911.

38. Hanseeuw BJ, Betensky RA, Schultz AP, Papp KV, Mormino EC, Sepulcre J, et al. Fluorodeoxyglucose metabolism associated with tau-amyloid interaction predicts memory decline: Tau, Amyloid, FDG, and Memory in Normal Aging. Ann Neurol. 2017;81:583–596.

39. Scott MR, Hampton OL, Buckley RF, Chhatwal JP, Hanseeuw BJ, Jacobs HIL, et al. Inferior temporal tau is associated with accelerated prospective cortical thinning in clinically normal older adults. NeuroImage. 2020;220:116991.

40. Hanseeuw BJ, Betensky RA, Jacobs HIL, Schultz AP, Sepulcre J, Becker JA, et al. Association of Amyloid and Tau With Cognition in Preclinical Alzheimer Disease: A Longitudinal Study. JAMA Neurol. 2019;76:915.

41. Rabin JS, Neal TE, Nierle HE, Sikkes SAM, Buckley RF, Amariglio RE, et al. Multiple markers contribute to risk of progression from normal to mild cognitive impairment. NeuroImage: Clinical. 2020;28:102400.

42. van der Kant R, Goldstein LSB, Ossenkoppele R. Amyloid-β-independent regulators of tau pathology in Alzheimer disease. Nat Rev Neurosci. 2020;21:21–35.

43. Harrison TM, Du R, Klencklen G, Baker SL, Jagust WJ. Distinct effects of beta-amyloid and tau on cortical thickness in cognitively healthy older adults. Alzheimer’s & Dementia. 2020:alz.12249.

44. Papp KV, Buckley R, Mormino E, Maruff P, Villemagne VL, Masters CL, et al. Clinical meaningfulness of subtle cognitive decline on longitudinal testing in preclinical AD. Alzheimers Dement. 2020;16:552–560.

Connectomic-Genetic Gradients Within the Tau Spreading Backbone of the Aging Brain

Victor Montal[a,b,c]; Ibai Diez[a,d;] Chan-Mi Kim[a]; William Orwig[a]; Elisenda Bueichekú[a]; Raquel Gutiérrez-Zúñiga[a], Alexandre Bejanin[b,c]; Jordi Pegueroles[b,c]; Oriol Dols-Icardo[b,c]; Patrizia Vannini[d,e]; Georges El-Fakhri[a]; Keith A. Johnson[a]; Reisa A. Sperling[d]; Juan Fortea[b,c]; Jorge Sepulcre[a,d]

(a) Gordon Center for Medical Imaging, Department of Radiology, Massachusetts General Hospital and Harvard Medical School, Boston, Massachusetts, USA; (b) Memory Unit, Department of Neurology, Hospital de la Santa Creu i Sant Pau, Biomedical Research Institute Sant Pau, Universitat Autonoma de Barcelona, Barcelona, Spain; (c) Center of Biomedical Investigation Network for Neurodegenerative Diseases (CIBERNED), Madrid, Spain; (d) Athinoula A. Martinos Center for Biomedical Imaging, Massachusetts General Hospital and Harvard Medical School, Charlestown, Massachusetts, USA; (e) Center for Alzheimer research and treatment, Department of Neurology, Brigham and Women's Hospital, Harvard Medical School, Boston, MA

In preparation (2021)

ABSTRACT

A key hallmark of Alzheimer Disease (AD) pathology is the accumulation of tau protein in the form of neurofibrillary tangles across large-scale networks of the human brain cortex. Currently, it is still unclear how tau accumulates within specific cortical systems, and whether in situ genetic traits play a role in this circuit-based propagation progression. In this study, using two independent cohorts of cognitively healthy older participants, we reveal the backbone of tau spreading and its connectomic intersections with high-resolution transcriptomic genetic data. We observed that specific connectomic-genetic gradients exist along the tau spreading network. Particularly, we identified 577 genes that significantly accompany the spatial spreading of tau; a set of genes in which APOE and glutamatergic synaptic genes (e.g. SLC1A2) play a central role. Thus, our study characterizes neurogenetic topological vulnerabilities in distinctive brain circuits of tau spreading and suggests that drug development strategies targeting the gradient expression of this set of genes should be explored to help stop or prevent the accumulation of tau.

INTRODUCTION

The most common form of dementia, Alzheimer Disease (AD) is one of the biggest public health challenge today. Moreover, its prevalence is expected to double in the coming 20 years increasing its burden on society[1]. AD is characterized by the abnormal accumulation of amyloid and tau, which either alone or more probably in combination, might be among the most significant factors of disease progression. Advances in the development of novel high-affinity radiolabels have enabled the study of tau accumulation in vivo[2]. Specifically, tau-PET (also named FTP-PET for the specific Flortaucipir tracer) has been reported to detect early local tau pathology in preclinical AD[3], showed good concordance with histopathological data, and accurately recapitulated the Braak neuropathological staging of neurofibrillary tangles (NFT)[2,4,5]. Such pathological accumulation of tau has been directly linked to longitudinal atrophy[6], and is predictive of memory decline and clinical progression[7]. Thus, it is crucial to better understand, preemptively detect, and individually predict tau accumulation in order to treat AD.

The pathological accumulation of amyloid and tau are not randomly distributed but rather follow a stereotypical spatial pattern that follows large-scale networks, suggesting that AD is a network-afflicting brain disease. Accordingly, recent studies have focused not only on signal intensity changes, but also on the large-scale network relationship of molecular binding affinity between distributed brain regions using both dimensionality reduction approaches[8,9] and high-resolution network analyses[3,10]. However, it is still unknown whether tau accumulation relates to cerebral local in situ genetic traits that might cause or influence the circuit-based propagation of tau. Recent research has focused on analyzing the genetic and metabolic fingerprint that might characterize a regional vulnerability in the most affected areas[11,12]. Concerted efforts have been directed to study the local region properties using post-mortem data, from cellular morphology to cell-type specific gene expression[13,14]. Thus, previous neuroimaging-genetic studies have mainly focused on the spatial relationship between gene expression and diverse neuroimaging measures but have neglected the connectomic signatures of AD-related pathology or the topographic integration between the large scale networks underlying tau propagation and the local constitutive genetic expression patterns.

Here, we aimed to characterize the network stereotypical pattern of tau accumulation and the spatial gene expression gradients across the cortical mantle suggesting a regional

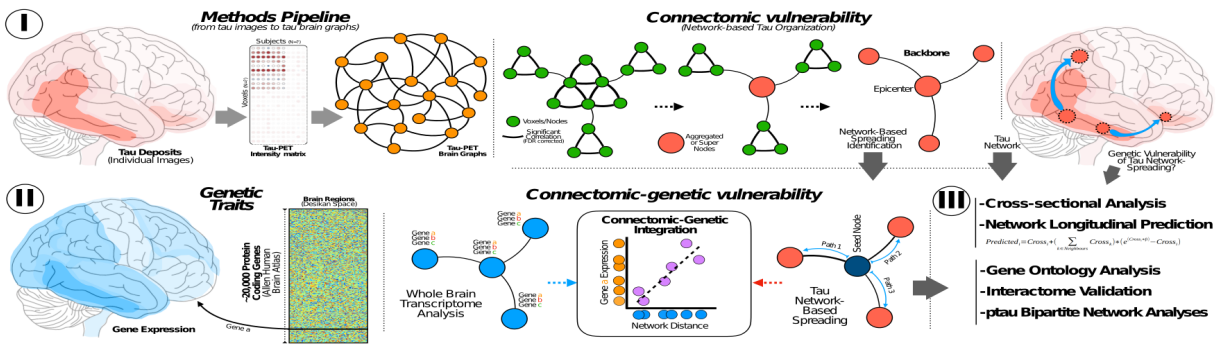

Figure 1. Methodological summary. I) For each pair of voxels of tau-PET (or FTP-PET), we computed the pairwise Pearson correlation to obtain a population connectivity (adjacency) matrix to further apply the node-aggregation algorithm to retrieve the Tau-PET network backbone. II) AHBA dataset with transcriptome information from 10,027 genes in 180 regions from the Glasser atlas are projected to the super-nodes from the NAA to investigate the relationship between gene expression and network-distance from the left entorhinal. III)

vulnerability that accompanies tau propagation. Using two independent samples of cognitively unimpaired participants from the Harvard Aging Brain Study (HABS) and Alzheimer's Disease Neuroimaging Initiative (ADNI) cohorts, we first developed a novel graph theory algorithm to obtain the backbone tau-PET network across cortical areas in the aging brain and assess its utility to predict one and two-year tau accumulation. This data-driven strategy led us to identify and analyze regions that encompass the whole continuum of the Braak staging. Thereafter, we studied how the network-wise propagation of tau within the backbone network was related to the local expression of genes using the AHBA high-resolution transcriptome dataset[15]. Such analysis allowed us to identify a set of genes, representing the connectomic-genetic gradients of gene expression that characterize the regional vulnerability along the tau spreading network. We then studied the biological significance and potential implications of these protein coding genes based on their genetic functional components, interactomic properties and relationship with NFT-related proteins. The integration of large-scale connectomic information with high-resolution gene expression data allowed us to describe gradients of neurogenetic vulnerability of tau spreading in the human cerebral cortex.

RESULTS

Tau-PET Backbone-Graph Follows Tau Accumulation Patterns of preclinical AD

Using cross-sectional data from a subset of amyloid positive cognitively unimpaired participants from HABS (N=19) and ADNI (N=52) with no follow-up data, we studied the FTP-PET signal changes in preclinical AD across different brain systems using a graph theory approach. We developed a node-aggregation algorithm (NAA, Fig 1-I) that aggregates groups of nodes with converging information, into a set of regions of interest, here referred to as super-nodes, that characterize the system information of in vivo tau accumulation in preclinical AD (online methods). By applying the NAA, we obtained 58 super-nodes encompassing medial and lateral temporal regions, cuneus and precuneus, and posterior cingulate cortex, temporoparietal areas, and portions of the inferior frontal

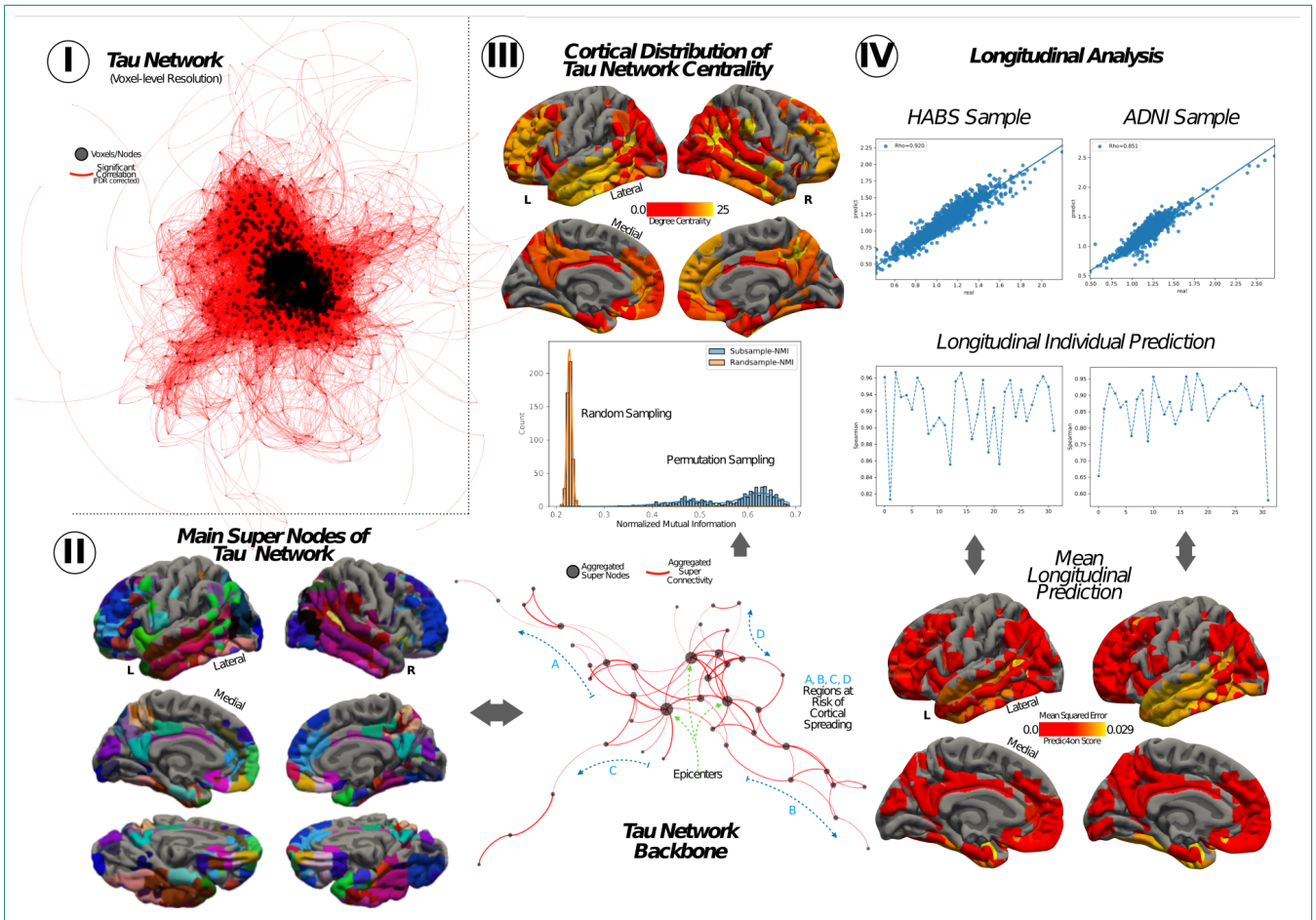

Figure 2. Tau-PET network backbone. I) The initial voxel-wise network. II) The 58 nodes resulting from the Node-Aggregation Algorithm (NAA), its network representation and the histogram resampling the robustness of our results over 500 permutations with a subset of 50 participants. III) The topographical degree centrality measure of the tau network backbone. IV) Scatterplot of the association between predicted and real Tau-PET, the individual correlation for each of the participants and the MSE error per ROI.

cortex, including areas in the whole spectrum of Braak staging (Fig 2-II). Importantly, we confirmed the robustness of the super-nodes size and localization with a permutation approach using 500 random subsets of 50 participants from the original sample and assessing their overlap with the original network (Fig 2-II). The similarity between the permutations from the subsets were significantly larger compared to the null distribution created from 500 permutations of synthetic super-nodes (online methods). When studying the importance of each super-node in the network, as measured by the degree centrality, we identified hub super-nodes with a number of connections over the mean, including the middle temporal gyrus, inferior temporal gyrus and precuneus (Fig 2-III).

Next, we assessed the accuracy of the prediction of regional tau accumulation in a non-overlapping longitudinal cohort from HABS (N=32; 2-year follow-up) and ADNI (N=32; 1-year follow-up). Compared to other approaches that use the

(structural or functional) connectome as a proxy to predict the longitudinal tau accumulation, we instead took advantage of the previously computed FTP-PET backbone graph. Overall, when considering the pool of all super-nodes mean FTP-PET signal from all the participants, we found a high association between the real longitudinal FTP-PET and the predicted FTP-PET, for both the HABS cohort (rho=0.92) and in ADNI (rho=0.85). We also found high associations at the individual level for both cohorts (HABS= 0.92+/-0.04, ADNI=0.87+/-0.08). We then studied the reliability in the regional prediction of tau accumulation, assessing the mean squared error (MSE) between predicted and real FTP-PET signal for each super-node, in each cohort separately. The super-node with the maximum error was the left lateral temporal gyrus, with a MSE value of 0.026 in ADNI and 0.028 in HABS (Fig 2-IV).

Table 1. Sample Characteristics

	HABS	ADNI
Sample (N)	51	85
Sample long (N)	32	32
Age (median, IQR)	79.2 [73.7-82.9]	74.8 [69.6-79.1]
Sex (female %)	62.74	57.64
metaROI FTP-PET, SUVr (median, IQR)	1.15 [1.11-1.22]	1.19 [1.15-1.25]

Genetic Vulnerability of Tau Network Spreading

Next, we combined high-resolution gene expression data from the AHBA with the previously computed FTP-PET backbone network to identify which genes showed a gradient of transcriptomic expression related to the network-based tau spreading. For each super-node, we computed the network distance to the left entorhinal, where those regions with shorter distance regions would be next regions to be affected by tau spreading (online methods). When we assessed the association between each super-node distance from the seed and the transcriptome expression from the 10,027 genes in the AHBA, we identified a set of 744 statistically significant associations (Fig 3-II; FDR < 0.001). The expression of 414 of the genes were positively associated with network-based distance to seed with a Spearman rho>0.55, whereas 330 genes were negatively associated with network-based distance with a Spearman rho < -0.56. Of note, all obtained genes remained significant when applying a permutation-based approach where the backbone FTP-PET network links where randomly interchanged to generate random maps of different spreading patterns, which suggests that the relationship between the gradient of gene expression and the network-wise distance was dependent on the FTP-PET backbone structure (Suppl. Material 1). Among the 744 genes, 167 could not be validated with the transcriptome data of the ROS/MAP participants – a cohort with bulkRNA sequencing of more than 700 participants in the continuum of AD-, and were thus excluded from further analyses. From the resulting 577 genes, 122 were significantly differentially expressed when comparing HC vs AD in the ROS/MAP cohort.

Interactome and Gene Ontology Analyses

To assess the biological meaning of our 577 tau network-related genes (TNG), we focused on their molecular physical interactions and cellular component overrepresentations (Fig3). The Panther GO analysis revealed a set of enriched genes involved in neuron structure (main axon, dendritic spine, and neuronal cell body), the synapsis (postsynaptic density and presynaptic membrane) and the Schaffer collateral in the hippocampi (FWE < 0.05; Fold Enrichment > 2). We then analyzed the importance of each gene within the TNG-interactome network using a curated set of gene-

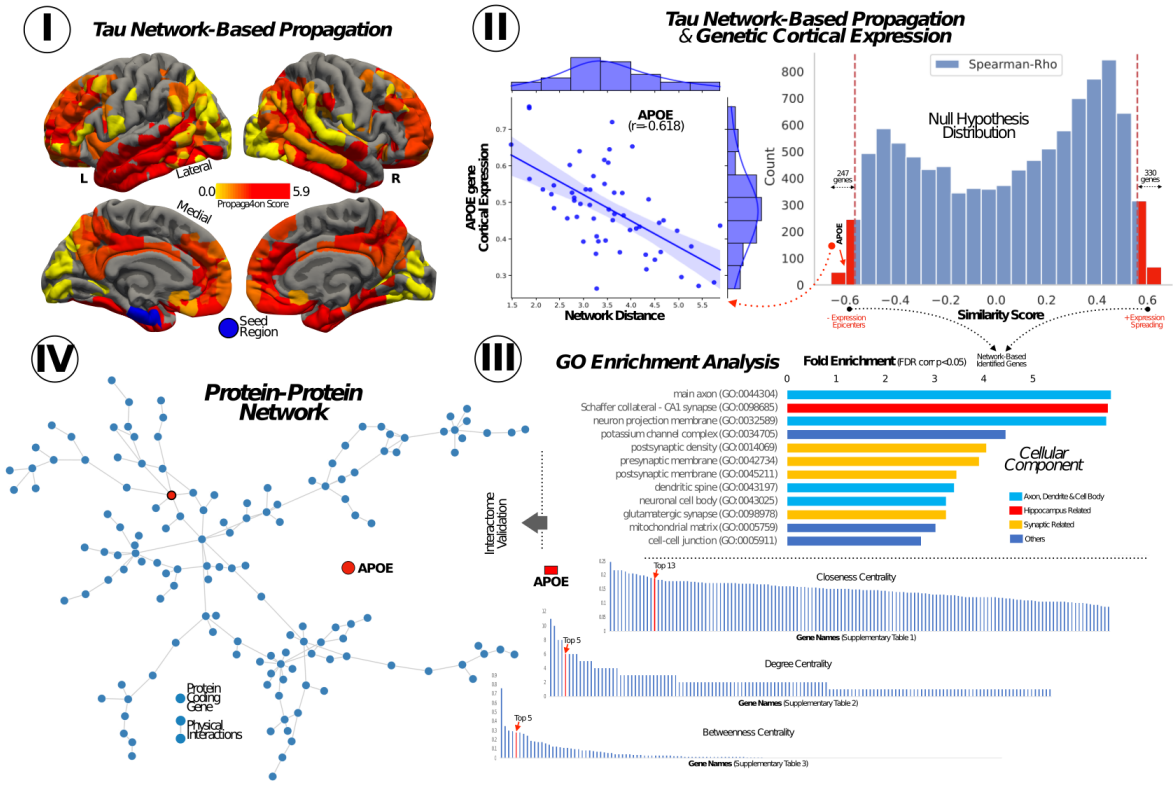

Figure 3. Connectomic-genetic gradient within the Tau-PET network. I) Surface representation of the network-based distance of each super-node to the left entorhinal. II) Histogram of the association between gene expression and network-based distance for 10,027 genes and the scatterplot for APOE. III) Cellular components over-representation based on Panther-GO. IV) Gene-gene network based on physical interaction and the centrality measure for its genes

gene physical interaction from Genemania (online methods). We found that MAPK3 (top1) and APOE (top6) had a central role in these genetic interactions, being the genes with higher degree, betweenness and closeness centrality (Suppl Table 1). We validated our results studying the relationship between our 577 TNG and the 74 pTau-interactome genes recently described by Drummond and colleagues 16, computing a bi-partite network to display the relationship between those two sets of genes (online methods). We found that most of the TNG were associated with pTau-interactome genes (Fig 4-I). Importantly, these associations were non-random, as shown in the ad-hoc permutation-based analyses (Fig 4-II, online methods), suggesting a high affinity between the TNG and pTau-interactome genes, compared to random neuro-genes. Specifically, the mean degree and the unique number of genes interconnecting the TNG to the pTau-interactome were significantly higher (a mean degree of 0.8 and 108

unique genes compared to lower than 0.3 mean degree and lower than 65 unique genes for the random permutations). We did not find that these associations were driven by a group of genes in any specific cellular component GO-term. We also studied which TNG were more directly related to more protein expression in NFT, as measured in Drummond et al. We found that APOE and SLC1A2, the two only TNG related to MAPT, had a strong influence in the level of NFT protein expression (Fig 4).

DISCUSSION

In this study, using two independent cohorts of cognitively unimpaired older participants (HABS and ADNI), we characterized the in vivo accumulation of tau pathology in large-scale networks using a novel graph theory approach and demonstrated its potential to be used as a proxy for the prediction of longitudinal tau accumulation in preclinical AD. Moreover, we integrated the tau large-scale network information with high-resolution transcriptomic genetic data to characterize the gradient of neurogenetic vulnerability related to the spreading of tau across brain circuits. We found that 577 genes specifically predispose the spread of tau; a set of genes in which APOE and glutamatergic synaptic genes (SLC1A2) have central roles.

Our study integrated high-resolution cortical gene expression information with neuroimaging connectome data to investigate the underlying biological pathways of AD-related pathology spreading. Several recent studies have focused on assessing the relationship between gene expression and both imaging signal intensity[17,18] and statistical differences[19,20]. For example, Grothe and collaborators (2018) showed that the topographic expression of APP and MAPT was related to amyloid accumulation and neurodegeneration in AD, respectively. Recently, our group expanded these results by studying the biological basis of both tau and amyloid propagation, finding an over-representation of genes associated with lipid metabolism 10. Our approach in the present manuscript builds on the aforementioned studies, but with a key innovation: we developed a method to integrate gene expression data into the FTP-PET network to study the association between them. Concretely, instead of assessing the relationship between signal intensity and gene expression, we integrated the network-based distance from the entorhinal cortex to all the subsequent regions, to evaluate if the network spreading of tau accumulation was related to a gradient of gene expression.

In contrast to the consensus in the literature that tau spreads in a prion-like manner, recent findings have cast doubt on the notion that all tau accumulation is only driven by cell-cell transmission. It has been suggested that tau accumulation could be a result of both spreading and local amplification/phosphorylation, in addition to local vulnerability[21,22]. For example, Meisl and colleagues (2020) have recently shown that the tau accumulation rate in animal models is more related to local amplification than seed spreading. In this sense, several studies have suggested a specific cellular/molecular vulnerability driving (or modulating) the downstream neurodegeneration (and tau spreading) process[13,23,24]. However, most studies have only assessed whether local regional vulnerability (i.e. study if the cellular-composition, genetic and molecular environment for a specific region) present such selectivity to accumulate tau. Thus, when integrating global-brain information, such genetic vulnerabilities have been studied using intensity maps, which do not account for biological spreading or the network-wise nature of tau accumulation. In the present study, we studied the gradient of change in the gene expression from healthy young individuals across several brain regions, in conjunction with the network of tau

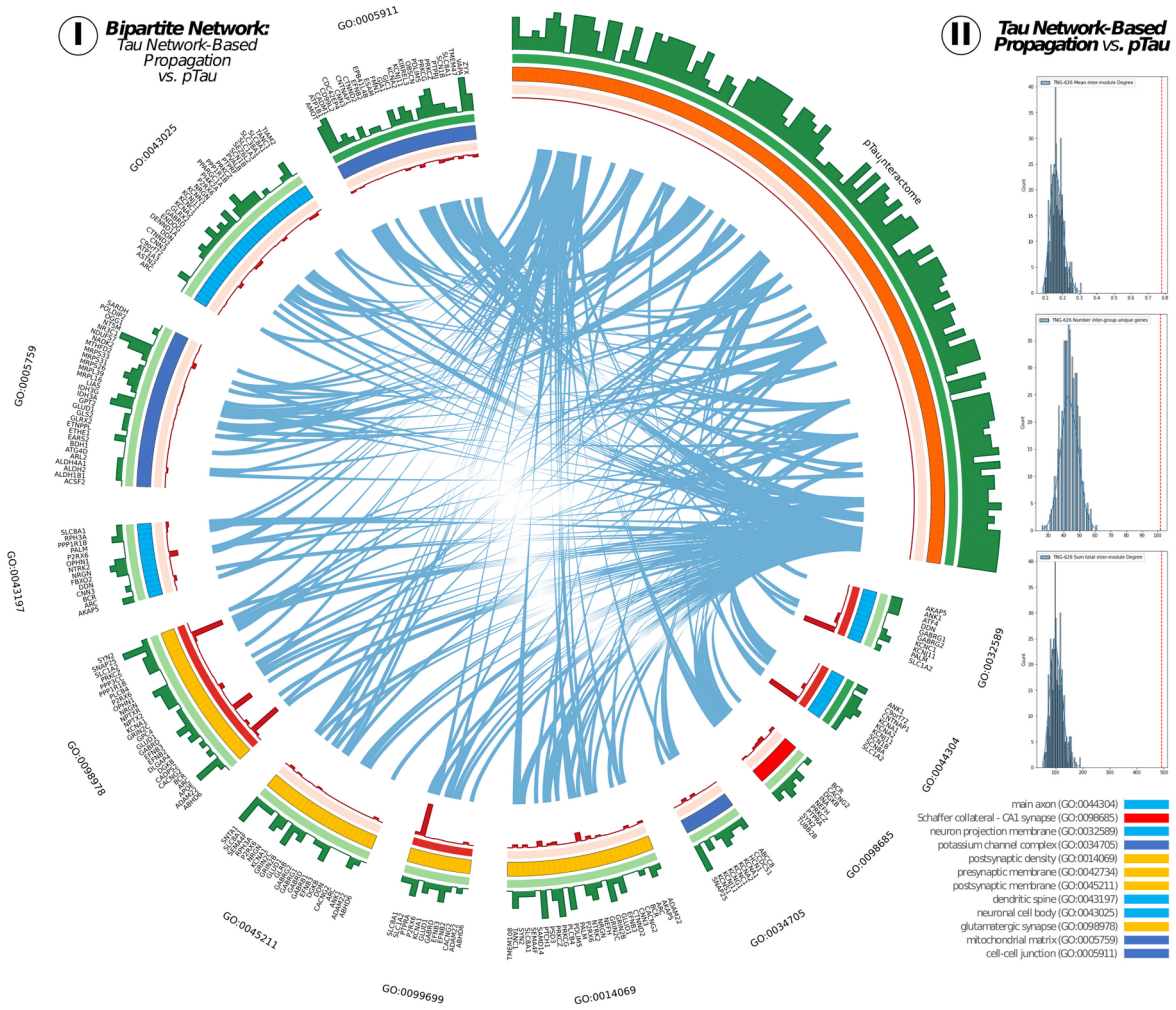

Figure 4. Tau network-related genes (TNG) are associated to pTau-interactome genes. I) The circular layout of the bi-partite network. Links between the TNG and pTau-interactome sets are shown in blue. Green bars represent the gene degree within each set and red bars represent the amount of protein expressed in NFT of the pTau-interactome connected to each TNG.

deposition, to disentangle the gradient genetic fingerprint of regional vulnerability leading to tau spread. We observed that the set of TNG is overrepresented by various genetic pathways suggesting regional vulnerability, such as glutamatergic synaptic ontologies. Previous research has described that glutamatergic excitatory neurons are more vulnerable to AD[25], and conversely, that the pathways of genes overexpressed in such neurons are strongly related to tau accumulation[13]. Here, we show that gene SLC1A2 (or EAAT2) is associated with tau network spreading and pTau genetic profiles. SLC1A2 is localized in the neuron and glia membrane and its main function is to clear glutamate from

the synaptic cleft. The association between SLC1A2 and tau is in agreement with the hypothesis that excitatory neurons are more vulnerable to tau pathology. Several studies have also pointed to its importance in cognitive decline where lower expression of this gene in astrocytes and neurons was associated to worse cognitive performance[26]. Additional studies using animal models and bioinformatic approaches have also identified SLC1A2 as a potential candidate for drug development in AD[27].

Whereas historically APOE has been more associated with amyloid pathology rather than with tau, we found that it has a central role in our TNG interactome, highlighting its potential relevance in the vulnerability of tau accumulation as well[10]. Moreover, our bipartite network analyses showed that APOE has a high indirect influence in the expression of proteins in NFT, due to its physical interaction with MAPT. Several recent studies have found a direct association between ApoE4 and the proliferation of tau in animal models[28]. In fact, the removal/reduction in ApoE, specifically ApoE expressed on astrocytes, has been shown to decrease tau accumulation and decrease tau-mediated neurodegeneration[29,30]. Such cellular vulnerability has also been recently reported in human neurons where ApoE drive selective neurodegeneration[31]. Importantly, both APOE and SLC1A2 showed a negative correlation between their expression and FTP-PET network-based distance, suggesting that early areas to accumulate tau might be more vulnerable due to higher basal expression of both genes, where a transcriptome alteration of their expression might have a stronger impact in tau accumulation. Our results would suggest that the stereotypical pattern of the spread of tau follow the gradient of expression of APOE and SLC1A2, where a pathological alteration of its expression could affect more severely, and earlier, those brain regions with higher expression and network-wise proximity to the entorhinal cortex.

Our investigations used network information to obtain a robust backbone representation of the FTP-PET network, aggregating groups of nodes which share connectivity profiles. As a result, we obtained a low dimensional connectome that overcomes previous limitation when studying topological and temporal tau alterations using high-dimensionality PET network studies, such as redundant link information (caused by inherent local smoothing of the data) and extensive computational resources. Notably, our method identified, using a sample of amyloid positive cognitively unimpaired individuals, a pattern of co-accumulation in both early Braak stages (e.g., entorhinal, or inferior temporal)[32] and neocortical regions affected at late Braak stages 2 suggesting that slight increases in FTP-PET in Braak V/VI might also be meaningful in early stages of the disease. We also propose that the backbone FTP-PET network might be a reliable proxy to predict longitudinal tau accumulation. Strongly grounded on the prion-like spreading of tau, several studies in the literature have proposed various propagation models to accurately predict longitudinal tau accumulation based on the structural or functional connectomes[33–36.] Contrary to such approaches, we explored the possibility to first, use data-driven backbone-nodes instead of cortical parcellation atlas - which are not generated from and for FTP-PET data - and second, use the backbone FTP-PET connectome as a proxy for the spreading of tau, instead of focusing on the structural or functional connectome. In this sense, we obtained high significant correspondence between the real and predicted longitudinal tau accumulation both at individual level and at region of interest level. Further work is nonetheless needed to validate this model in later stages of the disease, where the amount of accumulation of tau per year is increased.

Overall, our analyses identified a gradient gene-expression signature of cell-susceptibility to accumulate tau along the different Braak areas. Our results highlight the key role of neuron- and synapse-related genes, such as APOE and SLC1A2, in the stereotypical pattern of tau spread. Moreover, the multi-genetic findings presented in this study support recent views about the different patterns of spreading of tau, where substantial individual differences in the topological gene expression profile and its local vulnerability could explain the different pathways through which tau would propagate.

METHODS

Participants

We included a total of 490 participants from two large studies. We included 145 participants from our cohort, the Harvard Aging Brain Study (HABS, https://habs.mgh.harvard.edu/), a cohort of cognitive aging and preclinical AD recruited from the community conducted at Massachusetts General Hospital (MGH); and 345 cognitively unimpaired participants from the Alzheimer's Disease Neuroimaging Initiative (ADNI; http://adni.loni.usc.edu/), a multi-center study designed to accelerate the discovery of biomarkers indicating progression of Alzheimer's disease pathology. ADNI was launched in 2003 as a public– private partnership led by principal investigator M. W. Weiner. The primary goal of ADNI has been to test whether serial magnetic resonance imaging (MRI), PET, other biological markers and clinical and neuropsychological assessment can be combined to measure the progression of MCI and early-onset AD. For up-to-date information, see http://adni.loni.usc.edu.

At study entry, all the included participants were assessed as cognitively clinically normal, with clinical dementia rating value of zero. Participants were included based on the following inclusion criteria: i) baseline tau-PET, ii) baseline amyloid-PET and, iii) a structural T1-weighted MRI. We tested demographic study differences using the Mann-Whitney U Test and chi square test.

Structural MRI

Structural 3D T1-weighted were acquired in 3 Tesla scanner, using a magnetization-prepared rapid-acquisition gradient-echo (MPRAGE) sequence. The T1-weighted MPRAGE structural images had a resolution of at least 1.3 x 1.3 x 1.3 mm voxels. All the T1-weighted images were preprocessed with Freesurfer v6.0 (https://surfer.nmr.mgh.harvard.edu/) as previously described[37].

Tau PET

Tau burden was measured in both cohorts using the Flortaucipir (FTP-PET) tracer (formerly AV1451 or T807). Acquisition parameters for each study have been described elsewhere[2]. FTP was preprocessed using previously published in-house pipelines (Jorge Sepulcre et al. 2018). Briefly, we computed the SUVr parametric maps normalizing the FTP intensity by the mean cerebellar grey matter intensity. We co-registered the FTP map to T1 using Freesurfer's mri_coreg. We computed the T1-MNI registration using SPM12. We then normalized the FTP-PET SUVr maps to the MNI space concatenating the PET-T1 and the T1-MNI registration. All FTP-PET maps were down-sampled at the normalized space to 8-mm isotropic voxel to study the high-dimensional data without computational limitations. For subsequent analyses, and to discard cortical brain regions with off-target FTP-PET binding, we select only those voxels were the fitting of the FTP-PET signal for the whole sample of participants with a 2-component Gaussian Mixture Model outperformed the fitting of a single Gaussian, using the Akaike Information Criteria to compare

between both models[33] [Suppl. Fig 2]. This is founded in the idea that if a certain voxel is strongly contaminated by off-target binding, partial volume effect, or none of the included participants do present abnormal AD-related binding, data should show a skewed distribution (one gaussian). Voxels following this pattern were excluded for subsequent analyses. After visual inspection on the raw FTP-PET intensity image, and FTP-PET to T1 registration, we excluded 65 participants due to miss-alignment during the registration and low SNR quality of the raw FTP-PET images.

Amyloid PET

HABS participants were injected with 10-15 mCi 11C-PiB intravenously as a bolus and followed immediately by a 60-min dynamic PET scan in 3-D mode. PiB-PET images were co-registered to T1-MRI using mri_coreg from Freesurfer. Dynamic PIB-PET was modeled with a Logan model, using the cerebellar GM as reference region to generate parametric Logan DVR images. For each participant, we computed the amyloid burden as the mean from a cortical composite including frontal, lateral temporal, and parietal, and retrosplenial (FLR) regions as defined using the Desikan-Killiany atlas, as in previous studies[2]. PIB-PET positivity was computed using a threshold of Logan DVR > 1.2, previously computed in the HABS sample derived from a Gaussian mixture modeling[38]. For ADNI participants, we download the amyloid burden composite directly from their webpage (12 Feb 2020). Details for FBP-PET and FBB-PET acquisitions are described elsewhere (http://adni.loni.usc.edu/wp-content/uploads/2012/10/ADNI3_PET-Tech-Manual_V2.0_20161206.pdf). Briefly, FBP-PET and FBB-PET images were co-registered to the T1-MRI Freesurfer processed image and computed the weighted mean inside a cortical summary region that is made up of frontal, anterior/posterior cingulate, lateral parietal, lateral temporal regions, normalized by the signal intensity of the whole cerebellum to obtain an amyloid burden FBP-PET and FBB-PET SUVr scalar value[39]. We used a previous validated threshold of FBP-PET > 1.11 and FBB-PET > 1.08 to assess amyloid positivity. We end up with 136 amyloid positive participants across the two samples.

Tau-PET and Backbone Graphs

Contrary to conventional intensity-based PET imaging studies, recent methodological advances have allowed the study of FTP-PET signals across different brain systems using high-dimensional network-based approaches 3,10. Due to the intrinsic shared properties, as well as local gaussian smoothing of the PET signal, nodes in high-dimensional networks might be interrelated between them, sharing link information, and including redundancy in the analyses which result into technical caveats (such as computational time or difficulties to get significant results due to high-dimensional multiple comparisons corrections). In the present study, we developed a novel node-aggregation algorithm (NAA) with the intention of i) integrating all the converging information and ii) obtaining a backbone or minimal graph characterization of the FTP-PET network. Moreover, such an approach will result in a set of meaningful data-driven ROIs for tau uptake, compared to conventional atlas-based approaches, where the delineation of the ROIs might be mining-less for the study of in vivo tau pathology.

Computation of high-dimensional FTP-PET association matrix (or connectivity matrix) has been explained in detail elsewhere[10]. Briefly, for each pair of voxels within the previously obtained FTP-PET grey matter mask, we computed the Pearson r correlation and its corresponding p-value using the cross-sectional sample of participants (N=71). We corrected for multiple comparisons using a

threshold of FDR q < 0.005 and selected the top 20% correlations. The resulting association matrix was used as input to the NAA. The aim of NAA is to iteratively identify the set of nodes with maximum shared information and aggregate them. Thus, we first computed the number of 2-simplex (i.e., set of 3 nodes interconnected) for each node of the high-dimensional matrix using equation 1:

$$2-Simplex_j = \sum_{k \in N} [\sum_{i \in N} A_{ji} * A_{ik}] * bin(A_{jk})$$

where N is the total number of nodes, A is the voxel-wise adjacency matrix and j,k,i are nodes. After computing the number of 2-simplex per voxel, we, searched for the node with highest number of 2-simplex and aggregate all the interconnected nodes into a new super-node (Fig 1). We repeated the aggregation of nodes iteratively, using the original adjacency matrix, till there is not any set of 2-simplex in the network. Afterwards, we computed the edge/link between two super-nodes as the mean of the correlation between all the nodes that are part of the super-nodes, which resulted into the minimal FTP-PET network. We studied the stability of the resulting network with a permutation approach by re-running the algorithm 500 times in a subset of 50 random participants and computed the spatial normalized Mutual Information (NMI) comparing the permuted-sample vs original sample network. To estimate the significance of our findings, we created a null-distribution generating 500 synthetic maps of super-node (same extension as the original super-nodes) to evaluate the NMI between random maps and the original backbone FTP-PET network. We studied the resulting minimal network computing each super-node degree as the sum of weighted links that arise from each super-node (Fig 2). For visualization purposes, we projected the set of super-nodes and the degree map to Freesurfer fsaverage standard space using mri_vol2surf.

Longitudinal Individual Prediction of tau-PET Accumulation

A subset of 64 participants had longitudinal FTP-PET data (32 HABS participants at 2 years, 32 ADNI participants at 1 year follow-up). We designed a propagation model grounded on recent in vivo findings[36,40], but instead of using structural or functional connectome information to define the connectivity between different regions, we used as a propagation skeleton the FTP-PET network driven by the NAA approach. We defined the longitudinal model propagation as:

$$longTau_j^p = crossTau_j^p + (\sum_{k \in N} crossTau_j^p * A_{jk}) * (e^{crossTau_i^p * \beta} - crossTau_j^p)$$

where j refers to super-node, p to participant, A is the adjacency matrix, crossTau is the cross-sectional mean FTP-PET on super-node j and participant p, and BETA is the regularization parameter. We estimated the BETA parameter using the Powell optimizer as implemented in the SciPy python package. We performed three statistical analyses to evaluate the performance of our model to predict longitudinal data. For each cohort, we first computed the Spearman Rho between the predicted and real longitudinal FTP-PET pooling all the super-nodes from all the participants together. We then estimated the intra-participant agreement using the Spearman Rho coefficient to evaluate individually the accuracy of the model. Finally, we assessed the accuracy of the prediction on a regional basis, computing the mean standard error (MSE) for each one of the super-nodes, displaying the values in the cortical surface.

Network-Brain-Gene Association Relationship

In the present study we have developed a novel approach that integrates spatial high-resolution gene expression within the network structure of tau accumulation. This strategy brings a novel framework to incorporate gene expression data into brain connectivity circuits, rather than just investigate spatial overlaps between transcriptomic and neuroimaging phenotypes. The rationale behind such an approach is to study whether the network of tau spreading from an initial seed point (entorhinal) is also reflected in a gradient of constitutive gene expression within the network, reflecting brain vulnerability to tau propagation. We used a surface anatomical transformation of the cortical transcription profiles of 10027 protein-coding genes that fullfilled a quality control filter, based on 58,692 measurements of gene expression in 3,702 brain samples obtained from the left hemisphere of 6 adult human participants of the AHBA[41,42]. Gene expression was averaged within 180 cortical areas from the Glasser et al atlas[43]. Based on previous reports of hemisphere-symmetry in the cortical gene expression, we mirrored the left hemisphere gene expression to the right hemisphere. Since our NAA approach creates data-driven ROIs that do not match the Glasser parcellation, we computed the gene expression within each super-node as the weighted average of each region from the Glasser atlas that co-localized with each super-node, resulting into a gene expression matrix of 58 regions (the number of super-nodes in the backbone FTP-PET network) by 10027 genes. To assess the network-based spreading, we selected as seed with the highest degree of entorhinal overlap in our data, namely the left hemisphere entorhinal, previously identified as a starting point of tau-pathology spreading in AB positive individuals[32], and we computed the distance between nodes using the inverse weight of the links, and based on Dijsktra algorithm, which resulted in a single value of network distance from each super-node to the entorhinal. Then, for each gene, we computed the Spearman Rho coefficient between gene expression and network distance. We selected the significant correlations using a Benjamin-Hochberg FDR $q < 0.001$. Moreover, we studied if the pattern of genes significantly associated with distance from the entorhinal were network-topography dependent, generating a null-model computation of the distance and the calculation of the Spearman Rho after permuting randomly the super-node edges 1000 times.

Bulk RNAseq Differential Expression

We included bulkRNAseq gene expression derived from the dorsolateral prefrontal cortex of 792 participants from the ROS/MAP cohort. A detailed description of the cohort and patient characteristics can be found elsewhere[44]. Participants were categorized as HC (N=260), mild cognitive impaired (N=206) or AD (N=326) based on clinical status. Details on sample collections, tissue and RNA preparation and quality control are provided in previously published work[44]. We downloaded the ".bam" files for each participant data from the ROS/MAP repository (https://adknowledgeportal.synapse.org/Explore/Studies/DetailsPage?Study=syn3219045). To assess the deferentially expressed (DE) genes set, we compared gene expression from 55765 genes of HC against AD using DESeq2 (Love, Huber, and Anders 2014), controlling by age at death, sex, education, library preparation and library batch and extra batch effects as detected by the SVAseq package[45]. We considered significant genes with p-value after correction with FDR $q < 0.05$, as usually done in DE analyses[46].

Tau Network-Based Genes Interactome and Gene Ontology Analysis

We characterize the biological meaning of gene sets from the tau network-based genes (TNG) using Gene Ontology (GO) cellular component profile (Panther DB; default set of parameters[47]). Then, we analyzed the relationship between TNG imputing their interactome using Genemania[48] which returned the gene-gene network based on a curated list of gene physical interaction. From the resulting network, we compute the relevance of each gene computing three centrality measures: closeness, degree and betweenness using Cytoscape[49].

Tau Network-Based Genes and NFT Bipartite Network

Finally, we investigate the relationship between our TNG results (577 genes) and an overlapping NFT-pTau affinity purification-mass spectrometry derived profile that has recently been reported as the pTau-interactome (74 genes)[16]. First, using Genemania, we create the bi-partite network of the relationship between the TNG and the pTau-interactome genes. We studied the relationship between the two sets of genes using three measures: i) mean inter-set degree, ii) number of genes inter-connecting from each gene-set and iii) the total sum degree. To estimate their significance, we generated a null distribution of these parameters using a random set of of neuro-genes obtained from the bulkRNAseq data from the ROS/MAP cohort: 577 TNG vs 74 random genes. Finally, using the information of the amount of protein expressed by each gene of the pTau-interactome in NFTs, as published in Drummond et al, we computed the importance of each of the TNG as the mean of expressed protein for each of its connected genes in the pTau-interactome. This is grounded in the idea that one gene in the TNG might be more relevant to tau pathology if it is related to a gene that does express a lot of proteins in the NFT. We used CIRCOS[50] to visualize the inter-group links, the intra-group degree (green histogram), the GO-term mean inter-set degree and the protein-based importance of each gene (red-histogram). For visualization purposes, we only plot genes present in the GO-terms, which resulted in some genes being displayed more than once.

ACNOWLEDGEMENTS

We thank the investigators and staff of the Harvard Aging Brain Study, Massachusetts Alzheimer's Disease Research Center, the individual research participants, and their families and caregivers. We also thank the PET Core of the MGH, the Harvard Center for Brain Science Neuroimaging Core and the Athinoula A. Martinos Center for biomedical imaging support. This project is supported by the US National Institute of Aging grants (R01AG061811, and R01AG061445 to J.S. and R01AG061083 to P.V. and J.S). Moreover V.M was funded by the Institute of Health Carlos III (FI18/00275) and by the Centro Investigacion Biomedica en Red Enfermedades Neurodegenerativas (CIBERNED). Dr Bejanin was supported by a Miguel Servet I grant (CP20/00038) from the Carlos III Health Institute.

REFERENCES

1. Zang, Z., Lin, P. & Levey, A. Monetary Costs of Dementia in the United States To. N. Engl. J. Med. 369, 487–489 (2013).

2. Johnson, K. A. et al. Tau positron emission tomographic imaging in aging and early Alzheimer disease. Ann. Neurol. 79, 110–119 (2016).

3. Sepulcre, J. et al. In vivo Tau, Amyloid and Grey Matter Profiles in the Aging Brain. J. Neurosci. In press, 7364–7374 (2016).

4. Schöll, M. et al. PET Imaging of Tau Deposition in the Aging Human Brain. Neuron 89, 971–982 (2016).

5. Marquié, M. et al. [F-18]-AV-1451 binding correlates with postmortem neurofibrillary tangle Braak staging. Acta Neuropathol. 134, 619–628 (2017).

6. La Joie, R. et al. Prospective longitudinal atrophy in Alzheimer's disease correlates with the intensity and topography of baseline tau-PET. Sci. Transl. Med. 12, 1–13 (2020).

7. Sperling, R. A. et al. The impact of amyloid-beta and tau on prospective cognitive decline in older individuals. Ann. Neurol. 85, 181–193 (2019).

8. Hoenig, M. C. et al. Networks of tau distribution in Alzheimer's disease. Brain 141, 568–581 (2018).

9. Ossenkoppele, R. et al. Tau covariance patterns in Alzheimer's disease patients match intrinsic connectivity networks in the healthy brain. NeuroImage Clin. 23, 101848 (2019).

10. Sepulcre, J. et al. Neurogenetic contributions to amyloid beta and tau spreading in the human cortex. Nat. Med. (2018) doi:10.1038/s41591-018-0206-4.

11. Mrdjen, D. et al. The basis of cellular and regional vulnerability in Alzheimer's disease. Acta Neuropathol. 138, 729–749 (2019).

12. Fu, H., Hardy, J. & Duff, K. E. Selective vulnerability in neurodegenerative diseases. Nat. Neurosci. 21, 1350–1358 (2018).

13. Leng, K. et al. Molecular characterization of selectively vulnerable neurons in Alzheimer's disease. Nat. Neurosci. 24, 276–287 (2021).

14. Mathys, H. et al. Single-cell transcriptomic analysis of Alzheimer's disease. Nature 2, (2019).

15. Shen, E. H., Overly, C. C. & Jones, A. R. The Allen Human Brain Atlas: comprehensive gene expression mapping of the human brain. Trends Neurosci. 35, 711–714 (2012).

16. Drummond, E. et al. Phosphorylated tau interactome in the human Alzheimer's disease brain. Brain 143, 2803–2817 (2020).

17. Acosta, D., Powell, F., Zhao, Y. & Raj, A. Regional vulnerability in Alzheimer's: The role of cell-autonomous and transneuronal processes. Alzheimer's Dement. 1–13 (2018) doi:10.1016/j.jalz.2017.11.014.

18. Seidlitz, J. et al. Transcriptomic and cellular decoding of regional brain vulnerability to neurogenetic disorders. Nat. Commun. 11, 1–14 (2020).

19. Diez, I. & Sepulcre, J. Neurogenetic profiles delineate large-scale connectivity dynamics of the human brain. Nat. Commun. 9, 3876 (2018).

20. Grothe, M. J. et al. Molecular properties underlying regional vulnerability to Alzheimer's disease pathology. Brain 1–17 (2018) doi:10.1093/brain/awy189.

21. Raj, A. et al. Combined Model of Aggregation And Network Diffusion Recapitulates Alzheimer's Regional Tau-PET. Brain Connect. 1–42 (2021) doi:10.1089/brain.2020.0841.

22. Meisl, G. et al. Amplification, not spreading limits rate of tau aggregate accumulation in Alzheimer's disease. bioRxiv (2020) doi:10.1101/2020.11.16.384727.

23. Freer, R. et al. A protein homeostasis signature in healthy brains recapitulates tissue vulnerability to Alzheimer's disease. Sci. Adv. 2, 1–8 (2016).

24. Cornblath, E. J. et al. Computational modeling of tau pathology spread reveals patterns of regional vulnerability and the impact of a genetic risk factor. Sci. Adv. 1–16 (2021).

25. Arnsten, A. F. T., Datta, D., Tredici, K. Del & Braak, H. Hypothesis : Tau pathology is an initiating factor in sporadic Alzheimer ' s disease. Alzheimers. Dement. 1–10 (2020) doi:10.1002/alz.12192.

26. Sharma, A. et al. Divergent roles of astrocytic versus neuronal EAAT2 deficiency on cognition and overlap with aging and Alzheimer's molecular signatures. Proc. Natl. Acad. Sci. U. S. A. 116, 21800–21811 (2019).

27. Foster, J. B. et al. Enhancement of tripartite synapses as a potential therapeutic strategy for Alzheimer's disease: A preclinical study in rTg4510 mice. Alzheimer's Res. Ther. 11, 1–19 (2019).

28. Jablonski, A. M. et al. Astrocytic expression of the Alzheimer's disease risk allele, ApoEε4, potentiates neuronal tau pathology in multiple preclinical models. Sci. Rep. 11, 1–18 (2021).

29. Litvinchuk, A. et al. Apolipoprotein E4 Reduction with Antisense Oligonucleotides Decreases Neurodegeneration in a Tauopathy Model. Ann. Neurol. (2021) doi:10.1002/ana.26043.

30. Wang, C. et al. Selective removal of astrocytic APOE4 strongly protects against tau-mediated neurodegeneration and decreases synaptic phagocytosis by microglia Article Selective removal of astrocytic APOE4 strongly protects against tau-mediated neurodegeneration. Neuron 1–18 (2021) doi:10.1016/j.neuron.2021.03.024.

31. Zalocusky, K. A. et al. Neuronal ApoE upregulates MHC-I expression to drive selective neurodegeneration in Alzheimer's disease. Nat. Neurosci. 24, 786–798 (2021).

32. Sanchez, J. S. et al. The cortical origin and initial spread of medial temporal tauopathy in Alzheimer's disease assessed with positron emission tomography. Sci. Transl. Med. 13, eabc0655 (2021).

33. Vogel, J. W. et al. Spread of pathological tau proteins through communicating neurons in human Alzheimer's disease. Nat. Commun. 11, 2612 (2020).

34. Franzmeier, N. et al. Functional brain architecture is associated with the rate of tau accumulation in Alzheimer's disease. Nat. Commun. 11, 347 (2020).

35. Raj, A. Graph Models of pathology spread in Alzheimer's Disease: An Alternative to Conventional Graph Theoretic Analysis. Brain Connect. 1–61 (2021) doi:10.1089/brain.2020.0905.

36. Yang, F. et al. Longitudinal predictive modeling of tau progression along the structural connectome. Neuroimage 237, 118126 (2021).

37. Montal, V. et al. Biphasic cortical macro and microstructural changes in autosomal dominant Alzheimer disease. Alzheimer's Dement. in press, 1–11 (2020).

38. Mormino, E. C. et al. Amyloid and APOE ε4 interact to influence short-term decline in preclinical Alzheimer disease. Neurology 82, 1760–1767 (2014).

39. Landau, S. M. et al. Amyloid-β imaging with Pittsburgh compound B and florbetapir: comparing radiotracers and quantification methods. J. Nucl. Med. 54, 70–7 (2013).

40. Jack, C. R. et al. Predicting future rates of tau accumulation on PET. Brain 143, 3136–3150 (2020).

41. Diez, I. & Sepulcre, J. Unveiling the neuroimaging-genetic intersections in the human brain. Curr. Opin. Neurol. 34, 480–487 (2021).

42. Arnatkevic, A., Fulcher, B. D. & Fornito, A. A practical guide to linking brain-wide gene expression and neuroimaging data. Neuroimage (2019) doi:10.1016/j.neuroimage.2019.01.011.

43. Glasser, M. F. et al. A multi-modal parcellation of human cerebral cortex. Nature 536, 171–178 (2016).

44. De Jager, P. L. et al. Data descriptor: A multi-omic atlas of the human frontal cortex for aging and Alzheimer's disease research. Sci. Data 5, 1–13 (2018).

45. Leek, J. T. Svaseq: Removing batch effects and other unwanted noise from sequencing data. Nucleic Acids Res. 42, e161 (2014).

46. Dols-Icardo, O. et al. Motor cortex transcriptome reveals microglial key events in amyotrophic lateral sclerosis. Neurol Neuroimmunol Neuroinflam 7, 1–12 (2020).

47. Mi, H., Muruganujan, A. & Thomas, P. D. PANTHER in 2013: Modeling the evolution of gene function, and other gene attributes, in the context of phylogenetic trees. Nucleic Acids Res. 41, 377–386 (2013).

48. Mostafavi, S., Ray, D., Warde-Farley, D., Grouios, C. & Morris, Q. GeneMANIA: A real-time multiple association network integration algorithm for predicting gene function. Genome Biol. 9, (2008).

49. Paul Shannon, 1 et al. Cytoscape: A Software Environment for Integrated Models. Genome Res. 13, 426 (2003).

50. Krzywinski, M. et al. Circos: An information aesthetic for comparative genomics. Genome Res. 19, 1639–1645 (2009).

SUPPLEMENTARY MATERIAL

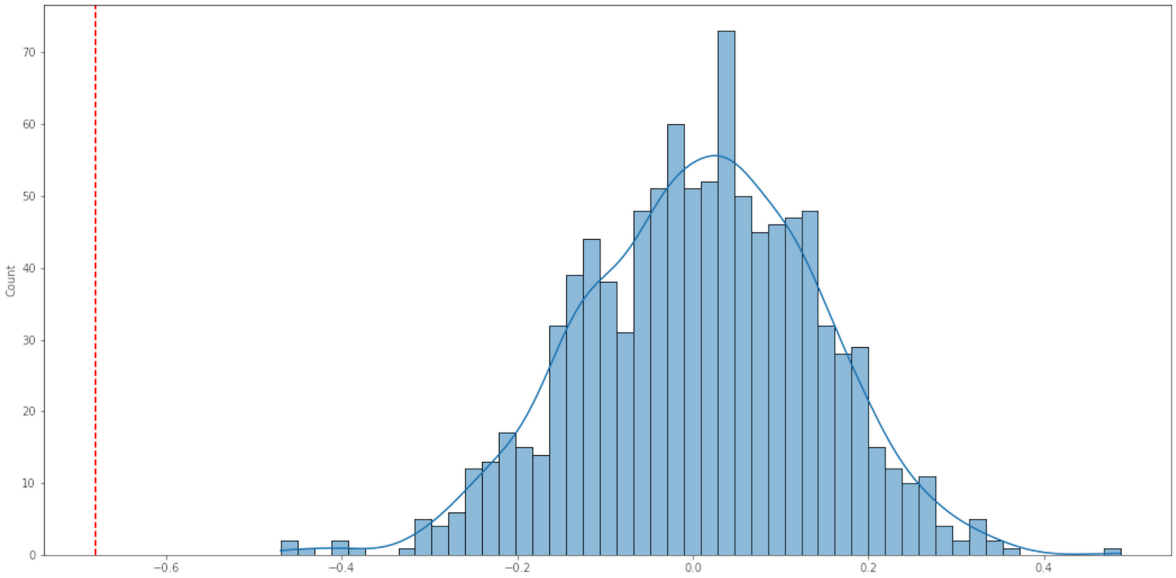

Suppl. material 1. Spearman correlation histogram of the null-model of the association between APOE gene expression and distance from entorhinal after randomly permuting the super-node edges 1000 times. In red, the Spearman correlation using the original FTP-PET network backbone.

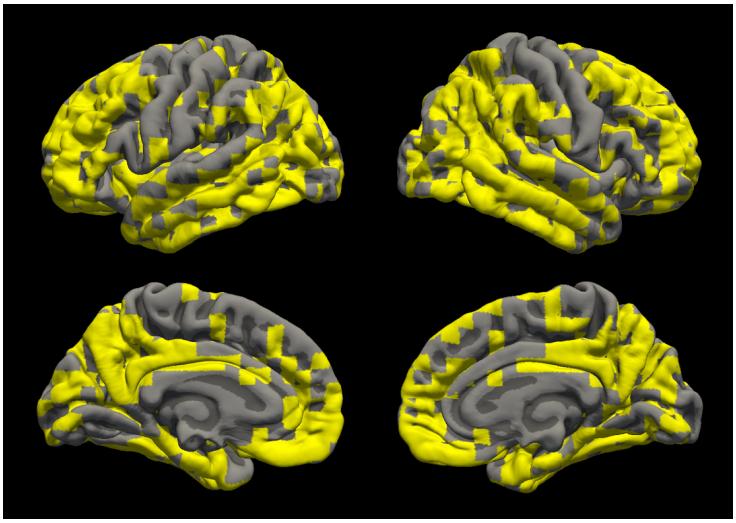

Suppl material 2. Surface rendering of the mask of regions used to compute the FTP-PET adjacency matrix. These are the areas were the FTP-PET signal follow a 2-component GMM in AB+ participants.

4. Discussion

In this thesis we studied the cortical changes and regional vulnerability along the AD continuum using MRI and PET biomarkers (structural, diffusion and spectroscopy MRI and tau PET) as well as other multiomics data (microarray expression data). Concretely, in study 1, we investigated the biphasic trajectory of cortical thickness and cortical diffusivity in the largest sample of ADAD available worldwide. In study 2, we investigated the pattern of the inflammation and neuron-integrity metabolite alterations along the AD continuum, and its relationship to cortical thickness and core-AD biomarkers, in a sample of adults with DS. In study 3, we investigated the relationship between cortical diffusivity and tau-PET in preclinical AD, and its prognostic value. Finally, in study 4, we investigated the regional vulnerability of tau spreading combining tau-PET and high-resolution spatial microarray data using graph-theory tools. Overall, these four studies illustrate the complexity of cortical alteration (both in terms of imaging markers and genetic vulnerability) in AD, with a focus on the preclinical phase of the disease.

4.1 A Biphasic Model of Cortical Macro- and Micro-structural Changes

At the start of this thesis, our group had previously reported a biphasic trajectory of cortical changes in preclinical AD. We first demonstrated in 2010 using a small cohort of ADAD, that decades before clinical symptoms, participants with ADAD showed increased cortical thickness and decreased cortical diffusivity[51]. In 2011, we showed that increased cortical thickness could also be found in early stages of preclinical AD in those participants with transitional Aβ values[69]. This study also suggested that the relationship between cortical thickness and CSF Aβ could be non-linear. However, in 2014, in a different cohort (ADNI) we showed that this non-linear relationship was due to the confounding effect of an amyloid and tau toxic interaction[70]. In particular, we showed that those cognitively unimpaired participants with abnormal amyloid, but normal tau levels had increased cortical thickness, but those with both abnormal amyloid and tau showed more atrophy with respect cognitively unimpaired participants with normal biomarkers. More recently, using a large Spanish multicentre cohort of cognitively unimpaired participants, we showed that the cortical macrostructural changes (cortical thickness) were accompanied by changes in the cortical microstructure that supported that amyloid-related inflammation was the probable cause of the increases in cortical thickness[54]. In particular, A+T- participants had increased thickness and decreased diffusivity and A+T+ participants had more atrophy and increased diffusivity, compared to A-T- subjects (Annex 1, first co-author of the paper, but included in Dr Vilaplana thesis). One of the caveats of the previous work was that we were using group-wise analyses based on biomarker status (i.e not taking into account the specific temporality of events along the disease continuum) and thus could not ascertain the temporality of changing points (ie. when in the disease process the inflexion point occurred).

Therefore, and building on these previous works, we aimed to mathematically estimate the inflexion point where cortical thickness changed from thickening to atrophy, and where cortical diffusivity

changed from decreasing to increasing taking advantage of the largest sample of ADAD. In Study 1, we identified for the first time, that the inflexion point for the cortical dynamics is around 15 years prior to symptom onset, but that the increases in thickness and decreases in diffusivity already started over 2 decades before. Of note, we also showed that these changes parallel the changes in core AD biomarkers. Importantly, our group was the first to propose a conceptual framework and a biological hypothesis to explain the increases of cortical thickness and decreases of diffusivity in early phases of preclinical AD. In particular, we posit that the pathological cortical thickening and decreased diffusivity in early preclinical AD is driven by early amyloid-related inflammation (Figure 4). In this sense, there is converging evidence in the literature suggesting that the pathological accumulation of amyloid drives to astroglial[97] and microglial activation and recruitment[98]. Moreover, recent neuropathological studies have pointed to an increased cortical thickness related to more amyloidosis, even in symptomatic stages of the disease[99]. In our model, we hypothesize that such glia recruitment/activation would result into adding new diffusion barriers limiting the extracellular cortical water displacement, resulting into decreased diffusivity, as previously explored in animal models[100]. The association between cortical thickening and increase neuroinflammation have been shown by our group in a pilot study[72] with a small sample of ADAD and deprenyl-PET – an astrocytosis in-vivo marker, and by other who assessed the association between microglia activation measured using microglia PET and increased cortical thickness in prodromal AD[101,102]. In our biological model, we consider that the inflexion point and the subsequent atrophy / increases in diffusivity will arise from the toxic synergistic effect between amyloid and tau[103]. In this sense, several authors have studied the subgroup of A+T+ preclinical participants, finding atrophy in medial temporal regions[104], a finding that we have also replicated in our studies[54,70].

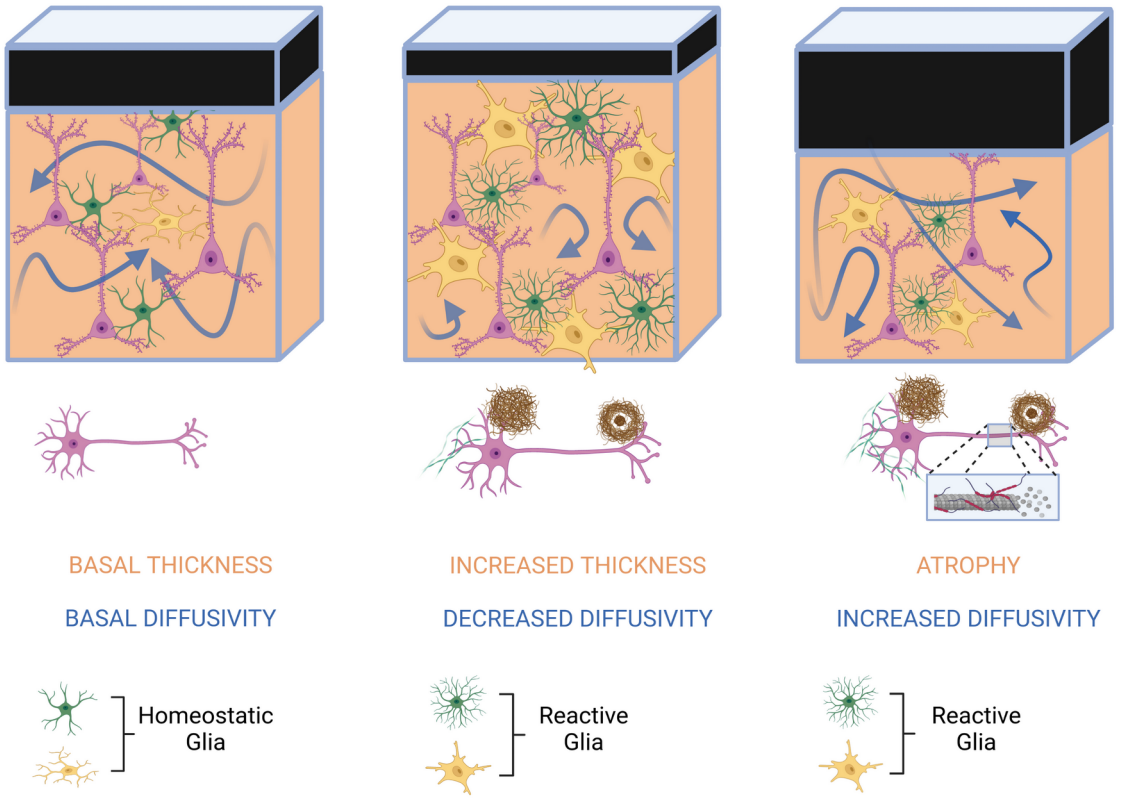

Figure 4. Biological rationale for the biphasic model of cortical changes. (Left) basal state with homeostatic glia, and no pathological amyloid nor tau; (Middle) Amyloid positivity result into reactive glia, increased cortical thickness and decreased cortical diffusivity; (Right) Amyloid and tau positivity result into reactive glia, increased atrophy and increased cortical diffusivity

Whereas our group have consistently identified such biphasic trajectory, the reported results in the literature are despair and, apparently, conflicting. These discrepancies might arise by inaccurate modelling of the data (i.e. imposing a linear model in their statistical analyses and/or neglecting the toxic synergistic effect of amyloid and tau at late stages of the preclinical AD phase). In this sense, previous studies have also shown pathological cortical thickening in relation with amyloid deposition, but provide a different interpretation. An example is the study published by Johnson et al, who found increased thickness in the Wisconsin Registery cohort, who only mentioned it as "unexpected finding"[105]. This study did not assess the effect of tau, but was performed in a relatively young cohort (mean age 61) and thus more likely to have A+/T- individuals than A+/T+ and less age-related atrophy. Another example is the paper by Chetelat et al[106], who associated the thickening in preclinical AD to "cognitive reserve" in the Australian Imaging, Biomarker & Lifestyle Flagship Study of Ageing (AIBL)

cohort, but only when excluding those with subjective cognitive complaints, also probably selecting more likely less advanced individuals. Other groups have found no cortical changes along the preclinical stage[107] or even atrophy related to amyloidosis[108], probably as a result of only considering linear models and/or mixing together participants in different phases of the disease that might obscure the biphasic phenomena (i.e pooling together A+T- participants - which show thickening - and A+T+ - which present atrophy – masking the biphasic trajectory of changes). Nevertheless, since our 2014 and 2017 papers, more groups have considered the toxic synergy between amyloid and tau and have consistently found the biphasic trajectory of cortical changes in independent cohorts and concurred with our biological interpretation to justify their findings. Some examples are a recent study from the European Prevention of AD cohort with more than 1500 participants, where Ingala et al found significant increases in grey matter in A+T- participants[67], a manuscript by Harrison et al using the Berkeley Aging Cohort Study[109] and a recent manuscript by Vogt et al using the Wisconsin Registry for Alzheimer's Prevention cohort[110]. Our biphasic model has also been found in independent cohorts of ADAD. For example, our group have repetitively found the biphasic model in the PICOGEN cohort[51,111], it has also been observed in the PSEN1 mutation Colombian cohort[112], in the Karolinska Insititute Swedish cohort[72], the Chinese Familial Alzheimer Disease Network[113] and has also been replicated in DIAN[114].

Based on our hypothesis that the cortical thickening and decreased cortical diffusivity would be a result of an inflammatory process, we decided to further study such relationship using different inflammatory markers. We first showed that YKL-40, a marker of astrogliosis[115] which was increased in later stages of the disease, is related to tau and atrophy in temporal regions that was stronger in A+ participants[116]. Later, we investigated the relationship between astrogliosis, measured using Deprenyl-PET and cortical thickness and cortical diffusivity in a preclinical cohort of ADAD[72]. Finally, in Study 2 we decided to study neuroinflammation alterations in the AD continuum using MRS - and more concretely the measurements of myo-inositol - and correlate it with diverse cortical alterations. Thus, our primary hypothesis for Study 2 based on our biphasic model was that mI would be increased very early in the disease, and that it would be related to cortical thickening. However, when we analysed the trajectories of mI along the disease continuum in a large cohort of DS, we found that mI, similarly to what we had found in the aforementioned YKL-40 study, is mainly altered in symptomatic stages of the disease, and that it was related to atrophy and core-AD biomarkers of neurodegeneration. Of note, we found that despite that YKL-40 and mI have a similar temporality and both measure astrogliosis, the two measures do not correlate. This is consistent with the existence of different populations of astroglia with different gene expression and different markers observed in the neuropathology[83,84] (e.g. YKL is only found only in a subset), and more broadly reflects the complexity of neuroinflammation in AD.

Importantly, despite our unexpected results, in Study 2 we reported for the first time the trajectory of MRS-driven markers along the AD continuum, and its relationship to cortical thickness and biochemical biomarkers. We were able to capture the effects of the trisomy (the mI transporter is expressed in chromosome 21), and found that adults with DS had increased mI compared to non-euploid participants at all ages, but that further increased in symptomatic stages of the disease as it had been described in sporadic AD[117]. This finding further reinforces that although most AD biomarkers show the same temporality and magnitude of changes in DSAD and sporadic AD, it is very important to assess the starting points as there might be neurodevelopmental differences that must be taken into account[118].

4.2 Implications for disease modelling

A key result from our research present in this thesis, is that the use of linear models is not appropriate to study the complex cortical changes occurring in the AD continuum. The non-linear trajectory of changes can be ascertained in two ways (Figure 5). First, in the ADAD studies, because of the predictability of disease onset, we can calculate the estimated years to symptom onset in mutation carriers at the individual level, and temporally locate participants along the disease. This estimated years to onset concept a good proxy to ascertain the disease cronopathology and enable the study of the cortical changes (or other biomarkers) continuously (Figure 5-A). When using a large dataset such in DIAN it becomes apparent that the cortical changes are better modelled with a quadratic function over a linear one. The biphasic trajectory is missed if only linear models are tested.

The second way is to consider the participants biomarkers profiles and specifically stratify the analyses based on the biomarker profiles of the individual participants. As exemplified in Figure 5-B (for didactic purposes using the hypothetical data in ADAD, but which can also be applied to sporadic AD), mixing up participants with different biomarker profiles leads to erroneous interpretations. For example, a study evaluating the linear relationship between cortical thickness and amyloid deposition, without considering the effect of tau might find (as it has been the case) increased cortical thickness, no relationship or atrophy depending on the relative compositions of A+T- and A+T+ individuals.

Another difficulty is the presence of confounding factors (and their relationships to core AD biomarkers). One of the most significant confounding factors in sporadic AD studies, and more importantly in preclinical AD, is age[16]. This is because age, in the absence of AD biomarker abnormalities, is strongly associated with atrophy[119–121], even from young ages[122], on the one hand, but it is also associated with biomarker positivity (both amyloid and tau) on the other[123]. Thus, the increase in the prevalence of amyloid positivity both in PET and CSF with age has been consistently described in the literature[124,125]. Furthermore, several studies have also reported an association between ageing and

tau accumulation in the mesial temporal in cognitively unimpaired subjects[123,126]. Critical for the purposes of this thesis, the increases in amyloid burden that we have repeatedly found to be associated with thickening in the absence of tau would be mitigated because amyloid positivity is likely to be found in older individuals, who have age-related atrophy (and are more likely to have higher tau pathology). These conflicting effects explain some of the results in a previous study from our group[71], in which, A+T- individuals most often showed an attenuation in the rates of atrophy with respect A-T- individuals rather longitudinally (rather than actual longitudinal thickening), although cross-sectionally this translated into thicker cortex in the group comparison[54]. It also explains the fining of thinning in the medial temporal lobe, which is very likely to have tau pathology and thus exhibit the toxic interaction (of note the fact that different cortical regions could be at different stages is predicted in Jack models).
Thus, we need to control for the confounding effects of age (both positive -for tau- and negative-for amyloid) on the correlational analyses between brain structure and other AD biomarkers (Figure 5-C). Importantly, including age as a covariate does not control effectively for this effect. One of the most widely used strategies in the literature to regress-out the ageing effect is to use normative values, for example, based on the W-score approach[127]. This is the approach we used in the Study 1 of this thesis. We again could show that this enabled us to show cortical thickening in the critical period in which there is amyloid accumulation, but no tau pathology. Overall, to fully capture the cortical changes in AD we must use more complex models than the ones commonly used in the last decades. It is also crucial to have an appropriate study design (considering the target population, stratification, age confounding effect, etc) in addition to using adequate analytical and statistical models. These multifactorial effects overt the cortical structure (i.e ageing-related atrophy, amyloid, and tau interaction-related atrophy and amyloid-related thickening) highlights the technical and statistical difficulties when studying cortical alterations along the AD continuum (Figure 5).

The biphasic model of cortical alterations in AD supported by the works of this thesis could also help explain some paradoxical findings in recent clinical trials. Trials using drugs that target amyloid clearance have repeatedly shown a paradoxical atrophy in the context of successful amyloid removal. For example, in 2007 Fox and colleagues reported that participants treated with the AN1792 vaccine showed greater atrophy compared to the placebo group[128]. Recent studies on the effect of verubecestat (a BACE-1 inhibitor) also reported stronger atrophy in treated patients compared to the placebo group[129], even though BACE inhibitors do not necessarily impact the synapse integrity[130].

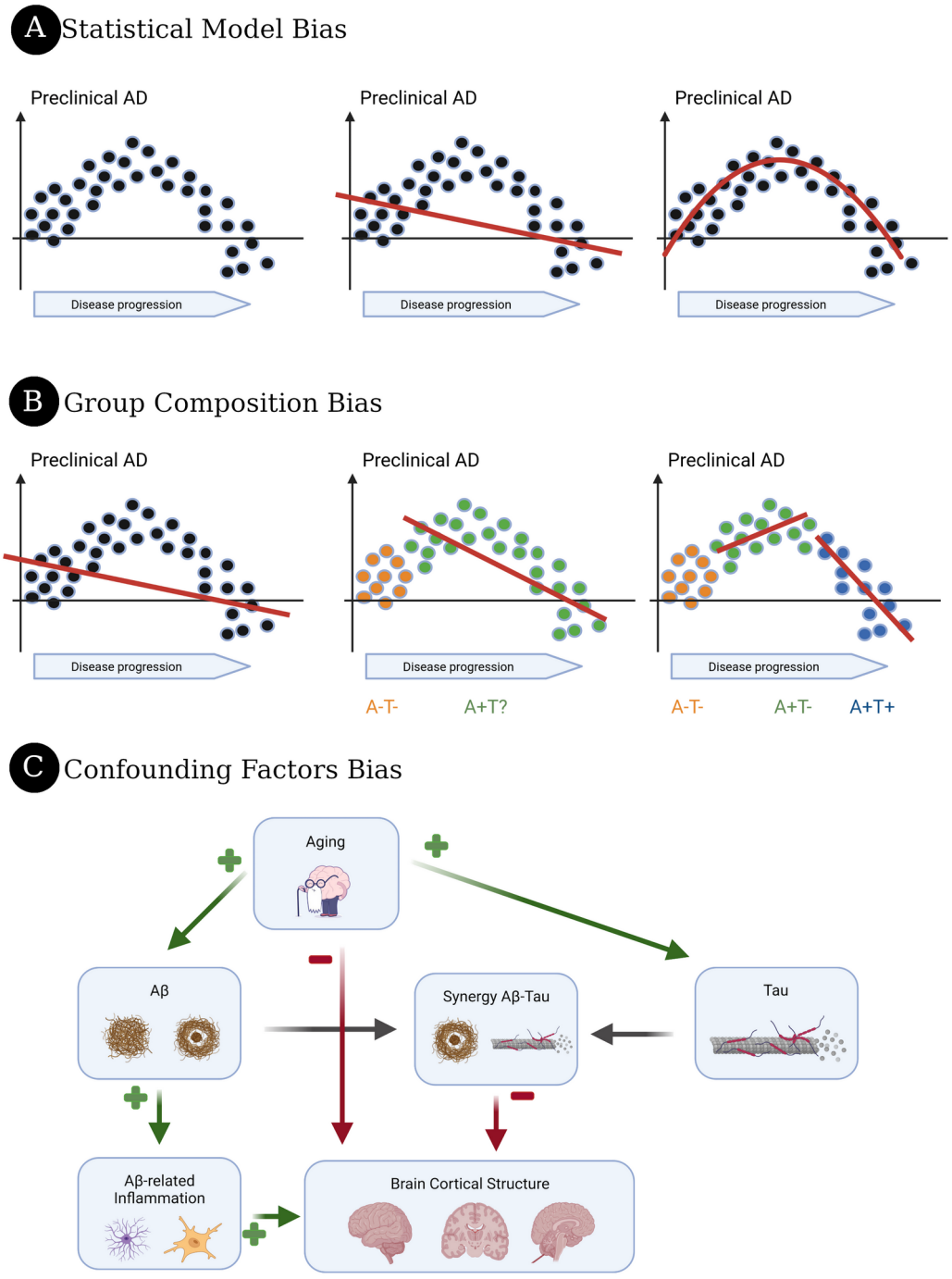

Figure 5. Data modelling complexity in AD studies. (A) Statistical model bias for data fitting; (B) Group composition bias for data fitting; (C) multiple confounding-effects for data interpretation

In a recent promising Phase II anti-amyloid trial using donanemab, the treated group had accelerated whole brain atrophy after an effective clearance of amyloid as compared with the placebo group[131]. We hypothesize that this (extra) atrophy is not a pathological/deleterious effect of these drugs, but an expected effect of removing the amyloid-related inflammatory-response. Such interpretation over these recurrent findings in anti-amyloid trials highlight the need to reconsider the biphasic model, both when interpreting the results, and when defining imaging-based primary or secondary endpoints in clinical trials.

Another important implication of the biphasic model is that it greatly expands the time window in which MRI can capture changes. The current dogma in the field is that MRI is only sensible to capture and track structural alterations 7 years before clinical symptoms manifest[132,133]. However, in the context of the biphasic model and as it has been shown in Study 1, cortical structures start to change more than 20 years prior to symptoms onset. Thus, MRI-markers, such as cortical thickness and cortical mean diffusivity are promising markers to be integrated in clinical trials as primary or secondary endpoints, specially in measuring drug efficacy.

Whereas the work presented in this thesis have answered important questions about the dynamics of cortical alteration in the AD continuum, further work is needed to better comprehend and more accurately model early alterations. We need to better understand how the accumulation of amyloid and NFT, measured in-vivo using PET, might affect cortical thickness and cortical diffusivity, both locally and non-locally. Furthermore, we need to revisit the individual and synergetic effect along the AD continuum of each pathological hallmark (i.e amyloid and tau) after controlling by the multifactorial confounding factors such as age-related alterations. In addition, even though we only focused on grey matter alterations, several studies in ADAD and in sporadic AD[134–136] have pointed to white matter alterations in preclinical AD related to amyloid and tau alterations. Thus, it is important to also study how amyloid and tau pathology might cause structural and connectivity alterations in fibre tracks and subsequent effect in the cortex via diasquisis, and how such white matter alterations fit within the proposed biphasic model.

4.3 The Effects of the AD Inflammasome Complexity in MRI Outcomes

A fundamental element to explain the biphasic trajectories of cortical changes is neuroinflammation. Glia cells have received much less attention than neurons in AD pathophysiology. Only recently, studies started to highlight the complex dynamics of neuroinflammation along the AD continuum. These complex (and non-linear) changes in basic, animal and human studies[137–140] make the study of the relationship between cortical alterations and glia complex. This complexity is partially reflected in

Study 2, in which we observed two unexpected results: that mI was only altered in late stages of the disease (compared to other reactive astrocytosis markers such as GFAP[141] or deprenyl-PET[35] shown to be altered early in the disease) and second, that it did not correlate with CSF YKL-40, another marker of astrocytosis[115]. The latter is especially significant as both mI and YKL-40 elevations have a similar temporality, a similar cellular origin, but do not correlate. This finding is in agreement with the fact that YKL-40 is only expressed in a subset of astrocytes[115] and that recent single cell RNA seq studies showed several subpopulations of glia with very different (genetic) profiles[84,142].

Indeed, the novel microscopic and transcriptomic studies have shown the heterogeneity glia cells. We are only beginning to understand how these cells transition from homeosis to (importantly) both protective and toxic states in relation with the AD pathophysiology. For example, using single-cell RNA-seq, Mayers et al. showed that only a subtype of astroctyes cells is altered in late-stages of the disease[83]. In a follow-up paper, Habibib et al. demonstrated, using mice models, that there is a specific subtype of astrocytes that is gradually altered in the AD continuum[84]. Similarly, Keren-Shaul al showed that there is a specific subtype of microglia that is activated in late-stages of AD, which they named DAM (Disease-Associated Microglia)[143]. Such heterogeneity in glia alterations have recently led to a re-thinking of the vague term “reactive astrocyte or reactive glia”[144].

An extra layer of complexity to comprehend neuroinflammation in AD is understanding the temporality of these alterations. Indeed, neuroinflammatory changes follow a non-linear or non-monotonic temporal trajectory of changes. For example, using an in-vivo tracer of reactive astrocytes that binds to Monoamine oxidase B (MAO-B), namely C11- deprenyl, collaborators from Karolinska Institute have shown both in animal models and autosomal dominant AD, that there are early increases in deprenyl uptake in the preclinical stage of the disease that decrease in the symptomatic stage of the disease[35]. On the contrary, YKL-40, another marker of reactive astrogliosis, has been shown to be increased mainly in the symptomatic stages of the disease[145], much later than deprenyl-PET. Similarly, microglia alterations also follow a non-linear non-monotonic trajectory. For example, several studies have shown that soluble triggering receptor expressed on myeloid cells 2 (sTREM2), which is mainly expressed in microglia, is altered in prodromal stages of the disease, to later decrease in late-AD, as shown both in sporadic and familial AD[29,139]. Another example is the findings using the PK11195-PET – a tracer that binds to the benzodiazepine receptor in the mitochondria and which is overexpressed in activated microglia. The uptake of this tracer seems to have two peaks with disease progression: one at late preclinical-early prodromal AD, followed by decreases in later prodromal AD, and another peak early in the dementia stage[140].

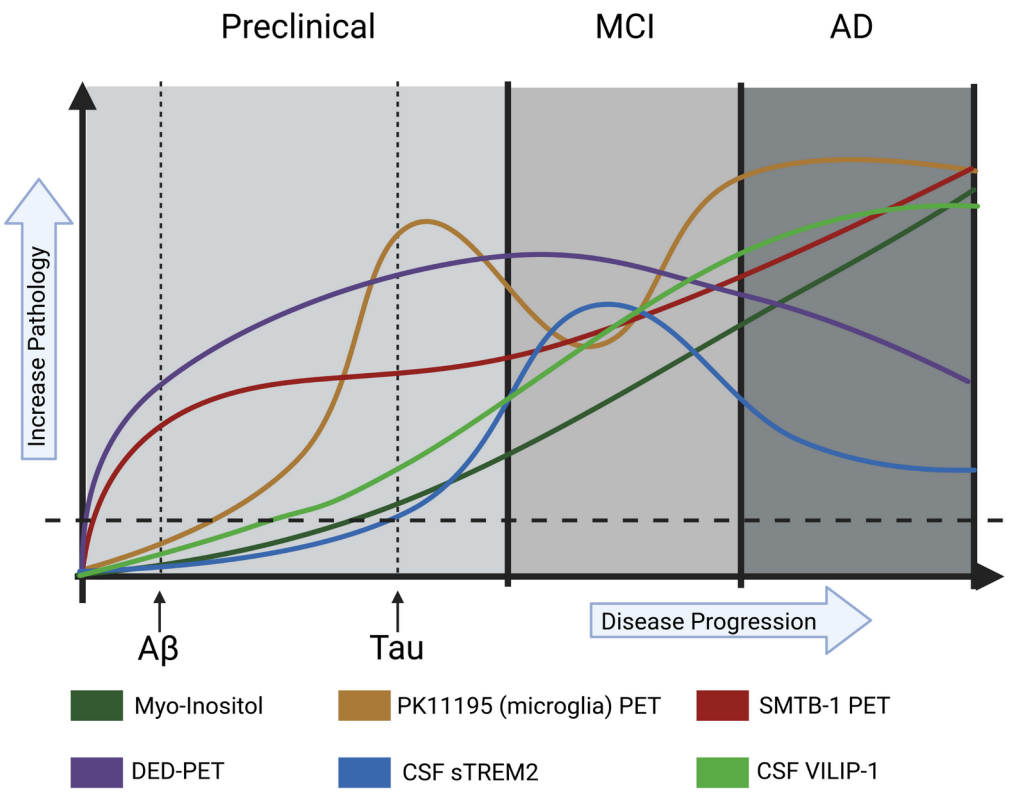

Figure 6. Inflammasome complexy along the AD continuum. Diverse inflammatory markers have different trajectories along the disease continuum. Estimations based on literature reports.

The complexity of neuroinflammation has important implications when evaluation the biphasic model. First, it is clear that lumping together all inflammation markers under the label "neuroinflammatory markers" is a oversimplification that leads inevitably to erroneous interpretations of the findings. Such complexity can be observed in part by the work from our group, where the temporality of alterations and its relationship with cortical structure changes vary depending on the inflammation marker (e.g YKL-40, deprenyl-PET and mI). Second, the effect of inflammation over the cortical structure might be obscured by co-ocurring phenomena. The effect of tau-related and age-related atrophy, which is very strong specially in late stages of the disease, could mask the inflammatory-related thickening and decrease of diffusivity. As an example, a recent work by Gispert et al. found a pattern of increased grey matter volume related to sTREM2 in prodomal AD only when accounting for the amount of CSF pTau[146]. Third, recent findings have shown the interplay between glia cells and both amyloid and tau[97,147]. Thus, when evaluating cortical alterations along the AD continuum, it is important not only to

consider the amyloid and tau toxic interaction, but also the interaction (and not only additive) effect of glia, which might lead to unexpected findings specially in preclinical AD.

Given the increasingly recognized importance of glia alterations in AD, clearly demonstrated in GWAS studies[9], we should rethink the current framework to classify participants. This will result into better patient profiling, which might be important in the advent of novel anti-inflammatory clinical trials (e.g to increase TREM2 reactivity). Thus, we need to develop candidate inflammation markers for a correct participant recruitment. Importantly, as we shown in the present thesis, the use of MRI markers such as cortical thickness and cortical diffusivity might be used as a surrogate markeres of inflammation change, and could be included as secondary end-point in these anti-inflammatory trials.

The impressive advancement in biomarker discovery and validation in recent years offer unprecedented opportunities to study the neuroinflammatory changes along the AD continuum and to disentangle the relationship between neuroinflammation and cortical alterations. In addition to the aforementioned biomarkers summarized in Figure 6, some new biomarkers would be especially well suited to continue the study of the cortical biphasic changes. First, new imaging modalities such as diffusion-weighted MRS (DW-MRS) might help to dissect the different neuroinflammation processes. Whereas classic MRS only measure metabolites, DW-MRS has the capability to quantify the displacement of certain metabolites, providing also morphological/microstructural information[148]. Previous work with DW-MRS have shown its capability to measure not only increases in astrocytosis, but also a change in their morphology when they change to a reactive conformation[149–151]. This biomarker is thus promising to differentiate the moment at which glia start to react and undergo morphological changes. Second, with novel machine learning approaches, one could integrate information from several already-existing biomarkers to produce a model for neuroinflammation. This data-driven approach could help to disentangle the complexity and temporality at which each biomarker is altered, and its relationship to cortical structure. Finally, only a small number of papers have started to study, using neuroimaging data, the role that neuroinflammation have on the interaction between amyloid and tau, and its subsequent structural alterations[147]. The study on the role of inflammation on this toxic interaction necessary for cortical atrophy and cognitive decline might provide new targets for intervention and preventive therapies.

4.4 Cortical Diffusivity Biomarker as a Prognostic and Diagnostic Tool

During my MSc and at the beginning of this thesis, we developed a surface-based pipeline that mitigates the pitfalls of volumetric approaches when measuring the cortical microstructural alterations[54]. Concretely, we developed this technique to measure the effects of the amyloid-related inflammation on the cortical microstructure, under the assumption that this technique would capture glia recruitment and

activation as well as reactive cellular hypertrophy, all of which would result in more barriers to the movement of water. As reported in Study 1 (and previously in the 2017 paper, Annex I), we indeed found that cortical diffusivity was significantly decreased in early preclinical AD in A+T- participants. However, the performance of this technique in tracking neurodegeneration and astrodegeneration along the disease continuum, which would result in the removal of barriers and increased cortical diffusivity, was not tested. Therefore, we also studied the microstructural alterations in later stages of AD (and in other neurodegenerative diseases) and realized that cortical diffusivity was also a sensitive marker of neurodegeneration. In Study 1 we showed that cortical diffusivity was altered before cortical thickness (between the age-range of -10 and -5, compared to cortical thickness, which was altered between -5 and 0 years before symptom onset), and that the pattern of alterations was more widespread for cortical mean diffusivity compared to the atrophy maps. In Study 3, we wanted to evaluate the association of cortical diffusivity with the accumulation of NFT, as measured with flortaucipir uptake, in earlier stages of the disease. We found that the amount of NFT accumulation in early-Braak stages (such as the inferior temporal) was related to widespread increased diffusivity. Interestingly, the cortical regions where this association remained significant resembled the areas identified in Study 4 when generating the backbone tau network, which suggest that cortical diffusivity might be tracking early and subtle tau-related neurodegeneration. In Study 3, we also experimented the complexity of analysing the cortical alterations in preclinical AD. Specifically we had to segregate the cognitively unimpaired participants based on their amyloid profile. As previously aforementioned, to avoid mixing group of participants with different biomarker profiles that might obscure the diffusivity-neurodegeneration relationship, we restricted our analysis to A+ cognitively unimpaired participants. This was a crucial step, since we wanted to capture the association with the spread of tau, which only occurs in the presence of pathological levels of amyloid[152,153]. Thus, we highlighted again the need to correctly model the changes in the AD.

Study 1 and 3 of this thesis confirm the potential of cortical diffusivity to track neurodegeneration in AD. Furthermore, in parallel to the works of this thesis, cortical diffusivity has been shown to be a promising marker of neurodegeneration in several other neurodegenerative diseases. Specifically, we showed increased diffusivity in patients with the behavioural variant of frontotemporal dementia (bvFTD)[57] (Annex2 paper, co-first author, used in Dr Illan thesis), in ALS[59], in Multiple Sclerosis[58] and in primary progressive aphasia (under review). A key result from all these studies is the observation of cortical diffusivity alterations in the absence of atrophy. In this sense, in Illan et al. we showed that a subgroup of bvFTD participants that were visually categorized with “absent atrophy” by two neurologists, did present increased diffusivity in regions typically reported of suffer from neurodegeneration in bvFTD patients[57]. Our rationale behind the sensitivity of cortical diffusivity vs cortical thickness, is that microstructural changes precede overt neuronal loss and therefore, cortical

diffusivity can capture the earlier more subtle alterations. Indeed, in early stages of neurodegeneration, the loss of a small number of neurons and the loss in the arborization of dendrites might not be severe enough to result into a thinner cortex, but the microstructural local environment could change sufficiently to increase water displacement and, therefore result into increased cortical mean diffusivity.

After the publication of our 2017 paper in which we presented the surface-based approach to measure cortical diffusivity for the first time, there have been several studies that, based on our methodology, studied the profile of cortical microstructural alterations in AD. For example, Vogt et al. showed in a cohort of prodomal AD, that cortical diffusivity was more sensitive than cortical thickness to track neurodegeneration in MCI[55]. Similarly, Parker et al. showed that cortical diffusivity could also be used to measure neurodegeneration in early-onset AD[56]. All these works suggest that cortical diffusivity could improve the sensitivity to track neurodegeneration in the AD continuum. However, further work is needed to translate cortical mean diffusivity to clinical practice and clinical trials. First of all, we need to define a signature of microstructural changes in AD from which to derive a scalar metric to be used at the individual level, similarly to the approaches used in cortical thickness[41]. Indeed, one of the most common markers used to measure neurodegeneration in the average of cortical thickness in regions well-known to be atrophied in late stages of the disease. Thus, we need to create a signature (or fingerprint) map of which regions might be the most sensitive to track alterations in the whole AD continuum. The use of machine learning tools and variance analyses, in combination with association studies with in vivo tau PET studies and cognitive scores, might help identify the most promising regions to be included in such a cortical diffusivity signature to measure the AD microstructural changes.

Our measure of cortical diffusivity is based on one of the simplest models of DWI data: mean diffusivity as measured from the tensor decomposition (DTI) of DWI signal. However, in the last decade, there have been various advances in both DWI acquisition sequences and modelling. In terms of acquisition, there are now many protocols with different gradient directions (e.g high angular resolution diffusion imaging - HARDI[154]) and multi-shells acquisitions with several b-values, some of which at the cost of very long acquisition times, but which more accurately capture the water displacement. Regarding modelling, one of the most promising biological-based compartmental models is the neurite orientation dispersion and density imaging[155] (NODDI), which accounts for intracellular diffusivity (bounded by the membrane of neurites and myelin sheaths), anisotropic extracellular diffusivity (outside neurites and potentially including glial cells), and the CSF compartments diffusion (isotropic diffusion). Another promising model is diffusion kurtosis imaging[156] (DKI), which overcomes some assumptions in the DTI model, such as considering the water diffusivity a Gaussian process in the presence of high-strength gradients. In the context of these new, advanced, and promising alternatives, is there space for our simple DTI model? We believe there is. The two options are not mutually exclusive, and each one

provides benefits over the other. On the one hand, the use of NOODI (or other compartment models) offer clear advantages for research as it better captures the biology of the cortical alterations[157]. For example, NOODI enables the investigation of the amount of intra and extra cellular diffusivity that is disturbed due to an inflammatory process or the accumulation of amyloid[110]. However, in clinical practice, it is not yet feasible (in terms of time and cost) to acquire the data to compute NOODI-based metrics and to process it. In addition, due to the long acquisition time, using such sequences in certain populations (such as Down Syndrome or AD) might result into low quality images due to movement artifacts. Mean diffusivity as measured from the tensor decomposition (DTI) of DWI signal is already often included in many acquisition protocols, which facilitates its implementation in the clinical practice. We proved that it is feasible to obtain meaningful values of cortical diffusivity from a low number of gradient directions[54], which require a short time acquisition, making it interesting both in terms of costs and to minimize motion-related artifacts. Further work is required to compare both modelling frameworks, and to evaluate the additive value of using a complex acquisition/modelling over a simplistic approach, but the cortical mean diffusivity metric has important advantages in multi-centre studies and clinical trials. In this sense we have previously shown that with adequate harmonization processes, it is feasible to pool together data in multi-centre studies with different protocols, even with different number of directions[54] (and to some extent when the b-values differ). The more recent and complex acquisitions are much more sensitive to the acquisition protocols. Furthermore, it will be most probably easier to derive a scalar measure from a cortical signature (to be used at the individual level) from cortical mean diffusivity than from the more complex multi-compartment approaches. All these pragmatic factors make our metric of cortical mean diffusivity much easier to implement in multi-centre studies and clinical trials.

4.5 Integration of multiomics data study regional vulnerability in AD

During the study of the cortical microstructural alteration in Study 3, we realized that the pattern of microstructural changes resembled that of the spreading of tau along the Braak stages. This led us to inquire about the genetic fingerprint that could characterize (if existing) the regional vulnerability to the spread of tau, and the subsequent pattern of macro and microstructural changes. Concretely, we wanted to assess if the constitutive gradient of changes in gene expression in healthy individuals was related to the temporality of tau accumulation in preclinical AD.

To investigate these phenomena we needed to integrate data from different sources and at different scales. Recent advances in data acquisition and the development of new methodological frameworks have helped to solve this gap[88,158]. Moreover, novel statistical approaches have led to integrate (macroscale) neuroimaging data (such as atrophy or functional maps) with the (mesoscale) quantifications of gene expression. Taking advantage of the ABA high-resolution map of gene

expression, and the tau accumulation information obtained using tau-PET, in Study 4, we characterized the gradual change in the expression of certain genes that were related to the spread of tau.

In Study 4, we developed a novel methodology, based on graph theory tools for two different case scenarios. First, we developed an algorithm to obtain the backbone of tau-PET, which results into a minimal representation of the relationship between the accumulation of tau between different brain regions. Of note, although this algorithm was used for tau-PET data, it can be applied to other neuroimaging measures. In this sense, it would be interesting to investigate the pattern of accumulation of amyloid, which despite it is considered to occur globally (and simultaneously) in the whole cortical mantel (contrary to the Braak staging system). Our approach might elicit a backbone which could be used to provide more accurate quantifications or to study local and non-local relationships between amyloid and tau. Second, we developed a framework to integrate network information (such as network-based distance) with the genetic data from the ABA, that could be also used to investigate other source of data (such as amyloid accumulation or cortical diffusivity maps).

The integration of multiomics data, in conjunction with the tools develop in Study 4, could also be used to study the pathophysiological alterations underlying the cortical changes in the proposed biphasic model. The increase in cortical thickness and the decreases in cortical mean diffusivity in Study 1 were attributed to an amyloid-related inflammatory process. We are, nonetheless, aware that there is not an overlap between the identified regions and the pattern of amyloid accumulation. In other words, the response or consequences of amyloid accumulation might differ in the different areas. This heterogeneity in the response might reflect different local vulnerabilites. The methodology developed in Study 4 might enable us to answer some of these questions. However, a major caveat is that the RNA expression measurements used in Study 4 (and similar studies) are obtained from a small group of healthy adults, which might be useful to assess vulnerability but causation cannot be proven in such analyses. One conceivable promising study would be to study how bulkRNA gene expression would be related to cortical thickness, measured from ante-mortem MRI scans in a concrete region of interest, to explore the genetic fingerprint suggestive of cortical thickening. Similarly, it would be feasible to explore using gene RNA sequencing data, if the increases in myo-inositol found in Study 2 would be the result of alterations in the overall number of certain glia-type cells.

In Study 4 we performed several graph theory analyses to investigate the role of APOE in the spread of tau. Unfortunately, the focus on tau, impeded us to assess the impact of the other major pathological hallmarks, especially amyloid (and inflammation). The potential of graph theory analyses could expand the results of Study 4 to investigate the set of genes mediating the relationship between amyoid-plaques genes and tau-NFT genes, as it has been done in other clinical conditions[159]. Using a curated list of physical interactions, as well as known pathways interactions (e.g using Reactome database), we can create a network of genes that inter-connect both amyloid and tau-related genes (Figure 7). From such

amyloid-tau network, we could identify the group of genes more closely associated with the interaction between amyloid and tau and study its biological and cellular profile (Figure 7). Moreover, we could integrate those findings with large cohorts of post-mortem data to analyse which set of genes is altered early in the AD continuum. Overall, the use of graph theory tools to integrate multidimensional and multiscale data is a promising and powerful framework to investigate the pathological alterations along the AD continuum.

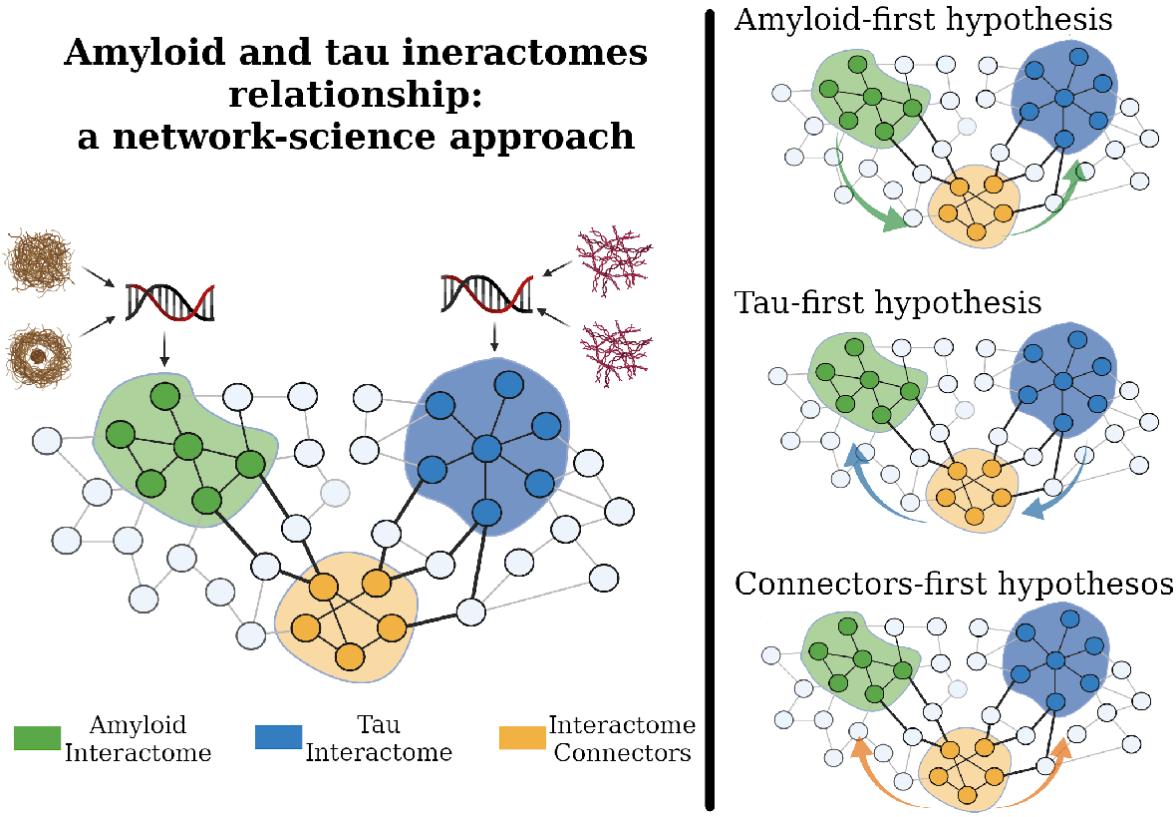

Figure 7. Study of the gene-interactions network between proteins encoded in amyloid plaques and NFT. (Left) Network construction to identify mediating genes (orange) between amyloid-related genes (green) and tau-related genes (blue); (Right) Hypothetical models to study the aetiology and causes of AD progression.

4.6 Limitations

The most important technical limitations of the works included in this thesis have already been acknowledged in the articles. Nevertheless, other conceptual limitations should also be acknowledged. First, the lack of an in-vivo measurement of astrocyte and microglia reactivity using PET. This could have been specially relevant in Study 1 and Study 2. In this sense, a pilot study published by our group showed that the early cortical thickening and decreased cortical mean diffusivity are associated to

astrocytosis[72] (measured using deprenyl-PET). It would be ideal to model the astrocytosis reactivity and how it impacts cortical changes in the DIAN cohort. Similarly, these inflammatory markers could also help disentangle the pathological alterations behind the myo-inositol increases in the cohort of Down syndrome participants. Another limitation is that at the design of Study 3, we only had the HABS cohort with available amyloid and tau PET data, with a diffusion MRI acquisition of sufficient quality. Currently, the increase of participants recruited in several public cohorts (such as ADNI or prevent-AD) would enable for a replication of the results in different cohorts, and more importantly to perform further analyses with increased statistical power. Finally, the only resource available for Study 4 of spatial high-resolution RNA sequence measurements was derived from the ABA, which is composed of healthy adults. There is not a similar database from AD patients. Despite the fact that we identify a gene expression profile to explain the regional vulnerability for the spread of tau, it would have been ideal to have a similar information-map in a cohort of AD participants, to measure the changes in gene expression that might underlie the vulnerability to the AD pathological alterations across the whole cortex.

4.7 General discussion

This doctoral thesis highlights the complexity on cortical alterations along the AD continuum and how we can study such dynamics using macrostructural, microstrucutral and genetic data. We used state-of-the-art neuroimaging software, and we also developed an in-house algorithm (cortical diffusivity) to study the preclinical cortical AD alterations. Our studies have: i) consolidated the biphasic model of cortical changes in preclinical AD, ii) shown the metabolite-related changes in late-stages of the disease, iii) demonstrated the potential of cortical diffusivity as a neurodegeneration marker and iv) proposed a gradient of gene-expression vulnerability associated to tau accumulation.

The consolidation of the biphasic model highlights the complexity of the AD pathophysiology and the importance of correctly modelling the cortical changes when considering MRI outcomes in AD preventive clinical trials. The validation of cortical diffusivity as a prognostic marker could result into its implementation in clinical practice and in clinical trials. Finally, the exploration of the genetic vulnerability to understand the spread of tau might help to identify novel pharmacological targets and to provide an analytical framework to integrate genetic and imaging data. Nonetheless, this thesis leaves even more open questions to better comprehend the pathophysiological drivers of the non-lineal cortical dynamics, the role of neuroinflammation, and the development of novel biomarkers to more accurately track preclinical AD, all of which are critical steps for the development of preventive therapies for this devastating disease.

5. Conclusions

Conclusions

The main conclusions of this thesis are:

1) Cortical thickness and cortical mean diffusivity in autosomal dominant Alzheimer disease follow a biphasic trajectory of changes. A non-linear trajectory greatly expands the performance of MRI to track the preclinical AD, reconciles conflicting data with respect the effects of amyloid accumulation on brain structure, and helps understand the (apparently) paradoxical trials in anti-amyloid therapies, in which the active arm was associated with increased atrophy.

2) Myo-inositol is constitutively increased in adults with Down Syndrome, but increases in symptomatic AD and is might be a non-invasive and cheap marker of neuroinflammation which could be used as an outcome measure in anti-inflammatory clinical trials.

3) Cortical mean diffusivity is a new biomarker that might have more sensitivity to detect and track neurodegeneration than cortical thickness. It correlates with tau-PET uptake in preclinical Alzheimer disease and has good prognostic performance. Therefore, it might be useful in clinical trials as a surrogate marker of tau accumulation and as an outcome measure of efficacy.

4) The pattern of topographical gradual change in gene expression suggest a regional vulnerability to tau accumulation. Identifying the genetic local vulnerability might help identify novel pharmacological targets to prevent AD.

6. References

1. 2021 Alzheimer's disease facts and figures. *Alzheimer's Dement.* **17**, 327–406 (2021).

2. Alexander, G. C. *et al.* Revisiting FDA Approval of Aducanumab. *N. Engl. J. Med.* **385**, 769–771 (2021).

3. Serrano-Pozo, A., Frosch, M. P., Masliah, E. & Hyman, B. T. Neuropathological alterations in Alzheimer disease. *Cold Spring Harb. Perspect. Med.* **1**, a006189 (2011).

4. Müller, U. C., Deller, T. & Korte, M. Not just amyloid: physiological functions of the amyloid precursor protein family. *Nat. Rev. Neurosci.* **18**, 281–298 (2017).

5. Reiss, A. B., Arain, H. A., Stecker, M. M., Siegart, N. M. & Kasselman, L. J. Amyloid toxicity in Alzheimer's disease. *Rev. Neurosci.* **29**, 613–627 (2018).

6. Hooper, C., Killick, R. & Lovestone, S. The GSK3 hypothesis of Alzheimer's disease. *J. Neurochem.* **104**, 1433–1439 (2008).

7. Braak, H. & Braak, E. Neuropathological stageing of Alzheimer-related changes. *Acta Neuropathol.* 239–259 (1991).

8. Hampel, H. *et al.* Developing the ATX(N) classification for use across the Alzheimer disease continuum. *Nat. Rev. Neurol.* **17**, 580–589 (2021).

9. Wightman, D. P. *et al.* A genome-wide association study with 1,126,563 individuals identifies new risk loci for Alzheimer's disease. *Nat. Genet.* **53**, 1276–1282 (2021).

10. Leyns, C. E. G. & Holtzman, D. M. Glial contributions to neurodegeneration in tauopathies. *Mol. Neurodegener.* **12**, 1–16 (2017).

11. Guttenplan, K. A. *et al.* Neurotoxic reactive astrocytes induce cell death via saturated lipids. *Nature* **599**, 102–107 (2021).

12. Mirra, S. S. *et al.* The Consortium to Establish a Registry for Alzheimer's Disease (CERAD). Part II. Standardization of the neuropathologic assessment of Alzheimer's disease. *Neurology* **41**, 479–486 (1991).

13. Thal, D. R., Rüb, U., Orantes, M. & Braak, H. Phases of Aß-deposition in the human brain and its relevance for the development of AD. *Neurology* **58**, 1791–800 (2002).

14. Del Río Hortega, P. Tercera aportación al conocimiento morfológico e interpretación funcional de la oligodendroglía. *Mem. Real Soc. Esp. Hist. Nat* (1928).

15. Weintraub, S., Wicklund, A. H. & Salmon, D. P. The neuropsychological profile of Alzheimer disease. *Cold Spring Harb. Perspect. Med.* **2**, a006171 (2012).

16. Livingston, G. *et al.* Dementia prevention, intervention, and care: 2020 report of the Lancet Commission. *Lancet* **396**, 413–446 (2020).

17. Jack, C. R. *et al.* NIA-AA Research Framework: Toward a biological definition of Alzheimer's disease. *Alzheimer's Dement.* **14**, 535–562 (2018).

18. Dubois, B. *et al.* Clinical diagnosis of Alzheimer's disease: recommendations of the International Working Group. *Lancet Neurol.* **20**, 484–496 (2021).

19. Gatz, M. *et al.* Role of genes and environments for explaining Alzheimer disease. *Arch. Gen. Psychiatry* **63**, 168–174 (2006).

20. Bateman, R. J. *et al.* Autosomal-dominant Alzheimer ' s disease : a review and proposal for the prevention of Alzheimer ' s disease. *Alzheimer's Res* **3**, 1–13 (2011).

21. Fortea, J. *et al.* Alzheimer's disease associated with Down syndrome: a genetic form of dementia. *Lancet Neurol.* **In press**, 930–942 (2021).

22. McCarron, M. *et al.* A prospective 20-year longitudinal follow-up of dementia in persons with Down syndrome. *J. Intellect. Disabil. Res.* **61**, 843–852 (2017).

23. Ryman, D. C. *et al.* Symptom onset in autosomal dominant Alzheimer disease: A systematic review and meta-analysis. *Neurology* **83**, 253–260 (2014).

24. Hansson, O. Biomarkers for neurodegenerative diseases. *Nat. Med.* **27**, 954–963 (2021).

25. Alcolea, D. *et al.* Feasibility of lumbar puncture in the study of cerebrospinal fluid biomarkers for Alzheimer's disease: a multicenter study in Spain. *J. Alzheimers. Dis.* **39**, 719–726 (2014).

26. Grothe, M. J. *et al.* Associations of Fully Automated CSF and Novel Plasma Biomarkers With Alzheimer Disease Neuropathology at Autopsy. *Neurology* **97**, e1229–e1242 (2021).

27. Toledo, J. B. *et al.* Nonlinear Association Between Cerebrospinal Fluid and Florbetapir F-18 β-Amyloid Measures Across the Spectrum of Alzheimer Disease. *JAMA Neurol.* **4283**, 571–581 (2015).

28. Wolters, E. E. *et al.* Regional [18F]flortaucipir PET is more closely associated with disease severity than CSF p-tau in Alzheimer's disease. *Eur. J. Nucl. Med. Mol. Imaging* **47**, 2866–2878 (2020).

29. Van Hulle, C. *et al.* An examination of a novel multipanel of CSF biomarkers in the Alzheimer's disease clinical and pathological continuum. *Alzheimer's Dement.* **17**, 431–445 (2021).

30. Ashton, N. J. *et al.* Plasma p-tau231: a new biomarker for incipient Alzheimer's disease pathology. *Acta Neuropathol.* (2021) doi:10.1007/s00401-021-02275-6.

31. Lleó, A. *et al.* Phosphorylated tau181 in plasma as a potential biomarker for Alzheimer's disease in adults with Down syndrome. *Nat. Commun.* 1–8 (2021) doi:10.1038/s41467-021-24319-x.

32. Moscoso, A. *et al.* Longitudinal Associations of Blood Phosphorylated Tau181 and Neurofilament Light Chain with Neurodegeneration in Alzheimer Disease. *JAMA Neurol.* **78**, 396–406 (2021).

33. Bailey, D., Townsend, D., Valk, P. & Maisey, M. *Positron Emission Tomography*. (Springer, 2005).

34. Villemagne, V. L., Doré, V., Burnham, S. C., Masters, C. L. & Rowe, C. C. Imaging tau and amyloid-? proteinopathies in Alzheimer disease and other conditions. *Nat. Rev. Neurol.* **14**, 225–236 (2018).

35. Rodriguez-Vieitez, E. *et al.* Diverging longitudinal changes in astrocytosis and amyloid PET in autosomal dominant Alzheimer's disease. *Brain* awv404 (2016) doi:10.1093/brain/awv404.

36. Chaney, A., Williams, S. R. & Boutin, H. In vivo molecular imaging of neuroinflammation in Alzheimer's disease. *J. Neurochem.* **149**, 438–451 (2019).

37. Greve, D. N. *et al.* Different partial volume correction methods lead to different conclusions: An 18F-FDG-PET study of aging. *Neuroimage* **132**, 334–343 (2016).

38. Pooley, R. A. Fundamental Physics of MR Imaging. *RadioGraphics* **25**, 1087–1099 (2005).

39. Braskie, M. N. & Thompson, P. M. A focus on structural brain imaging in the Alzheimer's disease neuroimaging initiative. *Biol. Psychiatry* **75**, 527–533 (2014).

40. Fischl, B. & Dale, a M. Measuring the thickness of the human cerebral cortex from magnetic resonance images. *Proc. Natl. Acad. Sci. U. S. A.* **97**, 11050–5 (2000).

41. Dickerson, B. C. *et al.* The cortical signature of Alzheimer's disease: regionally specific cortical thinning relates to symptom severity in very mild to mild AD dementia and is detectable in asymptomatic amyloid-positive individuals. *Cereb. Cortex* **19**, 497–510 (2009).

42. Cardinale, F. *et al.* Validation of FreeSurfer-Estimated Brain Cortical Thickness: Comparison with Histologic Measurements. *Neuroinformatics* **12**, 535–542 (2014).

43. La Joie, R. *et al.* Prospective longitudinal atrophy in Alzheimer's disease correlates with the intensity and topography of baseline tau-PET. *Sci. Transl. Med.* **12**, 1–13 (2020).

44. Alexander, D. C., Dyrby, T. B., Nilsson, M. & Zhang, H. Imaging brain microstructure with diffusion MRI: Practicality and applications. 1–26 (2016) doi:10.1002/nbm.3841.

45. Einstein, A. On the movement of small particles suspended in a stationary liquid demanded by the molecular-kinetic theory of heat. *Ann. Phys.* (1905).

46. Le Bihan, D. Looking into the functional architecture of the brain with diffusion MRI. *Nat. Rev. Neurosci.* **4**, 469–80 (2003).

47. Jelescu, I. O. & Budde, M. D. Design and Validation of Diffusion MRI Models of White Matter. *Front. Phys.* **5**, (2017).

48. Alexander, A. L., Lee, J. E., Lazar, M. & Field, A. S. Diffusion tensor imaging of the brain. *Neurotherapeutics* **4**, 316–29 (2007).

49. Basser, P. . Inferring Microstructural Features and the Physiological State of Tissues from Diffusion Weighted Images. *NMR Biomed.* **8**, 333–344 (1995).

50. Uluğ, A. M., Moore, D. F., Bojko, A. S. & Zimmerman, R. D. Clinical use of diffusion-tensor imaging for diseases causing neuronal and axonal damage. *AJNR. Am. J. Neuroradiol.* **20**, 1044–8 (1999).

51. Fortea, J. *et al.* Increased cortical thickness and caudate volume precede atrophy in psen1 mutation carriers. *J. Alzheimer's Dis.* **22**, 909–922 (2010).

52. Weston, P. S. J., Simpson, I. J. A., Ryan, N. S., Ourselin, S. & Fox, N. C. Diffusion imaging changes in grey matter in Alzheimer ' s disease : a potential marker of early neurodegeneration. *Alzheimers. Res. Ther.* **7**, 1–8 (2015).

53. Henf, J., Grothe, M. J., Brueggen, K., Teipel, S. & Dyrba, M. Mean diffusivity in cortical gray matter in Alzheimer's disease: The importance of partial volume correction. *NeuroImage Clin.* **17**, 579–586 (2018).

54. Montal, V. *et al.* Cortical microstructural changes along the Alzheimer's disease continuum. *Alzheimer's Dement.* 1–12 (2017) doi:10.1016/j.jalz.2017.09.013.

55. Vogt, N. M. *et al.* Cortical Microstructural Alterations in Mild Cognitive Impairment and Alzheimer's Disease Dementia. *Cereb. Cortex* bhz286 (2019) doi:10.1093/cercor/bhz286.

56. Parker, T. D. *et al.* Cortical microstructure in young onset Alzheimer's disease using neurite orientation dispersion and density imaging. *Hum. Brain Mapp.* 1–13 (2018) doi:10.1002/hbm.24056.

57. Illán-Gala, I. *et al.* Cortical microstructure in the behavioural variant of frontotemporal dementia: looking beyond atrophy. *Brain* **142**, 1121–1133 (2019).

58. Solana, E. *et al.* Regional grey matter microstructural changes and volume loss according to disease duration in multiple sclerosis patients. *Sci. Rep.* **11**, 1–11 (2021).

59. Illán-Gala, I. *et al.* Cortical microstructure in the amyotrophic lateral sclerosis-frontotemporal dementia continuum. *Neurology* **in-press**, 10.1212/WNL.0000000000010727 (2020).

60. Danielsen, E. & Ross, B. *Magnetic resonance spectroscopy diagnosis of neurological diseases*. (1999).

61. Klunk, W. E., Panchalingam, K., Moossy, J., McClure, R. J. & Pettegrew, J. W. N-acetyl-L-aspartate and other amino acid metabolites in Alzheimer's disease brain: a preliminary proton nuclear magnetic resonance study. *Neurology* **42**, 1578–1585 (1992).

62. Miller, B. L. *et al.* Alzheimer disease: depiction of increased cerebral myo-inositol with proton MR spectroscopy. *Radiology* **187**, 433–437 (1993).

63. Kantarci, K. *et al.* Regional metabolic patterns in mild cognitive impairment and Alzheimer's disease: A 1H MRS study. *Neurology* **55**, 210–217 (2000).

64. Harris, J. L., Choi, I. Y. & Brooks, W. M. Probing astrocyte metabolism in vivo: Proton magnetic resonance spectroscopy in the injured and aging brain. *Front. Aging Neurosci.* **7**, 1–8 (2015).

65. Dubois, B. *et al. Preclinical Alzheimer's disease: Definition, natural history, and diagnostic criteria*. *Alzheimer's & Dementia* vol. 12 (2016).

66. Hubbard, B. M., Fentonm, G. W. & Aanderson, J. M. A quantitative histological study of early clinical and preclinical Alzheimer's disease. *Neuropathol. Appl. Neurobiol.* **16**, 111–121 (1990).

67. Ingala, S. *et al.* Application of the ATN classification scheme in a population without dementia: Findings from the EPAD cohort. *Alzheimer's Dement.* **17**, 1189–1204 (2021).

68. McDade, E. *et al.* Longitudinal cognitive and biomarker changes in dominantly inherited Alzheimer disease. *Neurology* 10.1212/WNL.0000000000006277 (2018) doi:10.1212/WNL.0000000000006277.

69. Fortea, J. *et al.* Cognitively Preserved Subjects with Transitional Cerebrospinal Fluid ß-Amyloid 1-42 Values Have Thicker Cortex in Alzheimer Disease Vulnerable Areas. *Biol. Psychiatry* **70**, 183–190 (2011).

70. Fortea, J. *et al.* Cerebrospinal Fluid ß-Amyloid and Phospho-Tau Biomarker Interactions Affecting Brain Structure in Preclinical Alzheimer Disease. *Ann. Neurol.* **76**, 223–30 (2014).

71. Pegueroles, J. *et al.* Longitudinal brain structural changes in preclinical Alzheimer disease. *Alzheimer's Dement.* **9**, 1–11 (2016).

72. Vilaplana, E. *et al.* Cortical microstructural correlates of astrocytosis in autosomal- dominant Alzheimer ' s disease. *Neurology* **94**, 1:11 (2020).

73. Buckner, R. L. *et al.* Cortical Hubs Revealed by Intrinsic Functional Connectivity: Mapping, Assessment of Stability, and Relation to Alzheimer's Disease. *J. Neurosci.* **29**, 1860–1873 (2009).

74. Sepulcre, J. *et al.* In vivo Tau, Amyloid and Grey Matter Profiles in the Aging Brain. *J. Neurosci.* **In press**, 7364–7374 (2016).

75. Sepulcre, J., Sabuncu, M. R., Becker, A., Sperling, R. & Johnson, K. a. In vivo characterization of the early states of the amyloid-beta network. *Brain* **136**, 2239–2252 (2013).

76. Jones, D. T. Tau, amyloid, and cascading network failure across the Alzheimer's disease spectrum. *Cortex* **97**, 143–159 (2017).

77. Seeley, W. W., Crawford, R. K., Zhou, J., Miller, B. L. & Greicius, M. D. Neurodegenerative diseases target large-scale human brain networks. *Neuron* **62**, 42–52 (2009).

78. Raj, A., Kuceyeski, A. & Weiner, M. A Network Diffusion Model of Disease Progression in Dementia. *Neuron* **73**, 1204–1215 (2012).

79. Zhou, J., Gennatas, E. D., Kramer, J. H., Miller, B. L. & Seeley, W. W. Predicting regional neurodegeneration from the healthy brain functional connectome. *Neuron* **73**, 1216–27 (2012).

80. Fu, H., Hardy, J. & Duff, K. E. Selective vulnerability in neurodegenerative diseases. *Nat. Neurosci.* **21**, 1350–1358 (2018).

81. Mrdjen, D. *et al.* The basis of cellular and regional vulnerability in Alzheimer's disease. *Acta Neuropathol.* **138**, 729–749 (2019).

82. Muratore, C. R. *et al.* Cell-type Dependent Alzheimer's Disease Phenotypes: Probing the Biology of Selective Neuronal Vulnerability. *Stem Cell Reports* **9**, 1868–1884 (2017).

83. Mathys, H. *et al.* Single-cell transcriptomic analysis of Alzheimer's disease. *Nature* **2**, (2019).

84. Habib, N. *et al.* Disease-associated astrocytes in Alzheimer's disease and aging. *Nat. Neurosci.* 1–6 (2020) doi:10.1038/s41593-020-0624-8.

85. Shen, E. H., Overly, C. C. & Jones, A. R. The Allen Human Brain Atlas: comprehensive gene expression mapping of the human brain. *Trends Neurosci.* **35**, 711–714 (2012).

86. Diez, I. *et al.* Early-life trauma endophenotypes and brain circuit-gene expression relationships in functional neurological (conversion) disorder. *Mol. Psychiatry* **26**, 3817–3828 (2021).

87. Seidlitz, J. *et al.* Transcriptomic and cellular decoding of regional brain vulnerability to neurogenetic disorders. *Nat. Commun.* **11**, 1–14 (2020).

88. Sepulcre, J. *et al.* Neurogenetic contributions to amyloid beta and tau spreading in the human cortex. *Nat. Med.* (2018) doi:10.1038/s41591-018-0206-4.

89. Grothe, M. J. *et al.* Molecular properties underlying regional vulnerability to Alzheimer's disease pathology8 for the Alzheimer's Disease Neuroimaging Initiative*. 1–17 (2018) doi:10.1093/brain/awy189.

90. Chen, G. *et al.* Beyond linearity in neuroimaging: Capturing nonlinear relationships with application to longitudinal studies. *Neuroimage* **233**, 117891 (2021).

91. Jimenez, A. *et al.* Weight loss in the healthy elderly might be a non-cognitive sign of preclinical Alzheimer's disease. *Oncotarget* **8**, 104706–104716 (2017).

92. Euler, L. Solutio problematis ad geometriam situs pertinentis. *Comment. Acad. Sci. U. Petrop* (1736).

93. Barabási, A.-L. *Network Science*. (Cambridge University Press; 1er edición (5 Agosto 2016), 2016).

94. Bassett, D. S. & Sporns, O. Network neuroscience. *Nat. Neurosci.* **20**, 353 (2017).

95. Bullmore, E. & Sporns, O. Complex brain networks: graph theoretical analysis of structural and functional systems. *Nat. Rev. Neurosci.* **10**, 186–98 (2009).

96. Yu, M., Sporns, O. & Saykin, A. J. The human connectome in Alzheimer. *Nat. Rev. Neurol.* **0123456789**, (2021).

97. Perez-Nievas, B. G. & Serrano-Pozo, A. Deciphering the astrocyte reaction in Alzheimer's disease. *Front. Aging Neurosci.* **10**, 1–23 (2018).

98. Chen, W. T. *et al.* Spatial Transcriptomics and In Situ Sequencing to Study Alzheimer's Disease. *Cell* **182**, 976-991.e19 (2020).

99. Frigerio, I. CORTICAL THICKNESS IN ALZHEIMER'S DISEASE: DIFFERENTIAL CONTRIBUTIONS OF AMYLOID-BETA AND P-TAU LOAD. *ADPD 2021 Conf.* (2021).

100. Roitbak, T. & Syková, E. Diffusion barriers evoked in the rat cortex by reactive astrogliosis. *Glia* **28**, 40–8 (1999).

101. Hamelin, L. *et al.* Early and protective microglial activation in Alzheimer's disease: A prospective study using 18F-DPA-714 PET imaging. *Brain* **139**, 1252–1264 (2016).

102. Femminella, G. D. *et al.* Microglial activation in early Alzheimer trajectory is associated with higher gray matter volume. *Neurology* (2019) doi:10.1212/WNL.0000000000007133.

103. Busche, M. A. & Hyman, B. T. Synergy between amyloid-β and tau in Alzheimer's disease. *Nat. Neurosci.* **23**, 1183–1193 (2020).

104. Desikan, R. S. *et al.* Amyloid-β associated volume loss occurs only in the presence of phospho-tau. *Ann. Neurol.* **70**, 657–61 (2011).

105. Johnson, S. C. *et al.* Amyloid burden and neural function in people at risk for Alzheimer's Disease. *Neurobiol. Aging* **35**, 576–84 (2014).

106. Chételat, G. *et al.* Larger temporal volume in elderly with high versus low beta-amyloid deposition. *Brain* **133**, 3349–58 (2010).

107. Josephs, K. a *et al.* Beta-amyloid burden is not associated with rates of brain atrophy. *Ann. Neurol.* **63**, 204–12 (2008).

108. Becker, J. A. *et al.* Amyloid-β associated cortical thinning in clinically normal elderly. *Ann. Neurol.* **69**, 1032–42 (2011).

109. Harrison, T. M. *et al.* Distinct effects of beta-amyloid and tau on cortical thickness in cognitively healthy older adults. *Alzheimers. Dement.* 1–12 (2020) doi:10.1002/alz.12249.

110. Vogt, N. M. *et al.* Interaction of amyloid and tau on cortical microstructure in cognitively unimpaired adults. *Alzheimers. Dement.* 1–12 (2021) doi:10.1002/alz.12364.

111. Sala-Llonch, R. *et al.* Evolving brain functional abnormalities in PSEN1 mutation carriers: a resting and visual encoding fMRI study. *J. Alzheimers. Dis.* **36**, 165–75 (2013).

112. Fox-fuller, J. T. *et al.* Cortical thickness across the lifespan in a Colombian cohort with autosomal-dominant Alzheimer ' s disease : A cross-sectional study. *Alzheimer's Dement. J. Alzheimer's Assoc.* 1–11 (2021) doi:10.1002/dad2.12233.

113. Quan, M. *et al.* Effects of gene mutation and disease progression on representative neural circuits in familial Alzheimer's disease. *Alzheimers. Res. Ther.* **12**, 14 (2020).

114. Luckett, P. H. *et al.* Modeling autosomal dominant Alzheimer ' s disease with machine learning. *Alzheimer's Dement.* 1–12 (2021) doi:10.1002/alz.12259.

115. Querol-Vilaseca, M. *et al.* YKL-40 (Chitinase 3-like I) is expressed in a subset of astrocytes in Alzheimer's disease and other tauopathies. *J. Neuroinflammation* **14**, 1–10 (2017).

116. Alcolea, D. *et al.* Relationship between cortical thickness and cerebrospinal fluid YKL-40 in predementia stages of Alzheimer's disease. *Neurobiol. Aging* 1–6 (2015) doi:10.1016/j.neurobiolaging.2015.03.001.

117. Voevodskaya, O. & Sundgren, P. C. Myo-inositol changes precede amyloid pathology and relate to APOE genotype in Alzheimer disease. **0**, (2016).

118. Fortea, J. *et al.* Clinical and biomarker changes of Alzheimer's disease in adults with Down syndrome: a cross-sectional study. *Lancet* **395**, 1988–1997 (2020).

119. Anders M. Fjell. One year brain atrophy evident in healthy aging Anders. *J Neurosci* **29**, 15223–15231 (2010).

120. Fjell, A. M., McEvoy, L., Holland, D., Dale, A. M. & Walhovd, K. B. What is normal in normal aging? Effects of aging, amyloid and Alzheimer's disease on the cerebral cortex and the hippocampus. *Prog. Neurobiol.* **117**, 20–40 (2014).

121. Oh, H., Madison, C., Villeneuve, S., Markley, C. & Jagust, W. J. Association of gray matter atrophy with age, β-amyloid, and cognition in aging. *Cereb. Cortex* **24**, 1609–1618 (2014).

122. Frangou, S. *et al.* Cortical thickness across the lifespan: Data from 17,075 healthy individuals aged 3–90 years. *Hum. Brain Mapp.* 1–21 (2021) doi:10.1002/hbm.25364.

123. Braak, H. & Del Tredici, K. The preclinical phase of the pathological process underlying sporadic Alzheimer's disease. *Brain* **138**, 2814–2833 (2015).

124. Jack Jr, C. R. *et al.* Age-specific population frequencies of cerebral β-amyloidosis and neurodegeneration among people with normal cognitive function aged 50–89 years: a cross-sectional study. *Lancet Neurol.* **13**, 997–1005 (2014).

125. Mattsson, N. *et al.* Age and diagnostic performance of Alzheimer disease CSF biomarkers From the Clinical Neurochemistry Laboratory (N Supplemental data at www.neurology.org. (2012).

126. Knopman, D. S. *et al.* Entorhinal cortex tau, amyloid-β, cortical thickness and memory performance in non-demented subjects. *Brain* **142**, 1148–1160 (2019).

127. Bejanin, A. *et al.* Distinct Interplay Between Atrophy and Hypometabolism in Alzheimer's Versus Semantic Dementia. *Cereb. Cortex* 1–11 (2018) doi:10.1093/cercor/bhy069.

128. Fox, N. C. *et al.* Effects of Aβ immunization (AN1792) on MRI measures of cerebral volume in Alzheimer disease. *Neurology* **64**, 1563–1572 (2005).

129. Sur, C. *et al.* BACE inhibition causes rapid, regional, and non-progressive volume reduction in Alzheimer's disease brain. *Brain* **143**, 3816–3826 (2020).

130. Satir, T. M. *et al.* Partial reduction of amyloid β production by β-secretase inhibitors does not decrease synaptic transmission. *Alzheimer's Res. Ther.* **12**, 1–9 (2020).

131. Mintun, M. A. *et al.* Donanemab in Early Alzheimer's Disease. *N. Engl. J. Med.* **384**, 1691–1704 (2021).

132. Benzinger, T. L. S. *et al.* Regional variability of imaging biomarkers in autosomal dominant Alzheimer's disease. *Proc. Natl. Acad. Sci. U. S. A.* **110**, E4502-9 (2013).

133. Weston, P. S. J. *et al.* Presymptomatic cortical thinning in familial Alzheimer disease: A longitudinal MRI study. *Neurology* **87**, 2050–2057 (2016).

134. Araque Caballero, M. Á. *et al.* White matter diffusion alterations precede symptom onset in autosomal dominant Alzheimer's disease. *Brain* (2018) doi:10.1093/brain/awy229.

135. Collij, L. E. *et al.* White matter microstructure disruption in early stage amyloid pathology. 1–9 (2021) doi:10.1002/dad2.12124.

136. Nasrabady, S. E., Rizvi, B., Goldman, J. E. & Brickman, A. M. White matter changes in Alzheimer's disease: a focus on myelin and oligodendrocytes. *Acta Neuropathol. Commun.* **6**, 22 (2018).

137. Heppner, F. L., Ransohoff, R. M. & Becher, B. Immune attack: the role of inflammation in Alzheimer disease. *Nat. Rev. Neurosci.* **16**, 358–372 (2015).

138. Kinney, J. W. *et al.* Inflammation as a central mechanism in Alzheimer's disease. *Alzheimer's Dement. (New York, N. Y.)* **4**, 575–590 (2018).

139. Suárez-Calvet, M. *et al.* Early changes in CSF sTREM2 in dominantly inherited Alzheimer's disease occur after amyloid deposition and neuronal injury. *Sci. Transl. Med.* **8**, 34–38 (2016).

140. Fan, Z., Brooks, D. J., Okello, A. & Edison, P. An early and late peak in microglial activation in Alzheimer's disease trajectory. *Brain* aww349 (2017) doi:10.1093/brain/aww349.

141. Benedet, A. L. *et al.* Differences between Plasma and Cerebrospinal Fluid Glial Fibrillary Acidic Protein Levels across the Alzheimer Disease Continuum. *JAMA Neurol.* 1–13 (2021) doi:10.1001/jamaneurol.2021.3671.

142. Hasel, P., Rose, I. V. L., Sadick, J. S., Kim, R. D. & Liddelow, S. A. Neuroinflammatory astrocyte subtypes in the mouse brain. *Nat. Neurosci.* **24**, 1475–1487 (2021).

143. Keren-Shaul, H. *et al.* A Unique Microglia Type Associated with Restricting Development of Alzheimer's Disease. *Cell* **169**, 1276-1290.e17 (2017).

144. Escartin, C. *et al.* Reactive astrocyte nomenclature, definitions, and future directions. *Nat. Neurosci.* **24**, (2021).

145. Nordengen, K. *et al.* Glial activation and inflammation along the Alzheimer's disease continuum. *J. Neuroinflammation* **16**, 1–13 (2019).

146. Gispert, J. D. *et al.* Cerebrospinal fluid sTREM2 levels are associated with gray matter volume increases and reduced diffusivity in early Alzheimer's disease. *Alzheimer's Dement.* **0**, 614–629 (2016).

147. Pascoal, T. A. *et al.* Microglial activation and tau propagate jointly across Braak stages. *Nat. Med.* (2021) doi:10.1038/s41591-021-01456-w.

148. Palombo, M., Shemesh, N., Ronen, I. & Valette, J. Insights into brain microstructure from in vivo DW-MRS. *Neuroimage* **182**, 97–116 (2018).

149. Genovese, G. *et al. Inflammation-driven glial alterations in the cuprizone mouse model probed with diffusion-weighted magnetic resonance spectroscopy at 11.7 T*. vol. 33 (2020).

150. Ligneul, C. *et al.* Diffusion-weighted magnetic resonance spectroscopy enables cell-specific monitoring of astrocyte reactivity in vivo. *Neuroimage* **191**, 457–469 (2019).

151. De Marco, R. *et al.* Diffusion-weighted MR spectroscopy (DW-MRS) is sensitive to LPS-induced changes in human glial morphometry: A preliminary study. *Brain. Behav. Immun.* **99**, 256–265 (2022).

152. Mattsson-carlgren, N. *et al.* Aβ deposition is associated with increases in soluble and phosphorylated tau that precede a positive Tau PET in Alzheimer ' s disease. *Sci. Adv.* (2020).

153. Knopman, D. S. *et al.* Association of Initial β-Amyloid Levels With Subsequent Flortaucipir Positron Emission Tomography Changes in Persons Without Cognitive Impairment. *JAMA Neurol.* **55905**, (2020).

154. Chapter 8 - Moving Beyond DTI: High Angular Resolution Diffusion Imaging (HARDI). in *Introduction to Diffusion Tensor Imaging (Second Edition)* (eds. Mori, S. & Tournier, J.-D.) 65–78 (Academic Press, 2014). doi:https://doi.org/10.1016/B978-0-12-398398-5.00008-4.

155. Zhang, H., Schneider, T., Wheeler-Kingshott, C. A. & Alexander, D. C. NODDI: Practical in vivo neurite orientation dispersion and density imaging of the human brain. *Neuroimage* **61**, 1000–1016 (2012).

156. Jensen, J. H. & Helpern, J. A. MRI quantification of non-Gaussian water diffusion by kurtosis analysis. *NMR Biomed.* **23**, 698–710 (2010).

157. Fukutomi, H. *et al.* Neurite imaging reveals microstructural variations in human cerebral cortical gray matter. *Neuroimage* (2018) doi:10.1016/j.neuroimage.2018.02.017.

158. Diez, I. & Sepulcre, J. Unveiling the neuroimaging-genetic intersections in the human brain. *Curr. Opin. Neurol.* **34**, 480–487 (2021).

159. Maiorino, E. *et al.* Discovering the genes mediating the interactions between chronic respiratory diseases in the human interactome. *Nat. Commun.* **11**, 1–14 (2020).

7. Supplementary studies

Cortical microstructural changes along the Alzheimer's disease continuum

Victor Montal;[1,2,*] Eduard Vilaplana;[1,2,*] Daniel Alcolea[1,2] Jordi Pegueroles;[1,2] Ofer Pasternak[3] Sofia González-Ortiz;[4] Jordi Clarimón;[1,2] María Carmona-Iragui;[1,2] Ignacio Illán-Gala;[1,2] Estrella Morenas-Rodríguez;[1,2] Roser Ribosa-Nogué;[1,2] Isabel Sala;[1,2] María-Belén Sánchez-Saudinos;[1,2] Maite García-Sebastian;[5] Jorge Villanúa;[5,6] Andrea Izagirre;[5] Ainara Estanga;[5] Mirian Ecay-Torres;[5] Ane Iriondo;[5] Montserrat Clerigue;[5] Mikel Tainta;[5] Ana Pozueta;[7] Andrea González;[7] Eloy Martínez-Heras;[8] Sara Llufriu;[8] Rafael Blesa;[1,2] Pascual Sanchez-Juan;[7] Pablo Martínez-Lage;[2,5] Alberto Lleó;[1,2] Juan Fortea.[1,2]

(1) Memory Unit, Department of Neurology, Hospital de la Santa Creu i Sant Pau- Biomedical Research Institute Sant Pau-Universitat Autònoma de Barcelona, Barcelona, Spain. (2) Centro de Investigación Biomédica en Red de Enfermedades Neurodegenerativas. CIBERNED, Spain. (3) Departments of Psychiatry and Radiology, Brigham and Women's Hospital, Harvard Medical School, Boston, Massachusetts, USA. (4) Department of Radiology, Hospital del Mar, Barcelona, Spain. (5)Center for Research and Advanced Therapies and Memory Clinic. Fundacion CITA-alzheimer Fundazioa. Donostia/San Sebastian, Spain. (6) Donostia Unit, Osatek SA, Donostia University Hospital, San Sebastian, Spain (7) Servicio de Neurología, Hospital Universitario Marqués de Valdecilla, Santander, Spain (8)Center for Neuroimmunology, Hospital Clinic Barcelona, IDIBAPS, Barcelona, Spain.

Alzheimers Dement (2017) doi: 10.1016/j.jalz.2017.09.013

ABSTRACT

Cortical mean diffusivity (MD) and free water (FW) changes are proposed biomarkers for Alzheimer's disease (AD). We included healthy controls (N=254, HC), mild cognitive impairment (N=41, MCI) and AD dementia (N=31, dAD) patients. Participants underwent a lumbar puncture and a 3T-MRI. HC were classified following NIA-AA stages (Stage 0, N=220; Stage 1, N=25 and; Stage 2/3, N=9). We assessed the cortical MD, cortical FW and cortical thickness (CTh) changes along the AD continuum. Micro and macrostructural changes show a biphasic trajectory. Stage 1 subjects showed increased CTh and decreased MD and FW with respect the Stage 0 subjects. Stage 2/3 subjects showed decreased CTh and increased cortical MD and FW, changes that were more widespread in symptomatic stages. These results support a biphasic model of changes in AD, which could affect the selection of patients for clinical trials and the use of MRI as surrogate marker of disease modification.

BACKGROUND

Alzheimer's disease (AD) has a long preclinical phase in which several pathophysiological processes coexist before the appearance of the first clinical symptoms [1,2]. Despite the well-established description of brain atrophy in the symptomatic phase of AD, the structural trajectory of changes in preclinical AD is still controversial. It has been recently shown that β-amyloid interacts with cortical tau pathology to affect neurodegeneration [3–5]. The cortical changes might, however, be non-linear. There are several reports in different cohorts of an association between cortical thickening and brain amyloidosis, both in cross-sectional [4,6–10] and in longitudinal studies [11]. Based on those reports, we have previously proposed a model in which interactions between biomarkers in the preclinical phase of AD result in a 2-phase phenomenon: an initial phase of cortical thickening associated with brain amyloidosis, in the absence of tau, followed by a cortical atrophy phase, which occurs once tau biomarkers become abnormal [4].

New imaging biomarkers and extensive multimodal approaches could improve our understanding of the cortical changes along the AD continuum. For example, in the last decade, there has been a growing interest in diffusion-weighted imaging (DWI), which is sensitive to the microstructural properties of brain tissue [12]. Although most studies in the literature have used this technique to assess the microstructure in the white matter (WM) [13], DWI are also studied to reflect microstructural changes in the grey matter (GM). The mean diffusivity (MD) metric is often used in GM studies because the cortex is mostly an isotropic structure [8,12].

The number of GM diffusivity studies in AD to date is, however, limited, and all have small sample sizes. Based on these studies in familial [8,14] and sporadic AD [15], a biphasic trajectory of MD changes in the AD continuum has also been suggested [12]. Accordingly, in the pre symptomatic phase, MD would initially decrease because of cellular hypertrophy and/or inflammation (glial recruitment) [8,14]. Then, during the symptomatic phase, the progressive cellular loss and microstructural disorganization would cause the breakdown of diffusion barriers and leads to an increase in extracellular water and MD in vulnerable regions [12]. Therefore, this proposed biphasic trajectory of grey matter diffusivity changes would be similar to that described for cortical thickness (CTh) [4].

Another promising measure that can be derived from diffusion imaging is the free water fraction (FW)[16]. The proposed two-compartment model distinguishes the contribution of freely diffusing extracellular water from that of tissue-restricted water. It has been recently suggested that the FW component provides great sensitivity to detect

extracellular processes such as atrophy, cerebral edema or even neuroinflammation [17]. Moreover, the FW measure has been suggested as an important marker in the AD continuum [18–20].

We hypothesized that cortical diffusivity, cortical FW and CTh follow a biphasic trajectory of changes, where increases in CTh are associated with decreases in MD and FW in the early preclinical phase followed by atrophy associated with increased MD and FW in the symptomatic phase of the disease. Our objective was to study the cortical microstructural changes and their relationship with CTh along the AD continuum.

METHODS

Participants

A total of 449 subjects were recruited from 3 centers in Spain: Hospital de Sant Pau (HSP), Barcelona (n=263), Hospital Marqués de Valdecilla (HMV), Santander (n=22) and CITA Alzheimer, San Sebastián (n=164). We included cognitively normal healthy controls (HC), people with mild cognitive impairment (MCI) and AD dementia patients (dAD). All subjects underwent a lumbar puncture and a 3 Tesla MRI. A flowchart of the sample can be found in Fig. 1.

The HC (N=329) participants were unaffected relatives of patients in the three centers or volunteers who enrolled after hearing about the study in the media. The HC did not have cognitive complaints, they scored 0 on the clinical dementia rating scale (CDR) and their neuropsychological evaluation was normal for their age and education. Based on the CSF biomarker profile, and using previously published cut-off thresholds (Aß+ <550 pg/mL for CSF Aß1-42 and p-tau+ > 61 pg/ mL for CSF p-tau) [21], the HC subjects were classified into preclinical AD stages: Stage 0 (Aß-/p-tau-), Stage 1 (Aß+/p-tau-) and Stage 2/3 (Aß+/p-tau+). 23 subjects did not meet the NIA-AA preclinical staging criteria (Aß-/p-tau+) and were excluded from further analyses [1,11].

The MCI and the AD dementia subjects (N=120) were recruited at the HSP (SPIN cohort, http://santpaumemoryunit.com/). They all fulfilled the NIA-AA clinical criteria for probable AD dementia. From these, we selected only those with evidence of the AD pathophysiological process [22] according to CSF Aß1-42 and p-tau values [21]. Thus, 35 MCI and 1 dAD subjects were excluded because of a negative CSF AD profile.

More details about the recruitment and the assessments performed can be found elsewhere [21,23]. Briefly, all participants enrolled in this study were evaluated by neurologists with expertise in neurodegenerative diseases, and all had an extensive neuropsychological evaluation, as defined by the SIGNAL study (www.signalstudy.es). The complete neuropsychological battery can be found in [24].

The study was approved by the local Ethics Committee in each center following the ethical standards recommended by the Helsinki Declaration. All subjects gave their written informed consent.

MRI acquisition

3 Tesla MRIs were acquired at three different sites with different acquisition protocols. HMV subjects did not have DWI data. The acquisition parameters can be found in the supplementary material. Importantly, all centers had a structural acquisition of 1x1x1 mm isotropic resolution and a diffusion acquisition of at least 2x2x2 mm isotropic resolution.

CSF acquisition and analysis

CSF was acquired following international consensus recommendations, as previously described [21]. All the analyses were done in the Hospital of Sant Pau using

commercial ELISA kits (Fujirebio Europe). The interassay CV for all CSF determinations performed in this study was less than 15% [21].

Genetic Analysis

APOE genotype was determined as previously described [21].

Cortical thickness processing

Cortical thickness reconstruction was performed with Freesurfer package v5.1 (http://surfer.nmr.mgh.harvard.edu) using a procedure that has been described in detail elsewhere [25] (Fig. 2-Left) as previously reported [4,23]. A Gaussian kernel of 15 mm full-width at half maximum was applied to the subjects' CTh maps before further analyses as it is customary in surface based analyses [4,11,26]. From the remaining 390 subjects, 21 were excluded due to suboptimal image quality, which included subtle movement artifacts, poor SNR and gradient artifacts. Additional 43 subjects (11%) were excluded due to incorrect cortical segmentation by Freesurfer.

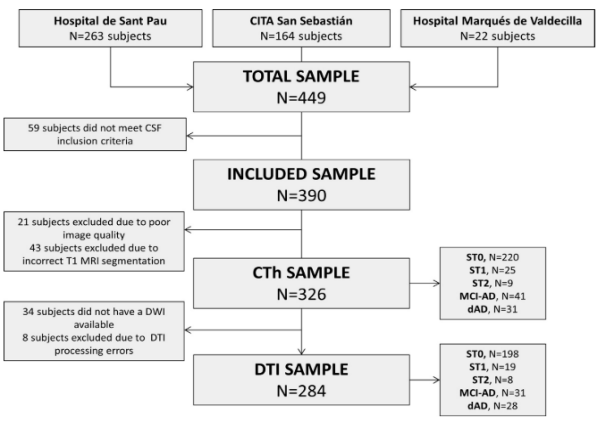

Fig. 1. Flowchart of the methodological procedures and the resulting samples after each process.

Cortical mean diffusivity processing

From the resulting 326 subjects, 284 were included for diffusion MRI analysis (34 had no raw data and 8 were excluded due to processing errors). We used a homemade surface-based approach based on the recent literature advances [27,28] to process cortical diffusion MRI, since the commonly used voxel-based morphometry (VBM) approach has limitations when used in GM analyses, where partial volume effects may bias cortical MD measurements [29] due to CSF signal inclusion in GM voxels. Moreover, VBM analyses are very sensitive to the smoothing kernel: different volume-based smoothing kernels provide diverse statistical results [30]. In order to mitigate these pitfalls, we used a surface-based DTI approach using the FSL package (http://fsl.fmrib.ox.ac.uk/fsl/fslwiki/, version 5.0.9) and, the Freesurfer package (v5.1). Further, to eliminate possible site biases on the diffusion MRI data, we applied a harmonization procedure using the ComBat toolbox [31], which was designed for multi-site studies. Please see harmonization details in the Supplementary material. The MD procedures are summarized in Fig. 2-Right and explained in detail in the Supplementary data. Briefly, the diffusion images were corrected for motion effects, skull-stripped, DTI tensor fitted and projected to the brain surface. A Gaussian kernel of 15 mm full-width at half maximum was applied to the subjects' mean diffusivity surface maps before further analyses [26]. Finally, the surface MD maps were harmonized and used for the statistical analyses.

All the MD analyses were repeated applying a partial volume (PV) correction especially designed for mean diffusivity studies [29]. Further detail can be found in the Supplementary material.

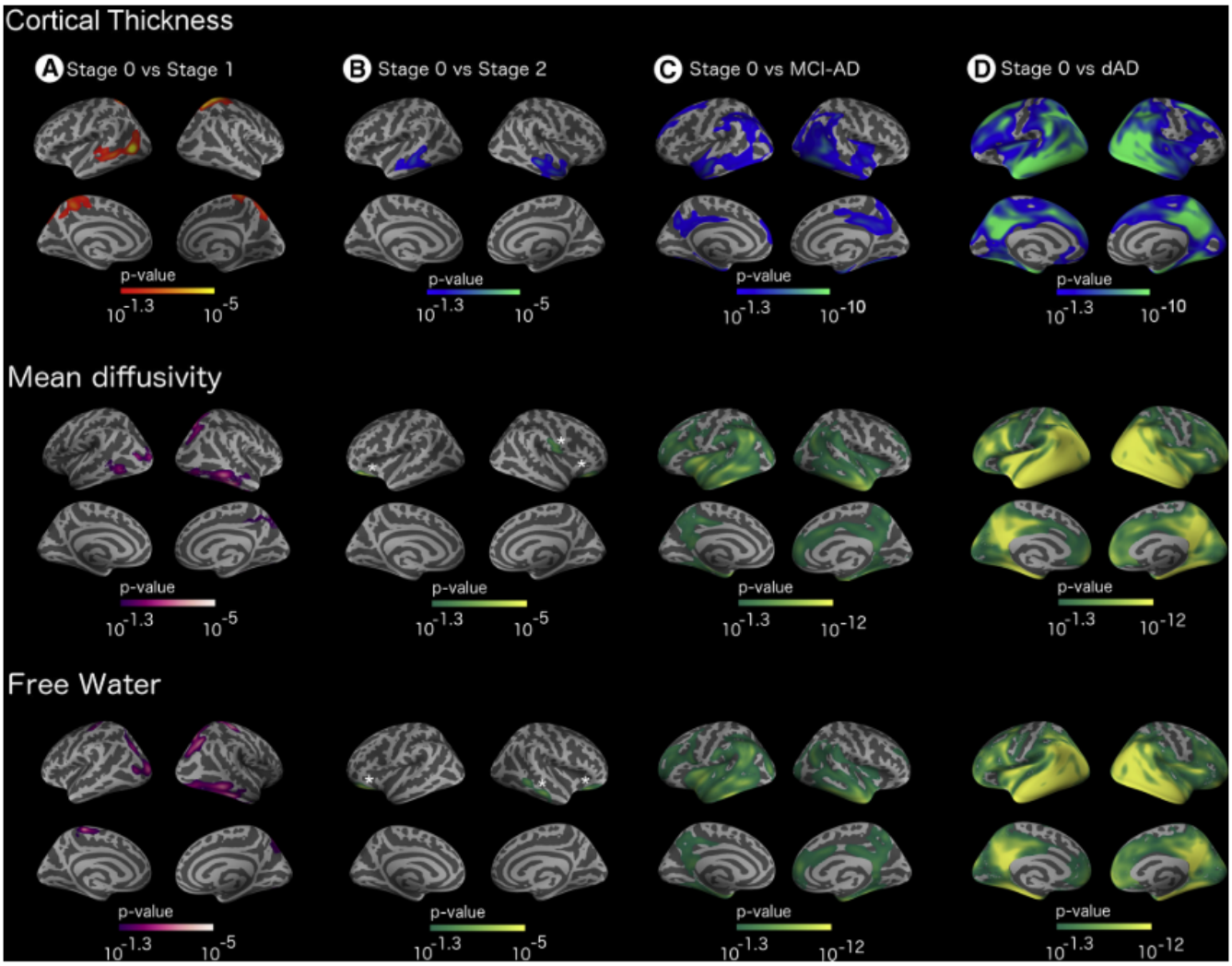

Fig. 3. Top. Cortical Thickness patterns in the AD continuum. (A) CTh differences in Stage 0 vs Stage 1 HC, (B) Stage 0 vs Stage 2 HC, (C) Stage 0 HC vs MCI-AD patients and (D) Stage 0 HC vs AD patients. Only clusters that survive family-wise error corrected p<0.05 are shown. All the analyses are adjusted by age, sex, center and *APOE*.

Mid. Cortical Mean Diffusivity patterns in the AD continuum. (A) MD differences in Stage 0 vs Stage 1 HC, (B) Stage 0 vs Stage 2 HC, (C) Stage 0 vs MCI-AD patients and (D) Stage 0 HC vs dAD patients. Only clusters that survive family-wise error corrected p<0.05 are shown. All the analyses are adjusted by age, sex and *APOE*.

Bottom. Free-water (FW) patterns in the AD continuum. (A) FW differences in Stage 0 vs Stage 1 HC, (B) Stage 0 vs Stage 2 HC, (C) Stage 0 vs MCI-AD patients and (D) Stage 0 HC vs dAD patients. Only clusters that survive family-wise error corrected p<0.05 are shown. All the analyses are adjusted by age, sex and *APOE*.

MD=Mean Diffusivity; FW=Free-water; CTh = Cortical Thickness; HC= Healthy Controls; MCI-AD= Mild cognitive impairment with evidence of an underlying AD pathophysiological process; dAD= Alzheimer's disease dementia with evidence of an underlying AD pathophysiological process.

For visualization purposes, different color-codes were used for MD/FW and CTh. For the MD/FW results, we used a green-yellow color-code and a purple-white color representation for positive and negative significant values, respectively. For CTh results, we used a gradient-blue scale color-code and a red-yellow color representation for negative and positive significant values, respectively. In the stage 2 vs stage 0 comparisons, significant clusters are highlighted with an asterisk for visualization purposes.

Cortical free-water processing

The FW maps were computed as previously reported [16]. Briefly, the FW maps were estimated fitting a regularized bi-compartment model to our DWI data. This model includes a "tissue" compartment and a FW compartment. Free water was defined as water molecules that are not hindered or restricted, and are hence extracellular, with a diffusion coefficient of water in body temperature. The FW metric stands for the fraction of the FW compartment in a certain voxel (i.e. percentage of a certain voxel). Once the FW maps were computed, they were projected to the surface, smoothed (kernel size of FWHM 15 mm) and finally were harmonized before further statistical analyses. Same as for the MD, all the analyses were repeated applying a partial volume correction before the surface projection (see Supplementary material).

Statistical methods

Demographic group analyses were made using R statistical software (https://www.r-project.org/). Comparisons between groups were performed using an ANOVA with Tukey post-hoc corrections for continuous variables and with a chi-square test for categorical variables.

We first performed group analyses for MD, FW and CTh with a 2 class general linear model, as implemented in Freesurfer, between Stage 0 HC and the rest of the preclinical and clinical AD stages. Then, significant regions were plotted in a box and whisker plots to better illustrate the dynamics across de AD continuum.Second, to assess the relationship between MD and CTh, a vertex by vertex partial correlation was computed between the CTh and MD values in the whole sample, HC and symptomatic AD. Specifically, a general linear model was created, being the MD the dependent variable of interest, using CTh as the independent variable and introducing age, sex and APOE4 status as nuisance variables. All the group analyses included age, sex and APOE4 status as covariates. Additionally, CTh analyses included the center as covariate. To avoid false positives, a Monte Carlo simulation with 10,000 repeats as implemented in Freesurfer (family-wise error [FWE], $p < 0.05$) was tested. Full details can be found in the Supplementary material. Only those regions that survived those multiple comparison were shown in the figures.

For the figure projection and design, we used a freely available python library to overlay the results into the standard surface (Pysurf: https://pysurfer.github.io/).

RESULTS

Demographics, CSF biomarkers and APOE genotype

Table 1 summarizes the demographics, CSF biomarker levels and neuropsychological assessments of the subjects. Three hundred and twenty-six subjects were finally included: 220 Stage 0, 25 Stage 1, 9 Stage 2/3, 41 MCI-AD and 31 dAD. There were no statistical differences in any variable between the CTh whole sample and the diffusion MRI subset.

Biphasic trajectory of changes in MD and CTh in the AD continuum

Fig. 3-top shows the CTh group-difference maps covaried by age, sex,and APOE4 status ($p<0.05$ FWE corrected). Stage 1 HC showed areas of increased CTh with respect to Stage 0 HC (Fig. 3-top A) in the middle temporal gyrus and precuneus, in the left hemisphere, and superior parietal areas, in both hemispheres. Stage 2/3 HC revealed regions of atrophy in the middle temporal areas bilaterally with respect to Stage 0 HC (Fig. 3-top B). The MCI-AD patients vs the Stage 0 HC comparison showed an atrophy map in the

fusiform gyrus, precuneus, posterior cingulate cortex (PCC) and temporoparietal areas in the right hemisphere, and in the middle temporal gyrus left hemisphere (Fig. 3-top C). The dAD patients revealed a widespread atrophy pattern that further extended to the superior frontal gyrus, the enthorinal cortex and the superior, middle and inferior temporal gyrus bilaterally (Fig. 3-top D).

Fig. 3-mid shows the MD group-difference maps, covaried by age, sex,and APOE4 status ($p<0.05$ FWE corrected). Stage 1 HC revealed lower MD values in comparison to Stage 0 HC (Fig. 3-mid A) in the left and right inferior and middle temporal gyrus, and in the right superior parietal areas. Stage 2/3 HC showed higher MD values in the left inferior frontal gyrus (Fig. 3-mid B). MCI-AD patients showed a widespread pattern of increased MD in both hemispheres, mainly in the temporal lobe, supramarginal and the PCC (Fig. 3-mid C). The dAD patients showed similar results that further extended to almost the entire cortical mantle with a preservation of primary motor and sensory areas (Fig. 3-mid D).

Fig. 3-bottom shows the FW group-difference maps covaried by age, sex,and APOE4 status ($p<0.05$ FWE corrected). Stage 1 HC presented lower FW values in comparison to Stage 0 HC (Fig. 3-bottom A) in superior parietal areas bilaterally and in right inferior and middle temporal areas. Stage 2/3 HC showed higher FW values in orbitofrontal cortex bilateraly and portions of the left middle temporal cortex (Fig. 3-bottom B). MCI-AD patients showed increases of FW in vulnerable AD areas (Fig. 3-bottom C) that are more widespread in the dAD(Fig. 3-bottom D).

Figure 4 shows a box-plot for the most significant region, illustrating the proposed theoretical dynamic trajectories for CTh, MD and FW in AD vulnerable areas.

We repeated all the analyses using perfectly number-balanced and age-, gender- and center-matched samples.

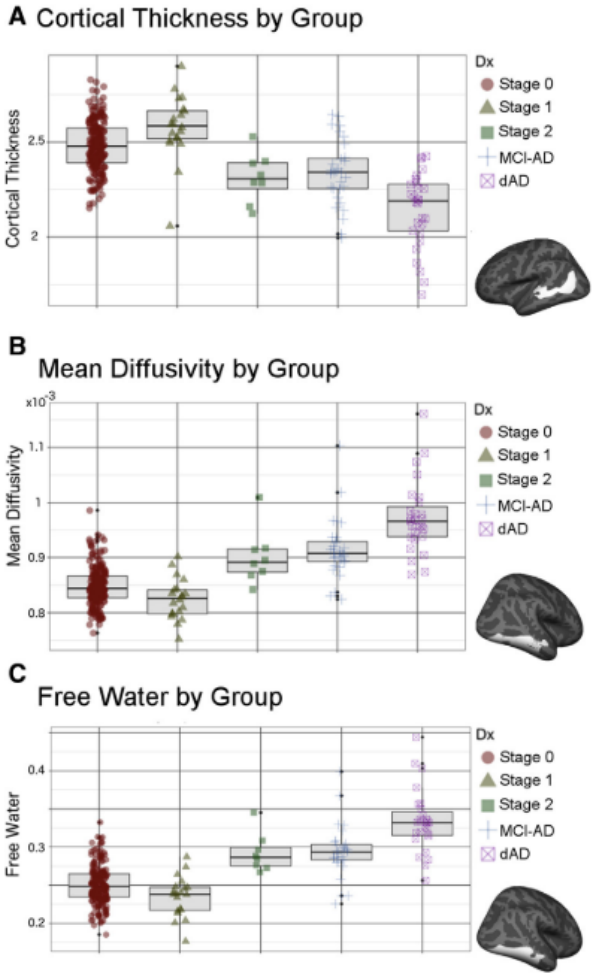

Fig. 4. Box and whisker plots illustrating the cortical dynamics in the AD continuum. Most significant cluster from the stage 0 vs stage 1 analyses were isolated, averaged and plotted by group. Specifically, A) Cortical thickness analyses, B) Mean diffusivity analyses and, C) Free Water analyses.. MCI-AD= Mild cognitive impairment with evidence of an underlying AD pathophysiological process; dAD= Alzheimer's disease dementia with evidence of an underlying AD pathophysiological process.

Also, the MCI analyses were repeated selecting the amnestic presentation forms (n=22). Then, we repeated the stage 0 vs stage 1 analysis without including APOE4 status as a covariate. Moreover, we repeated the MD stage 0 vs stage 1

analyses splitting by center. The results did not qualitatively change in any contrast (data not shown).

Finally, we repeated all the analyses presented applying a partial volume correction and the results did not change. Thus, only results uncorrected for partial volume are shown. The entire partial volume corrected results are shown in the Supplementary material Figure 1.

Cortical microstructural changes are intimately related to cortical thickness

The distribution of changes for both CTh and MD presented an overlapping pattern in the AD continuum. To further assess the relationship between CTh and MD, we performed a vertex-wise correlation analysis between CTh and MD values in the whole sample (N=284), in symptomatic patients (MCI and AD patients; N=59) and in HC (N=225) (Fig. Suppl 2), covaried by age, sexand APOE4 status. In the whole sample, the correlation was widely significant across almost the entire cortex (Fig. Suppl 2 A). These correlations were also found when HC (Suppl 2 B) and symptomatic patients (Suppl 2 C) were analyzed independently.

DISCUSSION

This study assesses the cortical microstructural changes and their relationship with CTh in the AD continuum in a large multicenter cohort. We found that micro and macrostructural brain changes are intimately related and that cortical MD, FW and CTh followed a biphasic trajectory of changes in AD (Fig. 4 and Fig. 5). In early preclinical AD (Stage 1), we observed cortical thickening and MD and FW decreases suggesting a relationship with amyloid deposition. In late preclinical AD (stage 2/3), and, especially in the symptomatic phase of the disease, there is increased MD, FW and atrophy in areas typically related to the AD-signature [32].

Our results confirm in another independent cohort, the biphasic trajectory of changes for CTh along the AD continuum. The finding of increased CTh in relation to brain amyloidosis has already been reported in several different cohorts in familial and sporadic AD in cross-sectional [4,7–10,33], and longitudinal studies [11]. The relationship between brain structure and CSF biomarkers, however, is still controversial. In fact, not all studies have reported increased CTh in relation to amyloid [34–37]. However, none of them have explicitly explored the influence of tau on these results. It's important to consider that, longitudinal studies by Desikan et al showed that volume loss [38] and cognitive decline [39] only occurs in the presence of both amyloid and tau alterations. On the other hand, brain atrophy in late preclinical AD stages and in symptomatic AD is very well established [32].

We found a similar 2-phase phenomenon for MD changes in preclinical AD, a trajectory of changes that had already been proposed in autosomal dominant AD [8,12]. In Stage 1 HC, we found decreases in cortical MD associated with the cortical thickening. In Stage 2/3 HC, and especially when comparing MCI and AD patients with respect to Stage 0 HC, we found a pattern of increased MD accompanied by cortical atrophy in AD vulnerable areas [32]. This study is the first to assess the entire AD continuum. The studies assessing the GM microstructural changes in AD are limited, and all of them with small samples sizes. These previous studies found MD decreases in asymptomatic familial AD [8,14]. Other studies with MCI and AD patients found MD increases in the symptomatic phase of AD [12]. The FW results present a high degree of overlap with the MD maps.

Our results confirm the proposed biphasic models for both CTh and diffusivity changes and FW (Fig. 5). Brain amyloidosis, in the absence of tau, would be related to pathological cortical thickening, decreased MD and

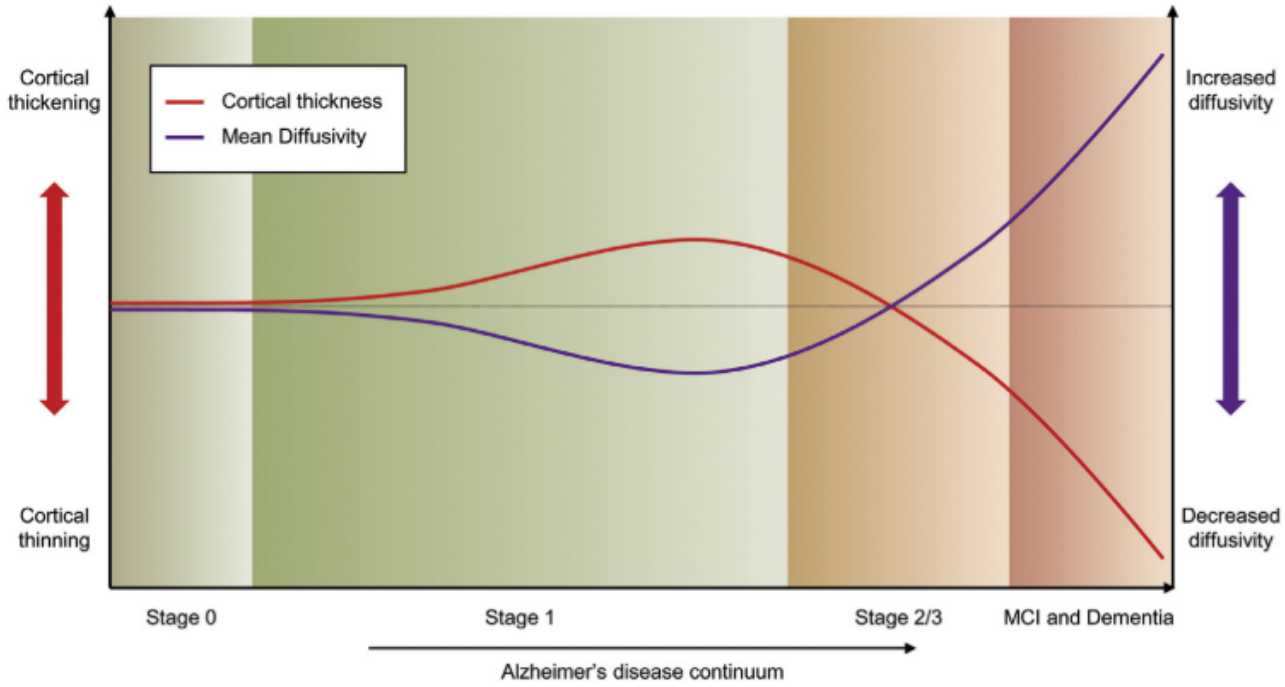

Fig. 5. Biphasic model of cortical thickness and mean diffusivity changes along the AD continuum. Proposed model for the trajectory of cortical changes in the Alzheimer's disease continuum. Cortical thickness is plotted in red while mean diffusivity is represented in purple. The color gradation between stages is used for illustrative purposes.

decreased FW, which would be followed by atrophy, increased MD and increased FW once tau markers become abnormal [4]. In this sense, Racine et al. found a correlation between amyloid deposition, as measured by PIB-PET, and decreased MD [15] in the Wisconsin Registry for Alzheimer´s Prevention (WRAP) cohort. Importantly, increased cortical volumes in relation to Aß deposition have been reported in a different work from the same cohort [7]. Of note, similar to the WRAP study, our cohort of HC is also relatively young and is also enriched for family history and APOE4 genotype. In both cohorts, increased CTh seems to be accompanied by decreased cortical MD values in preclinical AD. The increases in GM MD in symptomatic AD have been reported by several groups. Specifically, hippocampal MD has been found to be increased in MCI subjects who progressed to dementia compared with non-progressors [12]. In fact, hippocampal MD could be a better predictor for conversion to dementia than hippocampal volume itself [40]. Cortical MD has also been found increased in both MCI [41] and AD [42] patients. These MD increases have been related to cellular loss and microstructural disorganization, which would result in a breakdown of the usual barriers for water diffusion [12]. Again, the FW maps highly correlate with the MD results. Our interpretation is that the FW increases in the symptomatic phase of the disease would correspond with the same biological source as MD, which is likely extracellular.

We found a strong negative correlation between MD and CTh in the AD continuum. These data support an intimate relationship between the micro and macrostructural changes. This finding is in agreement with the inverse correlations between CTh and GM MD in a group of MCI patients reported by Jacobs et al [41]. However, previous studies have also proposed that microstructural changes precede changes in macrostructure [43]. Further studies are needed to confirm this hypothesis.

Our results are biologically plausible. We have previously discussed the rationale for the increases in CTh [4,9,11]. Both the increase in CTh and the MD and FW decreases in the early asymptomatic stage of AD might be caused by an amyloid-induced inflammatory response. This inflammation would trigger changes in cell volume (neuronal and glia swelling) and cell number (glia recruitment and activation) that could justify the decreases in cortical diffusivity [8,12,14]. In this respect, a recent paper showed that astrocyte activation is implicated in the very early stages of AD pathology [44]. Indeed, neuroinflammation and glial activation are increasingly recognized as early events in Alzheimer's, even before Aß1-42 deposition[45]. It has been shown that both cell hypertrophy and glial activation can alter the diffusion properties of tissue by adding new diffusion barriers[46]. Moreover, extracellular deposition of Aß fibrils could also contribute to the reduced cortical diffusivity [47], although this is still under debate [48]. The increases in cortical MD and FW are to be expected in the AD symptomatic phases due to the breakdown of microstructural barriers, such as myelin cell membranes and intracellular organelles, that would normally restrict water molecule motion [12]. This breakdown would be due to the synergy between amyloid and tau pathologies [5] that starts in late preclinical AD (Stage 2/3).

Our results have several clinical implications. First, our results suggest a potential use of cortical MD or FW as a biomarker for AD. Second, we expand our proposed model of a 2-phase phenomenon [4,11] to MD and FW, thus strengthening the role of pathogenic synergies between biomarkers and nonlinear trajectories of changes in hypothetical biomarker models of AD. Third, our results highlight the relevance of the NIA-AA preclinical AD research criteria in predicting different stages with different biology. Moreover, a multimodal approach with both CTh and diffusion measures might enable a better modeling of the cortical changes along the AD continuum. Finally, the results also have implications in clinical trials for preclinical AD. MRI measures are commonly used as surrogate markers of disease modification, but a linear trajectory of changes is always assumed. We suggest that a non-linear trajectory should be modeled, differentiating between the preclinical AD stages [11].

The main strengths of this study are the large number of subjects included in the sample and the surface-based analysis, which tries to overcome processing limitations and methodological concerns repeatedly reported in the literature [12,49]. Moreover, we applied different strategies to ensure that our results have strong biological basis. First, the results did not significantly changed when applying partial volume correction. Second, we included a harmonization processing step that mitigates the potential site variation in the acquisition protocols. Finally, were found qualitatively very similar results both with MD and FW (using different approaches to correct for partial volume effect). This study has also some limitations. First of all, the relatively young age of the HC accounts for the relatively small number of subjects in preclinical AD and in the suspected non-amyloid pathology (SNAP) group, despite the overall large sample size. This fact results in unbalanced preclinical stages

groups. Nonetheless, all the results survived correction for multiple comparisons and remained unchanged when using balanced groups for every analysis. The young age of both HC and symptomatic patients should be taken into account when comparing these results with other studies. Second, another important limitation is the indirect assessment of amyloid pathology and the lack of longitudinal follow-up. Only with longitudinal comparisons can we be sure that these stage 0 to stage 1 changes are due to progression rather than other intrinsic or longstanding differences (e.g. genetic) that cause both thicker cortices and a predisposition to amyloid deposition. Further studies with amyloid, tau and inflammation/glial activation PET as well as longitudinal diffusion MRI studies with harmonized protocols will help to confirm the sequence of alterations and the relationship between them. Third, this was a multicenter study with different diffusion protocols and number of directions. However, MD has been reported to be robust measure [50] and, as mentioned before, we also applied a novel and powerful harmonization processing step to address this issue. Nonetheless there was a relative imbalance of the group proportions at each site which might affect the algorithm. Diffusion MRI data is particularly prone to susceptibility artifacts. A common approach to correct for gradient distortions in EPI sequences is to use the gradient field map (https://fsl.fmrib.ox.ac.uk/fsl/fslwiki/FUGUE). Unfortunately, this acquisition is not available in our dataset so we could not perform a physics-based correction for EPI distortion. Therefore, despite the effort invested in harmonizing the diffusion sequences, we acknowledge that a clinical and physical phantom study would be required to more robustly detect possible sources of site biases in the data acquisition [51].

In conclusion, this study shows that cortical micro and macrostructure are closely related in AD. Cortical diffusivity follows a biphasic trajectory of changes: MD and FW initially decrease in the early preclinical phase and then increase in late preclinical and symptomatic stages. These results should be considered in clinical trials in the selection of subjects and in the modeling of the predicted changes to be expected with anti-amyloid therapies.

ACKNOWLEDGEMENTS

We thank the subjects and their families for their generosity. We want to acknowledge Laia Muñoz and Raul Nuñez for the laboratory and sample handling.

This work was supported by research grants from the Carlos III Institute of Health, Spain (grants PI11/02425 and PI14/01126 to Juan Fortea, grants PI10/1878 and PI13/01532 to Rafael Blesa, grants PI11/03035 and PI14/1561 to Alberto Lleó , grant PI12/02288 to Pascual Sánchez-Juan and grant PI15/00919 to Pablo Martinez-Lage) and the CIBERNED program (Program 1, Alzheimer Disease to Alberto Lleó and SIGNAL study, www.signalstudy.es), partly funded by Fondo Europeo de Desarrollo Regional (FEDER), Unión Europea, “Una manera de hacer Europa”. This work has also been supported by a “Marató TV3” grant (20141210 to Juan Fortea) and a grant from the Fundació Bancaria La Caixa to Rafael Blesa. This work was supported in part by Generalitat de Catalunya (2014SGR-0235). Moreover, this work has been supported by the Ministry of Economy and Competitiveness of Spain, the Basque Country Government, Obra social Kutxa and anonymous small private sponsors. As well as by the National Institutes of Health grants R01MH108574, P41EB015902, R01AG042512.

REFERENCES

[1] Sperling RA, Aisen PS, Beckett LA, Bennett DA, Craft S, Fagan AM, et al. Toward defining the preclinical stages of Alzheimer’s disease: recommendations from the National Institute

on Aging-Alzheimer's Association workgroups on diagnostic guidelines for Alzheimer's disease. Alzheimer's Dement 2011;7:280–92. doi:10.1016/j.jalz.2011.03.003.

[2] Villemagne VL, Burnham S, Bourgeat P, Brown B, Ellis K a, Salvado O, et al. Amyloid β deposition, neurodegeneration, and cognitive decline in sporadic Alzheimer's disease: a prospective cohort study. Lancet Neurol 2013;12:357–67. doi:10.1016/S1474-4422(13)70044-9.

[3] Wang L, Benzinger TL, Su Y, Christensen J, Friedrichsen K, Aldea P, et al. Evaluation of Tau Imaging in Staging Alzheimer Disease and Revealing Interactions Between β-Amyloid and Tauopathy. JAMA Neurol 2016;63110:1–8. doi:10.1001/jamaneurol.2016.2078.

[4] Fortea J, Vilaplana E, Alcolea D, Carmona-Iragui M, Sánchez-Saudinos M-BB, Sala I, et al. Cerebrospinal Fluid ß-Amyloid and Phospho-Tau Biomarker Interactions Affecting Brain Structure in Preclinical Alzheimer Disease. Ann Neurol 2014;76:223–30. doi:10.1002/ana.24186.

[5] Pascoal TA, Mathotaarachchi S, Mohades S, Benedet AL, Chung C-O, Shin M, et al. Amyloid-β and hyperphosphorylated tau synergy drives metabolic decline in preclinical Alzheimer's disease. Mol Psychiatry 2016:1–6. doi:10.1038/mp.2016.37.

[6] Chételat G, Villemagne VL, Bourgeat P, Pike KE, Jones G, Ames D, et al. Relationship between atrophy and beta-amyloid deposition in Alzheimer disease. Ann Neurol 2010;67:317–24. doi:10.1002/ana.21955.

[7] Johnson SC, Christian BT, Okonkwo OC, Oh JM, Harding S, Xu G, et al. Amyloid burden and neural function in people at risk for Alzheimer's Disease. Neurobiol Aging 2014;35:576–84. doi:10.1016/j.neurobiolaging.2013.09.028.

[8] Fortea J, Sala-Llonch R, Bartrés-Faz D, Bosch B, Lladó A, Bargalló N, et al. Increased cortical thickness and caudate volume precede atrophy in PSEN1 mutation carriers. J Alzheimers Dis 2010;22:909–22. doi:10.3233/JAD-2010-100678.

[9] Fortea J, Sala-Llonch R, Bartrés-Faz D, Lladó A, Solé-Padullés C, Bosch B, et al. Cognitively Preserved Subjects with Transitional Cerebrospinal Fluid ß-Amyloid 1-42 Values Have Thicker Cortex in Alzheimer Disease Vulnerable Areas. Biol Psychiatry 2011;70:183–90.

[10] Quiroz YT, Schultz AP, Chen K, Protas HD, Brickhouse M, Fleisher AS, et al. Brain Imaging and Blood Biomarker Abnormalities in Children With Autosomal Dominant Alzheimer Disease: A Cross-Sectional Study. JAMA Neurol 2015;2114:1–8. doi:10.1001/jamaneurol.2015.1099.

[11] Pegueroles J, Vilaplana E, Montal V, Sampedro F, Alcolea D, Carmona-iragui M, et al. Longitudinal brain structural changes in preclinical Alzheimer disease. Alzheimer's Dement 2016:1–11. doi:10.1016/j.jalz.2016.08.010.

[12] Weston PSJ, Simpson IJA, Ryan NS, Ourselin S, Fox NC. Diffusion imaging changes in grey matter in Alzheimer's disease: a potential marker of early neurodegeneration. Alzheimers Res Ther 2015;7:47. doi:10.1186/s13195-015-0132-3.

[13] Amlien IK, Fjell AM. Diffusion tensor imaging of white matter degeneration in Alzheimer's disease and mild cognitive impairment. Neuroscience 2014;276:206–15. doi:10.1016/j.neuroscience.2014.02.017.

[14] Ryan NS, Keihaninejad S, Shakespeare TJ, Lehmann M, Crutch SJ, Malone IB, et al. Magnetic resonance imaging evidence for presymptomatic change in thalamus and caudate in familial Alzheimer's disease. Brain 2013;136:1399–414. doi:10.1093/brain/awt065.

[15] Racine AM, Adluru N, Alexander AL, Christian BT, Okonkwo OC, Oh J, et al. Associations between white matter microstructure and amyloid burden in preclinical Alzheimer's disease: A multimodal imaging investigation. NeuroImage Clin 2014;4:604–14. doi:10.1016/j.nicl.2014.02.001.

[16] Pasternak O, Sochen N, Gur Y, Intrator N, Assaf Y. Free water elimination and mapping from diffusion MRI. Magn Reson Med 2009;62:717–30. doi:10.1002/mrm.22055.

[17] Lyall A, Pasternak O, Robinson D, Newell D, Trampush J, Gallego J, et al. Greater extracellular free-water in first-episode psychosis predicts better neurocognitive functioning. Mol Psychiatry 2017;doi:1–7. doi:10.1038/mp.2017.43.

[18] Maier-Hein KH, Westin CF, Shenton ME, Weiner MW, Raj A, Thomann P, et al. Widespread white matter degeneration preceding the onset of dementia. Alzheimer's Dement 2015;11:485–93. doi:10.1016/j.jalz.2014.04.518.

[19] Hoy AR, Ly M, Carlsson CM, Okonkwo OC, Zetterberg H, Blennow K, et al. Microstructural white matter alterations in preclinical Alzheimer's disease detected using free water elimination diffusion tensor imaging. PLoS One 2017;12:1–21. doi:10.1371/journal.pone.0173982.

[20] Fletcher E, Carmichael O, Pasternak O, Maier-Hein KH, DeCarli C. Early brain loss in circuits affected by Alzheimer's disease is predicted by fornix microstructure but may be independent of gray matter. Front Aging Neurosci 2014;6:1–9. doi:10.3389/fnagi.2014.00106.

[21] Alcolea D, Martínez-Lage P, Sánchez-Juan P, Olazarán J, Antúnez C, Izagirre A, et al. Amyloid precursor protein metabolism and inflammation markers in preclinical Alzheimer disease. Neurology 2015;85:626–33. doi:10.1212/WNL.0000000000001859.

[22] Jack CR, Albert MS, Knopman DS, McKhann GM, Sperling RA, Carrillo MC, et al. Introduction to the recommendations from the National Institute on Aging-Alzheimer's Association workgroups on diagnostic guidelines for Alzheimer's disease. Alzheimer's Dement 2011;7:257–62. doi:10.1016/j.jalz.2011.03.004.

[23] Alcolea D, Vilaplana E, Pegueroles J, Montal V, Sánchez-Juan P, González-Suárez A, et al. Relationship between cortical thickness and cerebrospinal fluid YKL-40 in predementia stages of Alzheimer's disease. Neurobiol Aging 2015;36:2018–23. doi:10.1016/j.neurobiolaging.2015.03.001.

[24] Sala I, Belén Sánchez-Saudinós M, Molina-Porcel L, Lázaro E, Gich I, Clarimón J, et al. Homocysteine and cognitive impairment. Relation with diagnosis and neuropsychological performance. Dement Geriatr Cogn Disord 2008;26:506–12. doi:10.1159/000173710.

[25] Fischl B, Dale AM. Measuring the thickness of the human cerebral cortex from magnetic resonance images. Proc Natl Acad Sci U S A 2000;97:11050–5. doi:10.1073/pnas.200033797.

[26] Kwon O, Park H, Seo S, Na DL, Lee J. A framework to analyze cerebral mean diffusivity using surface guided diffusion mapping in diffusion tensor imaging. Front Neurosci 2015;9:1–11. doi:10.3389/fnins.2015.00236.

[27] Wu M, Lu LH, Lowes A, Yang S, Passarotti AM, Zhou XJ, et al. Development of superficial white matter and its structural interplay with cortical gray matter in children and adolescents. Hum Brain Mapp 2014;35:2806–16. doi:10.1002/hbm.22368.

[28] Beer AL, Plank T, Meyer G, Greenlee MW. Combined diffusion-weighted and functional magnetic resonance imaging reveals a temporal-occipital network involved in auditory-visual object processing. Front Integr Neurosci 2013;7:5. doi:10.3389/fnint.2013.00005.

[29] Koo B-B, Hua N, Choi C-H, Ronen I, Lee J-M, Kim D-S. A framework to analyze partial volume effect on gray matter mean diffusivity measurements. Neuroimage 2009;44:136–44. doi:10.1016/j.neuroimage.2008.07.064.

[30] Jones DK, Symms MR, Cercignani M, Howard RJ. The effect of filter size on VBM analyses of DT-MRI data. Neuroimage 2005;26:546–54. doi:10.1016/j.neuroimage.2005.02.013.

[31] Fortin J-P, Parker D, Tunç B, Watanabe T, Elliott MA, Ruparel K, et al. Harmonization of multi-site diffusion tensor imaging data. Neuroimage 2017;161:149–70. doi:10.1016/j.neuroimage.2017.08.047.

[32] Dickerson BC, Bakkour A, Salat DH, Feczko E, Pacheco J, Greve DN, et al. The cortical signature of Alzheimer's disease: regionally specific cortical thinning relates to symptom severity in very mild to mild AD dementia and is detectable in asymptomatic amyloid-positive individuals. Cereb Cortex 2009;19:497–510. doi:10.1093/cercor/bhn113.

[33] Chételat G, Villemagne VL, Pike KE, Baron J-C, Bourgeat P, Jones G, et al. Larger temporal volume in elderly with high versus low beta-amyloid deposition. Brain 2010;133:3349–58. doi:10.1093/brain/awq187.

[34] Araque Caballero MÁ, Brendel M, Delker A, Ren J, Rominger A, Bartenstein P, et al. Mapping 3-year changes in gray matter and metabolism in Aβ-positive nondemented subjects. Neurobiol Aging 2015;36:2913–24. doi:10.1016/j.neurobiolaging.2015.08.007.

[35] Mattsson N, Insel PS, Nosheny R, Tosun D, Trojanowski JQ, Shaw LM, et al. Emerging β-Amyloid Pathology and Accelerated Cortical Atrophy. JAMA Neurol 2014;94121:1–10. doi:10.1001/jamaneurol.2014.446.

[36] Doré V, Villemagne VL, Bourgeat P, Fripp J, Acosta O, Chetélat G, et al. Cross-sectional and longitudinal analysis of the relationship between Aβ deposition, cortical thickness, and memory in cognitively unimpaired individuals and in Alzheimer disease. JAMA Neurol 2013;70:903–11. doi:10.1001/jamaneurol.2013.1062.

[37] Sala-Llonch R, Idland A-V, Borza T, Watne LO, Wyller TB, Brækhus A, et al. Inflammation, Amyloid and Atrophy in The Aging Brain: Relationships with longitudinal changes in cognition. J Alzheimer's Dis 2017. doi:10.3233/JAD-161146.

[38] Desikan RS, McEvoy LK, Thompson WK, Holland D, Roddey JC, Blennow K, et al. Amyloid-β associated volume loss occurs only in the presence of phospho-tau. Ann Neurol 2011;70:657–61. doi:10.1002/ana.22509.

[39] Desikan RS, McEvoy LK, Thompson WK, Holland D, Brewer JB, Aisen PS, et al. Amyloid-β--associated clinical decline occurs only in the presence of elevated P-tau. Arch Neurol 2012;69:709–13. doi:10.1001/archneurol.2011.3354.

[40] Müller MJ, Greverus D, Dellani PR, Weibrich C, Wille PR, Scheurich A, et al. Functional implications of hippocampal volume and diffusivity in mild cognitive impairment. Neuroimage 2005;28:1033–42. doi:10.1016/j.neuroimage.2005.06.029.

[41] Jacobs HIL, van Boxtel MPJ, Gronenschild EHBM, Uylings HBM, Jolles J, Verhey FRJ. Decreased gray matter diffusivity: A potential early Alzheimer's disease biomarker? Alzheimer's Dement 2013;9:93–7. doi:10.1016/j.jalz.2011.11.004.

[42] Scola E, Bozzali M, Agosta F, Magnani G, Franceschi M, Sormani MP, et al. A diffusion tensor MRI study of patients with MCI and AD with a 2-year clinical follow-up. J Neurol Neurosurg Psychiatry 2010;81:798–805. doi:10.1136/jnnp.2009.189639.

[43] Ringman JM, O'Neill J, Geschwind D, Medina L, Apostolova LG, Rodriguez Y, et al. Diffusion tensor imaging in preclinical and

presymptomatic carriers of familial Alzheimer's disease mutations. Brain 2007;130:1767–76. doi:10.1093/brain/awm102.

[44] Rodriguez-Vieitez E, Saint-Aubert L, Carter SF, Almkvist O, Farid K, Schöll M, et al. Diverging longitudinal changes in astrocytosis and amyloid PET in autosomal dominant Alzheimer's disease. Brain 2016:awv404. doi:10.1093/brain/awv404.

[45] Heneka MT, Carson MJ, Khoury J El, Landreth GE, Brosseron F, Feinstein DL, et al. Neuroinflammation in Alzheimer's disease. Lancet Neurol 2015;14:388–405. doi:10.1016/S1474-4422(15)70016-5.

[46] Roitbak T, Syková E. Diffusion barriers evoked in the rat cortex by reactive astrogliosis. Glia 1999;28:40–8.

[47] Mueggler T, Meyer-Luehmann M, Rausch M, Staufenbiel M, Jucker M, Rudin M. Restricted diffusion in the brain of transgenic mice with cerebral amyloidosis. Eur J Neurosci 2004;20:811–7. doi:10.1111/j.1460-9568.2004.03534.x.

[48] Thiessen JD, Glazner KAC, Nafez S, Schellenberg AE, Buist R, Martin M, et al. Histochemical visualization and diffusion MRI at 7 Tesla in the TgCRND8 transgenic model of Alzheimer's disease. Brain Struct Funct 2010;215:29–36. doi:10.1007/s00429-010-0271-z.

[49] Bendlin BB, Carlsson CM, Johnson SC, Zetterberg H, Blennow K, Willette A a., et al. CSF T-Tau/Aβ42 Predicts White Matter Microstructure in Healthy Adults at Risk for Alzheimer's Disease. PLoS One 2012;7:e37720. doi:10.1371/journal.pone.0037720.

[50] Yao X, Yu T, Liang B, Xia T, Huang Q, Zhuang S. Effect of increasing diffusion gradient direction number on diffusion tensor imaging fiber tracking in the human brain. Korean J Radiol 2015;16:410–8. doi:10.3348/kjr.2015.16.2.410.

[51] Teipel SJ, Reuter S, Stieltjes B, Acosta-Cabronero J, Ernemann U, Fellgiebel A, et al. Multicenter stability of diffusion tensor imaging measures: A European clinical and physical phantom study. Psychiatry Res - Neuroimaging 2011;194:363–71. doi:10.1016/j.pscychresns.2011.05.012.

SUPPLEMENTARY MATERIAL

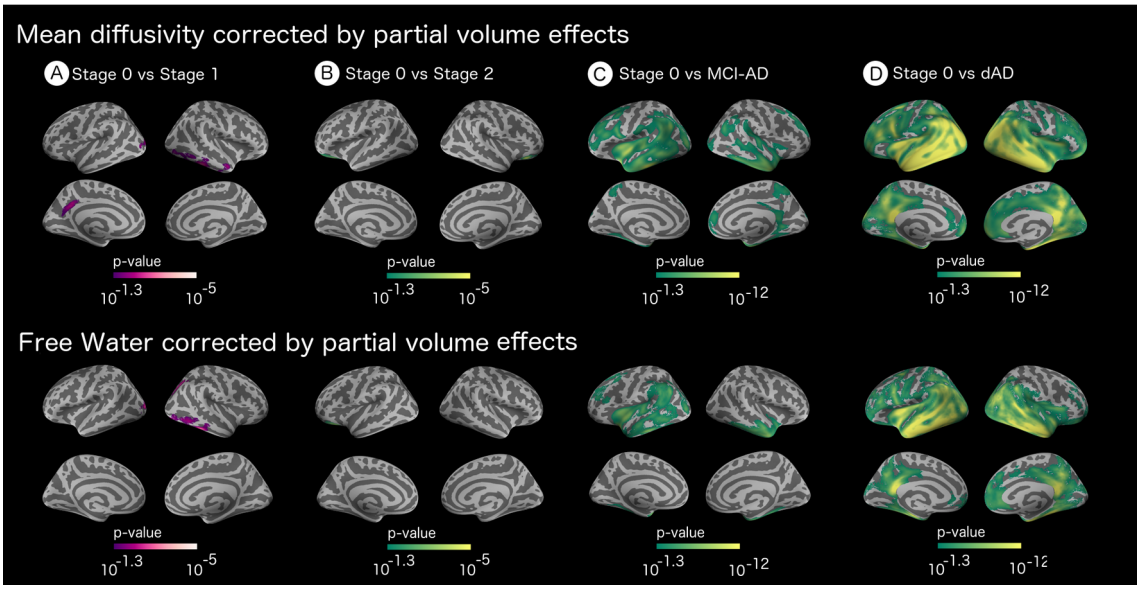

Suppl. Fig 1. Top. Cortical Mean Diffusivity patterns in the AD continuum. (A) MD differences in Stage 0 vs Stage 1 HC, (B) Stage 0 vs Stage 2 HC, (C) Stage 0 vs MCI-AD patients and (D) Stage 0 HC vs dAD patients.
Bottom. Free-water (FW) patterns in the AD continuum. (A) FW differences in Stage 0 vs Stage 1 HC, (B) Stage 0 vs Stage 2 HC, (C) Stage 0 vs MCI-AD patients and (D) Stage 0 HC vs dAD patients.

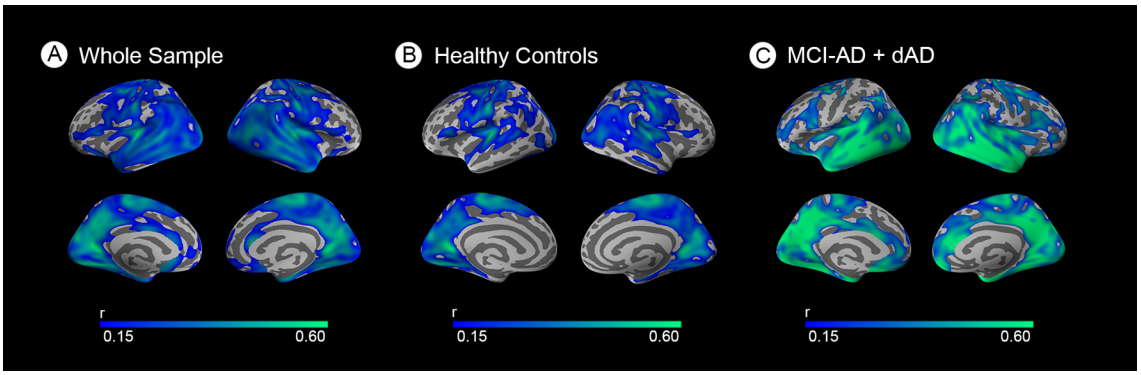

Suppl. Fig 2. Mean diffusivity correlates with cortical thickness. Vertex-wise partial correlation between mean diffusivity and cortical thickness for (A) the whole sample, (B) the cognitively healthy control group and, (C) the symptomatic group. Only clusters that survive family-wise error corrected p<0.05 are shown. All the analyses are adjusted by age, sex, centre and *APOE*

SUPPLEMENTARY METHODS

Site Harmonization

Briefly, the ComBat algorithm works on the MD data along with all the interest and nuisance variables, estimating and removing just the site effect, while maintaining the biological information.

Monte Carlo simulation

In this work we used the Monte Carlo simulation with 10000 repeats as implemented in Freesurfer. Briefly, this cluster-based method is based in the probability that a certain cluster of certain size is obtained by chance/noise. This probability is computed using Monte Carlo simulations where: 1) white Gaussian noise is synthesized in the standard space surface, 2) the noise is smoothed by a certain FWHM (data-dependent), 3) the smoothed values are thresholded using a thr>1.3 (i.e $p < 10\text{-}1.3$) and, 4) the maximum cluster size for the simulation is recorded. These steps are repeated 10000 times in order to generate a distribution of maximum cluster size generated by random noise. If our statistically significant cluster size is NOT smaller than the obtained during the Monte Carlo simulation more than 500 iterations ($p < 0.05$), the software considers that the cluster is not given by chance and survived multiple comparisons. This distribution is provided by Freesurfer (specifically, in the command mri_surfcluster)".

Dti processing

First, a rigid body transformation between the b=0 image and all the diffusion-weighted acquisition was applied to mitigate motion effects. After removing non-brain tissue using Brain Extraction Tool, diffusion tensors were fitted and MD was calculated using FSL's DTIfit command. A boundary-based algorithm as implemented in Freesurfer bbregister, was then used to compute an affine registration matrix between the skull-stripped b0 diffusion image and the segmented structural T1-weigthed volume. At this point, all b0 to T1 registrations were visually inspected in order to exclude those individuals with errors in the coregistration. Then, MD volumes were projected to each individual's surface space generated during the cortical segmentation. At each vertex, cortical MD was sampled using the middle point along the normal vector between white and pial surfaces using the Freesurfer's mri_vol2surf command, as it has been done in recent surface-based approaches. Then, the spherical registration computed during the CTh segmentation process was used to normalize each individual MD surface map to an average standard surface, enabling an accurate matching of cortical locations for the computation of further statistics

PV Correction for MD maps

In brief, after motion correction, tensor estimation and T1 – DWI registration, the images were introduced to the Koo et al PV toolbox. This toolbox computes the CSF contribution in each voxel, it then subtracts it and estimates the net MD value in the cortical GM. Only those voxels that contained at least a 30% of GM, as computed by Freesurfer's gtmseg, were considered for these analyses.

PV Correction for Free water maps

In this case, the corrected FW maps were the difference between the original FW and the percent of CSF in a given voxel as computed by FreeSurfer. Again, only voxels that contained more than 30% of GM as computed by Freesurfer were included in these analyses.

Cortical microstructure in the behavioral variant of frontotemporal dementia: looking beyond atrophy

Ignacio Illán-Gala[1,2]*; **Victor Montal[1,2]***; Sergi Borrego-Écija[3]; Eduard Vilaplana[1,2]; Jordi Pegueroles[1,2]; Daniel Alcolea[1,2]; Mª Belén Sánchez-Saudinós[1]; Jordi Clarimón[1,2]; Janina Turón-Sans[7]; Nuria Bargalló[4]; Sofía González-Ortiz[5]; Howard J. Rosen[6]; Maria Luisa Gorno-Tempini[6]; Bruce L. Miller[6]; Albert Lladó[3]; Ricard Rojas-García[7]; Rafael Blesa[1,2]; Raquel Sánchez-Valle[3], Alberto Lleó[1,2]; Juan Fortea[1,2,8]; on behalf of the Catalan Frontotemporal Dementia Initiative (CATFI) and the Frontotemporal Lobar Degeneration Neuroimaging Initiative (FTLDNI).

(1) Memory Unit, Department of Neurology, Hospital de la Santa Creu i Sant Pau, Biomedical Research Institute Sant Pau, Universitat Autònoma de Barcelona, Barcelona, Spain. (2) Centro de Investigación Biomédica en Red de Enfermedades Neurodegenerativas. CIBERNED, Spain. (3) Alzheimer's Disease and Other Cognitive Disorders Unit, Department of Neurology, Hospital Clínic, Institut d'Investigació Biomèdica August Pi i Sunyer, University of Barcelona, Barcelona, Spain. (4) Radiology Department, Hospital Clínic de Barcelona and Magnetic Resonance Image Core Facility, Institut d'Investigacions Biomèdiques August Pi I Sunyer (IDIBAPS), Barcelona. (5) Department of Radiology, Hospital del Mar, Barcelona, Spain. (6) Memory and Aging Center, Department of Neurology. University of California San Francisco, San Francisco, United States. (7) Neuromuscular Diseases Unit, Department of Neurology, Hospital de la Santa Creu i Sant Pau, Universitat Autònoma de Barcelona, Barcelona, Spain. (8) Barcelona Down Medical Center. Fundació Catalana de Síndrome de Down. Barcelona, Spain.

Brain (2019) doi: 10.1093/brain/awz031

Abstract

Cortical mean diffusivity has been proposed as a novel biomarker for the study of the cortical microstructure in Alzheimer´s disease. In this multicenter study, we aimed to assess the cortical microstructural changes in the behavioral variant of frontotemporal dementia; and to correlate cortical mean diffusivity with clinical measures of disease severity and CSF biomarkers (neurofilament light and the soluble fraction beta of the Amyloid precursor protein). We included 148 participants with a three-Tesla MRI and appropriate magnetization-prepared rapid gradient-echo and diffusion weighted imaging sequences: 70 behavioral variant of frontotemporal dementia patients and 78 age-matched healthy controls. The modified frontotemporal lobar degeneration clinical dementia rating was obtained as a measure of disease severity. A subset of patients also underwent a lumbar puncture for CSF biomarker analysis. Two independent raters blind to the clinical data determined the presence of significant frontotemporal atrophy to dichotomize the participants into possible or probable behavioral variant frontotemporal dementia. Cortical thickness and mean diffusivity were computed using a surface-based approach. We performed group comparisons of cortical thickness and cortical mean diffusivity between behavioral variant of frontotemporal dementia (both using the whole sample and probable and possible behavioral variant of frontotemporal dementia subgroups) and healthy controls. We also performed correlation analyses with the modified frontotemporal lobar degeneration clinical dementia rating score and CSF neuronal biomarkers. The mean diffusivity maps, in the whole cohort and in the probable behavioral variant of frontotemporal dementia group, showed widespread cortical areas with increased mean diffusivity that partially overlapped with cortical thickness, but further expanded to other behavioral variant of frontotemporal dementia-related regions. In the possible behavioral variant of frontotemporal dementia group, we found increased cortical mean diffusivity in frontotemporal regions (especially in the dorsolateral and medial prefrontal cortex of both hemispheres), but only minimal cortical thickness loss. Both mean diffusivity and cortical thickness correlated with measures of disease severity and CSF biomarkers. However, the areas of correlation with mean diffusivity were more extensive. Our data suggest that cortical mean diffusivity could be a sensitive biomarker for the study of the neurodegeneration-related microstructural changes in behavioral variant of frontotemporal dementia. Further longitudinal studies should determine the diagnostic and prognostic utility and the longitudinal change of this novel neuroimaging biomarker especially at the earliest stages of the disease.

INTRODUCTION

Frontotemporal lobar degeneration (FTLD) is a neuropathological construct encompassing multiple neurodegenerative diseases sharing partially overlapping patterns of frontal and/or temporal grey matter neurodegeneration (Bang et al., 2015). The behavioral variant of frontotemporal dementia (bvFTD) is a common clinical presentation of FTLD (Seo et al., 2018). Clinically, bvFTD is characterized by progressive personality changes followed by social, cognitive and functional deterioration (Ranasinghe et al., 2016). With the exception of genetically determined cases, the diagnosis of bvFTD relies on the clinical and neuroimaging features (Rascovsky et al., 2011; Wood et al., 2013). The refinement of the diagnostic criteria proposed by the frontotemporal dementia consortium has been an important step forward to improve the diagnosis of the bvFTD. Furthermore, these criteria have shown a good diagnostic value in pathology-confirmed cases (Balasa et al.,

2015; Chare et al., 2014; Perry et al., 2017; Rascovsky et al., 2011; Seo et al., 2018). In the frontotemporal dementia consortium criteria, the presence of frontal and/or temporal atrophy increases the diagnostic certainty once the clinical criteria for possible bvFTD are met. However, a number of patients are still misdiagnosed with other neurodegenerative and non-neurodegenerative diseases (Bang et al., 2015). Several factors, such as the absence of prominent cortical atrophy in up to a third of the patients (Ranasinghe et al., 2016; Rascovsky et al., 2011), may contribute to misdiagnosis. Conversely, possible bvFTD may include both neurodegenerative cases in early phases of the disease and non-neurodegenerative phenocopies (Gossink et al., 2016; Khan et al., 2012). Thus, the development of novel biomarkers able to increase the diagnostic certainty of FTLD is essential (Binney et al., 2017; Downey et al., 2015; Lam et al., 2013; Meeter et al., 2017). These are key aspects for the detection of patients with FTLD-related syndromes, especially at the earliest phase in clinical practice and for the selection of candidates to trials with protein-specific targeted therapies that may be more effective in earlier stages (Elahi and Miller, 2017).

Most neuroimaging studies in bvFTD have been focused on the cortical macrostructure with different metrics (grey matter density in voxel-based morphometry studies or cortical thickness in surface-based analyses) (Elahi et al., 2017; Mahoney, Simpson, et al., 2014; Meeter et al., 2017) or white matter microstructural properties (namely diffusor tensor imaging metrics such as, fractional anisotropy). However, diffusor tensor imaging can also be used to measure the magnitude of diffusivity (mean diffusivity), in the cerebral cortex (Weston et al., 2015; Montal et al., 2017). Higher cortical mean diffusivity values reflect microstructural disorganization and disruption of cellular membranes, and have been proposed as a sensitive biomarker which might antedate macroscopic cortical changes (Weston et al., 2015). However, only a single small study has assessed mean diffusivity changes in frontotemporal dementia (Whitwell et al., 2010). In this previous study no clear differences were found between gray matter density and gray matter mean diffusivity, as assessed on a voxel-based approach. However, the voxel-based approach may fail to capture the subtle tissue-specific changes that take place at the cortex level (Weston et al., 2015). As we have previously shown in Alzheimer's disease, cortical mean diffusivity can be accurately determined on a surface-based approach for the study of the microstructural changes that occur with disease progression and may antedate cortical thickness changes (Montal et al., 2017).

In bvFTD, there are no validated pathophysiologic biomarkers to reflect the underlying pathology, with the exception of pathogenic mutations that predict specific FTLD subtypes. However, CSF biomarkers may also contribute to our understanding of FTLD pathophysiology (Lleo et al., 2018; Meeter et al., 2017). Particularly, the CSF levels of neurofilament light (NfL) (an axonal cytoskeletal constituent essential for axonal growth) have shown to be a useful neurodegeneration biomarker in FTLD-related syndromes (Menke et al., 2015; Scherling et al., 2014). In addition to NfL, we have recently shown that the levels of the soluble fragment-beta of the Amyloid Precursor Protein (sAPPβ) (Alcolea et al., 2017) may be useful to track neurodegeneration in frontotemporal structures in frontotemporal dementia (Alcolea et al., 2017; Illán-Gala I et al., 2018).

In this multicentre study, we aimed to assess the cortical mean diffusivity changes in a large multicenter cohort of bvFTD patients, and to correlate these changes with clinical measures of disease severity (FTLD-CDR) and CSF biomarkers (NfL and sAPPβ). We hypothesized that cortical

mean diffusivity may be more sensitive than cortical thickness to detect the cortical changes associated with bvFTD.

METHODS

Participants

Participants were recruited in three different centers from two collaborative studies: The Catalan Frontotemporal Dementia Initiative (CATFI) and the Frontotemporal Lobar Degeneration Neuroimaging Initiative (FTLDNI).

The CATFI is a multicenter study focused on the development of novel biomarkers and therapeutic interventions for patients suffering from frontotemporal dementia. The CATFI study includes patients from three centers (Hospital de Sant Pau [HSP], Hospital Clínic de Barcelona [HCB] and Hospital Arnau de Vilanova). The principal investigator of the CATFI study is Dr. Alberto Lleó. The primary goals of FTLDNI are to identify neuroimaging modalities and methods of analysis for tracking FTLD and to assess the value of imaging versus other biomarkers in diagnostic roles. The Principal Investigator of FTLDNI is Dr. Howard Rosen at the University of California, San Francisco (UCSF). For up-to-date information on participation and protocol, please visit: http://memory.ucsf.edu/research/studies/nifd.

The inclusion criteria in this study were: (i) diagnosis of possible or probable bvFTD according to the frontotemporal dementia consortium criteria (Rascovsky et al., 2011); and (ii) 3T MRI study available for structural and cortical mean diffusivity analysis (see below for details). In both cohorts the diagnosis was made by neurologists with expertise in the evaluation the FTLD-related syndromes after an extensive neurological and neuropsychological evaluation. Moreover, patients were followed longitudinally at each center to ascertain if they presented a progressive clinical evaluation or developped a second FTLD-related syndrome (i.e. amyotrophic lateral sclerosis or a progressive supranuclear palsy phenotype).

Because the diagnosis of bvFTD has been related to non-neurodegenerative conditions in some cases that do not show the typical clinical progression, we identified bvFTD patients with increased certainty of underlying FTLD when any of the following criteria were met: (i) clinical evidence of disease progression (clinical deterioration evidenced during follow-up or progression to a second phenotype related to FTLD); (ii) genetic confirmation of FTLD (identification of a pathogenic mutation); (iii) confirmation of FTLD those patients with neuropathological evaluation available.

Fig. 1 shows the flowchart of the sample composition. A total of 192 participants with appropriate 3T structural and diffusion-weighted MRI were considered for analysis. Of these, 44 (23%) participants were excluded due to quality control issues or processing errors. All the excluded cases were bvFTD patients.

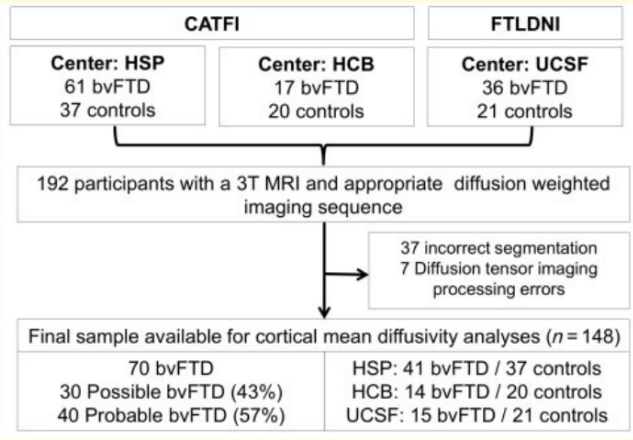

Figure 1. Flowchart of the sample composition.

Clinical measures of disease severity

The modified frontotemporal lobar degeneration clinical dementia rating (FTLD-CDR) was obtained as previously described, as a measure of disease severity the bvFTD (Knopman et al., 2008). Higher scores in the FTLD-CDR reflect a higher disease severity.

Genetic studies

Patients were screened for genetic mutations known to cause autosomal dominant inheritance of frontotemporal dementia as previously reported (Illán-Gala I et al., 2018; Perry et al., 2017).

Pathological assessment

Neuropathological assessments were performed at the Barcelona brain bank (n=1) or at UCSF (n=5) following previously described procedures (Tartaglia et al., 2010; Balasa et al., 2015). Pathology-proven FTLD cases were classified in one of the major molecular subtypes (tau, TDP-43, FUS or unclassifiable).

MRI acquisition

MRIs (3 T) were acquired at three different sites. The acquisition parameters by center can be found in the Supplementary Material. All centers had a structural MPRAGE T1-weighted acquisition of approximately 1 X 1 X 1 mm isotropic resolution and an EPI diffusion-weighted acquisition of at least 2.7 X 2.7 X 2.7 mm isotropic resolution.

Possible/Probable classification according to MRI atrophy on visual inspection

In order to determine the presence of significant frontotemporal atrophy consistent with the diagnosis of probable bvFTD according to the frontotemporal dementia consortium criteria (Rascovsky et al., 2011), all the MRIs from bvFTD participants analyzed in this study (n=114) were visually inspected by two independent raters blinded to the clinical data in order to determine the presence of significant frontotemporal atrophy to dichotomize the participants into possible bvFTD (bvFTD patients with a negative or conflicting atrophy rating) or probable bvFTD (bvFTD patients rated as positive atrophy by the two raters) (Rascovsky et al., 2011).

CSF sampling and analysis

A subset of 32 CATFI patients had also cerebrospinal fluid (CSF) available. We measured the CSF levels of NfL and sAPPβ as previously described (Alcolea et al., 2014; 2015; 2017). All biomarkers were analyzed at the Sant Pau Memory Unit Laboratory with commercially available ELISA kits (NF-light, Uman Diagnostics, Umea, Sweden; human sAPPß-w, highly sensitive, IBL, Gunma, Japan).

Cortical thickness processing

Cortical thickness reconstruction was performed with the Freesurfer package v5.1 (http://surfer.nmr.mhg.hardvard.edu) using a procedure that has been described in detail elsewhere (Fischl and Dale, 2000). All individual cortical reconstructions were visually inspected in a slice-by-slice basis to check for accuracy of the grey/white matter boundary segmentation. From the initial 115 bvFTD subjects with 3T MRI available from the three centers, 37 (32.2%) were excluded due to segmentation issues. Healthy controls scans did not require manual editing. Finally, each individual reconstructed brain was registered, and cortical thickness maps were morphed, to the fsaverage standard surface provided by Freesurfer, using a spherical registration, enabling an accurate inter-subject matching of cortical locations for the computation of further statistics. Prior to statistical analyses, we smoothed the cortical thickness maps using a Gaussian kernel with

Table 1. Sample demographics

Characteristics	Possible bvFTD	Probable bvFTD	All bvFTD	Cognitively healthy controls
n (% of bvFTD)	30 (43)	40 (57)	70 (100)	78
Age at symptom onset, years	60.2 ± 11.4	57.9 ± 8.8	58.8 ± 10	-
Age at MRI, years	65.8 ± 10.9	62.4 ± 9.2	63.8 ± 10	62.3 ± 6.1
Time from onset to MRI, years	5.5 ± 4.2	4.5 ± 3.1	4.9 ± 3.6	-
Sex Male/Female, n	24/6	27/13	51/19	26/52
Education, years	12.5 ± 5.6	13 ± 5.4	12.7 ± 5.5	13.4 ± 4.3
FTLD-CDR[†]	6.4 ± 3.7	8.3 ± 4	7.5 ± 4	-
Follow-up time, years	1.7 ± 1.4	1.9 ± 2	1.8 ± 1.7	-
Last reported phenotype	24 bvFTD 1 bvFTD with progressive aphasia 2 FTD-ALS 3 PSP-CBD	27 bvFTD 4 bvFTD with progressive aphasia 7 FTD-ALS 2 PSP-CBD	51 bvFTD 5 bvFTD with progressive aphasia 9 FTD-ALS 5 PSP-CBD	
Increased certainty of underlying FTLD (% of cases)	21 (70)[b]	38 (95)[a]	59 (84.3)	-
Definitive bvFTD (% of cases)	7 (23.3)	12 (30)	19 (27.1)	-

FWHM of 10mm as implemented in Freesurfer (Hagler et al., 2006).

Cortical mean diffusivity processing

We used a previously described home-made surface-based approach to process cortical diffusion MRI (Montal et al., 2017). Recent studies have shown the potential of surface-based methods to measure microstructural changes in neurodegenerative diseases (Montal et al., 2017; Parker et al., 2018) and the cortical architecture (Ganepola et al., 2017). An important advantage of these methods is the mitigation of partial volume effects or kernel-sensitive CSF

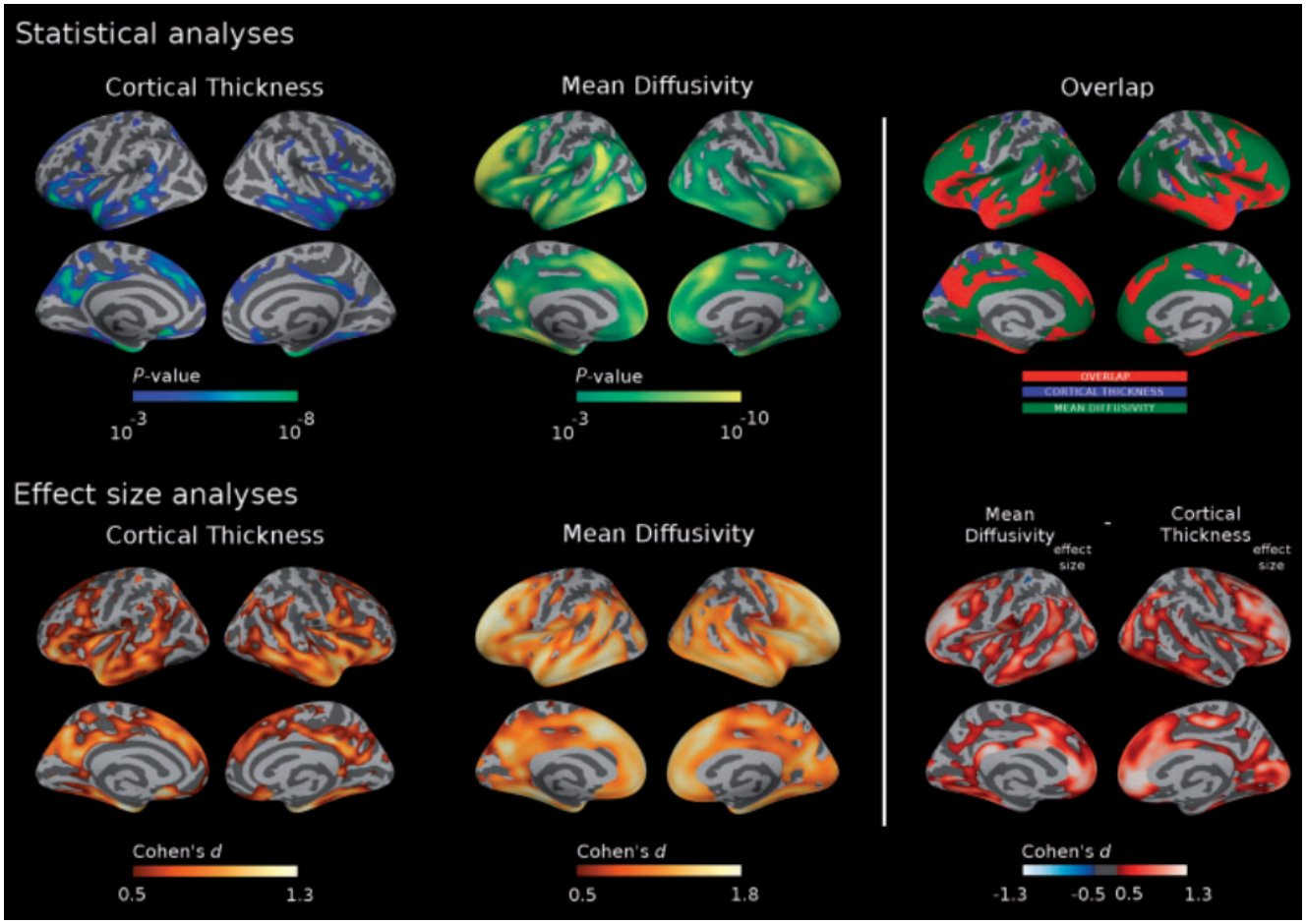

Figure 2. Group comparison of cortical thickness and cortical mean diffusivity between bvFTD and cognitively healthy controls. Top: Statistically significant results between all bvFTD and cognitively healthy controls for cortical thickness and cortical mean diffusivity. Regions in blue represent thinner cortex in the bvFTD group, whereas regions in green, represents higher cortical mean diffusivity in the bvFTD group. For illustration purposes, we included the overlapping map between both metrics (top-right). Cortical thickness analyses were adjusted for age, sex and center. Mean diffusivity analyses were adjusted for age and sex after a harmonization step. Only the clusters that survived familywise error correction $P<0.05$ are shown. Bottom: Medium to large effect sizes between the bvFTD and cognitively healthy controls for both cortical thickness and cortical mean diffusivity. The orange-gold colour represents higher effect size. In addition, the difference between both maps of effect size is displayed (bottom-right). The red-white colour represents gray matter areas where the cortical mean diffusivity has higher effect size than cortical thickness.

signal inclusion during the smoothing step (Coalson et al., 2018). Briefly, diffusion weighted imaging data were first corrected for motion effects applying a rigid body transformation between the b=0 image and the diffusion-weighted acquisitions. Then, after removing non-brain tissue using the Brain Extraction Tool, diffusion tensors were fitted, and mean diffusivity was computed using the FSL's dtifit command. We then computed the affine transformation between the skull-stripped b0 and the segmented T1-weighted volume using a boundary-based algorithm as

implemented in Freesurfer's bbregister. This approach takes advantage of the accurate segmentation of the white surface and pial surface obtained during the Freesurfer's segmentation (cortical thickness processing section), to accurately register the b0 and the T1-weighted image, maximizing the intensity gradient across grey matter and white matter between both volumes. At this point, all the diffusion to T1 registrations were visually inspected to exclude those subjects with an erroneous co-registration. Then, each individual mean diffusivity volume was sampled at the midpoint of the cortical ribbon (i.e half distance along the normal vector between the white matter surface and the gray matter surface) and projected to each individual surface reconstruction obtained during the Freesurfer processing, to create a surface map of cortical mean diffusivity (using Freesurfer's mri_vol2surf command). Finally, individual cortical mean diffusivity maps were normalized to an average standard surface using a spherical registration, enabling an accurate inter-subject matching of cortical locations for the statistical analyses. Prior to statistical analyses, we applied a Gaussian kernel of 15mm as implemented in Freesurfer, in order to obtain equivalent data effective smoothing between cortical thickness and cortical mean diffusivity (Bejanin et al., 2018; La Joie et al., 2012). The scripts used to process cortical mean diffusivity can be requested to the first authors.

Cortical mean diffusivity harmonization between centers

Diffusor tensor imaging metrics are very sensitive to acquisition parameters (Zhu et al., 2011). Thus, it is imprescindible to use harmonization approaches in order to mitigate center-specific differences in multicenter studies. Here, we applied a multi-center harmonization algorithm based on ComBat, in order to reduce center-specific differences in cortical mean diffusivity quantifications prior to any statistical analysis (Fortin et al., 2017). Briefly, ComBat uses an empirical Bayes framework to estimate the additive (mean) and multiplicative (variance) contribution of each site, at each vertex, for a specific diffusor tensor imaging metric, and corrects these effects. Importantly, this approach allows to include biological information (such as clinical group, age or biomarkers), and it has been reported to preserver within-site biological variability, increasing the statistical power.

Statistical methods

Group differences in the clinical and biomarker data were assessed using t-test or ANOVA for continuous variables, and Chi-square for dichotomous or categorical data. Biomarker values not following a normal distribution were log-transformed. Statistical analyses were performed with the IBM SPSS Statistics 25 (IBM corp.) software. Statistical significance for all tests was set at 5% (α=0.05), and all statistical tests were two-sided.

We first performed group comparisons for cortical mean diffusivity and cortical thickness with a two-class general linear model, as implemented in Freesurfer, comparing bvFTD and the cognitively healthy controls groups. These analyses were repeated for each center indepently. Moreover, as it has been reported that some possible bvFTD cases may represent either non-neurodegenerative cases or cases with a slowly progressive clinical course, we found relevant to compare the patterns of cortical thickness and cortical mean diffusivity in both the probable and possible subgroups. We then performed a vertexwise partial correlation analysis in the bvFTD group between the cortical mean diffusivity and cortical thickness and the log-transformed CSF sAPPβ and NfL values, in addition to the FTLD-CDR. Specifically, a general linear model was created, being mean diffusivity or cortical thickness the dependent variable of interest, and

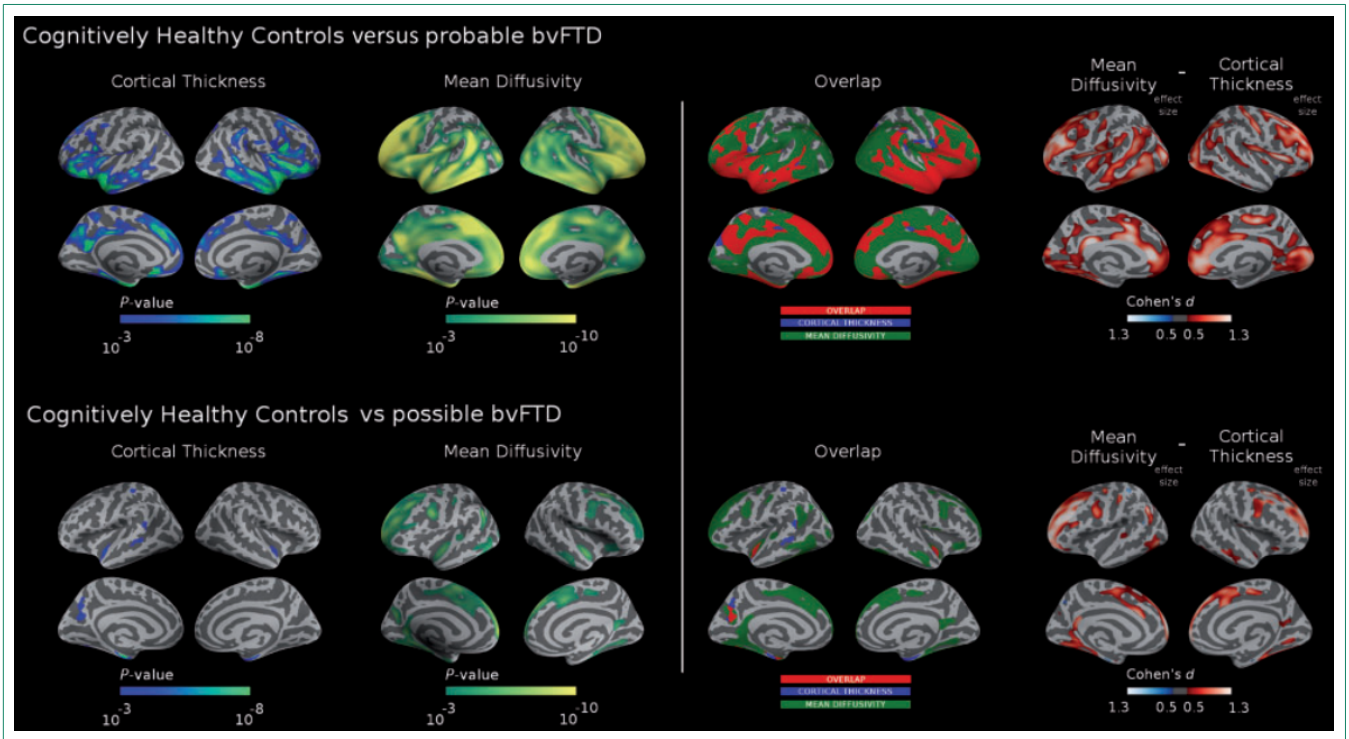

Figure 3. Group comparison of cortical thickness and cortical mean diffusivity between patients with possible and probable bvFTD and cognitively healthy controls. Cortical thickness and cortical mean diffusivity group comparisons between probable (top) and possible (bottom) bvFTD against cognitively healthy controls. On the right (top and bottom), we included the overlapping map between both metrics. Cortical thickness analyses are adjusted by age, sex and center. Mean diffusivity analyses were adjusted by age and sex after a harmonization step. Only clusters that survived familywise error correction (P<0.05) are shown. For visualization purposes, different color codes were used for cortical thickness and cortical mean diffusivity.

CSF values and FTLD-CDR scores the independent variables. We included age, sex, and center as nuisance variables in the cortical thickness analysis. In mean diffusivity analysis, only age and sex were included since diffusor tensor imaging data were already harmonized between centers in a previous step. The correlation between both metrics and FTLD-CDR was also assessed segregating the bvFTD group in possibles and probables. Only results that survived multiple comparisons (Family wise error < 0.05) based on Monte Carlo simulation with 10,000 repeats as implemented in Freesurfer are presented. We used a very stringent threshold of α=0.001 for the group analyses and a threshold of α=0.05 for the correlation analyses. A full description of the multiple comparisons methodology can be found in the Supplementary material.

In order to have a quantitative metric of the spatial differences between both groups; we computed the cortical thickness and cortical mean diffusivity vertex-wise effect sizes of the group comparison between bvFTD patients and cognitively healthy controls using the Cohen's d formula. We also computed the difference between the effect size maps of cortical mean diffusivity and cortical thickness to obtain a topographical representation of the sensitivity difference between both metrics.

For the figure projection and design, we used a freely available python library to overlay the results into the

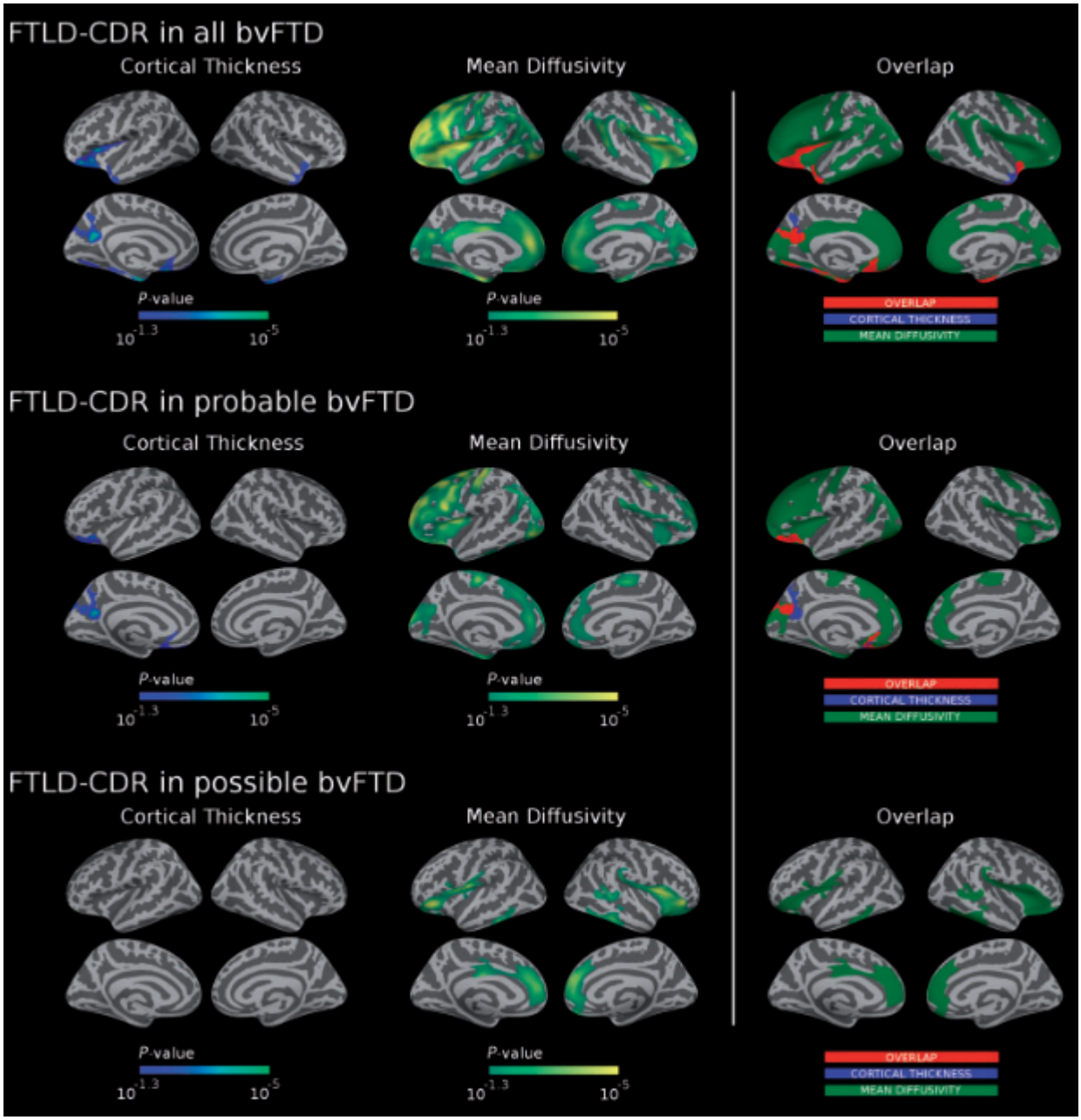

Figure 4. Relationship between cortical thickness and cortical mean diffusivity with the frontotemporal lobar degeneration clinical dementia rating score. Correlation of cortical mean diffusivity with the frontotemporal lobar degeneration clinical dementia rating score in the whole sample (top), probable bvFTD subgroup (middle) and possible bvFTD subgroup (bottom). Small regions of cortical thinning associated to higher FTLD-CDR scores (blue) were found in the probable subgroup, whereas extensive areas of increases of cortical mean diffusivity related to increases in FTLD-CDR scores (green) were found in both subgroups. Cortical thickness analyses were adjusted for age, sex and center. Mean diffusivity analyses were adjusted for age and sex after a harmonization step. The overlap between both maps is displayed on the right (top and bottom).

standard fsaverage surface (Pysurf: https://pysurfer.github.io)

RESULTS

Demographics and sample composition

Table 1 shows the demographics, clinical and neuroimaging features of the participants in the study. Age at MRI and years of education was similar between the bvFTD and HC groups but women were more frequent in the controls group than in the bvFTD group (χ2(1)=23.090; p<0.001). Age at symptom onset, age at MRI, time from symptom onset to MRI, sex distribution, education, FTLD-CDR, and follow-up time were similar between the possible and probable bvFTD groups. However, the proportion of patients with an increased certainty of FTLD at the end of follow-up was higher in the probable bvFTD group than in the possible bvFTD group (χ2(1)=8.089; p=0.004). As shown in Fig. 1, 44 out of 114 (40%) bvFTD participants were excluded because of segmentation or diffusion weighted imaging processing errors. The excluded patients had higher FTLD-CDR than the included bvFTD participants (t(92)=2.041; p=0.044; Supplementary Table 3).

Group comparison of cortical thickness and cortical mean diffusivity

Fig. 2 shows the cortical thickness and cortical mean diffusivity group comparisons between the bvFTD and cognitively healthy controls. The bvFTD group showed cortical thinning in the prefrontal cortex, the insula, the cingulate gyrus (anterior, dorsal and posterior), the orbitofrontal cortex, the anterior temporal pole, the lateral and medial temporal lobe, the angular gyrus and the precuneus. The mean diffusivity cortical map involved more regions than the cortical thinning map, encompassing the whole of the frontal and temporal cortices, and extending to posterior regions such as the inferior parietal and occipital lobe. As depicted in the overlap map included in Fig. 2, cortical thickness and cortical mean diffusivity maps showed a partial overlap but cortical mean diffusivity changes extended beyond the areas of cortical thinning. Of note, we observed similar patterns of cortical thickness and cortical mean diffusivity changes when each cohort was analyzed separately (data not shown).

Cortical thickness and cortical mean diffusivity in possible and probable bvFTD

We then assessed cortical thickness and cortical mean diffusivity separately in the possible and probable bvFTD subgroups (Fig. 3). In the probable bvFTD group we observed extensive clusters of cortical thinning that included essentially the same regions typically involved in the bvFTD that were observed in the Fig. 2. Similar to what we observed in the primary analyses the cortical mean diffusivity changes were more widespread than the cortical thickness changes (Fig. 3 top). In the possible bvFTD subgroup, we observed small clusters of cortical thinning in the insula, and the medial temporal lobe in both hemispheres. Interestingly, we observed extensive cortical mean diffusivity increases in the dorsal and medial prefrontal cortex, as well as in the supplementary motor cortex and the frontal pole in both hemispheres (Fig. 3 bottom).

Relationship between cortical thickness and cortical mean diffusivity with the FTLD-CDR

We next evaluated the capacity of cortical thickness and cortical mean diffusivity to reflect the disease severity in the bvFTD as measured by the FTLD-CDR scale. When pooling together all the bvFTD subjects, we observed an inverse correlation between FTLD-CDR scores and cortical

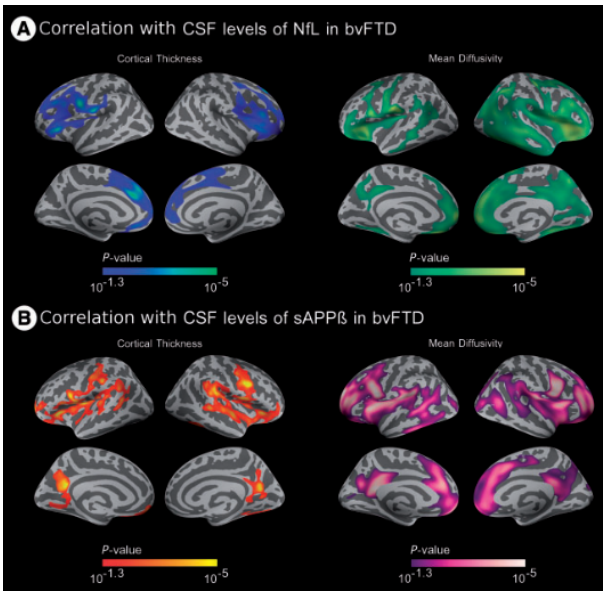

Figure 5. Correlation of cortical thickness and cortical mean diffusivity with CSF biomarkers Relationship of cortical thickness and cortical mean diffusivity with the CSF levels of Neurofilament light (NfL) (top) and the CSF levels of the soluble fraction beta of the amyloid precursor protein (sAPPβ) (bottom) in the subgroup of bvFTD participants with CSF sample available for analysis (n=32). As NfL and sAPPβ values were not normally distributed, we used log-transformed values for these biomarkers NfL levels negatively correlated with cortical thickness (blue) and positively correlated with cortical mean diffusivity (green). sAPPβ positively correlated with cortical thickness (red) and negative correlated with cortical mean diffusivity (purple). Cortical thickness analyses were adjusted for age, sex and center. Mean diffusivity analyses were adjusted for age and sex after a harmonization step. Only clusters that survived familywise error correction at P<0.05 are shown.

thickness in small clusters in the inferior frontal gyrus, the anterior insula, the anterior temporal pole and the medial temporal lobe in both hemispheres and a a correlation in the medial orbitofrontal cortex and in the precuneus in the left hemisphere. We observed larger clusters of significant positive correlations between cortical mean diffusivity and FTLD-CDR scores in both hemispheres (Fig. 4-top). Similar results were found when restricting the analyses to the probable bvFTD group (Fig. 4-middle). When restricting the analysis to the possible bvFTD, we did not find any correlation between cortical thickness and FTLD-CDR scores. However, cortical mean diffusivity was positively associated with FTLD-CDR scores in the anterior cingulate, frontal insula and lateral temporal in both hemispheres (Fig. 4-bottom).

Correlation of cortical thickness and mean diffusivity changes with CSF biomarkers

We finally assessed the correlation of cortical thickness and cortical mean diffusivity with CSF NfL and sAPPβ levels. CSF NfL levels were negatively correlated with cortical thickness in dorsolateral and medial prefrontal areas of the frontal lobe . The correlation between CSF NfL levels and cortical mean diffusivity included those areas, but also areas in the temporal and parietal lobes (Fig. 5 top). CSF sAPPβ levels were positively correlated with cortical thickness in regions of the prefrontal cortex, the insula, the temporo-parietal union and the lateral temporal cortex. The negative correlation between CSF sAPPβ levels and cortical mean diffusivity extended to more widespread frontal and temporal regions, as well as to posterior regions (Fig. 5-bottom).

DISCUSSION

In this study we investigated the value of cortical mean diffusivity as a biomarker in bvFTD in a large multicenter sample. We showed that cortical mean diffusivity was not only able to elicit those areas with cortical thinning, but also involved other areas that typically become affected with disease progression (Binney et al., 2017). Furthermore, we found cortical mean diffusivity increases in patients classified as possible bvFTD that had only minimal cortical thinning. Clinical measures of disease severity (FTLD-CDR) and CSF neuronal biomarkers (CSF NfL and sAPPβ levels)

showed a more widespread correlation with cortical mean diffusivity than with cortical thickness. Taken together, these findings suggest that cortical mean diffusivity might be more sensitive than cortical thickness to detect the earliest disease-related cortical changes in bvFTD.

Cortical mean diffusivity has been recently proposed as a sensitive biomarker for the detection of the earliest cortical changes in sporadic AD (Montal et al., 2017; Weston et al., 2015). We show, for the first time in bvFTD using a surface-based approach, that cortical mean diffusivity increases spread beyond the areas of cortical thinning in bvFTD, even in patients with possible bvFTD. Most previous studies using diffusor tensor imaging in bvFTD patients have focused on the white matter, probably because of the technical difficulties in the study of cortical microstructure (Papma et al., 2017). We identified a single previous small study (with 16 bvFTD patients) assessing cortical diffusor tensor imaging in the bvFTD using a volume-based approach (Whitwell et al., 2010). This study found overlapping patterns between atrophy and increases on mean diffusivity. Our study builds on these results using a larger sample, a surface-based approach, and the inclusion of bvFTD patients at milder disease stages. Consequently we were able to show the added value of cortical mean diffusivity as a more sensitive biomarker in bvFTD over cortical thickness.

We found minimal cortical thinning when comparing possible bvFTD patients and controls. However, we observed extensive cortical mean diffusivity increases in regions known to be affected in bvFTD (Schroeter et al., 2014; Brettschneider et al., 2014; Irwin et al., 2016). Moreover, we calculated effect size maps to quantify the impact of cortical thickness and cortical mean diffusivity for the differentiation of bvFTD patients from controls. Importantly, we obtained moderate to high net effect size favoring cortical mean diffusivity in critical bvFTD-related cortical regions such as the anterior cingulate, the prefrontal dorsal cortex and the insula. The suggestion that cortical mean diffusivity may be more sensitive than cortical thickness to detect the bvFTD cortical changes is further supported by our correlation analyses with the FTLD-CDR and CSF NfL and sAPPβ levels. Both the clinical measures of disease severity and the CSF biomarkers, they all showed a better correlation with cortical mean diffusivity than with cortical thickness. The FTLD-CDR has been validated as a tool for disease monitoring in clinical trials (Knopman et al., 2008). Although the FTLD-CDR scores also correlated with cortical thickness in some small frontotemporal clusters, we found a substantially widespread correlation with cortical mean diffusivity. Moreover, when restricting the analyses in the possible bvFTD subgroup, only associations between cortical mean diffusivity and FTLD-CDR scores were found. This finding supports a possible role for cortical mean diffusivity as a candidate neuroimaging biomarker for disease staging.

To further evaluate the role of cortical mean diffusivity as a neurogeneration biomarker, we investigated its correlation with CSF biomarkers in a subgroup of patients. NfL is one of the major constituents of the axonal cytoskeleton and plays an important role in axonal transport. The measurement of NfL levels both in the CSF and in serum correlates with disease severity, progression and survival in multiples neurodegenerative diseases (Landqvist Waldö et al., 2013; Meeter et al., 2016; Pijnenburg et al., 2015; Rohrer et al., 2016; Scherling et al., 2014; Wilke et al., 2016) (Alcolea et al., 2017). We also measured CSF sAPPβ levels, as we have previously shown that this biomarker correlates with frontotemporal neurodegeneration in FTLD-related syndromes (Alcolea D et al., 2017; Illán-Gala I et al., 2018). The association between cortical mean diffusivity and CSF

values further reinforce the notion that cortical mean diffusivity changes reflect the underlying neurodegeneration. Although we acknowledge that it is possible that some patients classified as possible bvFTD may not have underlying FTLD (Devenney et al., 2016; Gossink et al., 2015), recent studies in deep-phenotyped cohorts have shown that a significant proportion of bvFTD cases do not have frontotemporal atrophy and may be characterized by a slower disease course (Ranasinghe et al., 2016; Rascovsky et al., 2011). In the present study, 70% patients classified as possible bvFTD were found to have an increased certainty of underlying FTLD as suggested by follow-up, genetic and neuropathological information available. Indeed, longitudinal decline was observed in most possible bvFTD patients and psychiatric diagnoses were excluded by expert clinicians. Of note, two cases classified as possible bvFTD were found to have a C9orf72 expansion, a finding that has been previously reported in different cohorts (refs). Thus, we think that the patients classified as possible bvFTD are at high risk of having underlying FTLD and that our cortical mean diffusivity results support that at least a proportion of possible bvFTD patients have a neurodegenerative disease. Cortical mean diffusivity may be a relevant tool for increasing the diagnostic certainty in these “slowly progressive” bvFTD without overt frontotemporal atrophy (Davies et al., 2006; Khan et al., 2012).

Taken together, our findings support the role of cortical mean diffusivity as a novel potential neurodegeneration biomarker in bvFTD. We hypothesize that cortical mean diffusivity may be a sensitive tool for the refinement and monitoring of the very earliest cortical changes genetically-determined FTLD (Rohrer et al., 2015). Importantly, further longitudinal studies should explore the ability of cortical mean diffusivity to predict disease progression at the single-subject levels. Additionally, our study is the first to report the potential added value of cortical diffusor tensor imaging changes over cortical thickness in bvFTD. Further studies could explore the added value of the combined study of white and grey matter diffusor tensor imaging changes to improve pathological predictions (Downey et al., 2015; McMillan et al., 2014). All the aforementioned points are key aspects for candidate selection in clinical trials once protein-specific targeted therapies become available (Elahi and Miller, 2017).

The main strengths of this study are the relatively large number of bvFTD participants at a mild to moderate disease stage, and the surface-based analyses using a previously validated technique. This surface-based approach solves some of the limitations and methodological concerns that have been previously reported when using a voxel-based approach (Henf et al., 2018). Moreover, we enriched our description of the cortical mean diffusivity in the bvFTD with established clinical measures of disease severity and CSF biomarkers. This study has also some limitations. First, we acknowledge that a substantial part (up to 40% of the cases) of bvFTD cases were excluded because of segmentation or diffusor tensor imaging processing errors. Even though this is an inherent limitation of our surface-based approach, future improvements in T1 MRI acquisitions or the use of higher field MRIs, together with software improvements will likely reduce the number of subjects excluded due to segmentation errors. Of note, we observed that the excluded patients belonged to the probable bvFTD group (77.3% of the excluded cases) and were at a more advanced disease stage, as measured by the FTLD-CDR. Notwithstanding, cortical mean diffusivity may still provide valuable topographical information regarding the earliest cortical microstructural changes in patients at very mild disease stages (for example, sporadic bvFTD cases without overt cortical atrophy or even genetic cases) were

less segmentation errors are expected to occur. Second, it may be argued that there may be confounding results related to the different acquisition protocols across centers. However, the results presented in the current manuscript were obtained after using a validated state-of-the-art algorithm to harmonize diffusion data between centers (Fortin et al., 2017; Montal et al., 2017). Moreover, results were similar when analyzing each center independently regardless of the use of different diffusion weighted imaging sequences. Third, although we provide cross-sectional evidence that cortical mean diffusivity changes may be a novel sensitive metric to reflect neurodegeneration, further longitudinal studies and using presymptomatic mutation carriers should confirm that cortical mean diffusivity changes antedate cortical atrophy in patients with bvFTD. Fourth, because most of the included bvFTD cases did not have neuropathological evaluation, misdiagnosis could have occurred, especially in the possible bvFTD group. However, a high proportion of cases were found to have an increased certainty of underlying frontotemporal lobar degeneration when considering the available clinical, genetic and neuropathological information. Finally, as neuropathological evaluation was not available in most cases we were not able to explore the precise pathological correlates of the observed cortical mean diffusivity changes.

In summary, this study suggests that cortical mean diffusivity may be a valuable novel biomarker for the cortical mapping of neurodegeneration-related microstructural changes in bvFTD. Further longitudinal studies in different populations including preclinical mutation carriers should precise the diagnostic and prognostic utility especially at the earliest stages of the disease.

ACKNOWLEDGEMENTS

The authors thank the patients and their relatives for their support for this study. We also thank Laia Muñoz for technical assistance and María Carmona-Iragui, Estrella Muñoz-Rodríguez, Roser Ribosa for their collaboration in the recruitment of patients for this study.

REFERENCES

Agosta F, Galantucci S, Magnani G, Marcone A, Martinelli D, Antonietta Volontè M, et al. MRI signatures of the frontotemporal lobar degeneration continuum. Hum. Brain Mapp. 2015; 36: 2602–2614.

Alcolea D, Carmona-Iragui M, Suárez-Calvet M, Sánchez-Saudinós MB, Sala I, Antón-Aguirre S, et al. Relationship between β-Secretase, inflammation and core cerebrospinal fluid biomarkers for Alzheimer's disease. J Alzheimers Dis 2014; 42: 157–167.

Alcolea D, Martínez-Lage P, Sánchez-Juan P, Olazarán J, Antúnez C, Izagirre A, et al. Amyloid precursor protein metabolism and inflammation markers in preclinical Alzheimer disease. Neurology 2015; 85: 626–633.

Alcolea D, Vilaplana E, Suárez-Calvet M, Illán-Gala I, Blesa R, Clarimon J, et al. CSF sAPPβ, YKL-40, and neurofilament light in frontotemporal lobar degeneration. Neurology 2017; 89: 178–188.

Balasa M, Gelpi E, Martín I, Antonell A, Rey MJ, Grau-Rivera O, et al. Diagnostic accuracy of behavioral variant frontotemporal dementia consortium criteria (FTDC) in a clinicopathological cohort. Neuropathol Appl Neurobiol 2015; 4: 882-892

Bang J, Spina S, Miller BL. Frontotemporal dementia. Lancet 2015; 386: 1672–1682.

Bejanin A, La Joie R, Landeau B, Belliard S, La Sayette de V, Eustache F, et al. Distinct Interplay Between Atrophy and Hypometabolism in Alzheimer's Versus Semantic Dementia. Cereb. Cortex 2018

Binney RJ, Pankov A, Marx G, He X, McKenna F, Staffaroni AM, et al. Data-driven regions of interest for longitudinal change in three variants of frontotemporal lobar degeneration. Brain Behav 2017; 7: e00675.

Brettschneider J, Del Tredici K, Irwin DJ, Grossman M, Robinson JL, Toledo JB, et al. Sequential distribution of pTDP-43 pathology in behavioral variant frontotemporal dementia (bvFTD). Acta Neuropathol 2014; 127: 423–439.

Chare L, Hodges JR, Leyton CE, McGinley C, Tan RH, Kril JJ, et al. New criteria for frontotemporal dementia syndromes: clinical and pathological diagnostic implications. J Neurol Neurosurg Psychiatry 2014; 85: 865–870.

Coalson TS, Van Essen DC, Glasser MF. The impact of traditional neuroimaging methods on the spatial localization of cortical areas. Proc Natl Acad Sci U S A. 2018; 115: E6356–E6365.

Davies RR, Kipps CM, Mitchell J, Kril JJ, Halliday GM, Hodges JR. Progression in frontotemporal dementia: identifying a benign behavioral variant by magnetic resonance imaging. Arch Neurol 2006; 63: 1627–1631.

Devenney E, Forrest SL, Xuereb J, Kril JJ, Hodges JR. The bvFTD phenocopy syndrome: a clinicopathological report. J Neurol Neurosurg Psychiatry 2016; 87: 1155–1156.

Downey LE, Mahoney CJ, Buckley AH, Golden HL, Henley SM, Schmitz N, et al. White matter tract signatures of impaired social cognition in frontotemporal lobar degeneration. Neuroimage Clin 2015; 8: 640–651.

Elahi FM, Marx G, Cobigo Y, Staffaroni AM, Kornak J, Tosun D, et al. Longitudinal white matter change in frontotemporal dementia subtypes and sporadic late onset Alzheimer's disease. Neuroimage Clin 2017; 16: 595–603.

Elahi FM, Miller BL. A clinicopathological approach to the diagnosis of dementia. Nat Rev Neurol 2017; 13: 457–476.

Fischl B, Dale AM. Measuring the thickness of the human cerebral cortex from magnetic resonance images. Proc Natl Acad Sci U S A 2000; 97: 11050–11055.

Fortin J-P, Parker D, Tunç B, Watanabe T, Elliott MA, Ruparel K, et al. Harmonization of multi-site diffusion tensor imaging data. NeuroImage 2017; 161: 149–170.

Ganepola T, Nagy Z, Ghosh A, Papadopoulo T, Alexander DC, Sereno MI. Using diffusion MRI to discriminate areas of cortical grey matter. NeuroImage 2017

Gossink FT, Dols A, Kerssens CJ, Krudop WA, Kerklaan BJ, Scheltens P, et al. Psychiatric diagnoses underlying the phenocopy syndrome of behavioural variant frontotemporal dementia. J Neurol Neurosurg Psychiatry 2016; 87: 64–68.

Hagler DJ, Saygin AP, Sereno MI. Smoothing and cluster thresholding for cortical surface-based group analysis of fMRI data. NeuroImage 2006; 33: 1093–1103.

Henf J, Grothe MJ, Brueggen K, Teipel S, Dyrba M. Mean diffusivity in cortical gray matter in Alzheimer's disease: The importance of partial volume correction. Neuroimage Clin 2018; 17: 579–586.

Illán-Gala I, Alcolea D, Montal V, Dols-Icardo O, Muñoz L, De Luna N, et al. CSF sAPPβ, YKL-40, and NfL along the ALS-FTD spectrum. Neurology 2018 Ahead of Print

Irwin DJ, Brettschneider J, McMillan CT, Cooper F, Olm C, Arnold SE, et al. Deep clinical and neuropathological phenotyping of Pick disease. Ann Neurol 2016; 79: 272–287.

Khan BK, Yokoyama JS, Takada LT, Sha SJ, Rutherford NJ, Fong JC, et al. Atypical, slowly progressive behavioural variant frontotemporal dementia associated with C9ORF72 hexanucleotide expansion. J Neurol Neurosurg Psychiatry 2012; 83: 358–364.

Knopman DS, Kramer JH, Boeve BF, Caselli RJ, Graff-Radford NR, Mendez MF, et al. Development of methodology for conducting clinical trials in frontotemporal lobar degeneration. Brain 2008; 131: 2957–2968.

Koo B-B, Hua N, Choi C-H, Ronen I, Lee JM, Kim D-S. A framework to analyze partial volume effect on gray matter mean diffusivity measurements. NeuroImage 2009; 44: 136–144.

La Joie R, Perrotin A, Barré L, Hommet C, Mézenge F, Ibazizene M, et al. Region-specific hierarchy between atrophy, hypometabolism, and β-amyloid (Aβ) load in Alzheimer's disease dementia. J. Neurosci. 2012; 32: 16265–16273.

Lam BYK, Halliday GM, Irish M, Hodges JR, Piguet O. Longitudinal white matter changes in frontotemporal dementia subtypes. Hum. Brain Mapp. 2013; 35: 3547–3557.

Landqvist Waldö M, Frizell Santillo A, Passant U, Zetterberg H, Rosengren L, Nilsson C, et al. Cerebrospinal fluid neurofilament light chain protein levels in subtypes of frontotemporal dementia. BMC Neurol 2013; 13: 54.

Lleo A, Irwin DJ, Illán-Gala I, McMillan CT, Wolk DA, Lee EB, et al. A 2-Step Cerebrospinal Algorithm for the Selection of Frontotemporal Lobar Degeneration Subtypes. JAMA Neurol 2018

Mahoney CJ, Ridgway GR, Malone IB, Downey LE, Beck J, Kinnunen KM, et al. Profiles of white matter tract pathology in frontotemporal dementia. Hum. Brain Mapp. 2014; 35: 4163–4179.

Mahoney CJ, Simpson IJA, Nicholas JM, Fletcher PD, Downey LE, Golden HL, et al. Longitudinal diffusion tensor imaging in frontotemporal dementia. Ann Neurol 2014; 77: 33–46.

McMillan CT, Avants BB, Cook P, Ungar L, Trojanowski JQ, Grossman M. The power of neuroimaging biomarkers for screening frontotemporal dementia. Hum. Brain Mapp. 2014; 35: 4827–4840.

Meeter LH, Dopper EG, Jiskoot LC, Sánchez-Valle R, Graff C, Benussi L, et al. Neurofilament light chain: a biomarker for genetic frontotemporal dementia. Ann Clin Transl Neurol 2016; 3: 623–636.

Meeter LH, Kaat LD, Rohrer JD, van Swieten JC. Imaging and fluid biomarkers in frontotemporal dementia. Nat Rev Neurol 2017; 19: 109–419.

Menke RAL, Gray E, Lu C-H, Kuhle J, Talbot K, Malaspina A, et al. CSF neurofilament light chain reflects corticospinal tract degeneration in ALS. Ann Clin Transl Neurol 2015; 2: 748–755.

Montal V, Vilaplana E, Alcolea D, Pegueroles J, Pasternak O, Gonzalez-Ortiz S, et al. Cortical microstructural changes along the Alzheimer's disease continuum. Alzheimers Dement 2017; 14: 340–351.

Papma JM, Jiskoot LC, Panman JL, Dopper EG, Heijer den T, Donker Kaat L, et al. Cognition and gray and white matter characteristics of presymptomatic C9orf72 repeat expansion. Neurology 2017; 89: 1256–1264.

Parker TD, Slattery CF, Zhang J, Nicholas JM, Paterson RW, Foulkes AJM, et al. Cortical microstructure in young onset Alzheimer's disease using neurite orientation dispersion and density imaging. Hum. Brain Mapp. 2018

Perry DC, Brown JA, Possin KL, Datta S, Trujillo A, Radke A, et al. Clinicopathological correlations in behavioural variant frontotemporal dementia. Brain 2017; 140: 3329–3345.

Pijnenburg YAL, Verwey NA, van der Flier WM, Scheltens P, Teunissen CE. Discriminative and prognostic potential of cerebrospinal fluid phosphoTau/tau ratio and neurofilaments for frontotemporal dementia subtypes. Alzheimers Dement (Amst) 2015; 1: 505–512.

Ranasinghe KG, Rankin KP, Pressman PS, Perry DC, Lobach IV, Seeley WW, et al. Distinct Subtypes of Behavioral Variant Frontotemporal Dementia Based on Patterns of Network Degeneration. JAMA Neurol 2016; 73: 1078–1088.

Rascovsky K, Hodges JR, Knopman D, Mendez MF, Kramer JH, Neuhaus J, et al. Sensitivity of revised diagnostic criteria for the behavioural variant of frontotemporal dementia. Brain 2011; 134: 2456–2477.

Rohrer JD, Nicholas JM, Cash DM, van Swieten J, Dopper E, Jiskoot L, et al. Presymptomatic cognitive and neuroanatomical changes in genetic frontotemporal dementia in the Genetic Frontotemporal dementia Initiative (GENFI) study: a cross-sectional analysis. Lancet Neurol 2015; 14: 253–262.

Rohrer JD, Woollacott IOC, Dick KM, Brotherhood E, Gordon E, Fellows A, et al. Serum neurofilament light chain protein is a measure of disease intensity in frontotemporal dementia. Neurology 2016; 87: 1329–1336.

Scherling CS, Hall T, Berisha F, Klepac K, Karydas A, Coppola G, Kramer JH, Rabinovici G, Ahlijanian M, Miller BL, Seeley W, Grinberg LT, Rosen H, Meredith J Jr, Boxer AL. Cerebrospinal fluid neurofilament concentration reflects disease severity in frontotemporal degeneration. Ann Neurol 2014; 75: 116–126.

Schroeter ML, Laird AR, Chwiesko C, Deuschl C, Schneider E, Bzdok D, et al. Conceptualizing neuropsychiatric diseases with multimodal data-driven meta-analyses - the case of behavioral variant frontotemporal dementia. Cortex 2014; 57: 22–37.

Seo SW, Thibodeau M-P, Perry DC, Hua A, Sidhu M, Sible I, et al. Early vs late age at onset frontotemporal dementia and frontotemporal lobar degeneration. Neurology 2018; 90: e1047–e1056.

Suri S, Topiwala A, Mackay CE, Ebmeier KP, Filippini N. Using structural and diffusion magnetic resonance imaging to differentiate the dementias. Curr Neurol Neurosci Rep 2014; 14: 475.

Tartaglia MC, Sidhu M, Laluz V, Racine C, Rabinovici GD, Creighton K, et al. Sporadic corticobasal syndrome due to FTLD-TDP. Acta Neuropathol 2010; 119: 365–74.

Weston PSJ, Simpson IJA, Ryan NS, Ourselin S, Fox NC. Diffusion imaging changes in grey matter in Alzheimer's disease: a potential marker of early neurodegeneration. Alzheimers Res Ther 2015; 7: 47.

Whitwell JL, Avula R, Senjem ML, Kantarci K, Weigand SD, Samikoglu A, et al. Gray and white matter water diffusion in the syndromic variants of frontotemporal dementia. Neurology 2010; 74: 1279–1287.

Wilke C, Preische O, Deuschle C, Roeben B, Apel A, Barro C, et al. Neurofilament light chain in FTD is elevated not only in cerebrospinal fluid, but also in serum. J Neurol Neurosurg Psychiatry 2016; 87: 1270–1272.

Wood EM, Falcone D, Suh E, Irwin DJ, Chen-Plotkin AS, Lee EB, et al. Development and Validation of Pedigree Classification Criteria for Frontotemporal Lobar Degeneration. JAMA Neurol 2013; 70: 1411–7.

Zhu T, Hu R, Qiu X, Taylor M, Tso Y, Yiannoutsos C, et al. Quantification of accuracy and precision of multi-center DTI measurements: a diffusion phantom and human brain study. NeuroImage 2011; 56: 1398–1411.